**ADVERTIMENT**. La consulta d'aquesta tesi queda condicionada a l'acceptació de les següents condicions d'ús: La difusió d'aquesta tesi per mitjà del servei TDX (www.tesisenxarxa.net) ha estat autoritzada pels titulars dels drets de propietat intel·lectual únicament per a usos privats emmarcats en activitats d'investigació i docència. No s'autoritza la seva reproducció amb finalitats de lucre ni la seva difusió i posada a disposició des d'un lloc aliè al servei TDX. No s'autoritza la presentació del seu contingut en una finestra o marc aliè a TDX (framing). Aquesta reserva de drets afecta tant al resum de presentació de la tesi com als seus continguts. En la utilització o cita de parts de la tesi és obligat indicar el nom de la persona autora.

**ADVERTENCIA**. La consulta de esta tesis queda condicionada a la aceptación de las siguientes condiciones de uso: La difusión de esta tesis por medio del servicio TDR (www.tesisenred.net) ha sido autorizada por los titulares de los derechos de propiedad intelectual únicamente para usos privados enmarcados en actividades de investigación y docencia. No se autoriza su reproducción con finalidades de lucro ni su difusión y puesta a disposición desde un sitio ajeno al servicio TDR. No se autoriza la presentación de su contenido en una ventana o marco ajeno a TDR (framing). Esta reserva de derechos afecta tanto al resumen de presentación de la tesis como a sus contenidos. En la utilización o cita de partes de la tesis es obligado indicar el nombre de la persona autora.

**WARNING**. On having consulted this thesis you're accepting the following use conditions: Spreading this thesis by the TDX (www.tesisenxarxa.net) service has been authorized by the titular of the intellectual property rights only for private uses placed in investigation and teaching activities. Reproduction with lucrative aims is not authorized neither its spreading and availability from a site foreign to the TDX service. Introducing its content in a window or frame foreign to the TDX service is not authorized (framing). This rights affect to the presentation summary of the thesis as well as to its contents. In the using or citation of parts of the thesis it's obliged to indicate the name of the author

# Interaction between groundwater and underground constructions

## PhD Thesis

**Estanislao Pujades Garnes**

**Barcelona, September 2013**

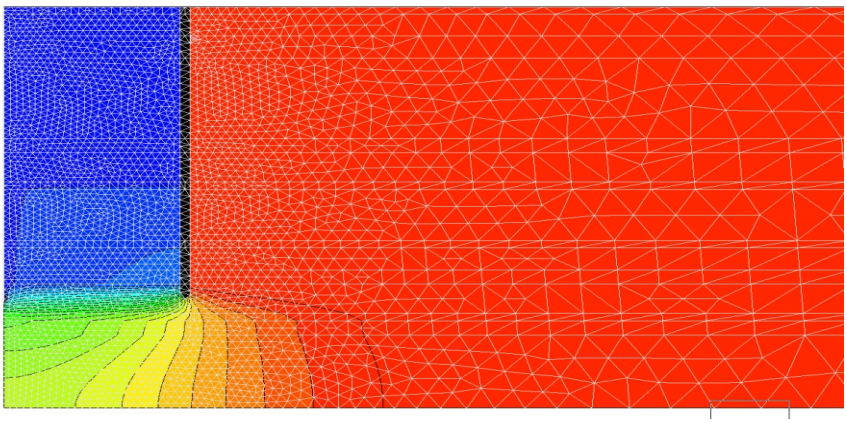

**Advisors:**
**Dr. Enric Vázquez Suñé**
**Dr. Jesús Carrera Ramirez**

**Hydrogeology Group (GHS)**
**Institute of Environmental Assessment and Water Research (IDAEA)**
**Spanish Research Council (CSIC)**
**Dept. Geotechnical Engineering and Geosciences, Universitat Politecnica de Catalunya, UPC-Barcelona Tech**

# Interaction between groundwater and underground constructions

PhD Thesis

Estanislao Pujades Garnes

Barcelona, September 2013

Advisors:

Dr. Enric Vázquez Suñé

Dr. Jesús Carrera Ramirez

**Hydrogeology Group (GHS)**

**Institute of Environmental Assessment and Water Research (IDAEA)**

**Spanish Research Council (CSIC)**

**Dept. Geotechnical Engineering and Geosciences, Universitat Politecnica de Catalunya, UPC-Barcelona Tech**

# I. Abstract

Underground constructions below the water table may be problematic if the role of groundwater is not properly acknowledged. Difficulties worsen in urban environments. Two aspects should be taken into account in the interaction between underground constructions and groundwater, 1) the impacts caused by the construction in the aquifers and 2) the difficulties that groundwater causes during the construction. Therefore, the design of an underground construction must be minimize the impacts in the underground environment as well as guaranteeing the safety of the workers and the integrity of adjacent structures. The adopted measures must not complicate the development of the construction and must not increase the total cost. To sum up, the construction must be efficient. These questions arose during the construction of the High Speed Train (HST) tunnel in Barcelona, which passes next to the Sagrada Familia. This thesis proposes answers to the questions which came up.

Two problems may arise when a construction intersects an aquifer, the drain and the barrier effect. While the former has been widely studied, the second has not been adequately formalized and this is the first aim of the thesis. Analytical solutions are obtained to compute the head variations caused by an underground impervious structure. The solutions allow computing of the impact under different circumstances and to design corrective measures. The proposed equations were verified by using the data from real underground constructions.

Subsidence caused by dewatering processes of deep excavations is feared. This fact affects the design. One option to reduce subsidences consist on deepen the enclosures (diaphragm walls, piles, jet-grouting piles) in order to avoid or minimise the dewatering. The second objective is to discuss the effectiveness of this measure, which rise the cost of the constructions, since drawdown caused by pumping are usually small and less dangerous (poorly differential) than is expected. Moreover, the pumping stabilizes the bottom of excavations. Therefore, to deepen the enclosures may be less efficient than combining short enclosures with deep pumping wells. Both alternatives must be compared. Thus, a number of dewatering scenarios, where the depth of the enclosures and the pumping wells are varied, are compared considering the safety, the outside affectations and the cost. Results show that combining deep pumping wells with short enclosures can become the most efficient method to perform excavations in preconsolidated soils.

Regardless of the method used to perform an excavation, the enclosure, always, plays an important role since it guarantees the stability of the excavation walls and prevents the entrance of lateral flow. The presence of small defects may lead to disastrous consequences, which would invalidate all the previous work oriented to develop an efficient construction. Therefore, given that the defects are relatively common, that the techniques used to detect defects are limited and that the groundwater behaviour taking into account underground structures can be predicted, the third objective of the thesis is to develop hydraulic methods to assess the state of an enclosure. These methods, specifically the Watertightness Assessment Test (WTAT), are used as much to estimate the effective parameters of the enclosure as to locate the defects.

Finally, the steps followed during the construction of the HST tunnel in Barcelona demonstrate the importance of the geological characterisation. If the soil is well known, all the aspects associated with the construction can be predicted accurately, which is crucial for designing an efficient underground construction. The geology, the hydrogeology and the historical processes suffered by the soil must be characterized accurately.

# II. Resumen

Las construcciones subterráneas realizadas por debajo del nivel piezométrico pueden ser problemáticas si no se reconoce el papel del agua subterránea. Las dificultades aumentan en ambientes urbanos. La interacción con el agua subterránea tiene lugar en las dos direcciones 1) los impactos causados por la construcción sobre el acuífero y 2) las dificultades que, durante la construcción, causará la presencia de agua subterránea. Por ello, el diseño de una construcción subterránea debe minimizar los impactos en el medio subterráneo y garantizar la seguridad de los trabajadores y la integridad de las estructuras adyacentes. Las medidas adoptadas no deben complicar en exceso el desarrollo de las obras ni sobrecargar el coste total de la obra. En resumen, la construcción debe ser eficiente. Estas preguntas surgieron durante la construcción del túnel para el Tren de Alta Velocidad (HST) en Barcelona, adyacente a la Sagrada Familia. En esta tesis se proponen respuestas a las mismas.

Los impactos sobre el acuífero pueden ser de dos tipos: el efecto dren y el efecto barrera. Mientras que el primero ha sido ampliamente estudiado, el segundo no ha sido formalizado adecuadamente, lo que constituye el primer objetivo de esta tesis. Para calcular las variaciones de nivel causadas por una estructura subterránea impermeable, se derivan ecuaciones para diversas condiciones de obra y para medidas correctoras. Se han verificado con datos de construcciones reales.

La subsidencia causada por el drenaje de excavaciones profundas es uno de los temores más condicionantes del diseño. Una de las maneras de reducirla, consiste en profundizar los recintos (pantallas, pilotes, columnas de jet-grouting) con el fin de evitar o minimizar el bombeo. El segundo objetivo de esta tesis es cuestionar la eficacia de estas medidas, que aumentan el coste de la construcción, ya que los asientos causados por el bombeo suelen ser pequeños y menos peligrosos (poco diferenciales) de lo temido. Además, el bombeo estabiliza la base de las excavaciones. Por ello realizar recintos más profundos puede ser menos eficiente que combinar recintos cortos y pozos de bombeo profundos. Es obvio que ambas alternativas deben compararse adecuadamente. Para ello, se han estudiado una serie de escenarios de drenaje que son comparados teniendo en cuenta la seguridad, las afecciones externas y el coste. Las variaciones entre los diferentes escenarios son las profundidades de los recintos y de los pozos de bombeo. Los resultados muestran que

combinar pozos de bombeo profundos con recintos cortos es el método más eficiente para llevar a cabo excavaciones en suelos preconsolidados.

Independientemente del método utilizado para llevar a cabo una excavación, el recinto, siempre juega un papel importante, ya que garantiza la estabilidad de las paredes de la excavación y evita la entrada de flujo lateral. La presencia de pequeños defectos puede tener consecuencias desastrosas, lo que haría inútil todo el trabajo previo orientado a desarrollar una construcción eficiente. Por lo tanto, dado que los defectos son relativamente comunes, que las técnicas utilizadas para detectar defectos son limitadas y que el comportamiento del agua subterránea puede ser predicho teniendo en cuenta las estructuras subterráneas existentes. El tercer objetivo de la tesis es desarrollar métodos hidráulicos para evaluar el estado del recinto de una excavación. Se muestra que estos métodos y, en particular, el ensayo de caracterización de impermeabilización permiten tanto estimar los parámetros efectivos del recinto como localizar los defectos.

Por último, los pasos seguidos durante la construcción del túnel para el Tren de Alta Velocidad en Barcelona evidencian la importancia de una buena caracterización geológica. Si el suelo es bien conocido, todos los aspectos asociados con la construcción pueden ser estimados con precisión, lo que resulta crucial para diseñar una construcción subterránea eficiente. La geología, la hidrogeología y los procesos históricos sufridos por el suelo deben ser bien conocidos.

# III. Resum

Les construccions subterrànies realitzades sota el nivell piezomètric poden ser problemàtiques si no es reconeix el paper de l'aigua subterrània. Les dificultats augmenten en ambients urbans. La interacció amb l'aigua subterrània té lloc en els dos sentits 1) els impactes causats per la construcció sobre l'aqüífer i 2) les dificultats que, durant la construcció, causarà la presència d'aigua subterrània. Per això, el disseny d'una construcció subterrània ha de minimitzar els impactes al medi subterrani i garantir la seguretat dels treballadors i la integritat de les estructures adjacents. Les mesures adoptades no han de complicar en excés el desenvolupament de les obres ni sobrecarregar el cost total de l'obra. En resum, la construcció ha de ser eficient. Aquestes preguntes van sorgir durant la construcció del túnel per al Tren d'Alta Velocitat a Barcelona, adjacent a la Sagrada Família. En aquesta tesi es proposen respostes a les mateixes.

Els impactes sobre l'aqüífer poden ser de dos tipus: l'efecte dren i l'efecte barrera. Mentre que el primer ha estat àmpliament estudiat, el segon no ha estat formalitzat adequadament, la qual cosa constitueix el primer objectiu d'aquesta tesi. Per calcular les variacions de nivell causades per una estructura subterrània impermeable, es deriven equacions per a diverses condicions d'obra i per a mesures correctores. S'han verificat amb dades de construccions reals.

La subsidència causada pel drenatge d'excavacions profundes és un dels temors més condicionants del disseny. Una de les maneres de reduir-la, consisteix a aprofundir els recintes (pantalles, pilotis, columnes de jet-grouting) amb la finalitat d'evitar o minimitzar el bombament. El segon objectiu d'aquesta tesi és qüestionar l'eficàcia d'aquestes mesures, que augmenten el cost de la construcció, ja que els seients causats pel bombament solen ser petits i menys perillosos (poc diferencials) del temut. A més, el bombament estabilitza la base de les excavacions. Per això realitzar recintes més profunds pot ser menys eficient que combinar recintes curts i pous de bombament profunds. És obvi que ambdues alternatives han de comparar-se adequadament. Per a això, s'han estudiat una sèrie d'escenaris de drenatge que són comparats tenint en compte la seguretat, les afeccions externes i el cost. Les variacions entre els diferents escenaris són les profunditats dels recintes i dels pous de bombament. Els resultats mostren que combinar pous de bombament profunds amb recintes curts és el mètode més eficient per dur a terme excavacions en sòls preconsolidats.

Independentment del mètode utilitzat per dur a terme una excavació, el recinte, sempre juga un paper important, ja que garanteix l'estabilitat de les parets de l'excavació i evita l'entrada de flux lateral. La presència de petits defectes pot tenir conseqüències desastroses, la qual cosa faria inútil tot el treball previ orientat a desenvolupar una construcció eficient. Per tant, atès que els defectes són relativament comuns, que les tècniques utilitzades per detectar defectes són limitades i que el comportament de l'aigua subterrània pot ser predit tenint en compte les estructures subterrànies existents. El tercer objectiu de la tesi és desenvolupar mètodes hidràulics per avaluar l'estat del recinte d'una excavació. Es mostra que aquests mètodes i, en particular, l'assaig de caracterització d'impermeabilització (WTAT) permeten tant estimar els paràmetres efectius del recinte com localitzar els defectes.

Finalment, els passos seguits durant la construcció del túnel per al Tren d'Alta Velocitat a Barcelona evidencien la importància d'una bona caracterització geològica. Si el sòl és ben conegut, tots els aspectes associats amb la construcció poden ser estimats amb precisió, la qual cosa resulta crucial per dissenyar una construcció subterrània eficient. La geologia, la hidrogeologia i els processos històrics soferts pel sòl han de ser ben coneguts.

# IV. Acknowledgements

This thesis is the end of my journey to obtain my Ph.D. It has been a challenging experience riddle of good and bad moments. However, I have felt supported during this time by several people. This thesis also belongs to them. I would like to express my gratitude to all of these people.

First and foremost, I want to thank my advisors, Enric Vázquez and Jesús Carrera for their continuous support, for their guidance, for giving me the opportunity to pursue my Ph.D in the Hydrogeology Group and mainly, for all that they have taught me.

A very special thanks to David G., who advices and helps me before starting my Ph.D. Maybe I would have given up the thesis without his support.

I would like to thank Diogo Bolster and Juan Hidalgo for providing valuable suggestions, comments and for their approval of this thesis.

I must also acknowledge all of the colleagues of the Hydrogeology group. Both, those who finished and those who still have left part of the way ahead. I am especially grateful to Danielle P., Francesca, Anna J., Victor V., Violeta V., Gonzalo S., Dani M., Silvia D., and Enkhbayar D., without forgetting those that shared with me the office for a long time, Marco B., and Pablo G.

Thanks also to my friends “Los Pachucas” for their support and walk with me not only during my Ph.D but during my 32 years of life. I am also very grateful to Bernat and Juanjo. They have taught me not to give up.

An special mention deserve all my family, both, those who are and those who are in a better place, for give me everything without expecting anything in return, for their confidence and for all the things that I have learned of them along these 32 years. They have made me as I am. Thanks to my two nephews, Vega and Alex for make me glad during the last part of my Ph.D. Thanks also to my brother, if he would not study geology, neither would I, and I would not have done this thesis. Special thanks for my parents, because besides many other things, they have taught me that anything is easy but all is reachable by constancy and effort.

I would like to express my heart-felt gratitude to Anna. I could not imagine how I would have finished this thesis without her constant love, encourage and support during the bad and good moments. I only hope that once completed our Ph.D.’s, we continue overcoming together the challenges that await us along life.

Finally, I would like to acknowledge ADIF, SACYR, INTECSA-INARSA and OHL for their support throughout the hydrogeological monitoring of the civil works. I also appreciate the final support from the Spanish Ministry of Science and Innovation (HEROS project: CGL2007-66748 and MEPONE project: BIA2010-20244); the Generalitat de Catalunya (Grup Consolidat de Recerca: Grup d'Hidrologia Subterrània, 2009-SGR-1057) and the AGAUR (Generalitat de Catalunya) through "the grant for universities and research centres for the recruitment of new research personnel (FI-DGR 2010, FI-DGR 2011 and FI-DGR 2012)".

*To my grandfather*

*Whatever your life's work is, do it well. Even if it does not fall in the category of one of the so-called big professions, do it well. As one college president said, "A man should do his job so well that the living, the dead, and the unborn could do it no better". If it falls your lot to be a street sweeper, sweep streets like Michelangelo painted pictures, like Shakespeare wrote poetry, like Beethoven composed music; sweep streets so well that all the host of Heaven and earth will have to pause and say, "Here lived a great street sweeper, who swept his job well". As Douglas Mallock says:*

*"If you can't be a pine on the top of the hill*
*Be a scrub in the valley, but be*
*The best little scrub by the side of the hill,*
*Be a bush if you can't be a tree.*

*If you can't be a highway just be a trail*
*If you can't be the sun be a star;*
*It isn't by size that you win or fail,*
*Be the best of whatever you are".*

***(The papers of Martin Luther King Jr.,Vol. III: Birth of a New Age)***

# V. Index

# VI. List of figures

# VII. List of tables

# 1. Introduction

## 1.1. Motivation and objectives

The development of urban environments often requires the construction of underground structures. These become deeper with time to avoid existing structures, which is possible thanks to the advances in construction technologies. Therefore, they are usually constructed below the water table, which increases construction difficulties. The interaction between the construction and the groundwater must be acknowledged to carry the works safely and to limit the impact over the natural behaviour of the aquifer. Interactions may occur and must be taken into account in both direction, the impact caused by the construction into the aquifer and the problems caused by groundwater during construction.

If the interaction between groundwater and underground structures is not properly considered, unforeseen events may occur. In fact, numerous accidents have occurred in recent years. The worst incident was the collapse of the Cologne's metro (Van Baars, 2011), where the historical archive building of Cologne collapsed and two people died. Apart from this, other disastrous accidents happened in Spain recently. During the High Speed Train (HST) tunnel construction by the "cut and cover method" in Bellvitge (Spain), a lot of sinkholes appeared. The sinkholes, which were caused by defects in the joints of the diaphragm walls, could affect the adjacent buildings and endanger the workers (Pujades *et al.,* 2012).

In recent years, apart from the incidents which occurred during the construction of tunnels, ecological disasters caused by underground constructions also have been reported. However, they did not have the same media impact as accidents. Some examples are the drain effects caused by a tunnel construction in the Northern Apenines (Italy) (Vincenzi *et al.,* 2008), the HST tunnel construction in Abdalajis (Spain) (Pulido *et al.,* 2008) or the HST tunnel construction in Pajares (Spain).

All these incidents, together with the collapse of a tunnel to extend the metro of Barcelona in 2005 (Van der Boom, 2011), contributed to the decisions taken during the HST tunnel construction in Barcelona. This tunnel belongs to the line Madrid-Barcelona-French frontier and crosses Barcelona linking the Sants and Sagrera stations. The particularity of this construction is that the tunnel passes adjacent to the Sagrada Familia Basilica, whose construction started at 1882 and is still on going, (Unesco World Heritage Site since 2005)

and below the "Casa Mila (La Pedrera)" (UNESCO World Heritage in 1984). Both monuments, which are visited by thousands of tourists, were designed by Antonio Gaudi. For this reason, the construction of the HST tunnel in Barcelona attracted the attention of politicians and public opinion, which feared for the safety of the Sagrada Famila given the recent disasters. Therefore, rigid safety measures were taken to avoid situations such as those described above and to prevent other types of accidents. Measures focused on avoiding events related to the presence of groundwater were proposed because the tunnel was constructed below the water level. In fact, events related with the presence of groundwater were the most feared and some measures, which overprotected the construction against groundwater, increased the costs. The tunnel construction was finished satisfactory and no serious accidents were noticed. However, a number of questions related with the interaction of groundwater and underground structures arose during the construction. Therefore, methods and solutions were developed to give an answer to these problems and to improve construction processes of underground structures below the water table.

When underground constructions intersect aquifers they may act as drains or barriers against natural groundwater flow (Vázquez-Suñè at al., 2005), causing environmental and economic impacts. A number of studies are focused in the drain effect caused by tunnels. It has been studied numerically, analytically and in real cases (Goodman *et al.,* 1965, Meiri, 1985, Li and Kagami, 1997, El Tani, 1999 and 2003, Kolymbas and Wagner, 2007, Vincenzi, 2009 and Butscher, 2012). However, the barrier effect has not been thoroughly studied. Generally, numerical models are used to quantify the head variations and to design solutions (if the barrier effect is considered) (Merrick and Jewell, 2003, Bonomi and Belleni, 2003, Ricci *et al.,* 2007 and Paris *et al.,* 2010). Nevertheless, building numerical models to compute the barrier effect may be complicated because considerable detail is necessary close to the obstruction. Analytical solutions are therefore useful. Unfortunately, few analytical equations are available (Marino and Kavvadas, 1997 and Deveughle and Zokimila, 2010) and their validity is limited. In part, these difficulties reflect that the barrier effect problem has not been adequately formalized.

Another concern arises when it is required to perform a deep excavation below the water table in an urban environment. Enclosures are generally deepened, which increase the cost of the construction, as far as a low hydraulic conductivity layer to reduce or eliminate the pumping since some authors associate large settlements to the drawdown caused by this (His and Small, 1992, Gue and Tan, 2004 and Roy and Robinson, 2009). However, other authors

argue that pumping is responsible for only a small part of the total soil movements. Other factors, such as wall deflection or problems arising during the construction of diaphragm walls or jet-grouting also contribute to settlements (Wong and Patron, 1993, Hwang *et al.,* 2006, Kung *et al.,* 2007 and Arai *et al.,* 2008). Moreover, settlements caused by pumping are fairly smooth in space, i.e. pumping will not cause large differential settlements. In addition, pumping settlements in preconsolidated soils, which is not unusual in a lot of cities due to the industrial evolution (Vázquez-Suñè *et al.,* 2005), are relatively small. Therefore, combining deep pumping wells with short enclosures (always respecting the minimum depth required structurally) could become an efficient method, because diaphragm walls give stability to the excavation walls and avoid lateral groundwater inflows, while pumping wells provide stable conditions at the excavation bottom. However, the efficiency of the different methodologies to develop excavation has not been compared taking into account the outside impacts, the safety and the costs. Moreover, enclosures are deepened sometimes using jet-grouting piles, whose impervious capacity is questionable at field scale.

Regardless of the method used to perform a deep excavation, the state of the enclosure plays an important part during the development of the works and in the success of the construction. On the one hand, defects in the enclosure located above the excavation bottom may cause the drag of soil towards the excavation, which may cause sinkholes outside. On the other hand, if the defects are located below the excavation bottom, the pore water pressure will be higher than expected and unstable conditions may arise. The presence of defects, which are relatively frequent (Bruce *et al.,* 1989), must be known before excavation, because defects can be repaired easily by injecting sealing substances or the dewatering system can be redesigned. But if they are noticed during excavation, reparation is difficult, because sealing substances are dragged towards the excavation due to the groundwater gradient, since the dewatering cannot be stopped. Although geophysical methods can be used to spot openings, their application is limited. Therefore, considering that groundwater evolution can be predicted, hydrogeological tools could be used to asses the state of enclosures before the excavation stage. In fact, Knight *et al.,* (1996) suggested a very limited solution and Vilarrasa *et al.,* (2012) proposed a method to establish the state of circular enclosures. However, the method has not been developed.

The characterisation of the soil is the most important step during underground constructions. Geological and hydrogeological characterisations are essential to predict and avoid undesired events. Another important fact is to know the historical processes suffered by

the soil. Specifically, large groundwater oscillations in the past contribute to increase the consolidation degree of the soil, and therefore, to improve the response of the soil in the event of future drops of head. Characterisation is also useful to design suitable dewatering systems, to predict all the impacts caused by the construction and to prevent undesired events. However, sometimes it is difficult to know some aspects of the soil, which causes differences between the observed and the expected. This happened during one of the excavations required by the HST tunnel in Barcelona, where despite following an exhaustive methodology, an unexpected behaviour of the soil was noticed.

Thus, the objectives of this thesis are:

1. To formalize the barrier effect definition, finding the variables that control the problem and deriving simple analytical solutions, which make it possible to estimate the barrier effect under different circumstances and design of corrective measures when underground constructions intersect aquifers.
2. To evaluate the effectiveness of deepening enclosures against a reduction of pumping for dewatering when this measure is only used to avoid outside effects (settlements) caused by pumping at deep excavations. In the same situations, one objective is to define the suitability of the jet-grouting technique when it is used to deepen and waterproof enclosures.
3. Propose hydraulics based methodologies to assess the state of underground enclosures prior to excavation. The methods must be applicable and should allow knowing the effective parameters of the enclosure and to locate defects.
4. To assess the role of geologic characterisation to achieve the goals of an underground construction. If the soil is well known, undesired events and problems can be prevented efficiently.

## 1.2. Thesis outline

This thesis consists of five main chapters (chapters 2 to 6) plus introduction (chapter 1), conclusions (chapter 7) and references list (chapter 8). The body of the thesis is based on publications that have already been published, accepted or submitted to international journals. The references to the publications are included in a footnote at the beginning of each chapter.

Chapter 2 gives a global view of the construction of the High Speed Train (HST) tunnel in Barcelona. This section reports the main characteristics of this construction, which leads to the questions answered at the thesis, and exposes the hydrogeological impacts caused around the Sagrada Familia. The tunnel was constructed with a Tunnel Boring Machine. It crosses Barcelona and passes below some emblematic monuments like The Sagrada Familia and La Pedrera. Both are UNESCO world heritages and a committee appointed by the UNESCO acted as external observers during the construction. This chapter exposes the procedure followed to estimate the affections caused by the tunnel around the Sagrada Familia and shows the measurements taken during the construction. Firstly, the geology of the site was described conscientiously to avoid unexpected events during the construction. The detailed geology allowed improving the previous predictions. Hydrogeological affections were predicted by using analytical and numerical tools. The main affection expected was a moderate barrier effect. In the same manner, an analytical method was used to estimate the soil movements caused by the changes in the groundwater behaviour induced by the construction. It was observed that the barrier effect would cause small heaves upgradient and small settlements downgradient. Predictions confirmed that the affections would be small and the tunnel was excavated. During and after the construction measures were taken to compare with the predictions and to avoid unexpected events. Groundwater behaved as was estimated and a moderate barrier effect was observed. In the same manner, soil movements, where short and long term movements could be observed, acted as was expected. The tunnel was finished successfully and the Sagrada Familia was not endangered. However, given the measurements the efficiency of a bored pile wall executed between the tunnel and the Sagrada Familia can be questioned. Similarly, an unexpected groundwater behaviour consequence of the construction of this wall was observed.

Chapter 3 studies the barrier effect caused by impervious structures constructed below the water table, which was one of the most feared affectations during the construction of the HST tunnel in Barcelona since underground structures act as barriers, causing heads to rise

upgradient and to fall downgradient. We define the barrier effect as the increase in head loss across the barrier with respect to the natural conditions prior to construction. We distinguish between regional (the minimum head loss observed at long distances) and local (the maximum head loss observed close to the structure) barrier effects. We use numerical and analytical methods to derive semi-empirical equations to quantify the two barrier effects for semi-permeable, partially penetrating (or fully penetrating but finite in length), and barriers with a by-pass in confined aquifers. The resulting equations depend on the barrier geometry and on the natural head gradient in the aquifer and they are easy to apply. We test their validity at two construction sites, obtaining excellent agreement between the computed and observed barrier effects.

Chapter 4 is concerned about methods to perform deep excavations in aquifers, which may be constructed by combining pumping with the cut and cover method. This chapter arises as an answer to the methods adopted for the construction of deep excavations required during the HST tunnel in Barcelona. The main requirement of the Administration was to reduce as much as possible the soil displacements. Thus, given that settlements are associated with pumping, the enclosures of the excavations were deepened more than was structurally necessary by diaphragm walls and jet-grouting piles without considering the efficiency of the dewatering system. We analysed the water-proofing efficiency of jet-grouting and the need for water isolation in preconsolidated sediments. We used data obtained from two shaft excavations during the construction of the high speed train tunnel in Barcelona located adjacent to the Sagrada Familia Basilica. Jet-grouting was characterised using pumping tests before and after the construction of the enclosure. A number of dewatering scenarios were considered at the two shafts by varying the depth of the enclosures. Settlements caused by dewatering were calculated analytically and numerically. The results show that jet-grouting reduces the permeability of the soil (90% reduction, from 5.5 to 0.6 m/day). However, this reduction only affected the pile area with the result that the necessary pumping rate was only reduced by 40% as in the case of the settlements outside the enclosure. However, settlements due to groundwater pumping are fairly smooth (i.e. the differential settlements are small) with low absolute values. Moreover they recover when pumping ceases. This rather elastic behaviour reflects the preconsolidated nature of the sediments in Barcelona and the fact that drawdowns concentrate at depth, causing little change in effective stress near the soil surface. Under these conditions, pumping does not pose a serious risk to settlements, and excavation costs can be lowered by constructing the enclosure at the minimum depth required

structurally. Also, an intense control of the pumping process may help reducing the conventional safety factors against heave.

Chapter 5 is focused on the defects that may be presents in diaphragm walls used to perform underground excavations below the water table. This question also arose during the HST tunnel construction, since small defects can entail negative consequences. Defects in diaphragm walls may cause flooding, which affects construction operations, and soil dragging, which may lead to subsidence and affect adjacent buildings outside the enclosure. Therefore, characterizing the state of the enclosure prior to excavation would be desirable. We propose doing so by analyze the response to groundwater pumping during dewatering. We use numerical modeling and analytical methods. The steady state heads along the enclosure and the variations in the flow behaviour during pumping depend on the state of the diaphragm walls. Monitoring of the heads is therefore proposed during drainage of the enclosure to characterize the diaphragm walls. An analytical solution in steady state and two transient state methodologies are presented. These methodologies are implemented to evaluate the state of the diaphragm walls used in the construction of a High Speed tunnel at Bellvitge near Barcelona, where large openings caused significant sediment drag, which provoked sinkholes outside the enclosure.

Finally, chapter 6 exposes the steps followed, the difficulties arisen and the solutions proposed to perform a deep excavation required by the High Speed Train tunnel in Barcelona. A common and effective method to perform this type of excavations consists in combine the cut and cover method with a drainage system. The success of the construction depends on the stability of the excavation bottom, which is reached by dropping the water pressure as much as necessary. Therefore, the drainage system must be chosen carefully and considering the hydrogeology of the site. If the excavation is performed in low hydraulic conductivity materials, wick drains or eductor wells can be used to drainage, even it is possible to excavate under undrained conditions. However, these techniques are risky, because the presence of not known thin conductivity layers below the bottom may leads to unstable conditions. Therefore, a detailed hydrogeological characterisation must be done to choose the best drainage system. The characterisation also allows constructing realistic numerical models to find the best dewatering system by simulating scenarios where the depth of the enclosure and the characteristics of the drainage are varied. However, although the design steps are precise, defects in the enclosure caused during its construction can entail the failure of the excavation. Therefore, the state of the enclosure must be known after the excavation stage since this can

be repaired or the dewatering system can be redesigned. Hydrogeological tools are suitable to this purpose.

In the shaft of the High Speed Train (HST) tunnel in Barcelona, the initial large scale geological characterisation suggested not using deep pumping wells. However, a detailed hydrogeological characterisation revealed the presence of thin transmissive layers inside the low hydraulic conductivity materials. Moreover, a Watertightness Assessment Test (WTAT), which consisted on pump inside the enclosure and observe outside, performed before the excavation stage shows a defect in the enclosure. As a result, the dewatering system was redesigned to assure stable conditions.

This chapter shows the importance of soil characterisation when deep excavations under the water table should be performed and the relevance of perform a WTAT before the excavation stage. As a result, a realistic working methodology arises, which allow to design stable deep excavations under the water table at urban areas.

Chapter 7 summarizes the main conclusions of the thesis.

In addition, there are four annexes that summarize the following information:

- Supplementary material of the chapters
- Scientific papers and proceedings related with this thesis
- Participation in congresses
- Projects developed and related with this thesis

# 2. Hydrogeological impact assessment by tunnelling in high sensitive sites

## 2.1. Introduction

The line of the High Speed Train (HST) "Madrid-Barcelona-France frontier" crosses Barcelona in the Southwest-Northeast direction. The stretch of Barcelona consists on a deep tunnel which was performed using a tunnel boring machine (TBM). The tunnel crosses the city without going under any building linking Sants and Sagrera stations. It goes under Provença, Diagonal and Mallorca streets and passes in front of the Sagrada Familia Basilica (Unesco World Heritage Site since 2005) and Casa Mila (Unesco World Heritage Site since 1984). The Basilica, whose construction commenced at 1882 and is on-going, was designed by Antonio Gaudi. This attracts thousands of tourists every year and is an icon of Barcelona. The proximity of the tunnel to the Sagrada Familia Basilica attracted the attention of politicians and citizens, because they feared for the safety of the Basilica during the construction.

This fear was increased by accidents and/or problems happened contemporary to the HST tunnel construction in Barcelona. In 2005, a tunnel to extend the line 5 of the metro of Barcelona collapsed during the construction stage affecting a lot of residents of the neighbourhood of El Carmel (Van der Boom, 2011). Fortunately, there were not dead. The tunnel collapsed because a geological fault, that was bad characterized. In the same manner, several problems appeared during the construction of other stretches of the HST line "Madrid-Barcelona-France frontier". For example, at Bellvitge neighbourhood that is located in the South of Barcelona. During the tunnel construction by the cut and cover method, several sink-holes appeared. These were caused by defects in the diaphragm walls and they could have affected neighbour buildings (Pujades *et al.,* 2012a). Other more media incidents, which happened when the HST tunnel was been performed, contributed to rise the concern about the construction. The most famous was the collapse of the Cologne's metro in 2009 (Van Baars, 2011).

As a result, the construction was projected carefully considering all the relevant aspects and predicting all the possible affectations caused by the tunnel. Additional safety measures were taken to avoid unexpected accidents and reduce the construction effects

**This chapter is based on the paper: Pujades, E, Vázquez-Suñé, E., Carrera, J., Culí, L., Jurado, A., 2013. Hydrogeological impact assessment by tunnelling in high sensitive sites. Submitted.**

around the Sagrada Familia and a strict monitoring was proposed during the construction. However, despite the changes carried out in the project and the detailed studies performed, the representatives of Sagrada Familia, some citizens associations and some political sectors did not support the construction. This generates citizen mobilizations against the tunnel and an intense political debate.

The previous project foresaw to construct the tunnel by the cut and cover method. However, this option was dismissed because the diaphragm walls would have created considerable affectations in the groundwater since the diaphragm walls interfered a big portion of aquifer. The head would have modified more than 3 m, which would have affected the capacity of the soil to support loads and would have caused soil movements (heave at the upgradient side of the tunnel and subsidence downgradient). Therefore, the tunnel was constructed by using a Tunel Boring Machine (TBM) to interfere less the aquifer. Protection measures were taken at the adjacent areas to Sagrada Familia. A wall of non-secant piles was constructed to reduce the tunnelling settlements under the Sagrada Familia and one shaft to repair the TBM was constructed before the Basilica to excavate the tunnel with the TBM in optimal conditions.

There are several aspects which must be considered when an underground construction is projected. Underground constructions in urban environments entail difficulties which increase when constructions are performed below the water table. These constructions may affect negatively the environment and both neighbour buildings and structures (Bonomi and Bellini, 2003, Chiocchini and Castaldi, 2011, Pujades *et al.,* 2012) if they are not designed and executed conscientiously.

Tunnels under water table may affect negatively the groundwater behaviour. Similarly, groundwater might difficult the construction increasing the costs. Moreover, if groundwater is not enough taking into account unexpected events can happen during the excavation. The most important effects that might be caused by a tunnel in the groundwater are the barrier effect and the drain effect (Vazquez-Suñe *et al.,* 2005). Barrier effect is caused by underground impervious structures located below the water table. These structures reduce the effective transmissivity of the aquifer, leading to a rise in the water table upgradient and a lowering downgradient (Ricci *et al.,* 2007, Deveughèle and Zokimila, 2010). On one hand, the rise of head upgradient may flood basements or parkings (Paris *et al.,* 2010), salinize the soil, affect the flora (Tambara *et al.,* 2003) and propagate contaminants contained in the unsaturated zone. Other geotechnical aspects caused upgradient are reduction of the bearing

capacity of the soil, expansion of heavily compacted fills, settlements of poorly compacted fills upon wetting and increase in loads on retraining systems or basements walls of buildings (Marino and Kavvadas, 1997). On the other hand, the barrier effect downgradient cause a drop of head which can promote seawater intrusion in coastal aquifers, ground subsidence, death of phreatophytes and the drying of wells and springs (Custodio and Carrera, 1989). Finally, the difference of water pressures between both sides leads to asymmetric loading for which buildings foundations have seldom been designed. Barrier effect can be assessed previously of the construction since it can be computed numerically and analytically (Pujades et al., 2012b). If the results show that the barrier effect is not acceptable, it can be minimised by using by-pass facilities (Kusumoto et al., 2003).

Drain effect is caused by non impervious tunnels, which are designed to drain water and to not support water loads. These tunnels cause a head drop that may have environmental and geotechnical consequences (Butscher, 2012). The drain effect has similar consequences than the head drop created at the downgradient side by the barrier effect. It may cause seawater intrusion in coastal aquifers, ground subsidence, the drying of wells and springs and the reduction of the base flow in rivers located in basins crossed by the tunnel (Li and Kagami, 1997, Vicenzi *et al.,* 2009). In addition, the drop of head and the flow towards the tunnel may rise the seepage from sewers waters introducing contaminants in the aquifer (Chae *et al.,* 2008). Drain effect consequences can be known accurately applying analytical solutions (Goodman, 1965, Meiri, 1985, El Tani, 1999 and 2003 and Kolymbas and Wagner, 2007).

The construction of tunnels by Tunnel Boring Machine (TBM) often requires the excavation of deep shafts (Ni and Cheng, 2011), which are used as maintenance, emergency and/or ventilation shafts. The dewatering needed to excavate in dry and safe conditions these shafts cause a drop in the head and modify the groundwater behaviour and the water pressure distribution around the shaft. The consequences motivated by the head drop are similar to the effects created by the drain effect. However, the drop is punctual. Apart from this, accidents occurred during the excavation of these shafts as siphoning or base heaves events may cause large soil movements endangering the nearby buildings.

Finally, tunnelling with TBM may cause soil settlements which can be divided in two, short and long term movements. Short term movements are caused mainly by the ground loss during the excavation. This fact redistributes the stress in the soil and results in a stress relief (Ercelebi et al., 2011). Total ground loss is the addition between the ground loss at the face of

the excavation, the ground loss around the shield and the ground loss behind the lining ring (Gatti and Casani, 2007). These settlements, which usually have a Gaussian shape where the maximum is located above the tunnel, are minimised by injecting compensation grouting. However, the movements are not eliminated completely. Long term movements are related with the groundwater redistribution pressure after the tunnelling and they are observed after the excavation process. Apart from these, accidents occurred during the drilling of the tunnel may cause large soil movements or sinkholes if a big quantity of materials are dragged towards the tunnel.

From all of the potential affectations summarized, settlements are the most significant impact. Therefore, efforts during the design and construction of the HST tunnel were aimed to avoid them. All the mentioned aspects were considered during the HST tunnel construction to avoid surprises during the works. Therefore a careful methodology was followed to minimise the risk. Firstly, the soil was characterized accurately to minimise unexpected events consequence of sudden changes of the drilled materials. Secondly, the construction was designed and its possible affectations were predicted by using analytical and numerical methodologies and finally, an exhaustive monitoring, which is exposed in this paper, was performed while the construction.

Thus, the objective of this paper is to demonstrate the utility of apply new and advanced methods for hydrogeological impact quantification during tunnelling construction processes. Furthermore, this shows how the exhaustive hydrogeological characterisation and the intense monitoring during the design and construction phases allow improving the decision making. The paper describes the behaviour, of the groundwater and the soil, observed during the different stages of the construction of the HST tunnel. The monitoring measures taken are commented and the main affectations are discussed.

## 2.2. Construction process

### 2.2.1. General aspects

Sagrada Familia is located in the centre of Barcelona. Its area is approximately 12000 $m^2$ (one block of buildings) and its actual height is around 150 m (Figure 2.1). The HST tunnel passes at 10 m from the Sagrada Familia. It is 30 m depth approximately and its radius is 5.8 m (Figure 2.1). The TBM crossed this area in October 2010. Note that there are two

more subway lines which cross the area (Line 5 and Line 2). These are shallower than the HST tunnel.

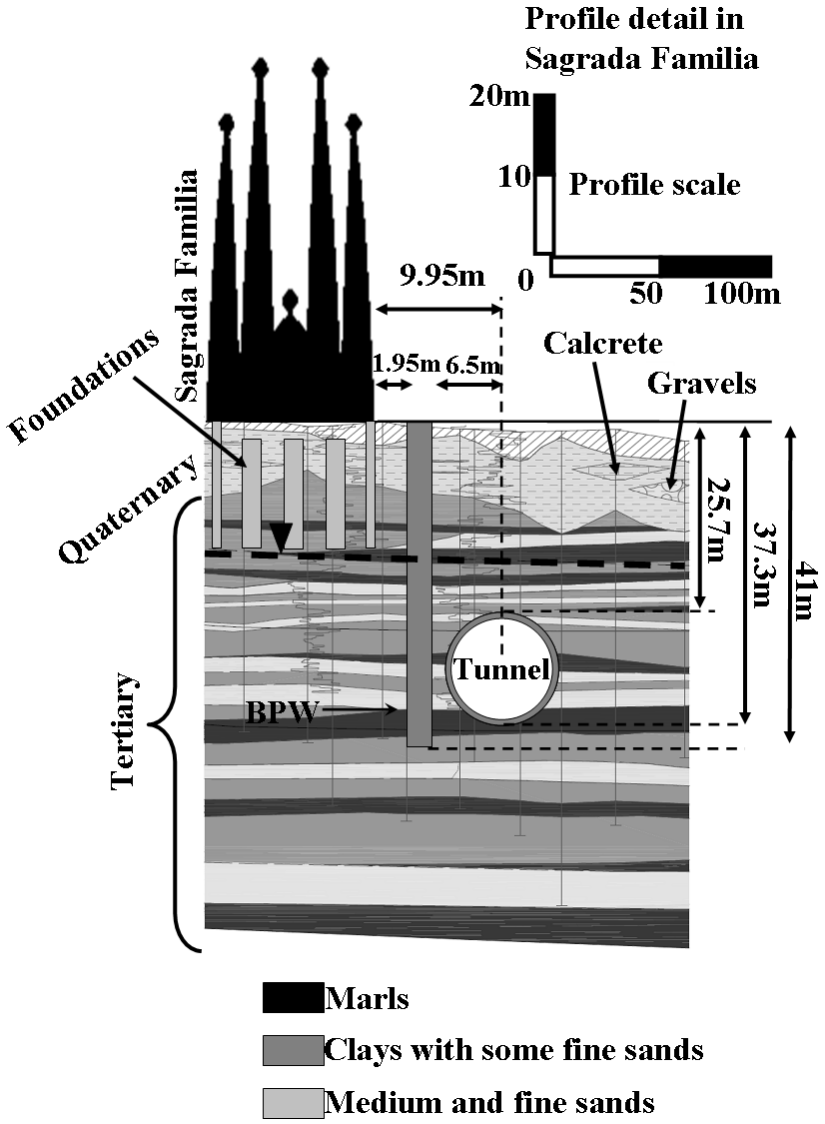


**Figure 2.1.** Detailed geology of the Sagrada Familia area. The tunnel and the BPW can be observed together with the Basilica and an scheme of its foundations.

A bored pile wall (BPW) was constructed to protect the Sagrada Familia in front of the movements caused by the TBM (Figure 2.1). This wall, which was formed by non secant piles, was 180 m length and 1.5 m width. The diameter of the piles was 1.5 m and they were constructed at each 2 m. As a result, there was a gap of 0.5 m between each two piles. The depth of the wall was 41 m and the piles were built using reinforced concrete. The piles were constructed before the TBM pass, between August 2009 and April 2010.

One maintenance shaft was excavated before the Sagrada Familia to repair and prepare the TBM to drill the most sensitive stretch of the tunnel. It was located in the crossroads between Mallorca and Padilla streets and it was named Padilla shaft. This was located at two blocks of buildings from Sagrada Familia (350 m) (Figure 2.2). The excavation of the shaft was performed using the "cut and cover" method combined with deep pumping wells. The enclosure consisted in diaphragm walls from the surface to 46.5 m depth and in jet-grouting secant piles from 42.5 m to 61.5 m depth. The maximum excavation depth was 41 m and the drawdown inside the pumping wells needed to assure stable (in front of bottom uplift) and dry conditions during the excavation stage was 45 m (58 m depth from the surface). Four pumping wells were used and the average flow rate pumped was 12 l/s. Jet-grouting enclosure, which was located in the bottom, has a relatively high hydraulic conductivity (Pujades et al., 2013a). As a result, during the dewatering stage, which took place in June 2010, drawdown was observed outside the enclosure.

### 2.2.2. Groundwater and soil characterisation

#### *2.2.2.1. Geology*

In general terms, the geology of Barcelona consists in Quaternary materials at the top and Pliocene materials at the bottom, which belongs to the Tertiary period. The Quaternary and the Tertiary materials make up the Barcelona's plain formation. The tunnel crosses mainly the Pliocene materials at the Sagrada Familia site. The shaft of Padilla crosses both, Quaternary and Pliocene (Figure 2.1 and 2.2).

Pliocene materials are grey clays, lutites and silts from sea deposits, and sequences of sand and/or fine gravels with silt-clay matrix. Pliocene deposits are an alternation of these lithologies. Fine sediments are predominant at the bottom. The number and thickness of layers with coarse sediments rise at shallower depths. Quaternary materials lie above the Pliocene. They can be divided in two: Pleistocene and Holocene. Pleistocene deposits are formed by gravels with clay matrix at the bottom of the sequence. These are alluvial fan deposits that are transformed in sands with clay matrix in the sea direction. Above, there are brown-yellow silts that are eolian deposits. They may contain calcareous nodules. At the top of this sequence there is a calcrete stratum. This serie may be repeated three times. Finally,

there are the Holocene deposits. These are the more recent and they are composed by several materials. The main deposits are:

- Torrential, alluvial and foothills deposits that are conformed by fine detrital sediments (red clays or silts).
- Gravel and sands from alluvial river deposits.
- Sands from coastal plain.

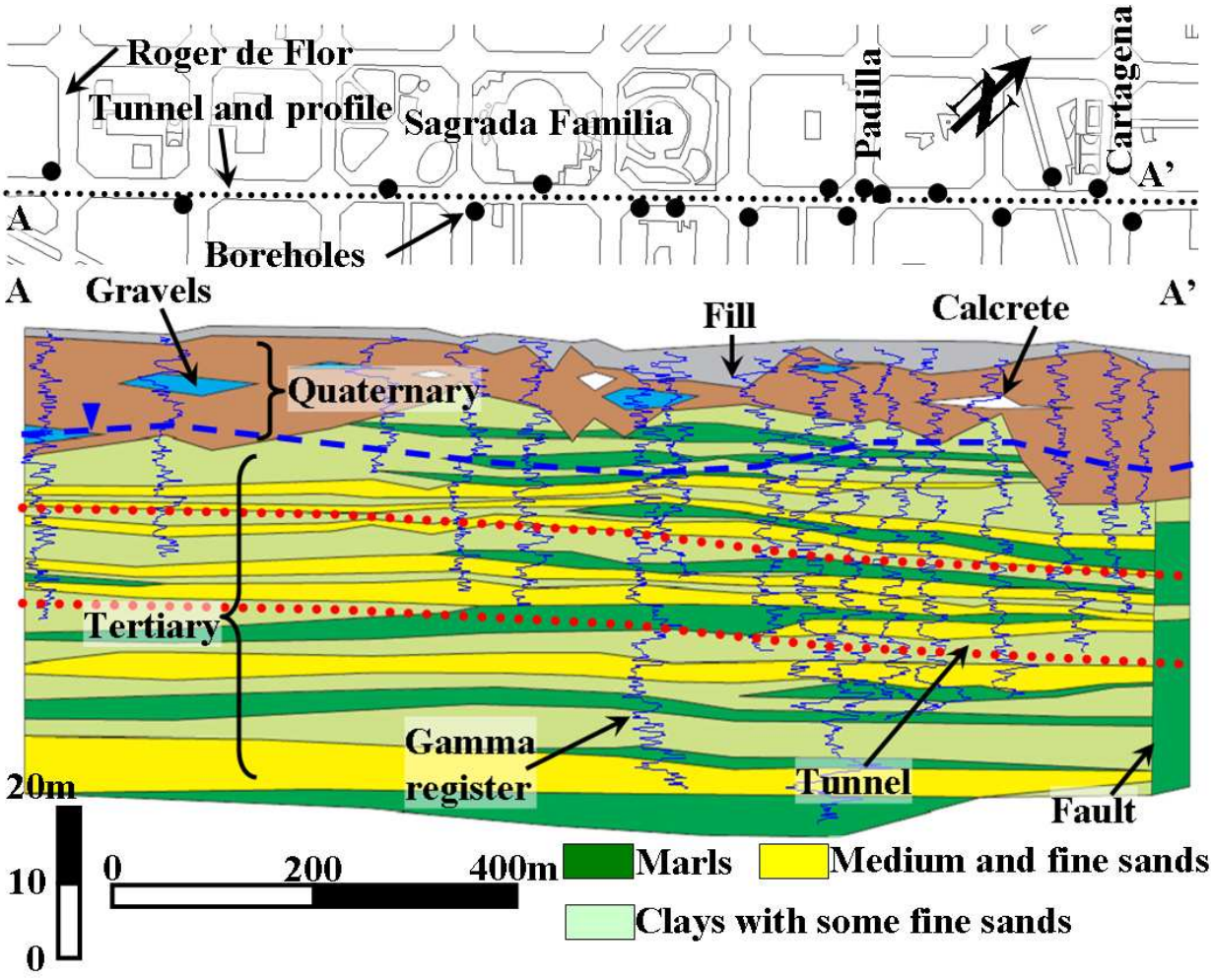


**Figure 2.2.** Plan view (up) of the surroundings of Sagrada Familia. Black points were the boreholes used to perform a detailed geological profile of the area (down). An important tool to execute the profile was the Natural Gamma Ray register from the boreholes. A fault was identified close to Cartagena street. The high vertical heterogeneity described was useful to predict the affectations.

A high detailed geology assessment was performed along the tunnel in order to know the lithology, the lateral and vertical continuity of the materials, and, in general, the geometry of the geological structures (Figure 2.2). This has been done by an accurate description of the materials observed at several boreholes preformed just before the construction. Moreover, the descriptions and photos from previous boreholes were examined. Apart from the borehole descriptions, a geophysical technique was used to improve the geology. This consists on a Gamma Natural Ray register, which allows corroborating the position of the layers and observing their lateral continuity and identify changes (Cripps and McCann, 2000). These works were very useful to perform a detailed profile, which considered accurately the position and geometry of the different materials. Figure 2.2 displays the detailed geological profile between Cartagena street, where a fault was identified, and Roger de Flor street. This profile was useful during the construction because all the lithology changes were identified. The antropic fill is 1-2 m thickness in all of the area, but it increases its thickness until 5 meters in the proximity of Sagrada Familia. Probably, this increase is consequence to the filling associated with the construction of Sagrada Familia and the two subway lines (L-2 and L-5). Quaternary materials are located below the fill. They have variable thickness along the profile varying from 20 to 1-2 m. Quaternary is formed by clays with some gravels, silts and sandy silts. All of them contain variable proportions of carbonate nodules. Discontinuous gravel deposits, which may belong to paleochanels, are observed. It is possible to observe no continuous calcrete deposits. At other locations of Barcelona the continuity of the calcrete allows delimitate the cycles of the tricycle formation because calcrete deposits are located above each cycle. Finally, there are the Pliocene materials. They are formed by the alternation of medium-fine sands, sandy marls and clayey marls. The different grain size depends on the position of the sea when they were sedimented. Fine materials are related with transgression events and coarse sediments with regression events. Pliocene is affected by faults which were identified in the profile. One of them is located in the Cartagena street. The identification of this fault before the tunnel construction was important because the drilled materials change significantly at both sides. Knowing the position of the faults is important because sometimes the TBM must be adapted to the new soil characteristics.

*2.2.2.2. Hydrogeology*

Hydrogeologically, Barcelona's plain can be considered as an aquifer with high vertical heterogeneity. Its effective transmissivity ($T_{eff}$) is 100-200 $m^2$/d. On one hand, the hydraulic conductivity ($K$) of the Quaternary clay layers ranges from 0.001 to 0.01 m/d and the $K$ of Quaternary sands and gravels layers ranges from 0.1 to 10 m/d. On the other hand, the $K$ of the Pliocene fine materials ranges from 0.001 to 0.01 m/d. The $K$ of the sand layers ranges from 0.1 to 10 m/d. These values were derived from the numerous hydraulic tests performed during the HST tunnel project and other projects.

Two pumping tests were performed near from Sagrada Familia (at the shaft of Padilla) to characterise hydraulically the soil. The first (August 2009) took 4 days (two of pumping and two of recovery) and the groundwater was pumped from one pumping well screened from the water table (located at 13 m depth) to 40m depth. The maximum drawdown reached in the well was 6 m while 5 l/s was the average flow-rate during the pumping. Two pumping wells were used in the second (January 2010) that was performed with some of the diaphragm walls constructed. In this case, it took 5 days (2 of pumping and 3 of recovery). The maximum drawdown reached in the well was 11m and the average flow rate was 10 l/s. The tests were interpreted by using the code TRANSIN-IV (Medina and Carrera, 1996), which allow to perform an automatic calibration (Carrera and Neuman, 1986a, Carrera and Neuman, 1986b, Carrera and Neuman, 1986c) and the hydraulic parameters of the layers were obtained (Pujades et al., 2013a).

Three more pumping were performed at the Padilla site, one to characterize hydraulically the jet-grouting enclosure (May 2012), other to dewater the excavation (June 2010) and the last to facilitate the entrance of the TBM in the shaft of Padilla (August 2010). In the former, the drawdown in the pumping well, which was located inside the excavation, achieved 18 m and the average flow-rate was 5 l/s. During the dewatering performed in June 2010, the maximum drawdown inside the excavation was 50 m. Finally, the last pumping, which was performed using six pumping wells located outside the enclosure, the maximum drawdown was 50 m. The huge drawdown produced was essential to drop the head outside the shaft of Padilla to facilitate the entrance of the TBM inside the enclosure.

Boreholes used in the geological description were used as piezometers to know the position of the water table. Most of them were screened completely but some were screened only at the deeper layers. Measures shown that the head was located at 17m depth,

approximately, at the surroundings of Sagrada Familia. Nevertheless, the piezometric level varied in depth. This was higher at a deep (55-60 m depth) sand layer (Pliocene). This layer has a piezometric head 5 m higher than the rest of the layers of the aquifer. This fact was also observed during the excavation of the shaft of Padilla. This information was important because the TBM had an extra-pressure of water at the layers located below the tunnel.

*2.2.2.3. Soil consolidation*

The consolidation degree of the soil is an important fact to predict soil movements caused by groundwater oscillations. In Barcelona, groundwater fluctuations produced by the proliferation of water consumer factories in the sixties (Vazquez-Suñe, *et al.,* 2005) caused the pre-consolidation of the soil. Therefore, the soil behaves elastically in front of groundwater oscillations when these are smaller than the drawdown caused during the water consumer factories period (Pujades, *et al.,* 2013b). As a result, if head variations caused by the construction are less than the head variations suffered historically, soil movements and water impacts will be small. While if the fluctuations are bigger, they may cause large movements. Historical head data at several piezometers was used to know the groundwater oscillations in the past. Some head measures are available around the Sagrada Familia since 1940 (Figure 2.3). In addition, head evolution was completed using the calibrated numerical model of Barcelona and considering data from historical recharge, pumpings and underground constructions (Vazquez-Suñe *et al.,* 2005). Head evolution was obtained from the upgradient and downgradient sides of the tunnel. Numerical results fit with measured data at both zones. The gradient along the time between upgradient and downgradient is more or less stable.

Head suffered important variations in the past century. This was 15 m below in the sixties, which was consequence of the industrial activity (Vazquez-Suñe, *et al.,* 2005). It is also observed a maximum at the beginning of the nineties. Currently, head is located 4 or 5 m below this maximum. The maximum level achieved by the head may be conditioned by the depth of the subway lines that cross the area (L5 and L2). Therefore, these tunnels may act as drains moderating the rise of the water table. The characteristics of the construction suggested that groundwater oscillations caused by the tunnel would be less than the historical oscillations. Therefore, soil movements caused by groundwater variations would be small and they would not endanger the Sagrada Familia or the buildings located in the area.

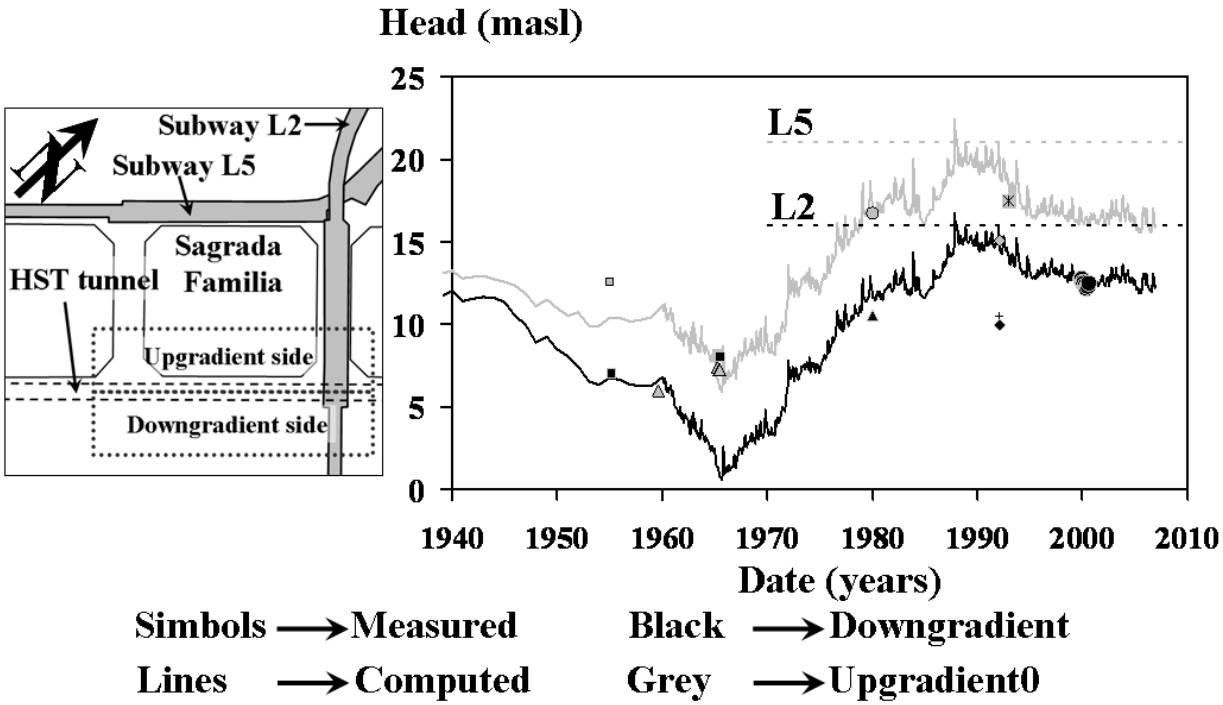


**Figure 2.3.** Historical head evolution at different piezometers located upgradient and downgradient of the tunnel. Numerical calculations (lines) match with the field measurements (symbols). The depth of the two metro lines (L2 and L5) seems to be related with the position of the head. The maximum drawdown was achieved at mid sixties. Black symbols belong to piezometers located downgradient while grey symbols represent the head of the piezometers located upgradient.

### 2.2.3. Analysis and impact assessment

#### *2.2.3.1. Hydrogeological predictions*

During the design stage of tunnels, the possible affectations caused by the construction must be computed. If the affectations are not acceptable, the design must be modified to reduce the impacts. Therefore, the possible affectations caused by the HST construction were predicted under different circumstances analytically and/or numerically. The drain effect was not considered given that the HST tunnel would be constructed with an impervious lining. Defects in the lining could have caused the entrance of water inside the tunnel, but this fact would have been punctual.

Head drop in Sagrada Familia caused by the pumpings in Padilla were not predicted basically because at the beginning only two pumpings were forecasted, one to know the hydraulic properties of the soil and the second to dewater the excavation. On one hand, the affectations of the former could not be known because the characteristics of the soil were not known yet. On the other hand, the affectations of the dewatering were not estimated because Sagrada Familia was too far and the pumping would be performed inside the enclosure.

The barrier effect was predicted numerically and analytically. Numerically by using the code TRANSIN-IV (Medina and Carrera, 1996), with visual interface of VISUAL TRANSIN (UPC, 2003). A multilayered numerical model, which represents the aquifers of Barcelona, was used. The validity of this model has been tested since it has been used to solve other hydrogeological problems in Barcelona. The construction was simulated as an impervious structure which crossed Barcelona and sectioned the half of the aquifer. Results, which were obtained in steady state, showed that the maximum barrier effect would be 1.25 m, and it was concentrated at some areas located close to the tunnel. It would decrease far from the tunnel. 1.25 m would be the maximum local barrier effect, while regionally the barrier effect would be close to 0.5 m. The distribution of the barrier effect is conditioned by the boundaries of the aquifer. In our case, the most of the barrier effect would be accumulated at the downgradient side. The drop caused by the local barrier effect downgradient would be 1 m while the rise upgradient would be less (0.25 m).

The barrier effect caused by the BPW and the tunnel at the surroundings of Sagrada Familia was obtained by using the equations proposed by Pujades et al., (2012b). On one hand, the barrier effect caused by the BPW constructed to protect Sagrada Familia was computed applying the Equation 1,

$$s_{BD} = \frac{s_B - i_N L_B}{i_N L_B} = \frac{K}{K_B} - 1 \qquad (1)$$

where $s_{BD}$ is the dimensionless barrier effect caused by a semi-permeable barrier, $i_N$ is the hydraulic gradient before the construction of the barrier, $L_B$, which is the characteristic length, is the width of the barrier and $K$ and $K_B$ are the hydraulic conductivities of the aquifer and the barrier respectively. On the other hand, the barrier effect caused by the tunnel construction was also computed using the equations proposed by Pujades *et al.,* (2012b) for partial barriers,

$$s_{BROD} = \frac{s_{BRO}}{i_N b} = \begin{cases} 0 & if \quad b_{bD} \le 0.1 \\ \frac{2}{3\pi} \ln\left( \frac{1}{5\pi b_{bD} \left(1 - b_{bD}\right)^6} \right) & if \quad b_{bD} > 0.1 \end{cases} \quad (2)$$

$$s_{BLOD} = \frac{s_{BLO}}{i_N b} = \begin{cases} 2b_{bD} & if \quad b_{bD} < 0.28 \\ \sqrt{\frac{3}{8}} \ln\left( \frac{2{b_{bD}}^{0.29}}{{b_{aD}}^2} \right) & if \quad b_{bD} \ge 0.28 \end{cases} \quad (3)$$

where $s_{BROD}$ is the regional dimensionless barrier effect, $s_{BRO}$ is the regional barrier effect, $b_{bD}$ is the dimensionless thickness cut by the barrier, $s_{BLOD}$ is the dimensionless local barrier effect, $s_{BLO}$ is the local barrier effect and $b_{aD}$ is the dimensionless thickness not cut by the barrier. Note that the characteristic distance to dimensionless the thickness is $b$. The dimensions were corrected using the anisotropy factor, which was obtained from the hydraulic characterisation of the site, since these must be corrected when the soil is heterogeneous in the flow direction. 0.01 was the natural groundwater gradient (before the construction) used to apply the equations.

The analytical barrier effect caused by the BPW was 5 cm, which is a relatively small barrier effect. This was not higher because the piles were not secant between them. Analytical barrier effects caused by the tunnel were 1.6 m for the local and 0.5 m for the regional effects. These values match with the numerical predictions. In the same manner, these values agree with the barrier effect observed at other areas of the construction (1.8 m) (Culí, 2011). The barrier effect observed at other areas also confirmed that this would be accumulated at the downgradient side (1.3 m of drop downgradient and 0.5 m of rise upgradient) (Culí, 2011).

*2.2.3.2. Soil behaviour predictions*

Groundwater modifications may affect the structure of the soil causing settlements or heaves depending on the groundwater behaviour. Maximum movements caused by groundwater fluctuations were calculated around Sagrada Familia by using the groundwater predictions. Soil movements were computed analytically by applying the equation proposed by Cashman and Preene (2001)

$$\rho_i = \gamma_W s_i D_i \alpha_i \quad (4)$$

where $\rho_i$ is the settlement of layer $i$, $\gamma_W$ is the specific weight of the water, $s_i$ is the drop of water pressure at each layer $i$, which is expressed in meters of water column, $D_i$ is the thickness of layer $i$ and $\alpha_i$ is the soil compressibility. The only parameter unknown is $\alpha_i$. However, this can be derived from the storage coefficient of each layer ($S_i$) taking into account the consolidation degree of the soil. As is mentioned, the soil of Barcelona is pre-consolidated (Pujades, *et. al.,* 2013b), and therefore, it behaves elastically. Thus, $S_i$ can be known given the equation proposed by Jacob (1950) and cited by Ferris (1962) for elastic aquifers

$$S_i = \gamma_W \theta_i D_i \left( \beta + \frac{\alpha_i}{\theta_i} \right) \quad (5)$$

where $\theta_i$ the soil porosity of layer $i$ and $\beta$ the water compressibility. It is possible to consider that $S_{Si} = \alpha_i$, assuming that $\beta$ is very small compared to $\alpha_i$ and $\gamma_W$=1 t/m$^3$, where $S_{Si}$ is the specific storage coefficient of layer $i$, which can be obtained from the interpretation of pumping tests. Therefore, settlements can be computed given $s$ and $S_S$. Note that the settlements were computed by assuming a value of $S_S$ of 0.00001, which belongs to the values observed at different pumping test performed during the construction. This methodology assumes only vertical movements, which is not true because horizontal movements also exist. However, this methodology allows approximating the displacements with an acceptable error (Pujades et al., 2013a).

Settlements induced by the barrier effect caused by the BPW and by the tunnel were computed. The value $S_B$ reflects the increase in head loss between both barrier sides (upgradient and downgradient) (Pujades et al., 2012b). Therefore, to evaluate the total soil movement caused by $S_B$, the increment observed upgradient (generally positive) is added to the increment observed downgradient (generally negative). Therefore, the value calculated represents the absolute value of the movements considering the heave upgradient and the settlement downgradient. Soil movements are calculated with the numerical and the analytical groundwater predictions by replacing in the Equation 4 the drawdown ($s$) by the predicted barrier effect ($S_B$).

The local displacement computed with the numerical groundwater predictions was 0.36 mm (0.29 mm of subsidence downgradient and 0.07 mm of heave upgradient). Regionally, the absolute value of movements caused by the barrier effect was 0.15 mm.

Similarly, soil movements were calculated using the analytical predictions for the barrier effect. On one hand, the absolute value of the soil movement caused by the BPW was 0.022 mm. Settlements were not big since the predicted groundwater fluctuations were small. On the other hand, soil movement caused by the barrier effect induced by the tunnel varied from 0.14 mm regionally to 0.46 mm locally. These values considered the addition between the movements at both sides of the barrier.

## 2.3. Monitoring and impact quantification

### 2.3.1. Groundwater monitoring points

Head behaviour was measured manually and automatically at several piezometers located around the Sagrada Familia (Figure 2.4a). The characteristics of these piezometers are exposed at Table 2.1. The great majority were screened completely with the exception of the piezometers PZ-5, PZ11 and PZ12, which were screened at deep layers. Figures 2.4b and 2.4c show the head variations during the construction upgradient and downgradient respectively.

| Name | Minimum screen depth (m) | Maximum screen depth (m) | Name | Minimum screen depth (m) | Maximum screen depth (m) |
|---|---|---|---|---|---|
| **PZ-2** | 0 | 38 | **PZ12** | 30 | 35.5 |
| **PZ-3** | 0 | 29.5 | **PZ-13** | 0 | 42 |
| **PZ-4** | 0 | 38.5 | **PZ-14** | 0 | 29.5 |
| **PZ-5** | 38 | 40 | **PZ-15** | 0 | 29.5 |
| **PZ-6** | 0 | 45.8 | **PZ-16** | 0 | 49.5 |
| **PZ-7** | 0 | 47.5 | **PZ-18** | 0 | 40 |
| **PZ-9** | 0 | 29.5 | **PZ-19** | 0 | 37.5 |
| **PZ11** | 30 | 25 | | | |

**Table 2.1.** Characteristics of the piezometers located around Sagrada Familia.

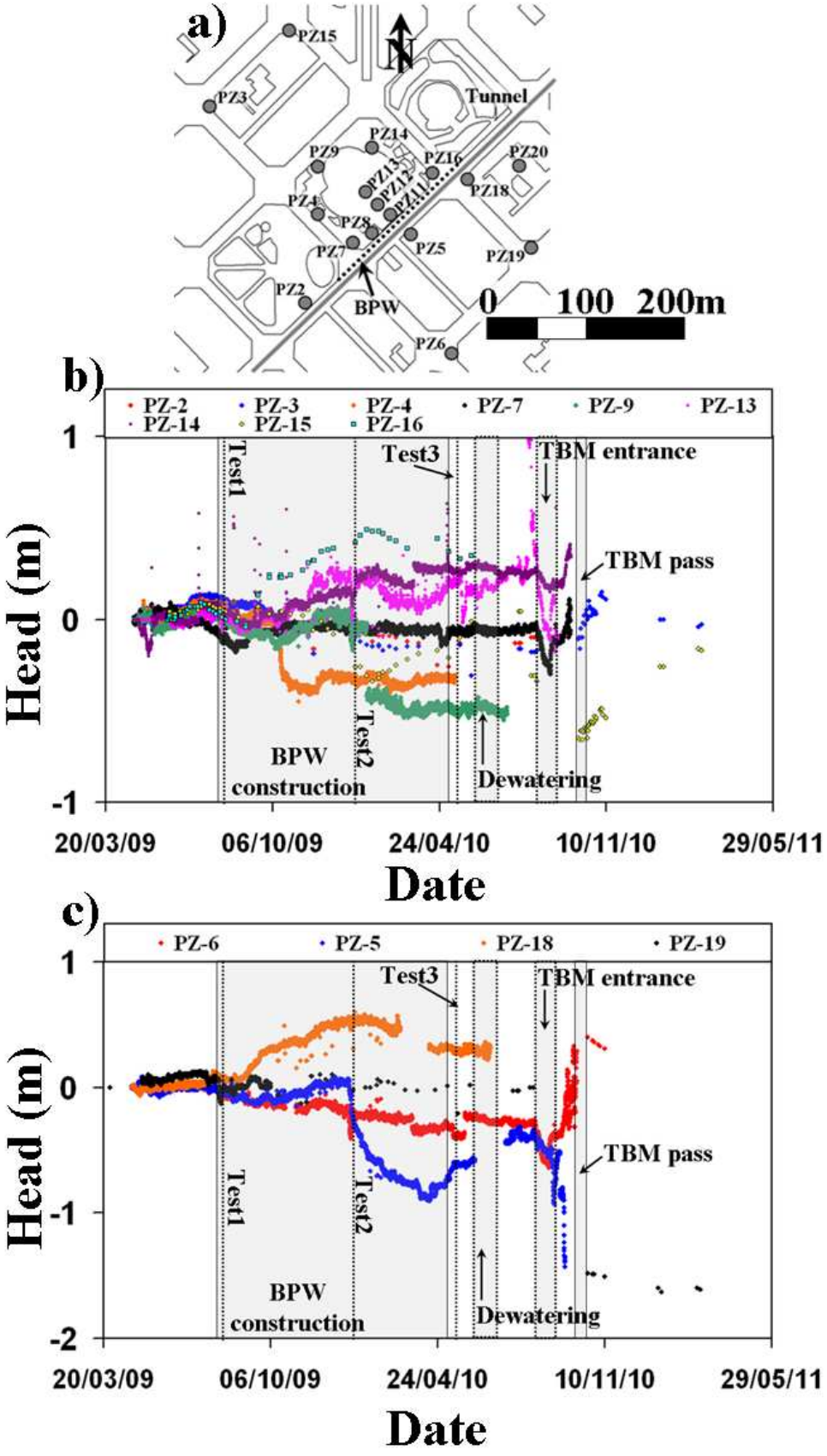


**Figure 2.4.** a) Distribution of the piezometers around Sagrada Familia. b) Head evolution of the piezometers located upgradient. c) Head evolution of the piezometers located downgradient.

### 2.3.2. Barrier effect caused by the BPW

The BPW did not create any barrier effect. At least, the barrier effect created was too small to be differentiated from the natural groundwater oscillations (±0.7 m according to the historical register). Only two piezometers located downgradient (PZ13 and PZ14) seemed to measure a possible barrier effect. Head rose 0.2 m at both. Probably, $S_B$ only was observed at these piezometers as a consequence of the heterogeneity of the soil. Maybe the materials where these piezometers were screened presents particularities which favoured the barrier effect. Possibly, they were located in a preferential way of the flow that may be partially interfered by one pile. But in general, the barrier effect caused by the wall was negligible.

### 2.3.3. Barrier effect caused by the tunnel

TBM drilling causes head oscillations, which magnitude depends on the conductivity of the soil. The oscillations are crated by pressure variations in the excavation chamber. If the oscillations are high, the water can spring up to the surface from the piezometers, which may create badly suspicious or fears. Therefore, piezometers located near the tunnel were sealed before the TBM pass to not increase the social alarm generated by the construction, since when the TBM started the perforation a great quantity of water well up from one piezometer causing the worry of the neighbours. Only some piezometers, which were located far from the tunnel, were preserved. As a result, during the tunnel construction around the Sagrada Familia only was possible to take measures in three piezometers (PZ3, PZ15 and PZ19). The piezometer located downgradient (PZ19) measured a drop of 1.6 m when the tunnel was constructed while the head in the piezometers located upgradient (PZ3 and PZ15) returned, more or less, to its initial position. The observations matched with the numerical predictions, which indicated that the barrier effect would be concentrated at the downgradient side of the tunnel. The magnitude of the barrier effect also correlated with the numerical and analytical predictions for the local barrier effect. In the same manner, the observations were similar to the barrier effect observed at other places of the construction (Culí, 2011).

### 2.3.4. Drain effect

No drain effect was observed at the piezometers once the tunnel was constructed. The head did not drop around the tunnel when this was constructed. This suggests that the lining of the tunnel had not significant defects.

### 2.3.5. Pumpings at the shaft of Padilla

Head evolutions at the piezometers of Sagrada Familia (Figures 2.4a and 2.4b) show that only the effects of three of the five pumpings performed at Padilla were observed. These were the two first pumping tests and the last dewatering performed to facilitate the entrance of the TBM into the shaft. These were the pumpings performed outside the enclosure or without the enclosure completed. The other pumpings were not observed since they were performed inside the enclosure, which due to the fear to the pumping settlements, was deepened more than was structurally necessary (Pujades et al., 2013a).

The first pumping test at the shaft of Padilla (200 m far away from Sagrada Familia) caused a maximum drawdown of 0.2 m, which was measured at PZ12, PZ11 and PZ19. At the other piezometers the drop observed was less. The maximum drawdown observed during the second pumping test was higher (0.3 m) and was observed in the piezometers PZ6, PZ13 and PZ11. During the last pumping, few piezometers were available since some of them were sealed. The maximum drop was observed at the piezometer PZ13 and it was 0.6 m. Summarizing, it was possible to observe in the Sagrada Familia site the effects of the pumpings performed at Padilla. However, the drawdown observed was too small to cause noticeable settlements.

### 2.3.6. Other hydraulic effects

An unexpected behaviour of the groundwater was observed at the piezometers PZ11 and PZ5 located upgradient and downgradient respectively. Initially, it was thought that the source was the second pumping test of Padilla. However, the drop was longer than the test (January 2010 until April 2010). These piezometers were located near from the BPW and four abrupt changes (Figure 2.5b) were observed at PZ11, which could be related with the

construction of four piles (PSF9, PSF7, PSF5 and PSF6) close to the piezometers (Figure 2.5a).

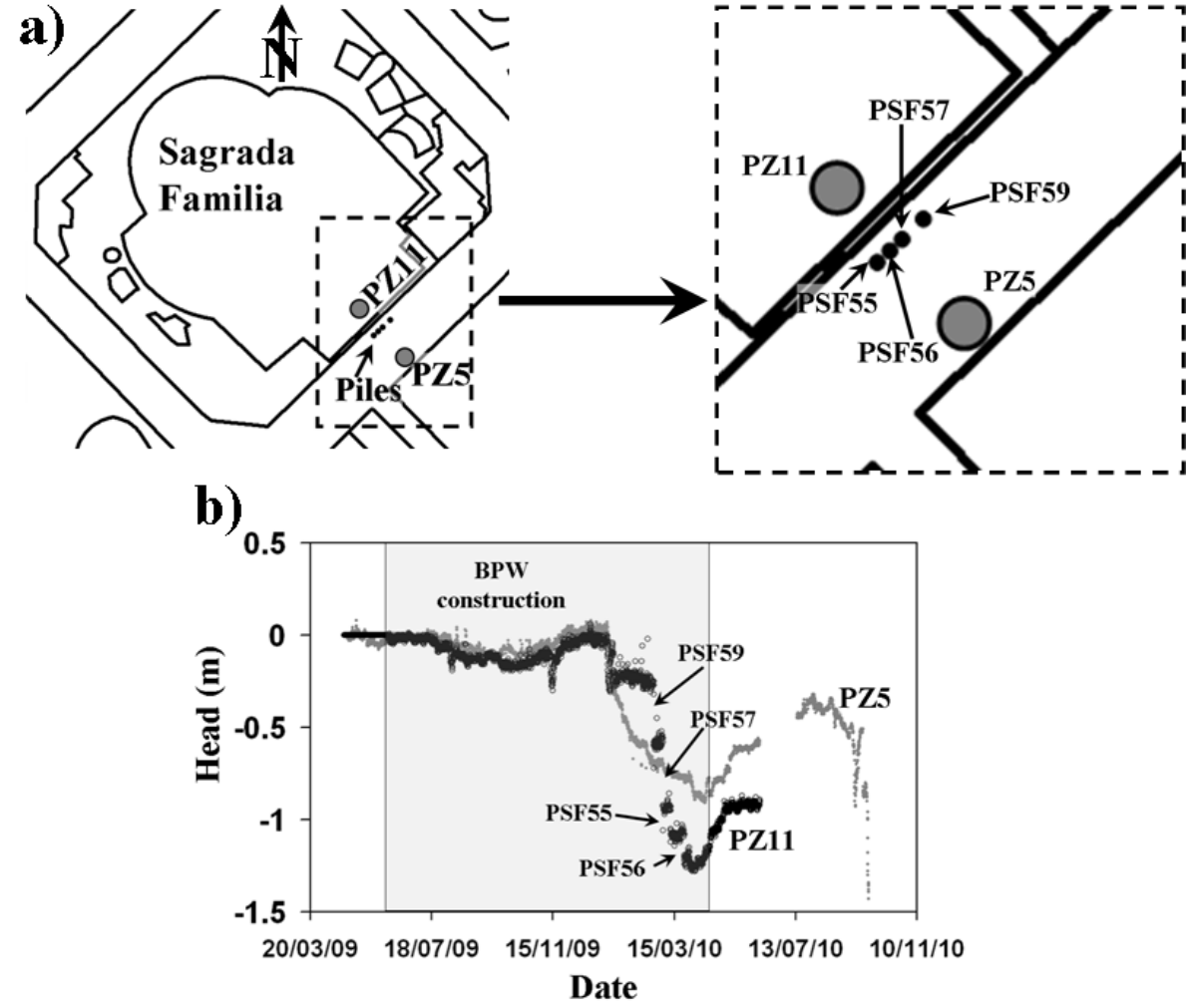


**Figure 2.5.** a) Location of the piles (PSF55, PSF56, PSF57 and PSF59) and the piezometers (PZ5 and PZ11). b) Head evolution of the piezometers PZ5 and PZ11. The drops correlated with the construction of the piles.

The relation between the piles and the drops is more visible at PZ11. The drop would have been caused by the hydraulic connection between different layers with different hydraulic head crossed by the piles. As is mentioned, the head at the deep layer was higher than the hydraulic head in shallow layers. PZ5 and PZ11 were only screened at deep layers; therefore, they measured the deep hydraulic head until the piles were constructed connecting different layers. At this moment, the hydraulic head at the deep layers dropped.

### 2.3.7. Soil movements

Soil movements were only measured during the pass of the TBM below Sagrada Familia. Probably, the construction of the BPW also generated soil movements, but during this time the monitoring points were not available. Soil movements started to be measured just before the pass of the TBM. Three parallel rows of monitoring points were located in front of the Sagrada Familia. One row was located on the upgradient side of the tunnel, other just above of the tunnel and the last at the downgradient side. Note that the BPW was located between the tunnel and the upgradient monitoring points (Figure 2.6). Soil movements are studied by comparing the movement upgradient, above and downgradient the tunnel at five sections (A, B, C, D and E in Figure 2.6).

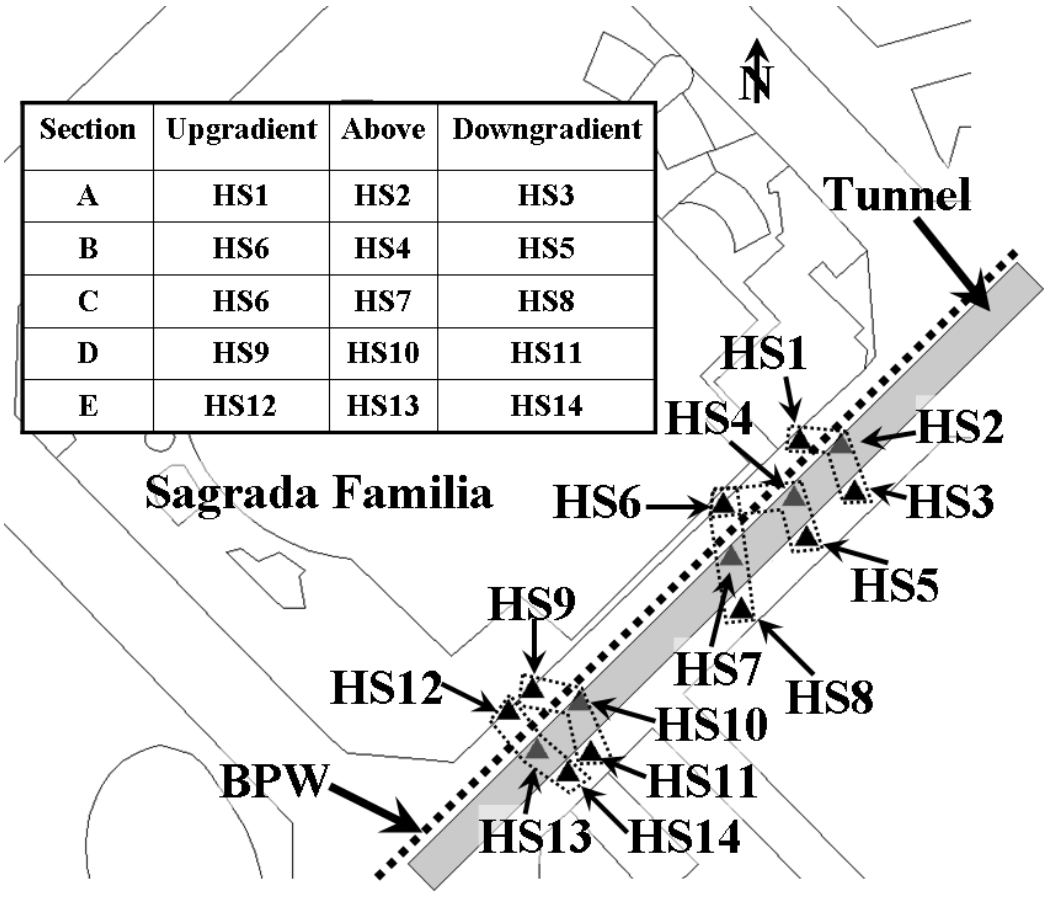


| Section | Upgradient | Above | Downgradient |
|---|---|---|---|
| A | HS1 | HS2 | HS3 |
| B | HS6 | HS4 | HS5 |
| C | HS6 | HS7 | HS8 |
| D | HS9 | HS10 | HS11 |
| E | HS12 | HS13 | HS14 |

**Figure 2.6.** Monitoring points used to observe the soil movements evolution during the construction. Five sections of monitoring points perpendiculars to the tunnel are used to evaluate the movements.

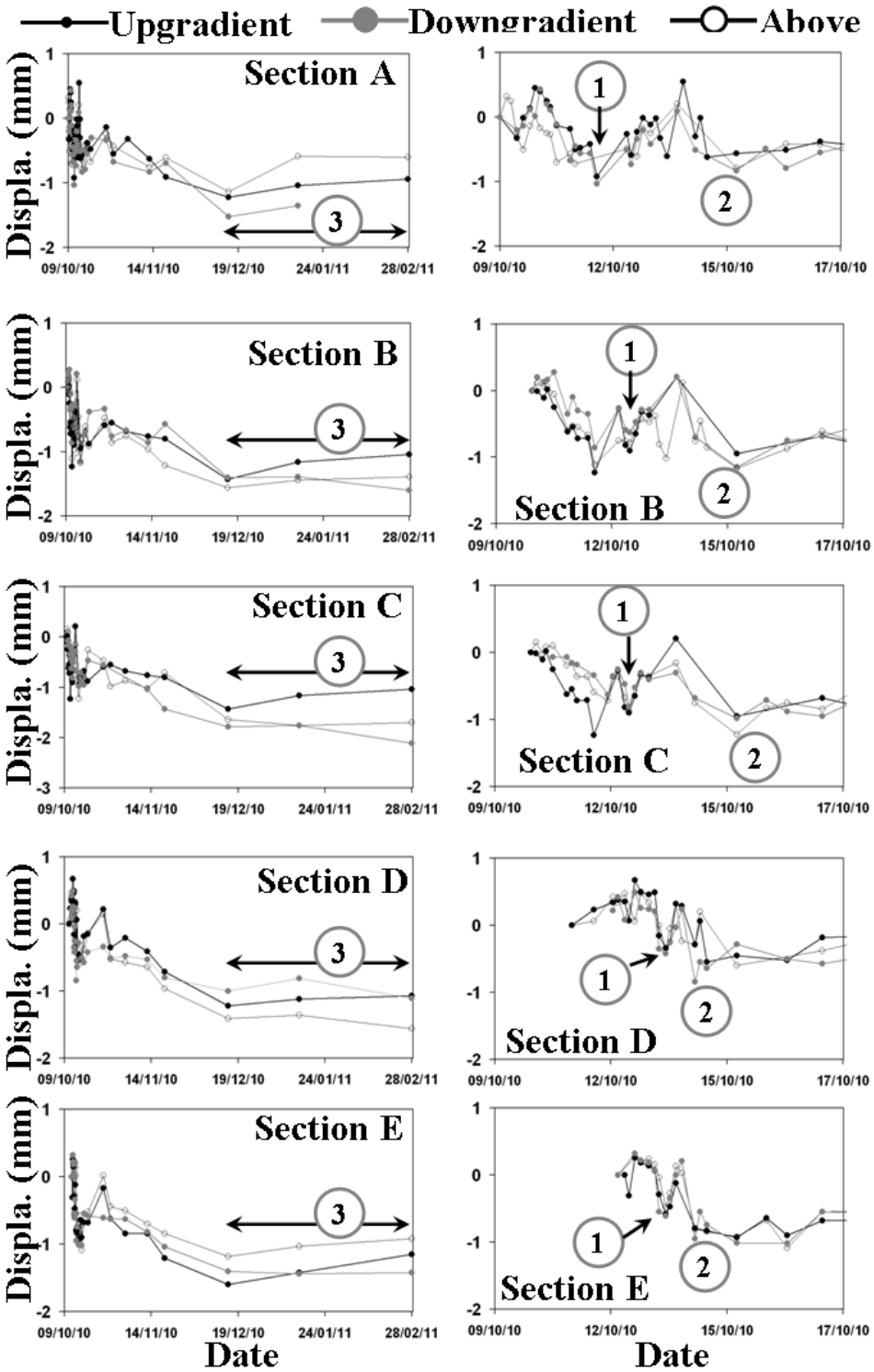


**Figure 2.7.** Soil movement evolutions in the different sections represented in the Figure 2.6. At the left, there are the displacements variations from the arriving of the TBM to Sagrada Familia to four months later while at the right there are zooms of the time where the tunnel was excavated below the Sagrada Familia. The right plots are useful to observe the short term movements. Points 1 and 2 are the times when the short time movements are observed to evaluate the affectations. In the left plots, data cover by the arrow with the number 3 is used to evaluate the long term movements.

Figure 2.7 displays on the left, the soil movement evolution from just before the arriving of the TBM to Sagrada Familia (9-10-2010) to the end of the monitoring (1-3-2011), and on the right, the soil movements only during the pass of the tunnel below the Sagrada Familia (from 9-10-2010 to 18-10-2010). Two main soil movements can be differentiate, the first is a short term movement related with the ground loss and the grout injection during the perforation process (this movement is shown at the right plots). It consists in a sharp drop (point 1 in the plots) followed by a rise and finally other long in time drop (point 2 in the plots), which could belong to a relaxation of the soil once the TBM passed. This evolution, which was observed in all of the monitoring points, had sharply oscillations which were caused by the pressure variations at the excavation chamber. This fact could be proved by comparing head and soil movement evolution during the tunnel perforation. This is performed using the data from one piezometer and three soil monitoring points located near from Sagrada Familia (Figure 2.8a and 2.8b). Head oscillations, which were caused by the water pressure variations in the excavation chamber, matched with the soil movements. The maximum settlements caused during the tunnel excavation, which are considered short term movements (points 1 and 2 in the plots) are summarized at Table 2.2. Although total soil movements were too small, they were similar at both wall sides. Therefore, the efficiency of the BPW may be questioned since this was designed to minimised or eliminate short term movements during the perforation at the upgradient side.

The second displacement differentiated was a long term soil movement. This movement is evaluated using the data during the period between December and the last measure (March 2011). This period is marked with the number 3 and an arrow in the left plots of Figure 2.7. This movement occurred once the TBM was moving away. Observations indicated that the movement depended on the position of the monitoring point in regard with the tunnel. Therefore, these movements could be caused by the groundwater fluctuations. Specifically, the soil behaviour could be related with the barrier effect created by the tunnel, because the monitoring points located upgradient registered a heave while they registered a drop or a smaller heave downgradient. $S_B$ started once the TBM was distant and it took time to affect the soil. Plots show that short term effects acted similarly in the three monitoring points of each section, but the behaviour is not the same and depends on the point after December. The difference between the increments upgradient and downgradient between both dates is the displacement which can be attributed to the barrier effect. Table 2.2 shows these increments which ranged between 0.3 and 0.7 mm, which agree with the predictions. The

behaviour of the soil located above the tunnel seems not to follow a clear tendency and this is difficult to relate with the barrier effect. Probably, the measures were altered by the excavation (ground loss and injections) since the monitoring points were too close to the drilled area. They are not used to evaluate the movements caused by the barrier effect.

| Section | Point | Settlement 1 (mm) | Settlement 2 (mm) | Movement $S_B$ (mm) | Difference $S_B$ (mm) |
|---|---|---|---|---|---|
| A | HS1 | -0.92 | -0.56 | 0.28 | - |
| | HS2 | -0.72 | -0.79 | 0.54 | |
| | HS3 | -1.03 | -0.83 | - | |
| B | HS6 | -1.23 | -0.95 | 0.39 | 0.59 |
| | HS4 | -1.11 | -1.17 | 0.17 | |
| | HS5 | -0.86 | -1.15 | -0.2 | |
| C | HS6 | -0.92 | -0.95 | 0.39 | 0.72 |
| | HS7 | -0.87 | -1.22 | -0.06 | |
| | HS8 | -0.81 | -0.98 | -0.33 | |
| D | HS9 | -0.34 | -0.45 | 0.15 | 0.26 |
| | HS10 | -0.34 | -0.6 | -0.15 | |
| | HS11 | -0.42 | -0.28 | -0.11 | |
| E | HS12 | -0.58 | -0.79 | 0.45 | 0.47 |
| | HS13 | -0.48 | -0.81 | 0.26 | |
| | HS14 | -0.61 | -0.95 | -0.02 | |

**Table 2.2.** Summary of the movements observed in the monitoring points of the defined section in Figure 2.6. Short term movements are Settlements 1 and 2, which belongs to the points 1 and 2 in the plots of the Figure 2.7. Long term movements are the movements caused by the barrier effect. The total movements of each section attributable to the barrier effect is shown at the right column.

Soil movements caused by the construction were also studied by considering their distribution at different stages of the construction (Figures 2.9a, 2.9b, 2.9c, 2.9d, 2.9e and 2.9f). This figure represents the total movements measured by the monitoring points since their installation. Figure 2.9a shows the soil position when the TBM was at the Marina street (just before to start the perforation below the Sagrada Familia). While Figure 2.9b shows the movement when the TBM had passed the Sardenya street (just after the perforation below the Sagrada Familia). Soil movement distribution also is displayed one, two, three and four months after the excavation of the tunnel below Sagrada Familia (Figures 2.9c to 2.9f). When the TBM was arriving to Sagrada Familia, it caused a heave (represented by triangles in the Figures) in front of the TBM. This heave was caused by the pressure applied over the soil

during the drilling. However, when the TBM passed and moved away, the ground settled (settlements are represented as circles in the Figures). Benefits of the BPW were not observed since movements during the TBM perforation were similar at both sides of the wall. The soil continued settling two months after the TBM pass. However, this recovered some during the third and the fourth months after the perforation. This recovering may be associated with the long term movement related with the groundwater behaviour. This can be observed in the Figure 2.10, where the variations from December to January (Figure 2.10a) and from December to March (Figure 2.10b) are represented. The barrier effect could have caused these movements. In general, soil heaves upgradient while it drops or heaves less downgradient.

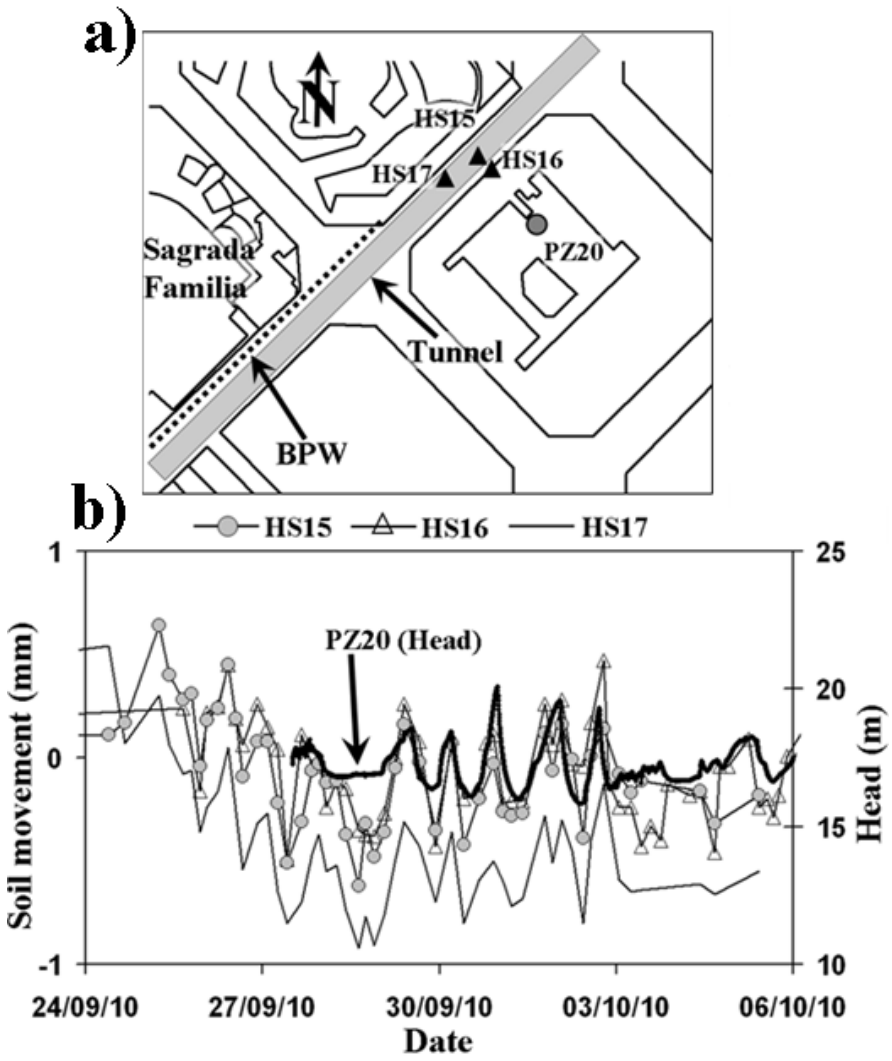


**Figure 2.8.** a) Monitoring points (HS15, HS16 and HS17) and piezometer (PZ20) used to observe the correlation between the head oscillations and the variations in the soil during the TBM pass.

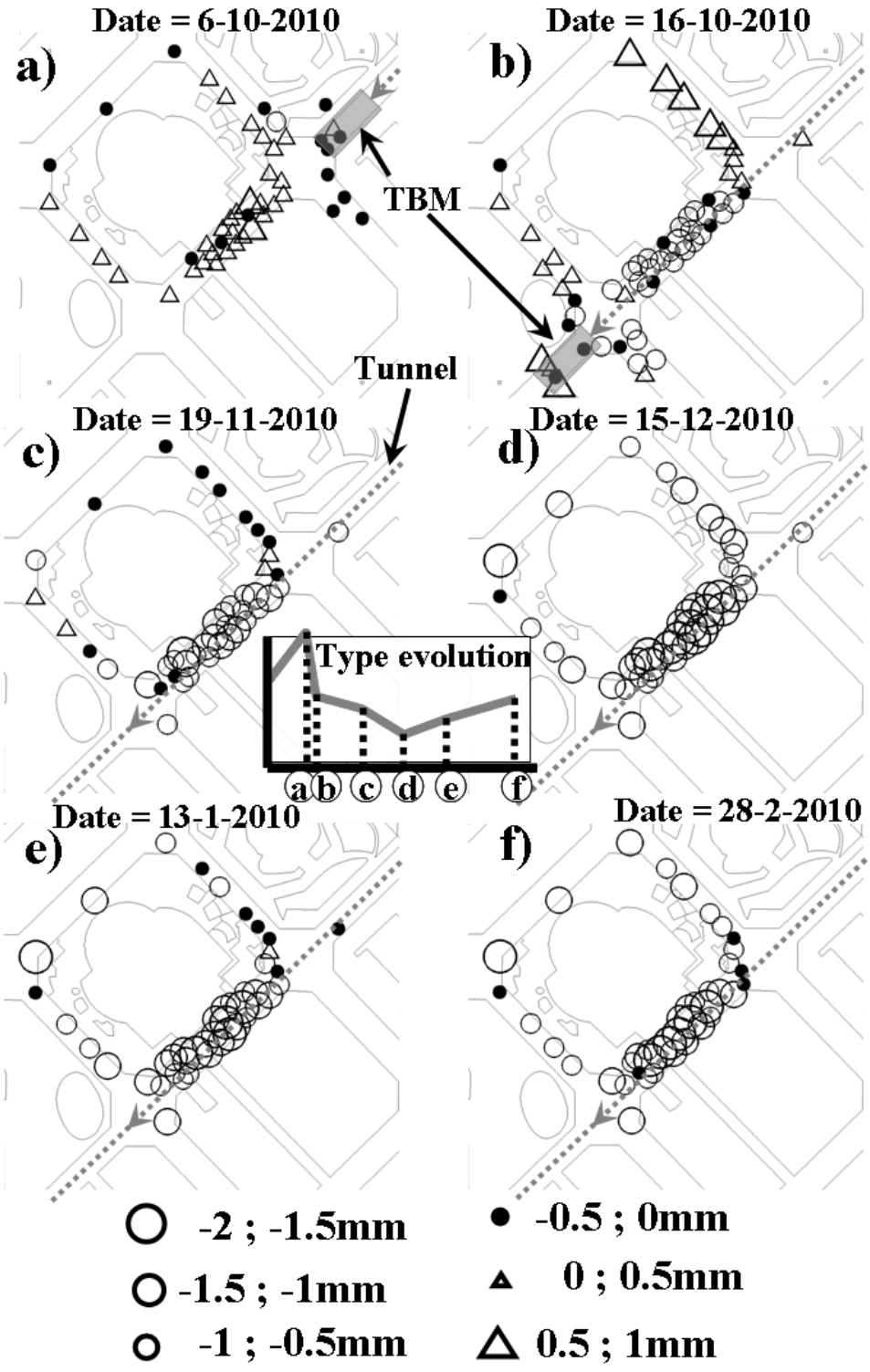


**Figure 2.9.** Soil movements distribution at several piezometers before and after the excavation of the tunnel. a) Movements just before the tunnel pass below Sagrada Familia. b) Movements just after the pass below Sagrada Familia. c), d), e) and f) represents the soil movements one, two, three and four months after the excavation of the tunnel below Sagrada Familia. In the middle, an schematic plot with the ideal behaviour is included to indicate at what moments of the evolution belongs each plan view.

Other soil movements, which were not measured, could have been the movements caused by the barrier effect generated by the BPW and the movements caused by pumping in Padilla. In the first case, it is shown that the barrier effect was very local and its magnitude was not big. Applying the Equation 4 to the maximum barrier effect observed, the different movements between upgradient and downgradient generated by the barrier effect would have been 0.06 mm. Following the same methodology but using the values of maximum drawdown observed during the three pumpings performed outside the enclosure, the settlements would have been 0.06 mm, 0.09 mm and 0.17 mm, for the first, second and fifth pumping. However, the soil would have recovered after these displacements given the elastic behaviour of the soil of Barcelona (Pujades et al., 2013b).

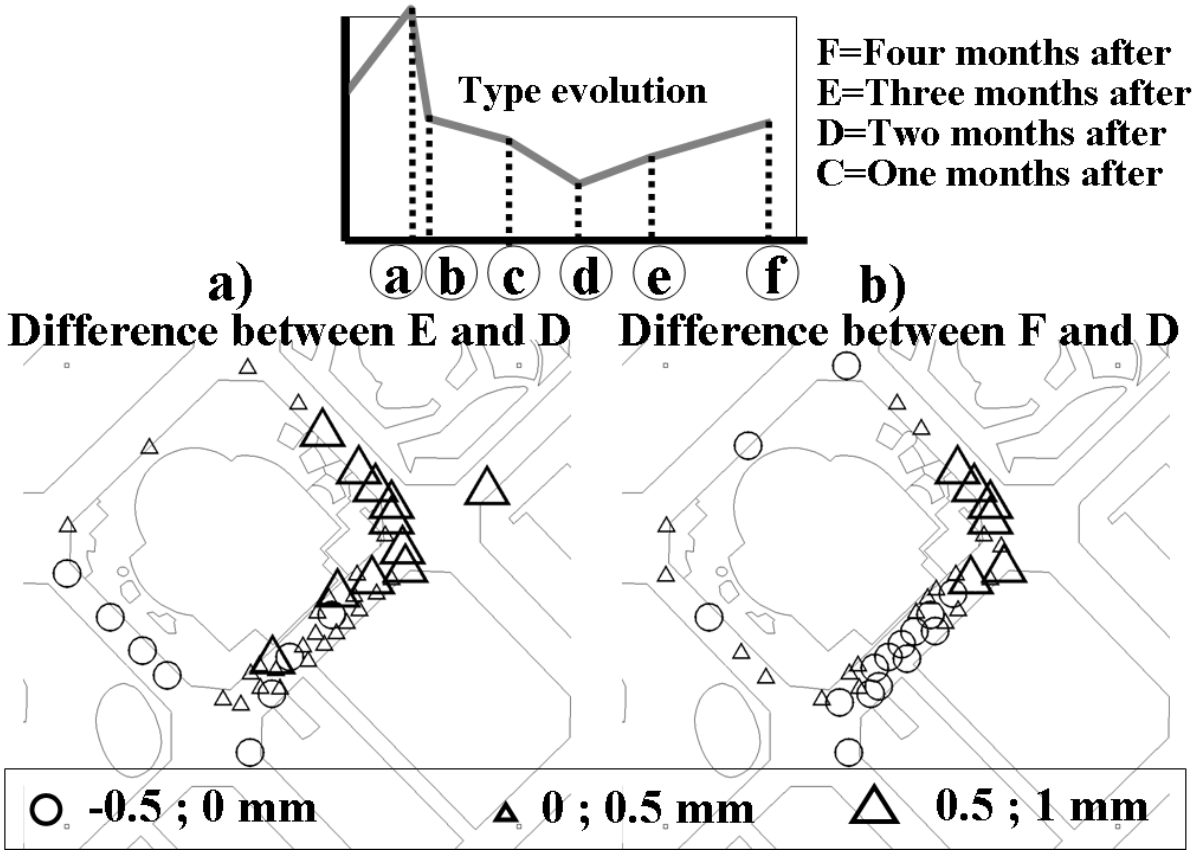


**Figure 2.10.** Soil movement distribution caused by the barrier effect. These movements represent the increments between December 2010 and March 2011. The plot with the ideal behaviour is included to indicate at what time belong the data used to obtain the plan views.

## 2.4. Discussion and conclusions

The construction of the HST tunnel that crosses Barcelona created a lot of controversy during the works. The fact that the tunnel passed below the Sagrada Familia attracted the attention of politicians and public opinion. Such was the case that a committee appointed by the UNESCO acted as external observers. As a result, the safety measures were increased during the construction to avoid unexpected events. Although no problems appeared during the construction and this was finished successfully, this paper exposes the previous tasks performed to predict the affectations of the construction and compares the predictions with the real measurements.

Affectations caused by an underground construction must be predicted before, because if they are too big, the construction can be redesigned. The characterisation of the soil is essential to perform suitable predictions. Therefore, the soil was characterised hydrogeologically using different techniques (borehole logging, Natural Gamma Ray and pumping tests). The geological profile was real since the following predictions matched with the measurements.

New analytical and numerical tools were used to predict the main affectation caused by the construction that was the barrier effect. Results matched with the observations taken during the construction. No barrier effect was observed as a consequence of the BPW construction while the barrier effect caused by the tunnel was around 1.6 m. This value also matches with the observations at other construction sites (Culí, 2012). A not predicted groundwater affectation was observed by the exhaustive monitoring. This consisted in a drop of head caused by the connection between layers with different head during the BPW construction. Piezometers screened in a deep sand layer, which had a head 5 m higher than the shallower layers, measured a drop when some close piles were drilled.

Two main soil movements could be differentiate when the tunnel was constructed, short and long term movements. Short term movements were observed during the drilling of the tunnel and were related with the ground loss and grout injection associated to the tunnel excavation. Moreover, small oscillations related with the water pressure variations in the excavation chamber were observed. Finally, long term movements were related with the groundwater behaviour once the tunnel was constructed. These were the movements caused by the barrier effect, which were predicted analytically using the stiffness parameters of the soil obtained from the storage coefficient. Results computed matched with the observations.

The safety measures taken during the HST tunnel construction like the BPW or the large monitoring rose the cost of the construction. However, these guaranteed that the construction developed in an unfavourable political and social context was finished in a safe manner.

Thus, the numerical and new analytical tools used are suitable to compute the hydrogeological impacts with a moderate error. However, a good characterisation is essential to obtain good results. Similarly, soil displacements caused by groundwater behaviour can be computed easily by using simple analytical equations. Obviously, if the problem is modelled with a coupled hydro-mechanical model, the estimations will be better. However, sometimes data and time to construct a reliable model are not available, and analytical equations become suitable. Methods used during the HST tunnel construction in Barcelona are appropriate since the predictions agreed with the observations.

# 3. Barrier effect of underground structures on aquifers

## 3.1. Introduction

Research has improved the construction of underground structures in cities (Tambara, *et al.,* 2003). They are successfully completed when rigorously and carefully planned (Jurado, *et al.,* 2011). However, it is essential to consider not only the construction stage but also the long term effects of these structures on the aquifer. When underground structures intersect aquifers, they may act as drains or barriers against the groundwater natural flow (Vázquez-Suñé, *et al.,* 2004), causing rise to environmental and economic impacts. A number of studies on underground constructions have focused on the evolution of pore pressure around the structure and on the characterization of the flow to its leaky parts, using analytical equations (Goodman, *et al.,* 1965; El Tani, 2003; Vilarrasa, *et al.,* 2011; Pujades, *et al.,* 2011) or numerical models (Font-Capó, *et al.,* 2011). However, few studies have dealt with the hydrogeological impacts of impervious structures (Deveughèle and Zokimila, 2010), which is the subject of this work.

Underground impervious structures modify the groundwater flow pattern because the structure reduces totally or partially the aquifer section. Thus, effective transmissivity is reduced, leading to a rise in the water table upgradient and a lowering downgradient (Ricci, *et al.,* (2007). These modifications of the water table can have negative consequences. Rising water levels may flood basements (Paris, *et al.,* 2010), promote soil salinization or affect flora by rotting the roots of plants (Tambara, *et al.,* 2003). Other impacts associated with the rise of heads include reduction of the bearing capacity of shallow foundations, expansion of heavily compacted fills under the foundation structures, settlements of poorly compacted fills upon wetting, increase in loads on retraining systems or basement walls of buildings, increase in the need for drainage in temporary excavations and propagation of contaminants contained in the partially saturated zone (Marinos and Kavvadas, 1997).

The lowering of heads on the downgradient side can cause seawater intrusion in coastal aquifers, ground subsidence, death of phreatophytes and the drying of wells and springs (Custodio and Carrera, 1989, Tambara, *et al.,* 2003). Moreover, the difference of water pressures between both sides of the underground structure leads to asymmetric loading for which building foundations have seldom been designed.

**This chapter is based on the paper: Pujades, E, López, A., Carrera, J., Vázquez-Suñé, E., Jurado, A., 2012. Barrier effect of underground structures on aquifers. Engineering Geology, 145-146, 41-49.**

Corrective measures exist to decrease these variations in the water table. In essence, corrective measures consist in collecting groundwater upgradient and in discharging it downgradient (Kusumoto, *et al.,* 2003). These measures that allow the groundwater to pass through the structure can be termed "bypasses".

Numerical models are used to quantify head variations and to design the solutions (Merrick and Jewell, 2003, Bonomi and Belleni, 2003, Paris, *et al.,* 2010 and Ricci, *et al.,* 2007). Building such models may be complicated because considerable detail is necessary close to the obstruction. Analytical solutions are therefore useful. Unfortunately, few analytical equations are available (Marinos and Kavvadas, 1997, Deveughele and Zokimila 2010) and their validity is limited. In part, this reflects that the barrier effect problem has not been adequately formalized.

Thus, the objective of this study is to formalize the problem of the barrier effect and to obtain analytical solutions for different barrier types.

## 3.2. Problem statement

### 3.2.1. Basic concepts and definitions

We define barrier effect ($s_B$) as the increase in head loss along flow lines caused by the reduction in conductance associated with an underground construction. Therefore

$$s_B = \Delta h_B - \Delta h_N \qquad (1)$$

where $\Delta h_B$ is the head drop across the barrier and $\Delta h_N$ is the head drop between the same points under natural conditions, i.e. prior to construction (Figure 3.1).

In general, the magnitude of $s_B$ depends on the location of the points across the barrier. The maximum head rise (or drop) commonly occurs close to the barrier and diminishes as distance is increased. In practice, therefore, it is important to distinguish between local ($s_{BL}$) and regional ($s_{BR}$) barrier effects

$$s_{BR} = \min\{s_B\} \qquad (2)$$

$$s_{BL} = \max\{s_B\} \qquad (3)$$

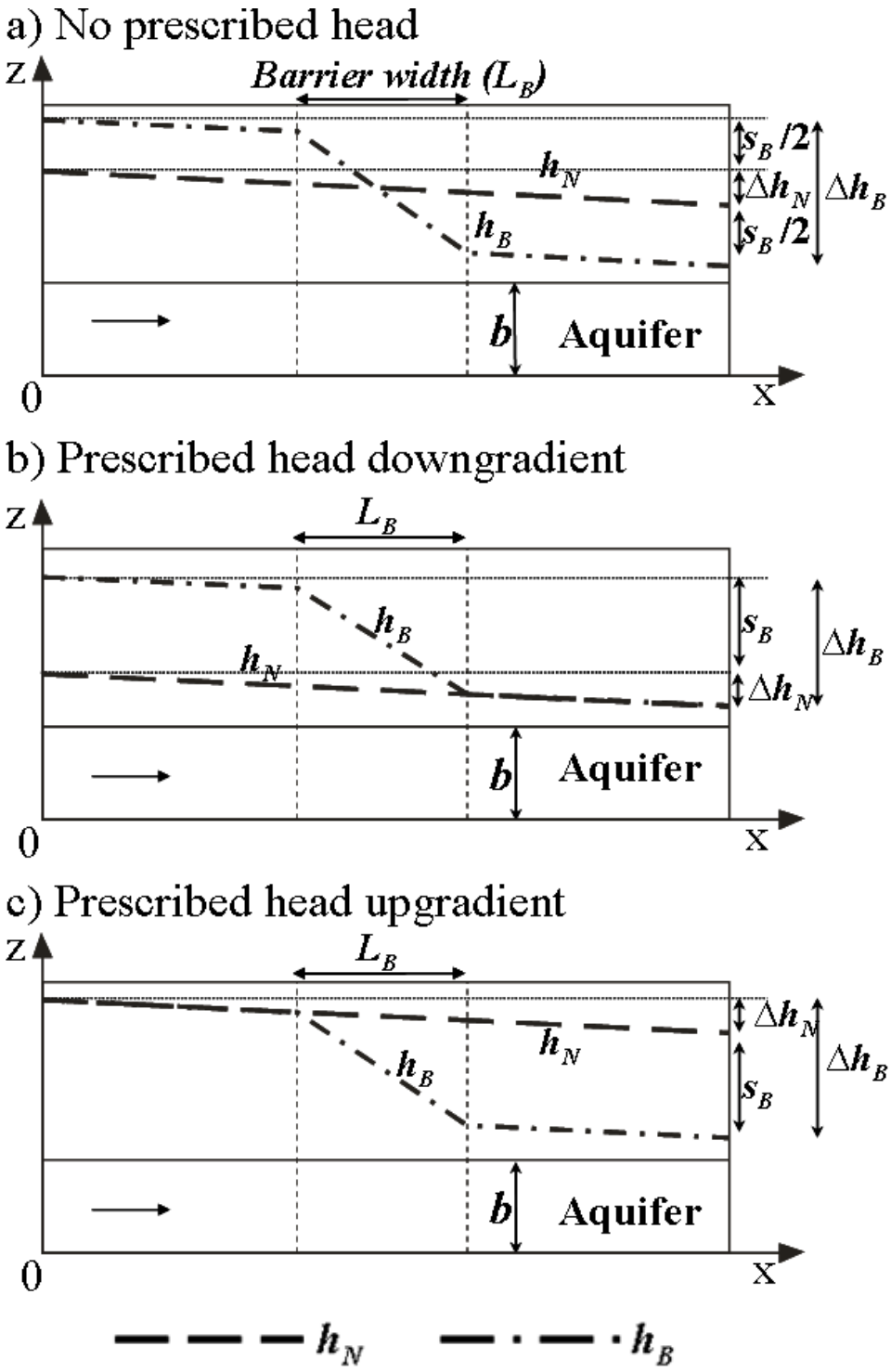


**Figure 3.1.** Cross section of an ideal aquifer whose transmissivity is reduced to an effective $T_B$ with respect to its natural initial $T$ over $L_B$. The head distribution before and after the barrier construction is displayed. Head variations depend on the boundary conditions, a) No prescribed heads, b) prescribed head on the downgradient side and c) prescribed head on the upgradient side. The type of boundary does not modify the value of $s_B$, which is the same in all cases. $h_B$ and $h_N$ are the head distributions with and without barrier.

The regional barrier effect is measured at long distances from the barrier, where groundwater flow lines are unaffected by the barrier. This occurs at distances from the barrier larger than the longest length partially cut by the barrier (width or thickness), e.g. this distance would be the aquifer thickness in the case of a barrier that cuts partially the whole width of an aquifer.

The actual impact of the barrier effect depends on the boundary conditions of the aquifer. When head is prescribed downgradient, the barrier effect is concentrated on the upgradient side of the barrier, causing heads to rise (case b in Figure 3.1), and vice versa (case c in Figure 3.1). On the other hand, in the absence of a prescribed head, the head rises upgradient of the barrier and drops downgradient (case a in Figure 3.1).

To compute $s_B$, we will assume that the flow through the aquifer remains unchanged because the total flow is controlled by outside factors (i.e, recharge or pumping). Otherwise, the barrier may reduce the total flow rate across the aquifer.

### 3.2.2. Governing equations

The equation that governs the problem in steady state can be written as

$$k\nabla^2 h = 0 \qquad (4)$$

where $h$ is head and $k$ is hydraulic conductivity, assumed constant. Commonly, aquifers are heterogeneous especially along the vertical direction (Velasco, *et al.,* 2011). Therefore, the vertical lengths to apply the analytical solutions need to be corrected using the anisotropic ratio ($a$) when the barrier forces a component of flow perpendicular to the stratification

$$k_h\left(\frac{\partial^2 h}{\partial x^2}+\frac{\partial^2 h}{\partial y^2}\right)+k_v\left(\frac{\partial^2 h}{\partial z^2}\right)=0 \qquad (5)$$

$$a=\sqrt{\frac{k_h}{k_v}} \qquad (6) \qquad \rightarrow \qquad k_h\left(\frac{\partial^2 h}{\partial x^2}+\frac{\partial^2 h}{\partial y^2}+\frac{1}{a^2}\frac{\partial^2 h}{\partial z^2}\right)=0 \qquad (7)$$

$$z'=az \qquad (8) \qquad \rightarrow \qquad k_h\left(\frac{\partial^2 h}{\partial x^2}+\frac{\partial^2 h}{\partial y^2}+\frac{\partial^2 h}{\partial z'^2}\right)=0 \qquad (9)$$

where $k_h$ and $k_v$ are hydraulic conductivities, in the horizontal and vertical directions, respectively.

### 3.2.3. Types of barrier

The following types of barriers can be distinguished: 1) semi-permeable barriers, 2) partial barriers, which do not completely obstruct one aquifer dimension, thickness or width (Figure 3.2a and 3.2b), 3) barriers that do not completely obstruct any aquifer dimension (barriers circumscribed in aquifers) (Figure 3.2c), and 4) barriers equipped with a system of bypasses (Figure 3.2d).

From a mathematical point of view, there is no difference between the two types of partial barrier.

Barriers circumscribed in aquifers are similar to partial barriers since we may ignore the thickness, which is not cut by the barrier, located above or/and below the structure.

Although bypass systems are designed to reduce the barrier effect, this is not totally removed. Bypass systems connect a water collection device upstream with a discharging device downstream through a pipe. These devices can be horizontal or vertical wells, possibly embedded in a gravel wall to improve their performance. The bypass studied in this chapter consists in fully penetrating wells.

### 3.2.4. Dimensionless form

The problem may be written in dimensionless form by dividing the barrier effect over the head drop that occurs over the barrier length under natural conditions

$$s_{BD} = \frac{s_B}{h_C} = \frac{s_B}{i_N d_C} \qquad (10)$$

Where $s_{BD}$ is the dimensionless barrier effect, $h_C$ is the characteristic head drop, $i_N$ is the natural gradient and $d_C$ a characteristic length that depends on the problem. Ideally, $s_{BD}$ should only depend on the geometrical features of the barrier.

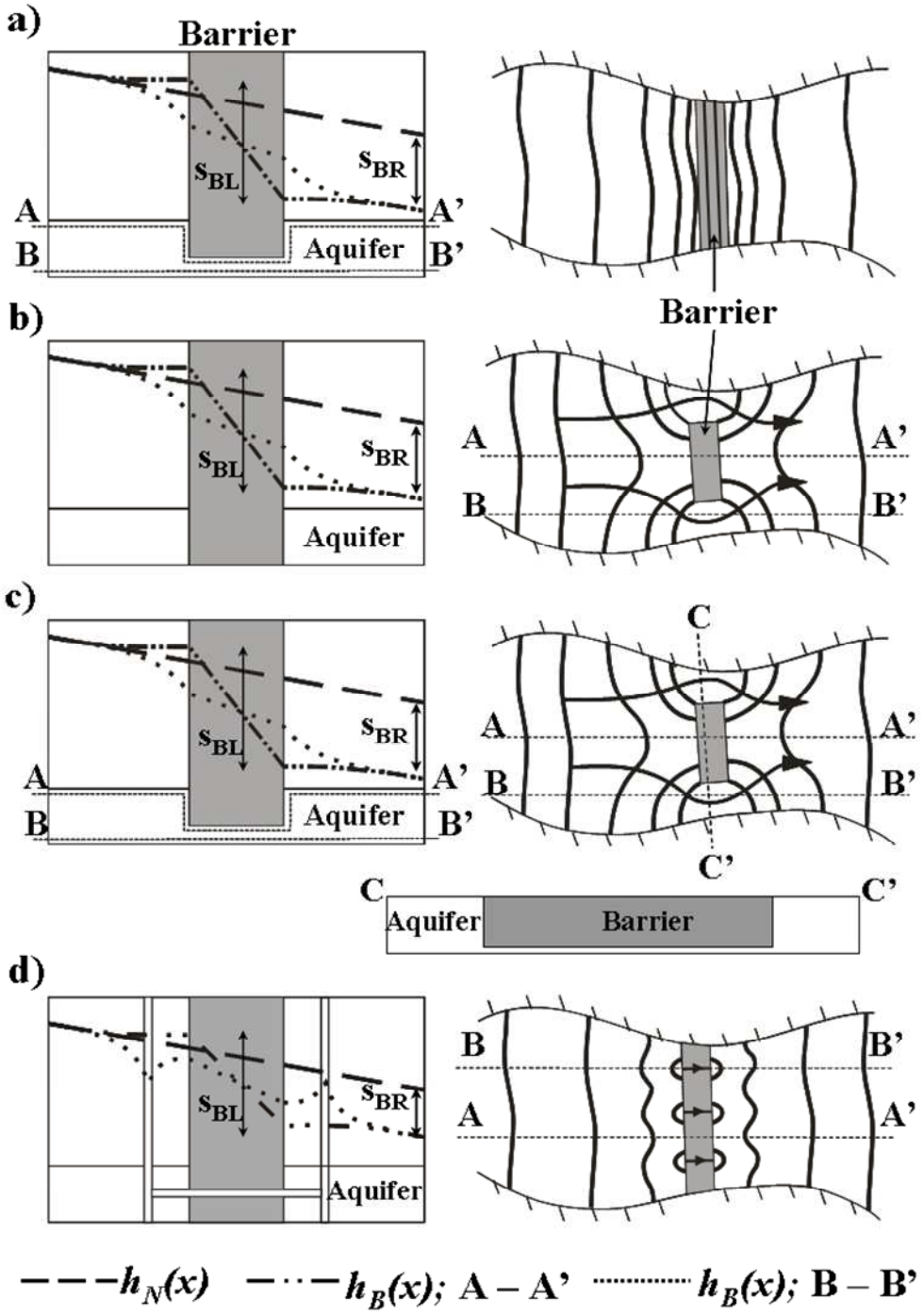


**Figure 3.2.** Cross sections (left) and plan views (right) of different types of barrier. $s_{BL}$ and $s_{BR}$ are shown in all cases. a) Partially penetrating infinite barrier. b) Completely penetrating finite barrier. c) Barrier included in aquifer. Section C-C' shows that the free area below the barrier is negligible. d) Barrier with bypass.

### 3.2.5. Semi-permeable barrier case

The above concepts are illustrated by the semi-permeable (fully-penetrating) barrier case, which can be regarded as paradigmatic. Consider a structure that

completely obstructs the aquifer and causes a reduction of the effective hydraulic conductivity over the constructed volume, but the flow rate continues crossing this area. Assuming that the flow rate across the aquifer is unaffected by the construction we can write

$$q_X = kbi_N = k_B b \frac{\Delta h_B}{L_B} \qquad (11)$$

where $b$ is the aquifer thickness, $q_X$ is the flow that crosses the aquifer, $k_B$ is the hydraulic conductivity of the barrier and $L_B$ is the width of the barrier. Ignoring the head loss across the barrier area (i.e. $i_N L_B << \Delta h_B$), we obtain

$$s_B = \frac{k}{k_B} i_N L_B \qquad (12)$$

The barrier length $L_B$ is the characteristic length. Combining equations (12) and (10), yields

$$s_{BD} = \frac{s_B}{i_N L_B} = \frac{k}{k_B} \qquad (13)$$

If the natural head gradient in the barrier area is not neglected, then

$$s_B\left(\text{in barrier area}\right) = \Delta h_B(\text{in barrier area}) - \Delta h_N(\text{in barrier area}) \qquad (14)$$

and

$$\Delta h_N(\text{in barrier area}) = i_N L_B \qquad (15)$$

Therefore

$$s_{BD} = \frac{s_B - i_N L_B}{i_N L_B} = \frac{k}{k_B} - 1 \qquad (16)$$

Notice that the actual $s_B$ depends on the barrier thickness. It is possible to characterize the barrier with a leakage coefficient ($\alpha_B$)

$$\alpha_B = \frac{q_X}{s_B} = \frac{kbi_N}{s_B} = \frac{kb}{s_{BD} L_B} \qquad (17)$$

The latter expression is general, i.e. given $s_{BD}$ and $k$ (or the aquifer transmissivity, $T$), it is possible to use Eq. (17) to derive the leakage factor $\alpha_B$. This can be used in some codes (Hsieh et al, 1993) to characterize barriers. Alternatively, the net effect of the barrier can be represented in models by assigning an effective transmissivity to the barrier $T_B = \alpha_B L_B$ over a band of width $L_B$. In the semi-permeable barrier case, this leads to $T_B = k_B b$, which is trivial.

### 3.3. Methodology

Except for the semi-permeable barrier, which was discussed above, the solutions to the other types of barrier are obtained using the following steps:

1. Study of the conceptual model setting and equations that govern flow behaviour.
2. Statement of the problem in dimensionless form and identification of the characteristic variables that govern the solution.
3. Preparation of a numerical model to compute $s_B$ for different values of the characteristic variables. We used the finite element code TRANSIN-IV (Medina and Carrera, 2003), with visual interface of VISUAL TRANSIN (UPC, 2003).
4. Performance of a conceptual and/or analytical study of the problem to predict the form of the terms in the analytical solution.
5. Fitting of the analytical terms to the numerical solution by multiple regression analysis. These analysis provide different functions of the variables that explain the behaviour of the system and allow us to calculate $s_B$. Each function has one regression coefficient ($R^2$) and the function with the regression coefficient closest to one is selected. The routine of IMSL DRBEST is used for the multiple regression analysis. This routine uses the Furnival and Wilson algorithm (1974).

### 3.4. Analytical expressions for $S_{BD}$.

#### 3.4.1. Partial barriers

As discussed in section 3.2, this type of barrier completely cuts only one aquifer dimension, i.e. either thickness or width (Figures 2a and b). Therefore, two types of partial barriers might be distinguished depending on the dimension cut. However, the two are equivalent from a mathematical point of view and share the same solution. In fact, differences between these two partial barriers are restricted to the meaning of the variables. For instance, we choose $b$ as a characteristic length, which is half the width of the aquifer in the fully penetrating finite barrier case (Figure 3.2b) or the aquifer thickness in the partially penetrating infinite case (Figure 3.2a). Assuming that the flow rate that cross the aquifer remains unchanged, the problem is fully defined in terms of the open fraction $b_a/b$ of the aquifer, where $b_a$ is the length of the aperture.

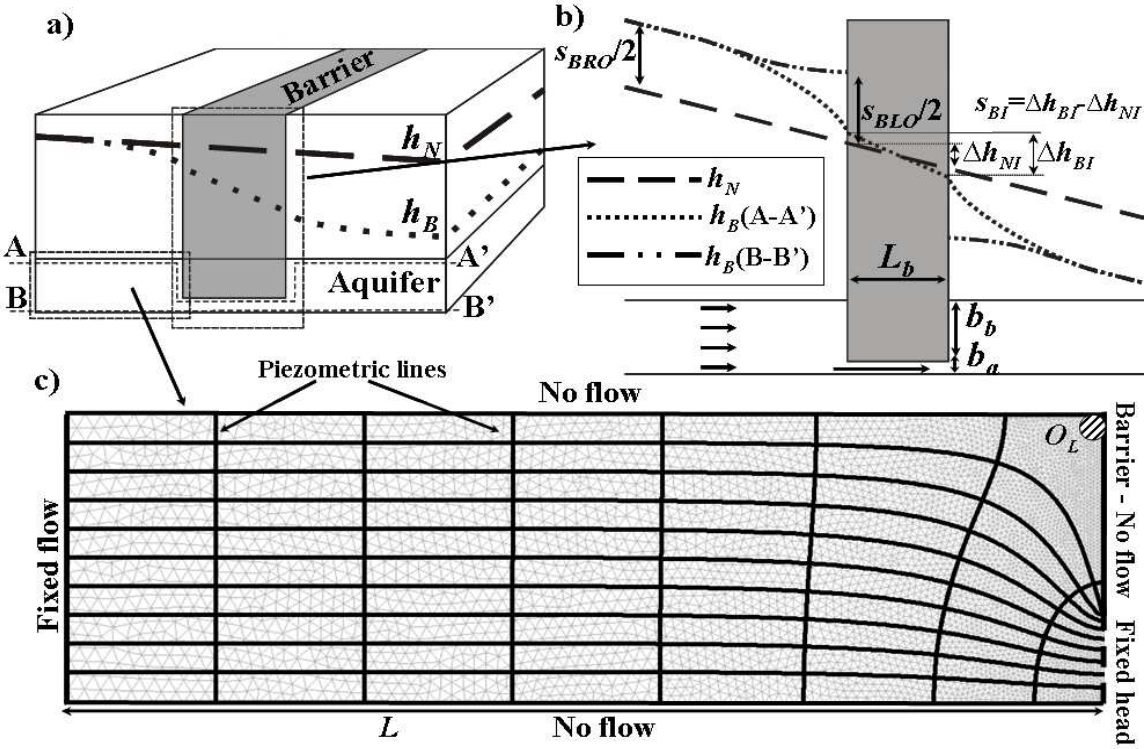


**Figure 3.3.** a) Schematic description of the barrier effect of a partially penetrating barrier with a long section of aquifer with a reduced thickness under the construction. b) The barrier effect consists of two terms: head loss below the construction and head loss by convergence into the opening. The computation grid is also shown (c). $s_{BRO}$ is the barrier effect between the aquifer boundary and the barrier, $s_{BRI}$ across the barrier and $\Delta h_{NI}$ the natural head through the barrier.

Note that the barrier effect can be divided into two terms (Figure 3.3b): the barrier effect between the aquifer boundary and the barrier ($s_{BO}$; $s_{BRO}$ or $s_{BLO}$) and

the barrier effect below the structure ($s_{BI}$). These two effects must be added to obtain the total barrier effect. The barrier effect resulting from the flux below the structure is given by the semipermeable barrier solution

$$s_{BI(L,L+L_B)} = \frac{q_X L_B}{k b_a} - \frac{q_X L_B}{k b} = i_N L_B \left( \frac{b}{b_a} - 1 \right) \qquad (18)$$

$$s_{BID(L,L+L_B)} = \frac{s_{BI}}{i_N L_B} = \frac{b}{b_a} - 1 \qquad (19)$$

where $s_{BID}$ is the dimensionless barrier effect below the barrier. This value, which could be negligible when $b>>L_B$, must be added to the barrier effect resulting from flow concentration towards the opening. This is discussed below.

3.4.1.1. Dimensionless regional barrier effect ($s_{BROD}$)

Several numerical results of the barrier effect have been obtained from the numerical model (Figure 3.3c) by varying $b_a$. For each run, the regional barrier effect is defined as the head rise at the outer boundary, where flux is prescribed. As shown in Figure 3.3c, flow in depth towards the opening is radial. Therefore we expect that the solution contains terms similar to Thiem equation. That are $\ln(b_{aD})$ and $\ln(b_{bD})$, where $b_{aD}$ and $b_{bD}$ are the dimensionless lengths of the aquifer cut and uncut by the barrier respectively ($b_{aD} = b_a/b$ and $b_{bD} = b_b/b$). Polynomial terms are also included similarly to the general hydrological equations to solve radial flow. We obtain an equation that is similar to that of Thiem, except for very large openings ($b_{bD} < 0.1$), when the regional barrier effect can be neglected

$$s_{BROD} = \frac{s_{BRO}}{i_N b} = \begin{cases} 0 & if \quad b_{bD} \le 0.1 \\ \dfrac{2}{3\pi} \ln\left( \dfrac{1}{5\pi b_{bD} \left(1 - b_{bD}\right)^6} \right) & if \quad b_{bD} > 0.1 \end{cases} \qquad (20)$$

and $R^2 =$ 1.00

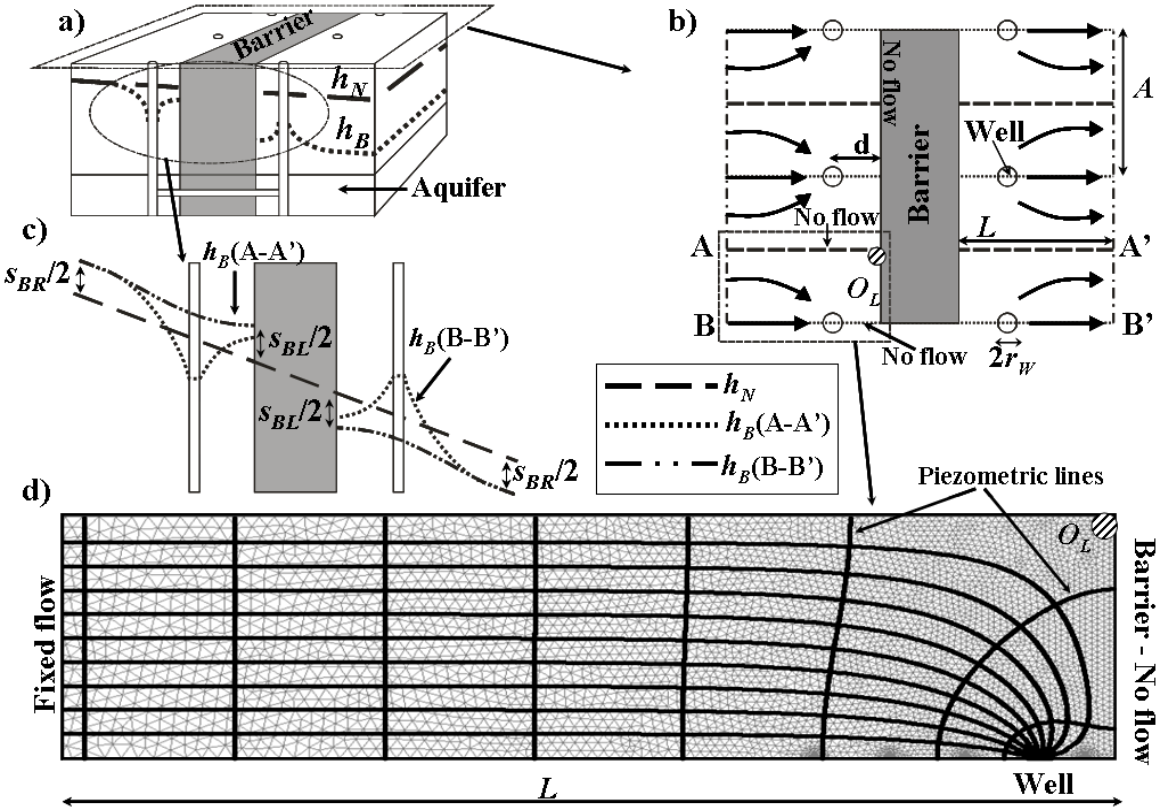


**Figure 3.4.** a) Schematic description of the barrier effect for barriers with a system of bypass. b) The problem can be studied as a pumping well surrounded by no flow boundaries. c) The barrier effect results from the flow convergence into the well. The computation grid is also shown (d).

Figure 3.5a displays the relationship between $s_{BROD}$ and $b_{aD}$. Note that numerical results (dots) match perfectly those obtained with Equation (20) (line). Note also that the barrier effect increases logarithmically when the opening is reduced. This increase is diminished when the aperture exceeds 30% of the aquifer thickness (vertical barrier) or width (horizontal barrier).

### 3.4.1.2. Dimensionless local barrier effect ( $s_{BLOD}$ )

The solution is obtained following the same steps adopted in the case of the regional barrier effect but evaluating the head variation at the local observation point $O_L$ (Figure 3.3c). Two situations must be distinguished. On the one hand, when the opening is small ( $b_{bD} > 0.28$ ), flow towards the opening is essentially radial with the result that the equation of the barrier effect is similar to that of Thiem. On the other

hand, when the opening is large ($b_{bD} > 0.28$), flow is linear and the head drop between $O_L$ (Figure 3.3) and the edge of the opening is equivalent to that of the natural gradient ($\Delta h = i_N b_b$). This value has to be multiplied by 2 to account for head loss on the downgradient side. The value 0.28 has no specific meaning, but simply results from the fitting procedures, which leads to the following equation:

$$s_{BLOD} = \frac{s_{BLO}}{i_N b} = \begin{cases} 2b_{bD} & if \quad b_{bD} < 0.28 \\ \sqrt{\frac{3}{8}} \ln\left(\frac{2b_{bD}^{\,0.29}}{b_{aD}^{\,2}}\right) & if \quad b_{bD} \geq 0.28 \end{cases} \quad (21) \qquad \text{and } R^2 = 1.00$$

The results of this approximation together with those of the numerical solution are shown in Figure 3.5b. Again, the fit is visually perfect (errors are smaller than 0.02 for $b_{aD} > 0.005$).

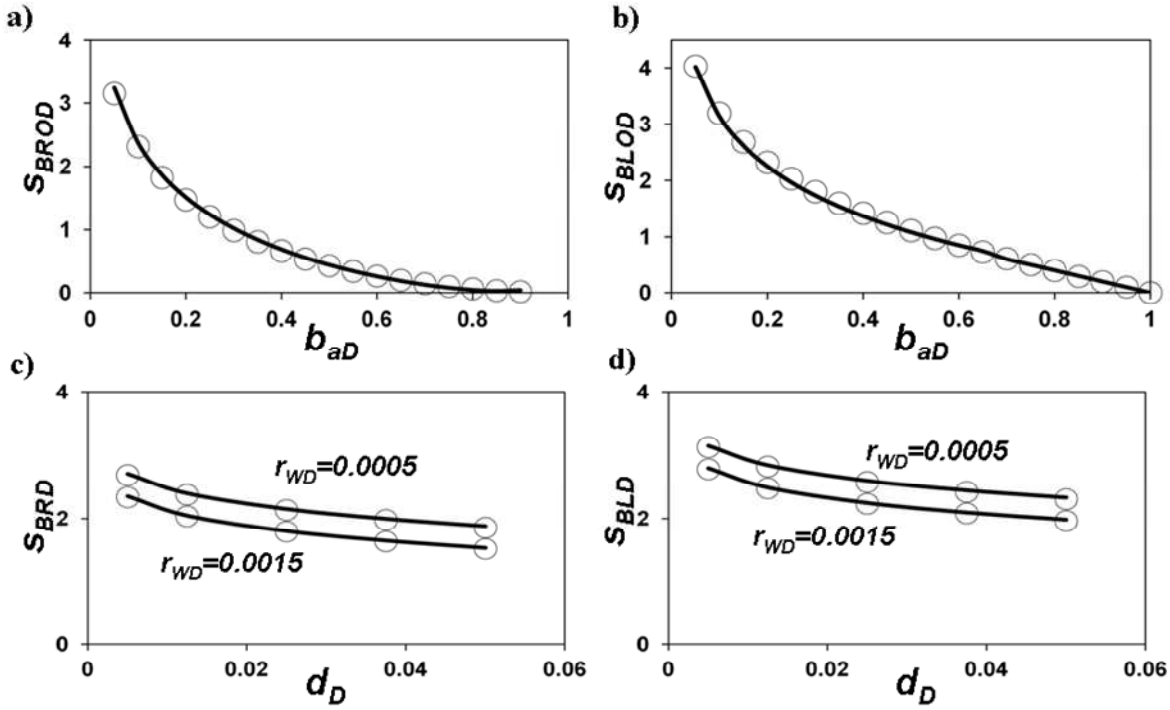


**Figure 3.5.** Dimensionless barrier effect, regional and local, versus some variables. Above-left a) $s_{BROD}$ vs. $b_{aD}$. Above-right b) $s_{BLOD}$ vs. $b_{aD}$. Below-left c) $s_{BRD}$ vs. $d_D$ for two well dimensionless radius (0.0005 and 0.0015). Below-right d) $s_{BLD}$ vs. $d_D$ also for two well radius.

### 3.4.2. Barrier with bypass

Bypasses can be used as a corrective measure to reduce $s_B$. They may be of several types (Kusumoto, *et al.*, 2003, Lopez, *et al.,* 2009). We analyze a bypass consisting of deep wells connected by a pipe through the underground construction (Figure 3.2d).

The system can be simplified for computational purposes as shown in Figure 3.4. Because of symmetry, the model domain is the rectangle bounded by the flow line along the wells and the axis perpendicular to the barrier located halfway between two adjacent wells. The intersection of this axis with the barrier is the point with highest head rise (point $O_L$ in Figure 3.4), where the local barrier effect is computed. The system is modelled by imposing a prescribed head at the well radius and the natural flux at the inflow boundary. All other boundaries are assumed to be impervious. The barrier effect is calculated as twice the difference between computed and natural heads at the inflow boundary (regional barrier effect) and at point $O_L$ (local barrier effect).

#### 3.4.2.1. Dimensionless regional barrier effect ( $s_{BRD}$ )

The problem can be solved analytically by means of the image theory or by using the solution for a drain in a long confined aquifer (Schneebeli, 1966, cited by Custodio and Llamas, 1983). The latter is simpler, but also requires the use of the image theory to accommodate the no flow boundary at the barrier. We consider two wells at $x = \pm d$, where $d$ is the distance between well and barrier. These two wells are equivalent to a single well of radius $\sqrt{2 r_W d}$ when $d << A$, where $A$ is the distance between wells and $r_W$ is the radius of the bypass well (Figure 3.4). Subtracting the natural head drop $i_N L$, where $L$ is the length to the furthest inflow boundary from the drawdown at the well, and dividing by $i_N A$ ( $A$ is the characteristic length) we obtain

$$s_{BRD} = \frac{s_{BR}}{i_N A} = \frac{1}{\pi} \ln \frac{A^2}{8\pi^2 r_W d} - \frac{2d - L_B}{A} \quad (22)$$

Figure 3.5c displays $s_{BRD}$ versus $d_D$ for two values of $r_{WD}$ (dimensionless well radius) using Equation (22) (lines) and the numerical model (dots) that overlap. The

regional barrier effect can be considerably reduced by increasing the well radius, e.g. constructing the well inside a gravel trench. The greater the distance ( $d$ ) from the well to the barrier, the greater the efficiency of the bypass. However, it is possible that the improvement obtained by placing the well further away from the barrier does not offset the increase in the difficulty of constructing the connecting pipe.

3.4.2.2. Dimensionless local barrier effect ( $s_{BLD}$ )

The solution of Schneebeli (1966 cited by Custodio and Llamas, 1983) can also be used to obtain the local barrier effect, using the same steps as above, which yields

$$s_{BLD} = \frac{s_{BL}}{i_N A} = \frac{1}{\pi} \ln \frac{A^2}{2\pi^2 r_W d} - \frac{2d - L_B}{A} + \frac{\pi d^2}{A^2} \quad (23)$$

Figure 3.5d displays the influence of $d$ and $r_{WD}$ on $s_{BLD}$. As in the case of $s_{BRD}$, the increase in $d$ and $r_{WD}$ diminishes the local barrier effect although the reduction is smaller than in the regional barrier effect.

## 3.5. Application

### 3.5.1 Introduction

We tested the validity of the above equations by applying them to the barrier effects at two underground construction sites: the tunnel for the High Velocity Train (HVT) in Barcelona (Spain) and a Railway Station (RS) at El Prat de Llobregat (Spain) (Figure 3.6). Only the local barrier effect was measured at both sites because the piezometers were close to the structures, which is not infrequent at most construction sites. Moreover, to achieve the steady-state barrier effect for long distances is time consuming.

The HVT in Barcelona was built using a Tunnel Boring Machine (TBM), which decreases the aquifer thickness. Thus, this may be regarded as a partially penetrating infinite barrier. Moreover, vertical hydraulic conductivity is smaller than the horizontal one. Therefore, this case illustrates the application of the anisotropy correction factor. At the RS at El Prat de Llobregat, the full thickness of the aquifer (but not its width) is

cut by the diaphragm walls. This case may therefore be regarded as a fully penetrating finite barrier.

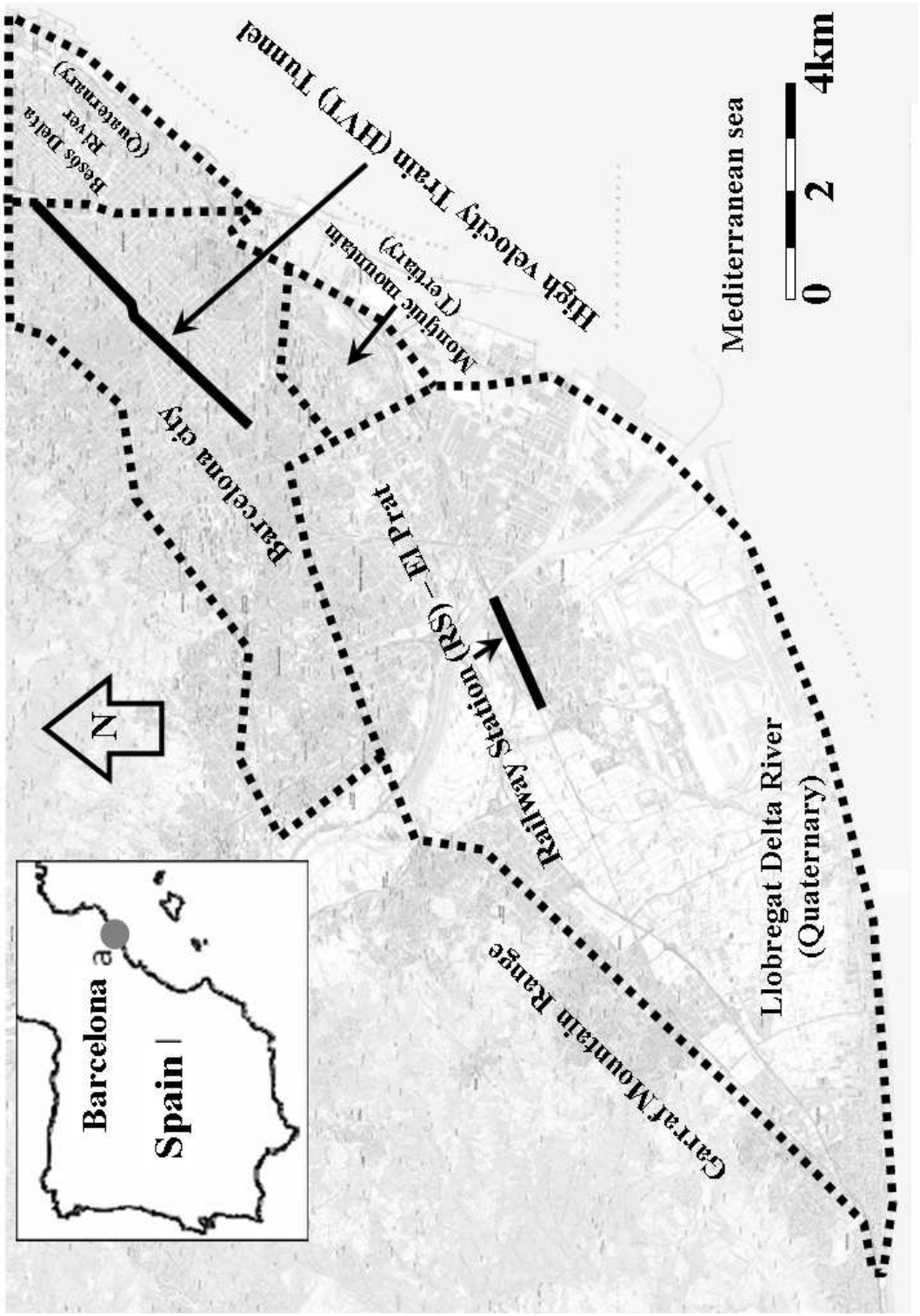


**Figure 3.6.** Study sites.

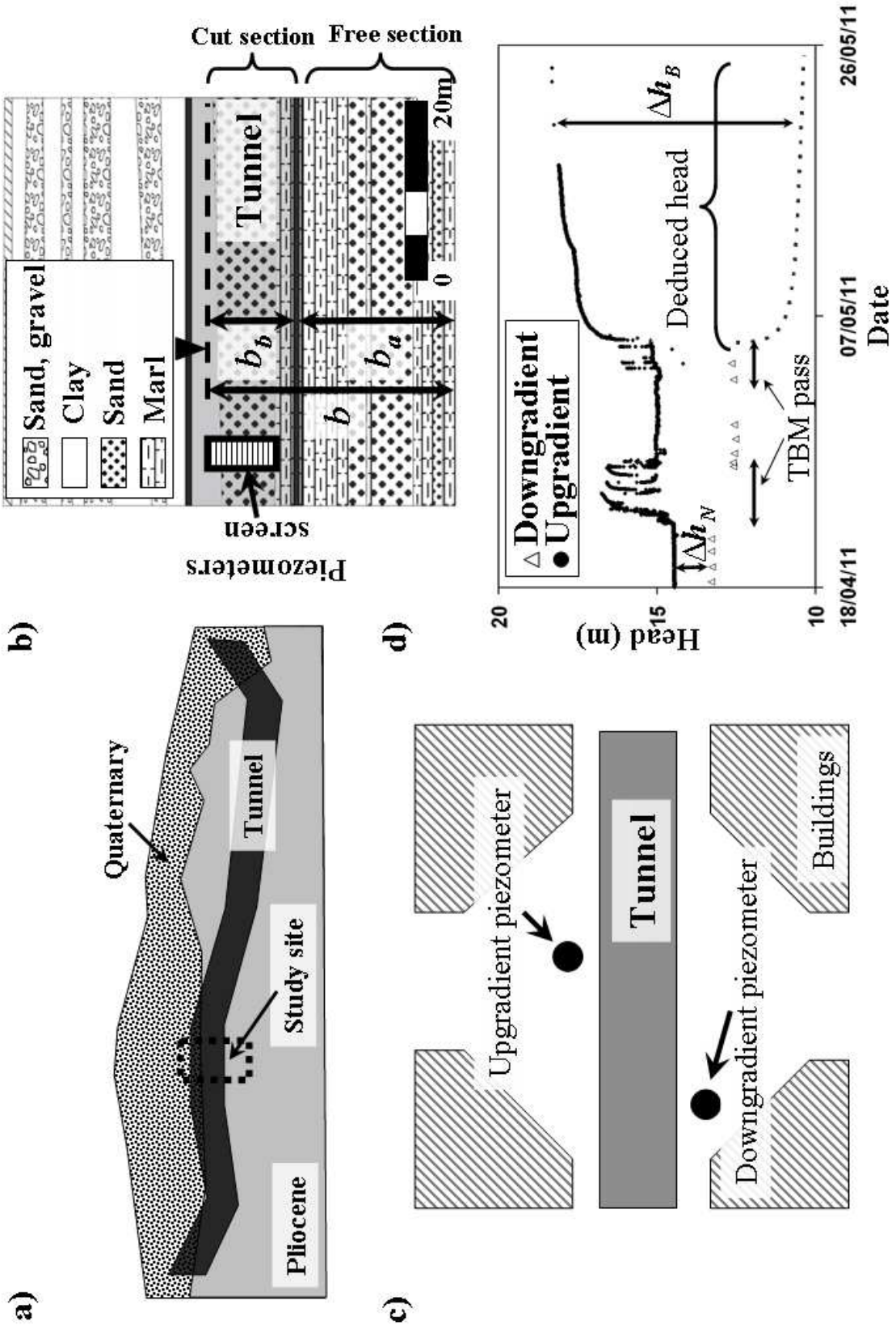


**Figure 3.7.** a) Tunnel section above Barcelona. b) Detailed geological section of the study site. c) Plan view of the study site. d) Head evolution at the piezometers.

### 3.5.2 HVT tunnel in Barcelona

The HVT tunnel crosses all the city of Barcelona penetrating the geological formation of the Barcelona plain. The length of the tunnel is 5.1 km. Permeable units under Barcelona include Tertiary (Pliocene) and Quaternary deposits. The Pliocene materials are the most affected by the tunnel, but it also cuts Quaternary deposits at some places (Figure 3.7a).

The Quaternary materials are made up of sequences of sand/gravel with clay matrix and silts with calcareous nodules. They contain levels of calcrete, which belongs to periods of no sedimentation. Sand/gravel layers with clay matrix are deposits from alluvial fans and the silt materials are eolian deposits. The percentage of clay varies, which can predominate at some layers. At the bottom, the Tertiary materials consist of very low permeability marls that contain high permeability sand strata (Figure 3.7b).

The Barcelona plain can be considered as an aquifer with high vertical heterogeneity, because it is formed by the alternation of different strata, but heads of the different layers are related. The effective transmissivity of the aquifer is 100-200 $m^2$/d. The Quaternary clays and the Pliocene marls display low hydraulic conductivity, ranging from 0.001 to 0.01 m/d. On the other hand, the hydraulic conductivity of the Quaternary sands and gravels ranges from 0.1 to 10 m/d, similar to Pliocene sands.

Two piezometers located in the middle of the tunnel route (Figure 3.7c) were monitored before and after tunnel construction. At this section, the tunnel is somewhat shallow and cuts the through the top portion of the aquifer. One piezometer was located upgradient and the other downgradient. Both piezometers were screened on the upper side of the aquifer (Figure 3.7b), where the maximum $s_{BL}$ was measured. Although the piezometer was broken during the construction of the tunnel, its data were used to obtain $i_N$ and $\Delta h_N$. Figure 3.7d displays the head evolution at both piezometers. It is observed a small step where the head rises at the upgradient side and drops symmetrically at the downgradient side at the beginning of May 2011. Later, the downgradient piezometer was broken, and then the head rise on the upgradient side is assumed to be equal (symmetrical) to the drop on the downgradient side. Therefore, the observed local barrier effect ( $s_{BL}^{obs}$ ) is given by

$$s_{BL}^{obs} = \Delta h_N - \Delta h_B = 8\ m$$

Figure 3.7d shows that $s_{BL}$ is produced when the TBM crosses the site. In this case, the barrier effects between the barrier and the aquifer boundary ($s_{BLO}$) and below the barrier ($s_{BI}$) are calculated and added. Given that $b_{bD} > 0.28$ and applying Equation (21), we obtain

$$s_{BLOD} = \sqrt{\frac{3}{8}} \ln\left( \frac{2{b_{bD}}^{0.29}}{{b_{aD}}^{2}} \right) = 0.97$$

And applying Equation (19), we obtain

$$s_{BID} = \frac{b}{b_a} - 1 = 0.76$$

The characteristic length of the vertical barrier effect is the aquifer thickness ($b$), which must be corrected for anisotropy. Computing the anisotropy ratio ($a$) (Equation 6) requires knowledge of the hydraulic conductivity distribution. $k_V$ and $k_H$ were calculated using the data of a pumping test, as the harmonic and arithmetic averages, respectively, of the hydraulic conductivities of the layers. i.e.

$$k_V = b\sum \frac{k_i}{b_i} = 0.008 \ \frac{m}{d} \qquad \text{and} \qquad K_H = \frac{\sum k_i b_i}{b} = 0.87 \ \frac{m}{d}$$

where $k_i$ is the hydraulic conductivity of each layer and $b_i$ is its thickness. Then,

$$a = \sqrt{\frac{k_h}{k_v}} = 10.21$$

Thus

$$b_C = b \cdot a = 22 \ m \cdot 10.21 = 224.6 \ m$$

where $b_C$ is the corrected thickness of the aquifer. Using $i_N = 0.035$, which was obtained with the head observations measured at both piezometers before the tunnel construction

$$s_{BLO} = s_{BLOD} i_N b_C = 7.6 \ m$$

Similarly, $s_{BI}$ is obtained from $s_{BID}$ as

$$s_{BI} = s_{BID} i_N L_B = 0.32\ m$$

and

$$s_{BL} = s_{BLO} + s_{BI} = 7.9\ m$$

This value is close to that of $s_{BL}^{obs}$ observed as a result of the tunnel construction (Figure 3.7d).

### 3.5.3 El Prat de Llobregat Railway Station

The El Prat de Llobregat RS is located in the middle of the Llobregat River Delta (Figure 3.8a). The Delta is delimited by the Garraf mountain range at the west, the sea at the south and east and the city of Barcelona at the north (Figure 3.6). This Delta have a complex structure as consequence of the sea level variations during the Quaternary (Tubau, 2004), but basically, contains two aquifers separated by a silt formation. The station was built using the "cut and cover" method. Diaphragm walls were used to perform the enclosure. Their depth was 29 m and they cut completely the shallow aquifer.

Both aquifers and the silt formation are quaternary deposits. At the top of the shallow aquifer, above the groundwater table, there are thin strata of flood plain clays, deposited during periods of overflowing of the river. In the bottom of the Delta, below the depth aquifer, there are Pliocene marls (Figure 3.8b). Aquifers are formed by sand and gravel deposits, and the silt formation is consequence of a marine transgression. Their thickness ranges form 12 to 20 m for the upper aquifer and from 4 to 12 m for the lower aquifer (Tubau, 2004).

Aquifer transmissivities range from 200 to 500 $m^2/d$ for the upper aquifer and from 1000 to 5000 $m^2/d$ for the lower aquifer. The silt layer can be considered as bottom boundary for the upper aquifer. Both aquifers constitute a valuable reservoir of water to the city of Barcelona. Therefore, they must be preserved and the underground constructions should not modify them.

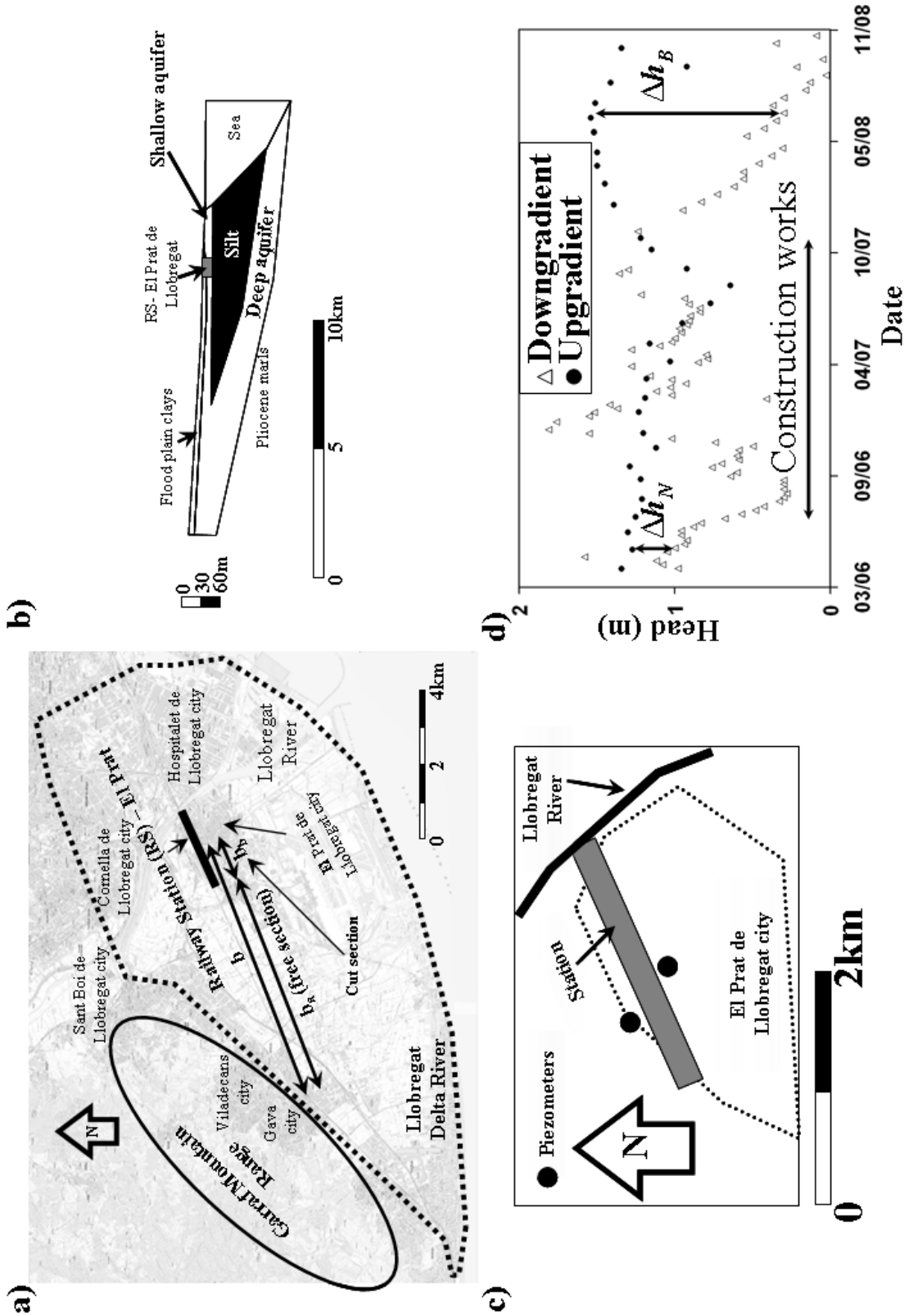


**Figure 3.8.** a) General plan view of the study site. b) Schematic profile of the aquifers distribution in the Llobregat Delta River. c) Detailed plan view. The piezometers were located close to the underground station. d) Head evolution at the piezometers.

As in the case of the HVT in Barcelona, $s_B$ was measured near the structure (Figure 3.8c) so that only $s_{BL}$ was measured. Head evolution (Figure 3.8d) was measured at two piezometers located on the upgradient and downgradient sides of the station. Both piezometers were screened at the shallow aquifer. $\Delta h_N$ was measured before the construction works start. Heads fluctuated a lot during construction, reflecting the diaphragm walls construction and the dewatering used during the excavation stage. After the end of construction, head rose upgradient and dropped downgradient. The difference between both is constant during 6 months. At this period $\Delta h_B$ is measured. Given $\Delta h_N$ and $\Delta h_B$, the observed local barrier effect can be obtained as:

$$s_{BL}^{obs} = \Delta h_N - \Delta h_B = 1.2\ m$$

Applying the equations proposed in this chapter and using the geometry of the Delta and the station (Figure 3.8a), $s_{BL}$ can be estimated. The methodology is similar to the case of the HVT except that no anisotropy correction is required. The RS constitutes a fully penetrating finite barrier, because the aquifer thickness is completely cut but not its width. Then, the length $b$ (5750m) is the distance between the middle of the RS and the Garraf mountain range. The length $b_a$ (4850m) is the distance between the edge of the RS and the Garraf mountain range. Finally, $b_b$ (900m) is the length of the half of the RS. In this case $b_{bD} = b_b / b = 0.16$. Therefore, using Equation (21), we obtain

$$s_{BLOD} = 2b_{bD} = 0.31$$

In this case, the barrier thickness is negligible because the gradient is much smaller than in the previous case with the result that $s_{BLO} \approx s_{BL}$. We calculate the natural gradient $i_N$ as $\Delta h_N / L_P$, where $L_P$ is the distance between the piezometers. This yields $i_N = 0.00066$, which is consistent with the piezometric surface (not shown). Therefore $s_{BL}$ yields

$$s_{BL} = s_{BLOD} i_N b = 1.19\ m$$

This value is again similar to $s_{BL}^{obs}$ when the construction was completed.

## 3.6. Conclusions

Underground constructions may cause head variations when intersecting an aquifer. Heads tend to rise upgradient at the obstruction and to fall downgradient. To quantify these variations, the barrier effect is defined as the increase in head drop along a streamline interrupted by a structure (Equation 1).

This increase is, in general, larger close to the obstruction (local barrier effect) than at long distances (regional barrier effect). But both barrier effects must be evaluated when assessing the impact of a tunnel.

We developed semi-empirical equations to quantify the regional and local barrier effects for several geometries of an obstruction. The equations are easy to apply. They only depend on the geometry of the barrier, which is known, and on the natural gradient prior to the construction, which can be easily obtained from the piezometric surface.

The resulting barrier effect can be used directly to assess acceptability or to derive the conductance of the barrier as input in numerical models to study alternative flow scenarios. In all cases, the barrier effect can be mitigated by the construction of bypass structures. The efficacy of bypasses can also be assessed using the equations proposed.

The validity of the equations proposed was tested at two construction sites. At both sites, the application of these equations was straightforward and yielded results that were close to the observations.

# 4. Deep enclosures versus pumping to reduce settlements during shaft excavations

## 4.1. Introduction

The growth of cities entails the construction of underground structures in urban areas. Several techniques can be used to excavate below the water table to prevent hydraulic heave or fluidisation of the excavation bottom according to EUROCODE 7 (Frank *et al.,* 2004). Some of the techniques avoid the inflow of groundwater into the excavation by waterproofing the walls, whereas others consist in dewatering. These methods can be combined to optimise effectiveness, increasing safety and lowering costs (Powers, *et al.,* 2007). For instance, the cut and cover method, which involves excavating between diaphragm walls, can be combined with pumping (Forth, 2004). Diaphragm walls ensure that the excavation walls are stable and prevent lateral groundwater inflow (Xanthakos, *et al.,* 1994) while pumping reduces the pore water pressure beneath the excavation. The depth of the walls must be sufficient to withstand the earth and water pressure towards the excavation (Lancellotta, 1995). This technique has been used for linear excavations such as tunnels (Pujades, *et al.,* 2009, Zhou, *et al.,* 2010), shafts or underground railway stations (Knight, *et al.,* 1996, Vilarrasa, *et al.,* 2012, Jurado, *et al.,* 2012). However, occasionally, diaphragm walls are lengthened as far as a low-permeability layer to reduce or eliminate pumping because some authors have reported large settlements due to drawdown caused by pumping (Hsi and Small, 1992, Gue and Tan, 2004, Roy and Robinson, 2009). We contend that the contribution of these measures (which will increase the cost) to safety is questionable because lengthening the diaphragm walls does not reduce pore pressures beneath the excavation.

Settlements caused by pumping are the critical issue. While most geotechnicians fear them, some authors argue that pumping is responsible for only a small portion of the total settlements. Other factors, such as wall deflection or problems arising during the construction of diaphragm walls or jet-grouting contribute significantly to settlements (Wong and Patron, 1993, Hwang, *et al.,* 2006, Kung, *et al.,* 2007, Arai, *et al.,* 2008). Obviously, the overall problem depends on the stiffness of the surrounding soil and the construction procedures.

**This chapter is based on the paper: Pujades, E., Vázquez-Suñé, E., Carrera, J., Vilarrasa, V., De Simone, S., Jurado, A., Ledesma, A., Ramos, G., Lloret, A., 2013. Efficiency of deep enclosures versus pumping to reduce settlements during shaft excavations. Accepted in Engineering Geology.**

Actually, settlements caused by drawdown are fairly smooth in space, i.e. pumping will not cause large differential settlements, except in cases of significant lateral changes in geological and geotechnical conditions. Uniform settlements do not damage buildings. Furthermore, pumping ensures stable and workable conditions at the bottom of the excavation (Pujades, *et al.,* 2012), which reduces wall deflection and the resulting settlements during excavation. Therefore, in general, pumping does not pose a serious risk, provided that it is well designed and performed in a controlled manner.

Sometimes, jet-grouting piles parallel to short diaphragm walls are used to deepen the enclosures (Forth, 2004). However, the waterproofing capacity of jet-grouting is debatable. Jet-grouting commenced in the 1970s to improve the shear strength of the soil (Fang, *et al.,* 1994) by injecting grout into fine particle soils (i.e. low hydraulic conductivity materials) (Berry, *et al.,* 1988). It involves injecting water-cement mixtures (and possibly other fluids such as air or water at high speed) into the soil (Tinoco, *et al.,* 2011). Jet-grouting is also used to reduce the hydraulic conductivity of soils (Davis and Horswill, 2002, Wen, 2005, Wong and Poh, 2005, Nikbakhtan, *et al.,* 2010) when high hydraulic conductivity layers are present. These layers contain coarse sediments. Although several authors (Forth, 2004, Saurer and Lesnik, 2011) favour this application of jet-grouting, few have provided values of jet-grouting hydraulic conductivity. Allan and Kukacka (1995) analysed core samples of a jet-grouted soil in the laboratory, obtaining low values in a low hydraulic conductivity soil ($8 \cdot 10^{-6}$ to $8 \cdot 10^{-8}$ m/d). On the other hand, Vilarrasa, *et al.,* (2012) quantified the transmissivity of a jet-grouting enclosure made to waterproof an excavation in a high hydraulic conductivity material. The transmissivity value obtained was two orders of magnitude lower than that of the original sediments, thus confirming the efficacy of jet-grouting in reducing the hydraulic conductivity of high permeability soils. However, this reduction may not be sufficient because of the small width of the jet-grouting wall. Furthermore, the evaluation of this reduction is global. Therefore, the risk of local problems is not eliminated, because most flow may concentrate in a few openings.

Therefore, given that deepening enclosures could not be efficient and that using jet-grouting does not guarantee success, the following questions may be raised: Is enclosures deepening a cost/effective measure against pumping? Is jet-grouting useful to this purpose?

These questions were raised during the construction of the shafts of the High Speed Train (HST) tunnel in Barcelona, Spain. The tunnel, which crosses Barcelona from SW to NE, was excavated adjacent to the Sagrada Familia Basilica (UNESCO World Heritage Site) using a Tunnel Boring Machine (TBM) (Figure 4.1a). The construction of the Basilica (designed by Antonio Gaudi), which commenced in 1882 and is on-going, attracted the attention of politicians and the press, who feared for the safety of the Basilica during the tunnel excavation. Emergency shafts were constructed every 700m of tunnel. Shafts were deep excavations performed with the cut and cover method. Safety measures were increased for the construction of the two shafts close to the Basilica (Figure 4.1) in the Bruc and Padilla streets. Three options were considered for the excavation of the shafts:

1. Short diaphragm walls: diaphragm walls are constructed at the minimum depth required structurally. Deep dewatering is essential to keep the excavation in dry and stable conditions.

2. Long diaphragm walls: diaphragm walls are deeper than the minimum depth required structurally. Generally, diaphragm walls are constructed with reinforced concrete as far as the minimum structural depth. The remaining walls are not necessarily reinforced.

3. Short diaphragm walls lengthened with jet-grouting: the depth of the diaphragm wall is the minimum required structurally.

The main requirement from the Administration was to reduce as much as possible the displacements on the buildings nearby. A value of 5 mm was defined as a warning limit for settlements. Therefore, the initial analyses of the shafts included a hydro-mechanical calculation of the excavation problem by means of PLAXIS finite element code, and displacements were predicted based on both, pumping and excavation of the shaft. However, as expected, settlements were very sensitive to the soil stiffness. Previous works developed about the hydrogeology of Barcelona indicated theat the stiffness parameters of the soil should be relatively high, as a consequence of the historical oscillations of the groundwater that preconsolidated the soil (Vázquez-Suñé *et al.,* 2005). However, the values used in the previous calculations were derived mainly from pressurometers, analysing the unloading-reloading phase. Now it is clear that those values were well below the actual stiffness of the soil for the strain level

applied. This aspect will be discussed later. Following that reasoning, the first option was discarded, as any contribution to settlements, even small, should be avoided if possible. Options 2 and 3 were chosen for excavating the shafts at Bruc and Padilla, respectively. No problems arose during (or after) the construction of the shafts, but the cost of the construction was considerably increased by these choices.

The present work addresses (1) the effectiveness of lengthening enclosures to avoid settlements caused by pumping and (2) the quantification of the hydraulic properties at real scale of a jet-grouting enclosure.

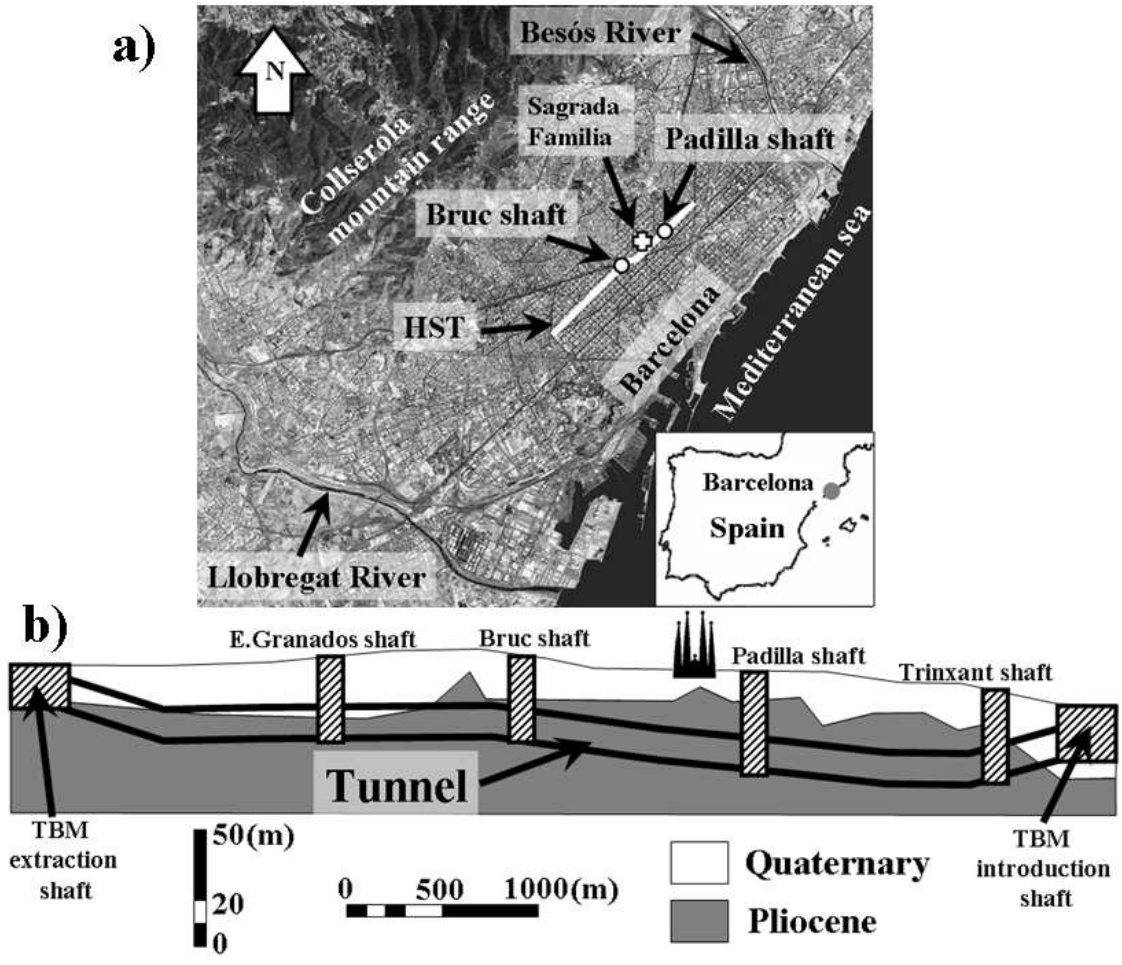


**Figure 4.1.** a) Plan view and geographical location of the study sites. b) Cross section of the tunnel with a schematic profile of the main geological formations.

## 4.2. Problem statement and basic concepts

### 4.2.1. Geographical, geological and hydrogeological description

Barcelona is located above Quaternary (above) and Tertiary (below) sediments. These materials lie above Palaeozoic and/or Triassic formations. In general, the tunnel penetrates Tertiary materials, but at some locations, it also crosses the Quaternary (Figure 4.1b).

Tertiary materials belong to the Pliocene age. They are made up of clays and grey marls as a result of sea deposits, and sequences of conglomerate with a sandy-clay matrix. Pliocene is characterised by an alternation of these lithologies. Fine sediments are predominant at the bottom, and the layers of coarse sediments increase in number and thickness at shallower depths.

The Pliocene is overlain by Quaternary materials which may be divided into: Pleistocene and Holocene. Pleistocene deposits are composed of gravels with a clay matrix at the bottom. These gravels are alluvial fan deposits that are transformed into sands with a clay matrix towards the sea. Overlying these alluvial materials are eolian deposits that consist of brown-yellow silts containing calcareous nodules. At the top of this sequence is a calcrete stratum. This series occurs three times. The Holocene deposits are composed of:

- Torrential, alluvial and foothills deposits made up of fine detritic sediments (red clays or silts).
- Alluvial gravel and sands.
- Coastal plain sands.

The geology of the study sites was characterised by a logging description and correlation profiles of several boreholes drilled at the two sites. Moreover, borehole Natural Gamma Ray Logging was also used to correlate the profiles. Figures 4.2a and 4.2b display the geological cross sections at Padilla and Bruc, respectively. It is possible to observe that the Quaternary and the Tertiary are divided into several strata of different textural and lithological properties.

Quaternary and Tertiary sediments can be considered as a single aquifer with considerable vertical heterogeneity. Its effective transmissivity ($T_{eff}$) is 100-200 $m^2$/d. The hydraulic conductivity ($k$) of clay layers ranges from 0.001 to 0.01 m/d and that of sand and gravel layers varies from 0.1 to 10 m/d. These values were derived from the numerous hydraulic tests performed during the HST tunnel project and other projects.

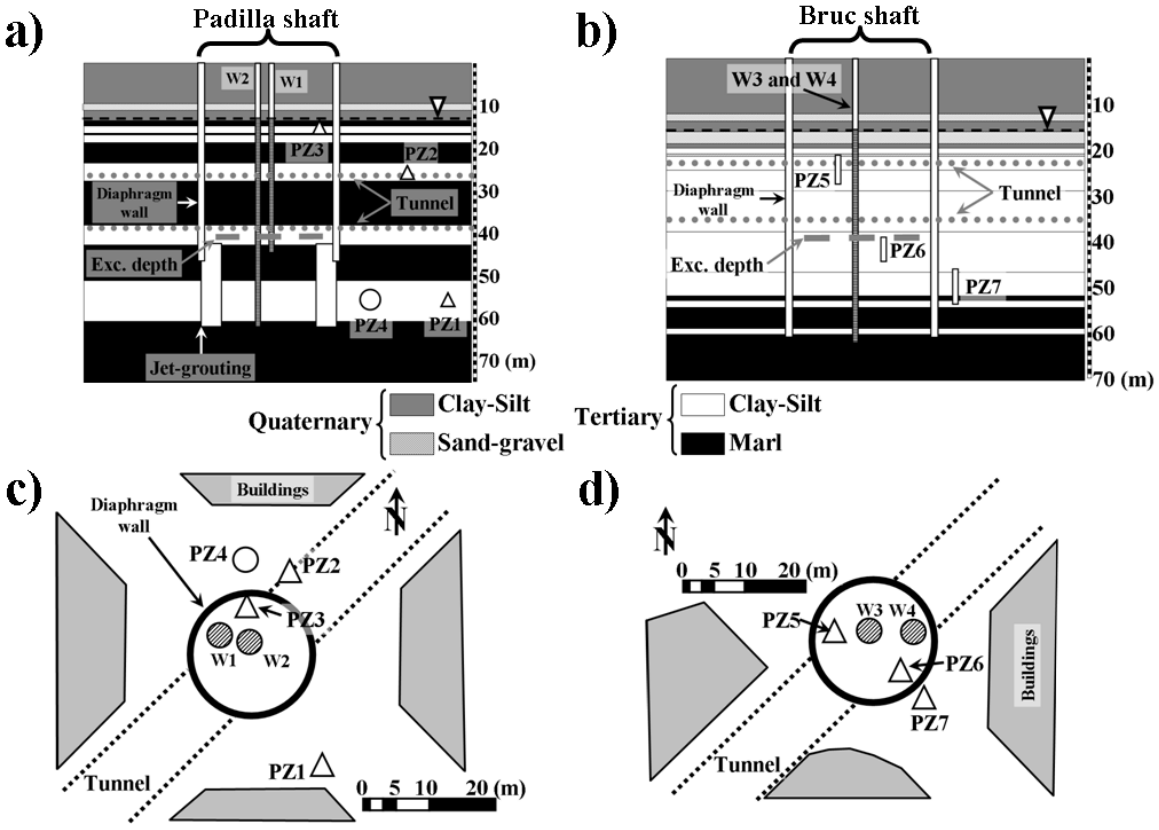


**Figure 4.2.** a) Geological profile of the shaft at Padilla. Triangles indicate the screen of the piezometers used during the first pumping test (PZ1, PZ2 and PZ3). The circle depicts the screen of the piezometer employed during the second pumping test (PZ4). W1 and W2 are the pumping wells used in the first and second pumping test, respectively. b) Geological profile of the shaft of Bruc with the screens of the piezometers employed during the pumping test (PZ5, PZ6 and PZ7) and the two pumping wells (W3 and W4). c) Plan view of the shaft at Padilla with the instruments used to perform the pumping tests. d) Plan view of the shaft at Bruc with the instruments employed to perform the pumping tests.

### 4.2.2. Soil state description

Knowledge of the hydrogeological history of the soil is essential to predict its response to dewatering. The structure and deformational characteristics of the soil depend on its geological history. As in many European cities, the early stages of urbanization in Barcelona were associated with an increase in industrial activity. Groundwater extraction by industry caused a significant lowering of groundwater levels. The subsequent decline of urban industries led to the recovery of groundwater levels (Vazquez-Suñe, *et al.,* 2005). A side effect of groundwater fluctuations is soil pre-consolidation. Thus, the soil in Barcelona behaves elastically whenever the groundwater oscillations do not exceed the maximum drawdown reached during the period of industrial activity. Since this maximum drawdown was approximately 10-15m at the Sagrada Familia Basilica, the current groundwater fluctuations usually remain in the swelling (elastic) branch of the oedometric curve.

| Characteristics of the double fluid jet-grouting | |
|---|---|
| Pressure injection of cement | 300 bars |
| Pumped rate of cement | Up to 400 l/min |
| Air pressure | 10-12 bars |
| Maximum quantity of cement | 1800 kg/m |
| Ratio water/cement | Between 1/0.87 and 1/1.05 |
| Ascent velocity | 6.5 m/min |
| Rotation velocity | 10 r.p.m |
| Diameter of nozzle | 4.6 mm |

**Table 4.1.** Characteristics of the jet-grouting used in the enclosure at Padilla.

### 4.2.3. Construction characteristics

Both shafts were circular (19.7m diameter) with depths of 41 and 40 m at Padilla and Bruc, respectively. The enclosures were lengthened as far as a Tertiary stratum of low-permeability to reduce pumping. Only the diaphragm walls were used for the enclosure of the Bruc shaft, reaching a depth of 61m. These walls were made of reinforced concrete from the surface to a depth of 45m which was the minimum depth required structurally. They were made of concrete from 45 to 61m depth. The Padilla enclosure consisted of 46.5m deep diaphragm walls made of reinforced concrete and jet-grouting piles from 42.5 to 61.5m depth (where the low permeability stratum is located). As a result, jet-grouting piles overlapped the diaphragm walls by 4m to ensure the sealing of the enclosure. The jet-grouting enclosure was located inside the enclosure of the diaphragm walls (Figure 4.2a). The jet-grouting used was double-fluid (Gavaskar, 1999) and its construction characteristics are given in Table 4.1.

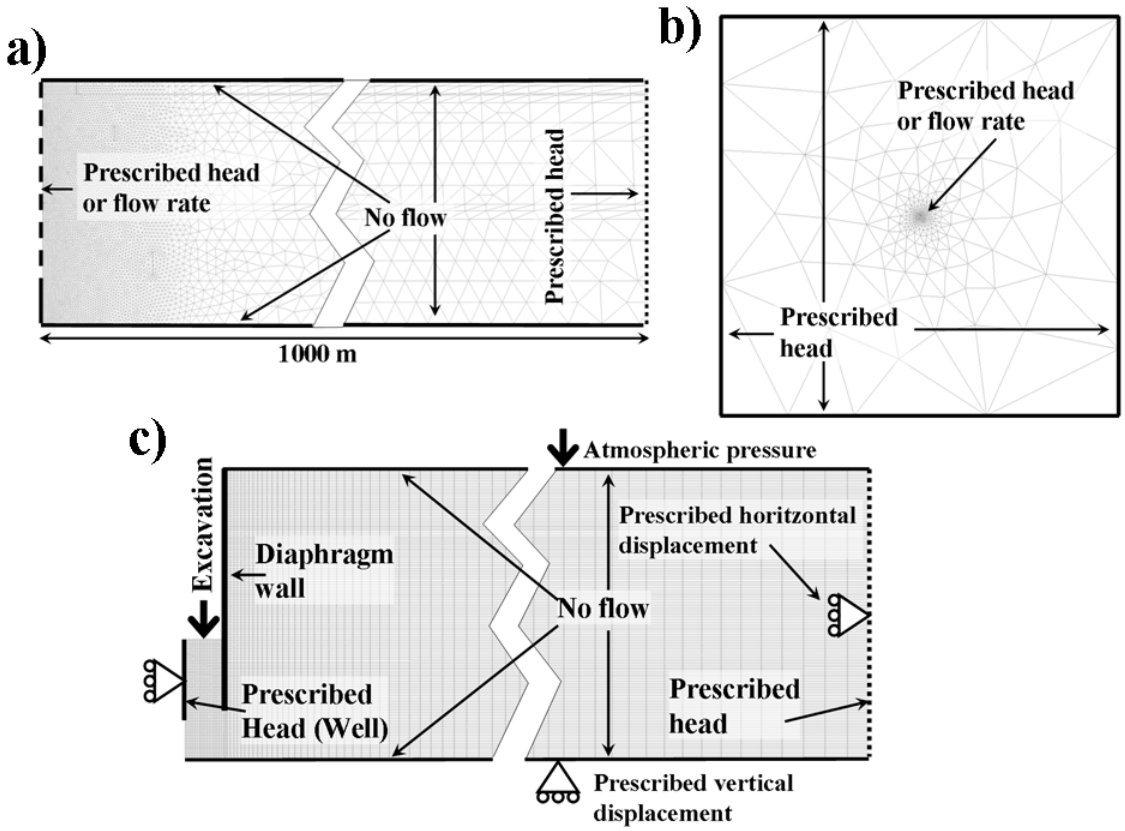


**Figure 4.3.** a) Axisymmetric hydrological model used to calibrate the pumping tests or to simulate the dewatering scenarios. b) Multilayer hydrological model employed to calibrate the pumping tests or to simulate the dewatering scenarios. c) hydro-mechanical model used to calculate the soil movements in different dewatering scenarios.

## 4.3. Basic concepts

### 4.3.1. Hydrological models

A number of hydrological numerical models were used to achieve the objectives. We used the finite element code TRANSIN-IV (Medina and Carrera, 2003 and Medina *et al.,* 2000), with visual interface of VISUAL TRANSIN (UPC, 2003) to construct the models. TRANSIN-IV can be used for several tasks, including simulation, parameter estimation, error and sensitivity analysis, model selection or experiment design. Its benefits to solve virtually a broad range of flow and transport problems have been proven numerous times (e.g., Usunoff *et al.*, 1992; Medina and Carrera, 1996; Iribar *et al*., 1997; Gomez *et al.,* 2010). Simulation entails defining the geometry, boundary conditions, hydraulic parameters (hydraulic conductivity and storage coefficient) and pumping rates, as described below.

Axisymmetrical and multilayer numerical models were employed depending on the geometry of each case (Figure 4.3a and 4.3b). Lateral boundaries were sufficiently far from the site to ensure that they were not affected by pumping; therefore the boundary condition applied at the boundaries was a prescribed head. Top and bottom were modelled as no flow boundaries because only the effect of pumping was analysed. Flow rate or head was prescribed at the pumping well depending on the objective of each simulation or the available data.

Numerical models were used to estimate the hydraulic parameters of the soil and the state of the enclosure by automatic calibration (also termed, parameter estimation, inverse problem or back analysis), employing the data measured during the pumping tests. Automatic parameter estimation was done with TRANSIN-IV using the methods of Carrera and Neuman, (1986a, b and c) and Medina and Carrera (2003). These models were also used to simulate a number of dewatering scenarios in order to come up with the best option. The safety factor and the outside settlement of each simulation were computed analytically by using numerical results.

### 4.3.2. Bottom stability (Safety Factor)

The results of several dewatering scenarios were compared. The main difference between them was the depth of the enclosure. The stability of the bottom of the excavation had to be ensured in all of them. Potential excavation problems caused by groundwater include fluidisation and base heave. Fluidisation may occur when the excavation is carried out in unconfined aquifers and base heave may take place when the excavation is undertaken above a confined aquifer (Cashman and Preene, 2001). In practice, positive (i.e., compressive) effective stresses are essential at all stages to address these two problems.

The vertical effective stress can be calculated by applying Terzaghi's equation in the vertical direction (Terzaghi and Peck, 1948)

$$\sigma'_V = \sigma_V - u \quad (1)$$

where $\sigma'_V$ is the effective vertical stress, $\sigma_V$ is the total vertical stress and $u$ is the water pressure. The total vertical stress is given by

$$\sigma_V = z\gamma_S \quad (2)$$

and the water pressure as

$$u = h\gamma_W \quad (3)$$

where $z$ is the depth of the point, $\gamma_W$ is the specific weight of the water, $\gamma_S$ the specific weight of the soil, which is taken as 20 kN/m$^3$, and $h$ is the piezometric head above the point. Unstable conditions are reached when $\sigma'_V \leq 0$. This occurs at excavations where the drainage system (wells and diaphragm walls) is not designed correctly. The drainage system must ensure that $\sigma_V > u$ or $\sigma_V / u > 1$ at each point below the excavation bottom. But in practice, owing to soil uncertainty, it is common to apply a safety factor ( $SF$ ) to guarantee stability. Thus, we adopted a $SF$ of 1.2,

$$SF = \frac{\sigma_V}{u} \geq 1.2 \quad (4)$$

According to EUROCODE 7 (Frank *et al*, 2004) the verification of hydraulic heave should be performed by comparing, at any point of the excavation bottom, the

total stress and the pore water pressure multiplied by the corresponding partial safety factors:

$$\gamma_{G,stb}\sigma_V = \gamma_{G,dst}u \qquad (5)$$

where $\gamma_{G,stb}$ and $\gamma_{G,dst}$ are the safety coefficients for stabilizing and destabilizing actions respectively. The Eurocode standards recommend $\gamma_{G,stb} = 0.9$ and $\gamma_{G,dst} = 1.35$ for this case. Despite that suggestion, we used a lower global safety factor of 1.2 due to the following reasons:

a) The Eurocode recommendation refers to straight walls, where the passive strength could be reduced dramatically if the soil effective stresses are reduced. In our case, the circular geometry of the shafts does not require any significant passive strength.

b) The Eurocode recommendation is based on a shallow pumping of the excavation bottom and not on a deep well pumping from the whole soil profile below the shaft, which is the case considered here. Therefore, the value of the pore water pressure could be measured (and controlled) directly from the pumping well, thus reducing the uncertainty of its value.

Given that soil is heterogeneous and that the drop of pressure is different in each geological layer, *SF* was computed for each meter below the bottom of the excavation. Shear resistance such as cohesion and friction forces were not considered, as usual in this type of analyses (Frank *et al.* 2004). However, since these forces are opposed to the water pressure effects, our calculations were conservative.

### 4.3.3. Settlement predictions

Settlements of each scenario due to dewatering were calculated using an analytical approximation and a coupled hydro-mechanical numerical model. The easier to apply analytical approximation is computed from the drawdown obtained from the hydrogeological numerical model. Results are compared with the numerical settlements obtained using the hydro-mechanical numerical model, which requires more time and dedication to compute the settlements. If the results are similar, analytical solutions

could be used as a preliminary assessment. Both methodologies require knowing the compressibility of layer *i* ($\alpha_i$), which can be derived from the storage coefficient using the equation proposed by Jacob (1950) and cited by Ferris *et al.,* (1962) for elastic aquifers,

$$\alpha_i = \frac{S_i}{\gamma_w D_i} - \theta_i \beta \qquad (6)$$

where $S_i$ is the storage coefficient, $D_i$ is the thickness of the layer, $\theta_i$ is the porosity and $\beta$ is the water compressibility, which is much smaller than typical soil compressibilities and is often neglected. In fact, if $\beta$ is neglected $S_{Si} = \alpha_i \gamma_W$, where $S_{Si}$ is the specific storage coefficient of the $i$th layer. Therefore, to calculate settlements caused by pumping, we only need know $S_{Si}$ (or $S_i$), which can be obtained from pumping test results.

The analytical computation was performed using the drawdown at different depths and distances derived from the flow model. Settlement at the top of the aquifer was calculated with the equation proposed by Cashman and Preene (2001), which assumes that all the displacements occur in the vertical direction,

$$\rho = \sum_i \gamma_W s_i D_i \alpha_i' \qquad (7)$$

where $\rho$ is the total settlement, $s_i$ is the drawdown in layer *i* and $\alpha_i'$ is the compressibility of each layer considering that the displacements take place only in the vertical direction. $\alpha_i'$ can be obtained from $\alpha_i$ applying

$$\alpha_i' = \alpha_i \frac{(1+\upsilon_i)}{3(1-\upsilon_i)} \qquad (8)$$

where $\upsilon_i$ is the Poisson ratio of the $i$th layer. To test the validity of the analytical method, we also computed settlements with a mechanical model, where it is considered that displacements caused by pumping need not be vertical.

The hydro-mechanical model was built using the finite element numerical code CODE_BRIGHT (Olivella 1994, Olivella, *et al.,* 1994, Olivella, *et al.,* 1996), which

may solve simultaneously the balance equations for heat transfer flow, air flow, solute transport and the mechanical equilibrium equations. Only the water balance and mechanical equilibrium equations (i.e., coupled hydro-mechanical problem) were considered here.. Figure 4.3c displays the boundary conditions of the model. The geometry and hydraulic boundary conditions were identical to those of the flow model, except that a prescribed head condition was imposed in the well. Mechanical boundary conditions consisted on restrict the horizontal movements in the pumping well (symmetry axis) and in the lateral boundary (opposed to the pumping well) and on restrict the vertical movements in the bottom of the model. The hydraulic parameters were also those of the flow model. Assuming linear elasticity, the only mechanical parameters required are Young's modulus ($E$) and Poisson ratio. Poisson ratio was assumed to be 0.35 for each layer. Young's modulus was obtained from compressibility, considering displacements in the three directions, as

$$E_i = \frac{3(1-2\upsilon_i)}{\alpha_i} \qquad (9)$$

## 4.4. Application

Application of the above procedures involves, first, characterising the aquifer, secondly, the enclosure, and thirdly, computing the settlements due to pumping. These steps are described sequentially below.

### 4.4.1. Hydraulic characterisation of the aquifer

#### *4.4.1.1. Padilla site*

One pumping test was performed at the site of Padilla to estimate the hydraulic parameters of the aquifer, before constructing the shaft walls. The pumping wells and the piezometers were designed in accordance with the geology of the area. The piezometers were screened at different depths to measure the hydraulic response in several layers. Figures 4.2a and 4.2c display the screen depth and the location of the three piezometers (PZ1, PZ2 and PZ3), and the pumping well used during the first pumping test (hydraulic characterisation) at Padilla (W1). Head measurements were obtained manually and automatically. Manual measurements followed a logarithmic

frequency to facilitate interpretation. Pressure sensors recorded heads each minute. The average pumping rate during the test, which was measured with an electromagnetic flow-meter, was 4.5 l/s. The pumping test lasted four days, two for pumping and two for recovery.

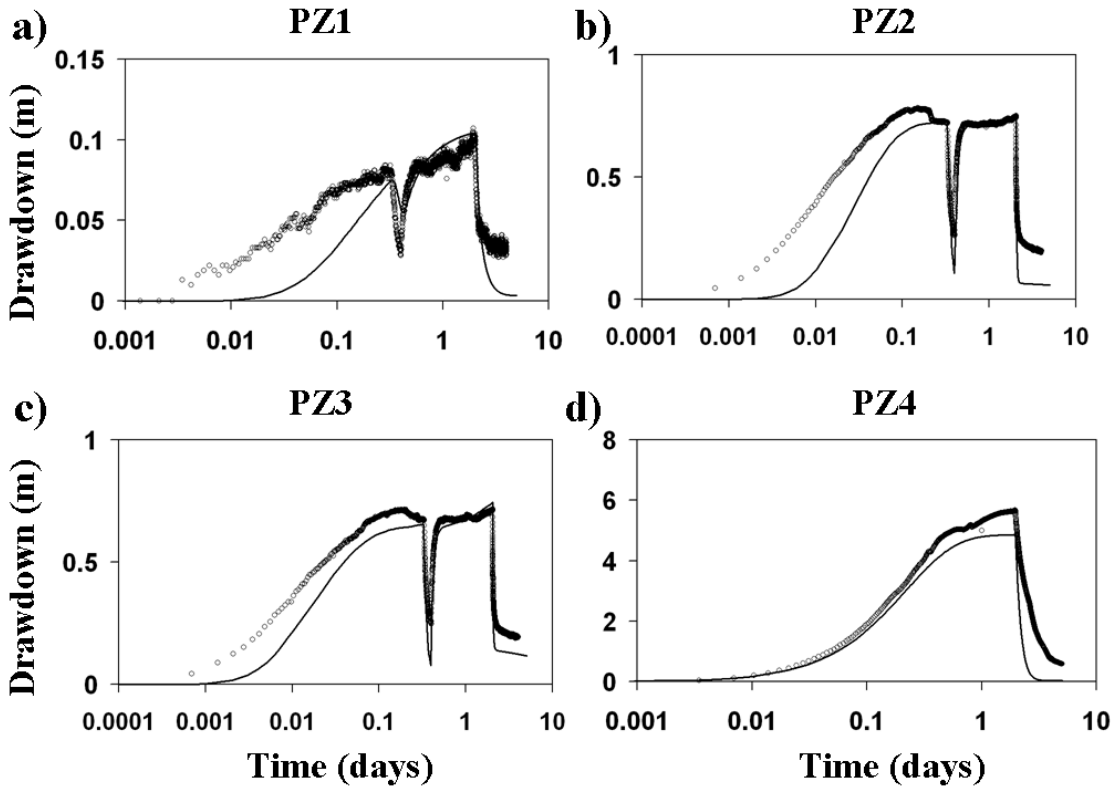


**Figure 4.4.** a), b) and c) Drawdown fitted curves of the piezometers located at Padilla (PZ1, PZ2 and PZ3 respectively). These are obtained from the numerical calibration of the first pumping test. d) Drawdown fitted curve at the piezometer used in the second pumping test at Padilla (PZ4). Note that dots are the measured drawdown while lines are the computed numerically.

The test was interpreted with an axisymmetrical model. Figures 4.4a, 4.4b and 4.4c show the fitted curves of the piezometers PZ1, PZ2 and PZ3 obtained after automatic calibration. Hydraulic parameters of the layers located below the water table are shown in Table 4.2. These results were verified by comparing the transmissivity obtained numerically (180 $m^2$/d) with the transmissivity obtained analytically by applying Jacob's method (200 $m^2$/d) (Cooper and Jacob, 1946).

*4.4.1.2. Bruc site*

Three piezometers were also used for the pumping test at Bruc (PZ5, PZ6, PZ7), carried out before the construction of the shaft walls. Figures 4.2b and 4.2d show their location and screen depth along with those of the two pumping wells used (W3 and W4). Head and pumping rate data were measured using the same tools as at Padilla. The average pumping rate was 10 l/s. The pumping test lasted four days, two for pumping and two for recovery.

| Lithology | Top depth (m) | Bottom depth (m) | $k$ (m/d) | $S_s$ ($m^{-1}$) | $E$ (MPa) |
|---|---|---|---|---|---|
| Clay | 0.0 | 13.5 | | | 50 |
| Sandy silt | 13.5 | 13.8 | 0.21 | 2.40E-01 | 132 |
| Silty calys with sand | 13.8 | 14.7 | 0.034 | 6.80E-05 | 132 |
| Fine - medium sands | 14.7 | 16.4 | 0.12 | 3.00E-05 | 300 |
| Silty clays | 16.4 | 16.8 | 0.042 | 5.10E-05 | 176 |
| Fine - medium sands with silt | 16.8 | 18.6 | 0.41 | 2.40E-05 | 375 |
| Sandy silt with sand layers | 18.6 | 23.4 | 0.3 | 6.40E-05 | 141 |
| Sands with some of clays | 23.4 | 27.6 | 0.3 | 5.90E-05 | 153 |
| Silty clays with some sand layers | 27.6 | 38.1 | 0.072 | 9.90E-06 | 909 |
| Fine - medium sands | 38.1 | 42.6 | 26.46 | 9.90E-06 | 909 |
| Marl | 42.6 | 51.0 | 0.0026 | 9.30E-06 | 968 |
| Medium sands | 51.0 | 60.7 | 5.5 | 9.80E-06 | 918 |
| Marl | 60.7 | 70.7 | 0.004 | 1.00E-05 | 900 |

**Table 4.2.** Description of the layers of Padilla, hydraulic conductivity and storage coefficient values obtained from the first pumping test at Padilla and values of $E$ used to the numerical computations. Note that the hydraulic values of the unsaturated zone were not known.

An axisymmetrical numerical model was used for estimating hydraulic parameters. Figure 4.5 displays the fit between calculated and measured drawdowns. Table 4.3 shows the hydraulic parameters of each layer. The effective transmissivity calculated using Jacob´s method was about 140-170 $m^2$/d, which compares well with that obtained by integrating values in Table 4.3.

| Lithology | Top (depth) | Bottom (depth) | $k$ (m/d) | $S_s$ ($m^{-1}$) | $E$ (MP) |
|---|---|---|---|---|---|
| Medium sand with clay matrix | 0 | 1.8 | | | 45 |
| Clay | 1.8 | 12 | | | 50 |
| Gravel and sand with clay matrix | 12 | 13.6 | | | 45 |
| Clay | 13.6 | 16 | | | 50 |
| Sand and gravel with clay matrix | 16 | 18.5 | | | 900 |
| Clay | 18.5 | 19.5 | 0.05 | 1.80E-01 | 938 |
| Fine - medium sand | 19.5 | 20.7 | 9.92 | 9.65E-06 | 933 |
| Marl | 20.7 | 21.2 | 0.20 | 9.23E-06 | 975 |
| Fine - medium sand | 21.2 | 24.3 | 3.95 | 9.07E-06 | 992 |
| Fine - medium sand with clay matrix | 24.3 | 28.8 | 4.12 | 8.93E-06 | 1008 |
| Medium - coarse sand with clay matrix | 28.8 | 37.7 | 4.91 | 9.42E-06 | 955 |
| Fine sand with clay matrix | 37.7 | 46.4 | 0.30 | 3.18E-05 | 283 |
| Fine - medium sand with clay matrix | 46.4 | 51.5 | 0.03 | 6.46E-06 | 1392 |
| Marl | 51.5 | 52.6 | 1.00E-03 | 6.19E-06 | 1454 |
| Fine - medium sand with clay matrix | 52.6 | 54.1 | 16.45 | 7.75E-06 | 1161 |
| Marl | 54.1 | 58.7 | 9.00E-04 | 4.99E-05 | 180 |
| Medium sand with clay matrix | 58.7 | 60 | 1.00 | 1.02E-05 | 884 |
| Marl | 60 | 70 | 1.00E-04 | 1.06E-05 | 849 |

**Table 4.3.** Description of the layers of Bruc, hydraulic conductivity and storage coefficient values obtained from the pumping test at Bruc and values of $E$ used to the numerical computations. Note that the hydraulic values of the unsaturated zone were not known.

### 4.4.2. Hydraulic characterisation of the enclosure

A second pumping test should be performed to analyse the state of an enclosure prior to excavation and dewatering in order to identify potential inflows during excavation (Pujades, *et al.,* 2012, Vilarrassa, *et al.,* 2012). If openings are detected (i.e., open joints between panels), these must be repaired or the dewatering must be re-designed. The test usually involves pumping inside and measuring inside and outside the enclosure. The diaphragm walls at the Bruc shaft reached a Tertiary stratum with low permeability. Therefore, no drawdowns were measured outside when pumping inside, which suggested that the enclosure was well made.

The enclosure at the Padilla shaft was lengthened using jet-grouting piles instead of diaphragm walls and significant drawdowns were observed outside when pumping inside. A pumping test was performed to quantify the hydraulic properties of the jet-grouting enclosure constructed below the diaphragm walls. The pumping well (W2), which was screened along aquifer thickness, was located inside the enclosure. A new piezometer (PZ4) was screened in the most transmissive layer cut by the jet-grouting piles (Figure 4.2c). This one replaced piezometer PZ1, which was damaged during the construction of the enclosure. Head and pumping rate measurements were taken

manually and automatically, as in the previous tests. The average flow rate pumped during the test was 5 l/s, and it also lasted four days, two for pumping and two for recovery.

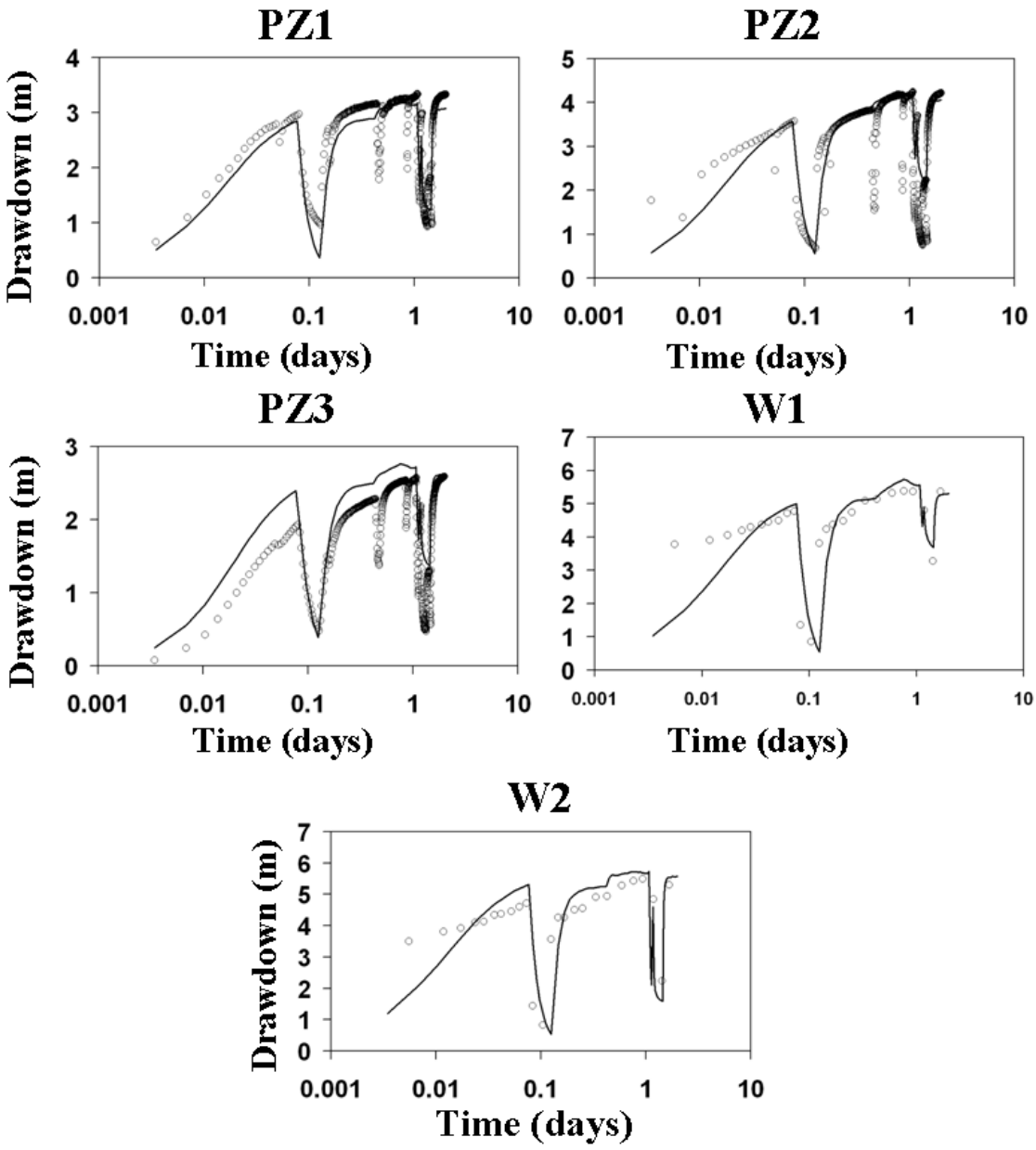


**Figure 4.5.** Drawdown fitted curves obtained from the numerical calibration of the pumping test performed at Bruc the PZ5, PZ6 and PZ7 piezometers and in the W3 and W4 pumping wells. Note that dots are the measured drawdown while lines are the computed numerically.

The test was calibrated numerically using a multilayer model (not an axisymmetrical one) because the pumping well was not located in the centre of the enclosure. The effective hydraulic conductivity of the jet-grouting enclosure obtained from calibration was 0.6 m/d. Figure 4.4d shows the fitted curve at PZ4.

### 4.4.3. Dewatering systems

The actual dewatering systems at both sites were compared with alternative scenarios. The comparisons considered the safety factor, the pumping rate and the outside settlements due to pumping. The minimum structural depth of the enclosure was maintained in all the scenarios. In addition, the pumping well where the head was prescribed to ensure stable conditions at the bottom of the excavation was located in the middle of the enclosure to facilitate comparison.

| Scenario | Settlement (mm) | | Pumping rate ($m^3$/d) |
|---|---|---|---|
| | Analytical | Numerical | |
| 1.Jet-grouting | 1.9 | 1.6 | 1300 |
| 2.Open bottom | 3.1 | 2.2 | 2150 |

**Table 4.4.** Predicted settlements calculated analytically and total pumping rate calculated numerically for the scenarios considered for the shaft at Padilla.

#### *4.4.3.1. Padilla site*

Two scenarios were considered at the Padilla shaft. The first one was identical to the actual excavation (46.5m deep diaphragm walls with jet-grouting piles that started at 42.5 meters and reached a depth of 61.5m). Jet-grouting piles were not applied at the bottom in the second scenario, so the enclosure consisted only of the diaphragm walls. Drawdown in the pumping well was prescribed to obtain a *SF* of 1.2. This implied that, in the first scenario, drawdown in the well had to be 45 m and in the second scenario, 60m. The corresponding pumping rates were 1300$m^3$/d and 2150$m^3$/d, respectively.

Settlements due to pumping were computed analytically (Equation 7) and numerically. Mechanical parameters (*E*) used in the hydro-mechanical numerical, which were obtained applying the Equation 9 and the results from the pumping test

interpretation, are shown at Table 4.2. The results at a distance of 20m from the pumping well are given in Table 4.4. Analytical settlements were 1.9 and 3.1mm for the first and second scenarios, respectively. The numerical model values were 1.6 and 2.2mm. Figure 4.6a displays the depth distribution of the settlements at a distance of 20m from the pumping well. Figure 4.6b shows the radial distribution of settlements at the surface and at the top of the saturated zone.

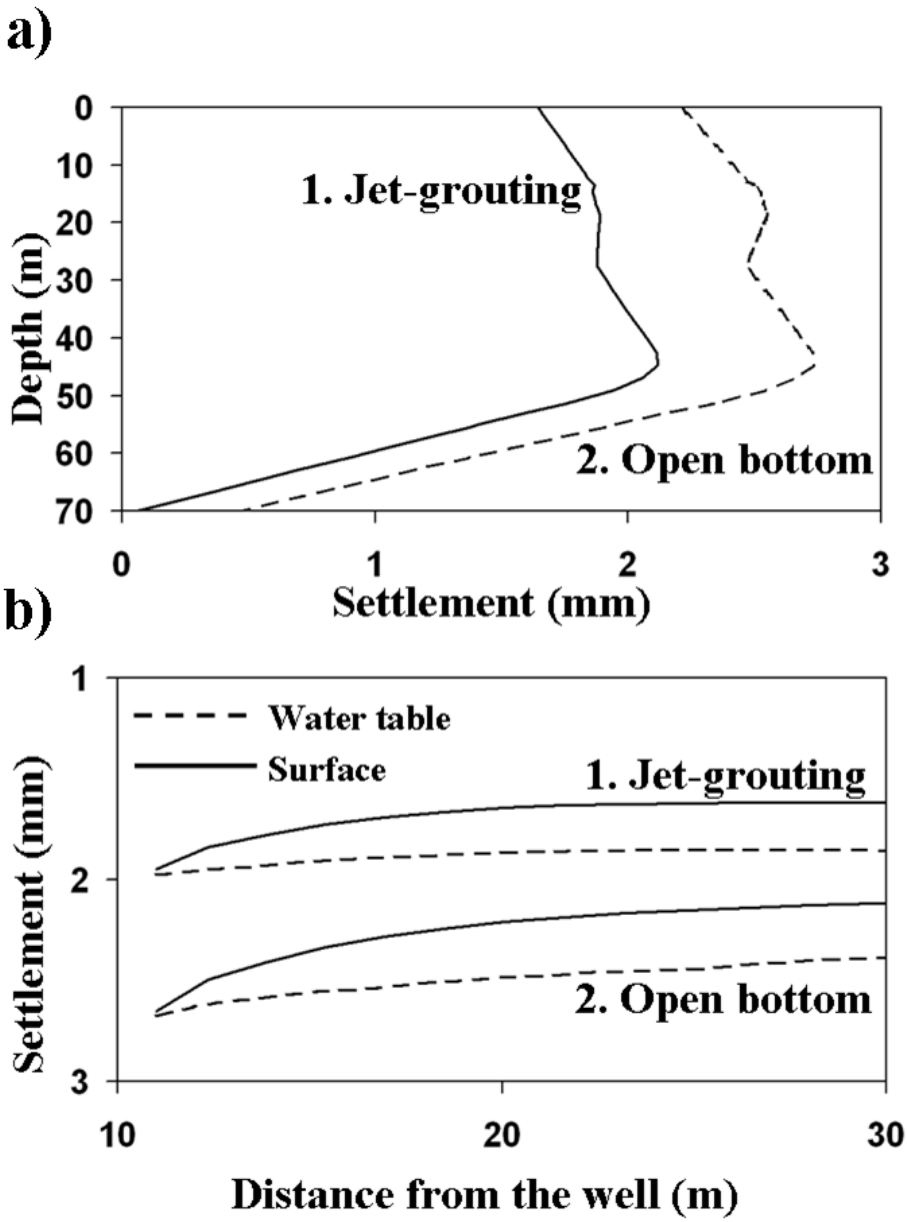


**Figure 4.6.** a) Settlements in depth at 20 meters from the pumping well in the scenarios proposed at Padilla. b) Total settlements at the surface and at the top of the saturated zone at different distances from the pumping well. Results are shown for the scenarios considered at Padilla. Note that the first scenario is the one used to carry out the excavation.

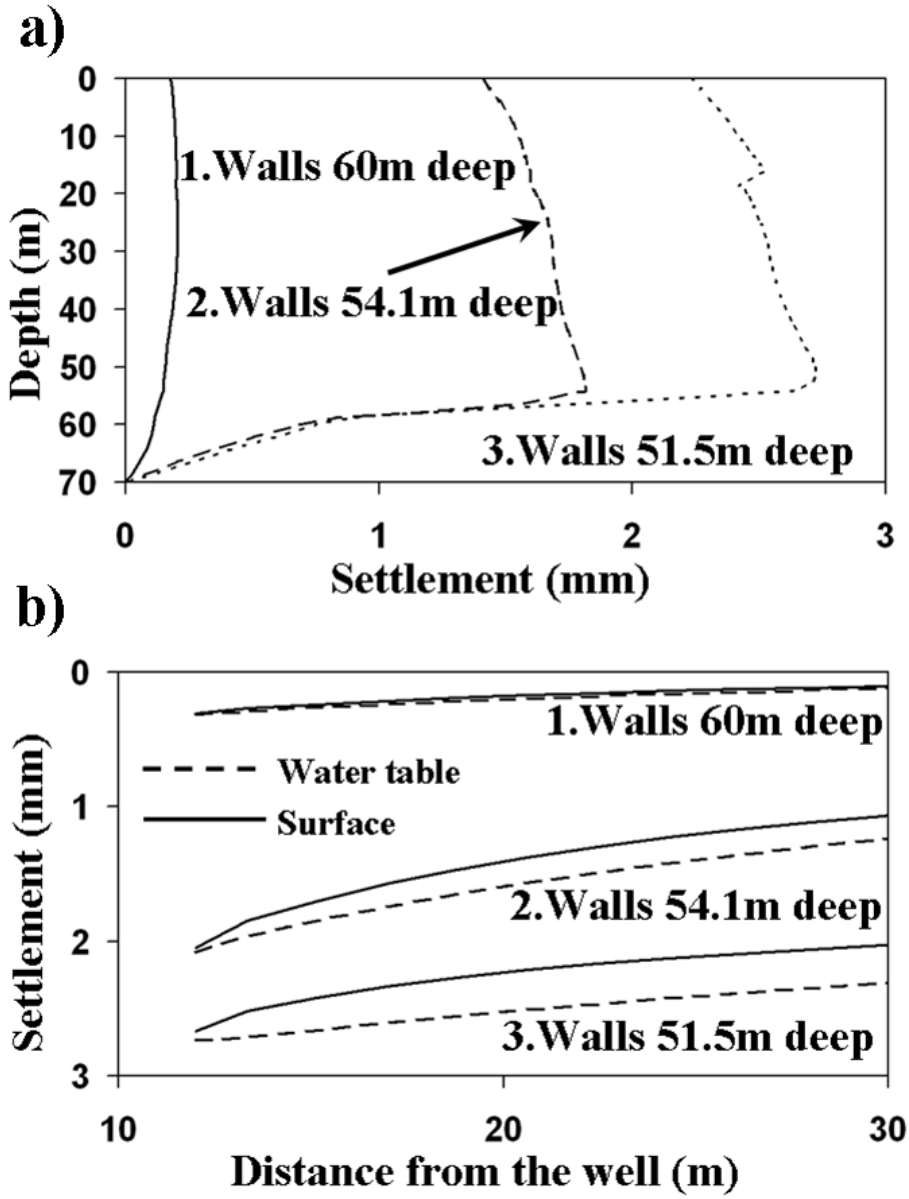


**Figure 4.7.** a) Distribution of settlements in depth at a distance of 20m from the pumping well in the scenarios considered at Bruc. b) Total settlements at the surface and at the top of the saturated zone at different distances from the pumping well. Results are given for the scenarios considered at Bruc. Note that the first scenario is the one used to carry out the excavation.

*4.4.3.2. Bruc site*

Three different scenarios were considered at the Bruc shaft. The first represented the actual enclosure (diaphragm walls reached a depth of 60m). The enclosures of the two other scenarios were shallower depending on the depth of the more transmissive

layers. In the second scenario, the diaphragm walls reached a depth of 54.1m, and in the third, a depth of 51.5m.

Drawdown in the well was calculated for the three scenarios to ensure safety conditions at the bottom of the excavation (Equation 4). The drawdown was 25m for the first, and 30m for the second and third scenarios. The corresponding pumping rates were 6, 45 and 520$m^3$/day, respectively.

Like in the Padilla site, the mechanical parameters (*E*) used in the hydro-mechanical numerical model to compute the soil displacements are shown at Table 4.3. These also were obtained applying the Equation 9 and the results from the pumping test interpretation. Figure 4.7a shows the vertical variations of the numerical settlements at a distance of 20m from the pumping well. The settlement is negligible in the first scenario. The maximum settlement in scenarios 2 and 3 is located at the bottom of the diaphragm walls. Figure 4.7b shows the total settlements at the surface and at the top of the saturated zone with respect to the distance from the pumping well. Analytical and numerical predictions of the settlements and of the pumping rate in the three scenarios are given in Table 4.5.

| Scenario | Settlement (mm) | | Pumping rate ($m^3$/d) |
|---|---|---|---|
| | Analytical | Numerical | |
| 1.Walls 60m deep | 0.001 | 0 | 6 |
| 2.Walls 54.1m deep | 1 | 1.5 | 45 |
| 3.Walls 51.5m deep | 2.4 | 2.3 | 520 |

**Table 4.5.** Predicted settlements calculated analytically and total pumping rate calculated numerically for the scenarios considered for the shaft at Bruc.

### 4.4.4. Actual Dewatering evolution

The solutions adopted to construct the enclosures were those that minimized pumping (i.e. the first scenarios at the two sites). As a result, no drawdown was measured outside the enclosure at Bruc. The enclosure reached an impervious layer and had no defects. For this reason, only the data collected during the excavation at the Padilla shaft are included in this study. Dewatering of the Padilla excavation started when the enclosure (diaphragm walls + jet-grouting) had been completed. It was executed by using four pumping wells (Figure 4.8a). Settlements were measured at the

monitoring points shown in Figure 4.8a. Figure 4.8b displays the evolution of the head during the dewatering at PZ4 and at one pumping well. Four pumping steps corresponding to the initiation of the pumping wells can be observed. The maximum drawdown was 45 meters inside the enclosure and some 20 meters outside the enclosure.

Figure 4.8c displays the evolution of the settlements at the 5 monitoring points. The elastic behaviour of the soil could be observed during the pumping test performed in mid May 2010. The surface settled during pumping (first half of the "test 2", shaded interval), but recovered its position when pumping ceased (second half of the shaded interval). Most settling occurred when pumping was not active and ground water heads were stable. A moderate fall of 1mm is observed in the plot between the second pumping test and the start of the excavation. Since the drop is homogeneous at all the monitoring points and since the jet-grouting enclosure was completed before the second pumping test, this drop can be attributed to a strain redistribution after injection of the grout and construction of the wall panels.

It may be observed that the rate of settling decreases, to the point and readings become stable until mid-June when the soil started to rise. This growth was about 0.5 and 0.8mm. The magnitude depends on the monitoring point. Subsequently, when the excavation ceased, which occurred approximately on 20 June, a sharp drop is observed in the plot. The drop, which was about 1mm was similar at all the monitoring points. A portion of this latter drop (0.8mm) was recovered at all the points when pumping stopped (on 30 June). .

The excavation stage started at the end of May, before the dewatering stage, which began when the excavation reached the water table. The decrease in the rate of settling, the stabilisation measured in late May, the rise observed on 15 June and the fact that settlements due to pumping were not observed at the beginning of dewatering are attributed to the rebound due to the unloading caused by the excavation (Zhang, *et al.,* 2013). In fact, pumping settlements were only observed when the excavation stage ceased. During the first stages of the dewatering stage, settlements due to pumping were probably compensated by the heave caused by the excavation process. They were not observed for this reason.

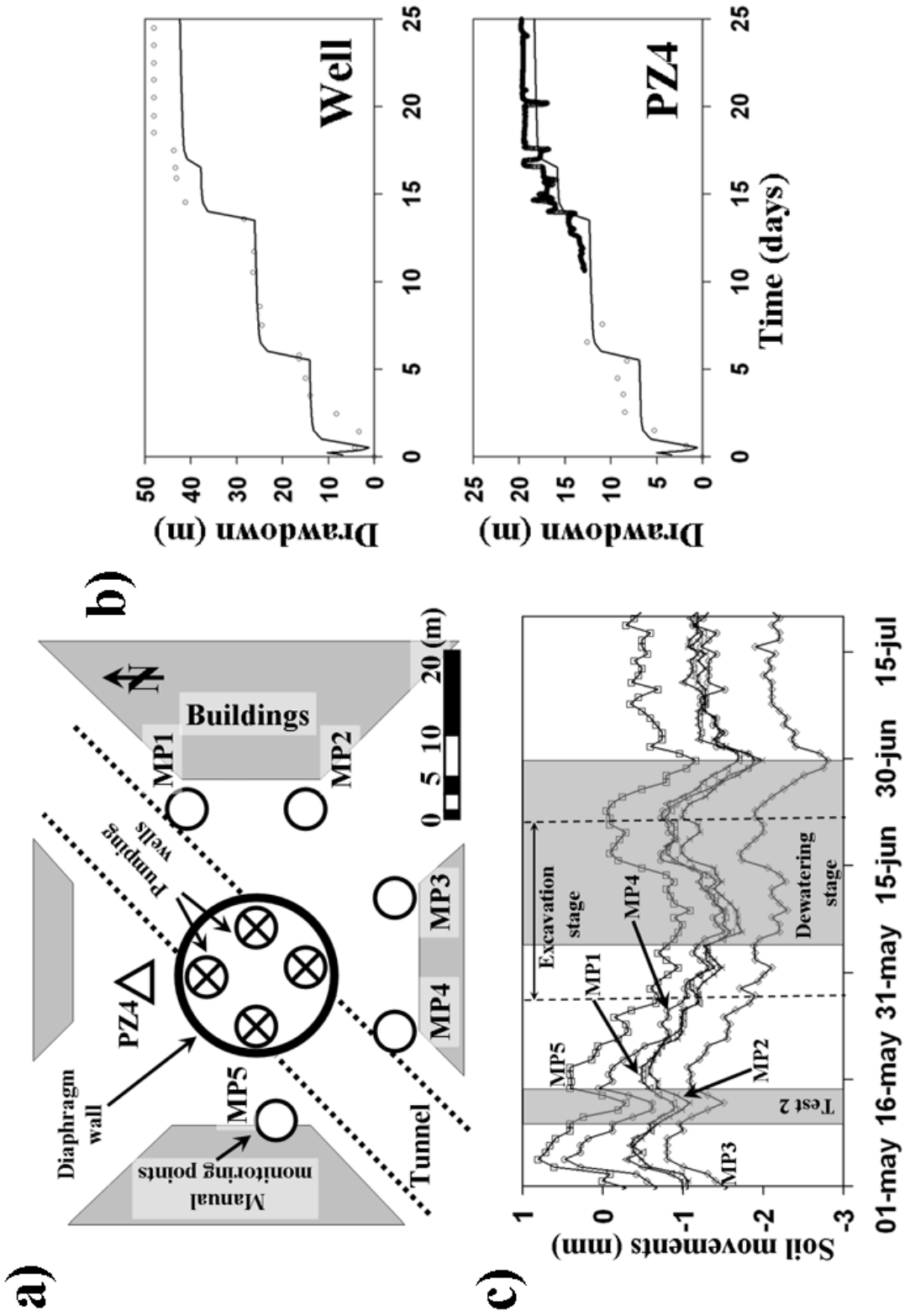


**Figure 4.8.** a) Plan view of Padilla during the dewatering. Circles are the monitoring points to measure the soil movements (MP1, MP2, MP3, MP4 and MP5). b) Measured (dots, notice that they are closely spaced at late time in PZ4) and computed (line) drawdowns from one of the pumping wells and the piezometer (PZ4) during the dewatering stage. c) Soil movements measured at the monitoring points (MP1 to MP5) at Padilla during construction.

The dewatering simulation gave suitable fits at PZ4 and at the pumping well (Figure 4.5b). The other piezometers proved to be unusable owing to the damage they suffered during the works. The computed numerical settlements were 1.6mm and the analytical, obtained with Equation 7, were 2.6mm. Both values were bigger than the movements observed (Figure 4.8c). The differences between the computed and the measured movements may be attributed to two factors. On the one hand, settlements were calculated at the steady state, which was not reached during dewatering. On the other hand, the rebound of the soil due to the unloading induced by the excavation, which was not modelled, gave rise to a contrary movement with respect to the pumping settlements. Therefore, the observed movements were the pumping settlements minus the soil heave due to the excavation.

## 4.5. Discussion

A number of measures are adopted to minimise soil movements when a deep excavation is undertaken under the water-table in an urban area. Quite often the design of pumping becomes an important issue in this context.

A dewatering system was designed to perform the shaft at Padilla with short diaphragm walls. But the enclosure was lengthened with jet-grouting piles to minimise drawdowns outside and to reduce the settlements caused by the dewatering. While jet grouting was originally developed to increase the shear strength of the soil, it is generally assumed that it can also be used to waterproof excavations. This concept is largely based on the results of laboratory tests (Allan and Kukacka, 1995), which suggest a very low permeability. However, because of the ideal conditions used in the laboratory the permeability may differ in the field. In fact, some un-grouted portions should be expected in patches of coarse sediments, which cannot be reached by the jet (Vilarrasa, *et al.,* 2012). These patches could concentrate groundwater flow and increase the effective permeability.

The hydraulic conductivity of the jet-grouting enclosure at Padilla was calculated by means of two pumping tests. One test was performed before the construction of the enclosure and the other subsequently. The results show that jet-grouting reduced the hydraulic conductivity of the area where it was performed, but

pumping was still necessary. The permeability of the area was reduced from 5.5 to 0.6 m/d. This value is in the range of the permeability of silty-sands. The reduction in permeability was significant (90%), but restricted to the jet grouting width, so that the reduction in the required pumping rate after comparison of the scenarios with and without jet-grouting was much smaller (from 2150 to 1300 $m^3$/day, or 40%)..

Two scenarios with different enclosure depths were compared at the Padilla shaft. In the first, the enclosure was 61.5m deep and consisted of diaphragm walls up to a depth of 46.5m and jet-grouting piles below. The second scenario involved only the use of the diaphragm walls. In terms of total enclosure surface, the first scenario required an additional 1182$m^2$ of jet-grouting which considerably increased the cost.

The results show that although the settlements are reduced when the enclosure is deeper they do not disappear. The total settlement with the shallow enclosure at 20m from the pumping well was 2.2mm (3.1mm if calculated analytically) whereas with the deeper enclosure it was 1.6mm (1.9 when calculated analytically). Their magnitude was similar and no dewatering scenario would have posed a risk to nearby buildings. Similarly, the pumping rate is reduced when the enclosure is lengthened, but it cannot be eliminated, because it is still necessary to guarantee stable conditions at the bottom of the excavation.

The results of the first scenario (diaphragm walls and jet-grouting), which was employed at Padilla, were compared with field measurements. The measured settlements during the construction show that the soil was stiff and its behaviour was elastic. Thus, the settlements due to pumping were small and recovered when pumping ended. Moreover, they were spatially smooth (i.e., differential settlements are small). Measured and computed settlements did not fit perfectly. Model results (analytical and numerical) were higher than the real measurements, although the difference was small (and the numerical ones slightly better). This can be attributed to the fact that computed settlements were obtained for steady state conditions, which was not achieved during dewatering. Moreover, the soil rebound due to the excavation that causes soil movements against the pumping settlements was not modelled. But, numerical and measured settlements may be comparable if these two considerations are taken into account. In such case, numerical predictions can be considered as a suitable option to approximate pumping settlements. The difference between the analytical and the

measured settlements was higher because the analytical solution considers that all the displacements occur in the vertical direction, which is not correct. But, still, the deviation is not high and the analytical methodology can also be used to approximate the values of pumping settlements in preconsolidated soils. Thus, both methodologies are useful for comparing the pumping settlements in several scenarios.

The storage coefficient of the soil, which was obtained from a pumping test, was used to determine some mechanical parameters of the soil. This is important because the mechanical properties were obtained without modifying the soil, which is not possible when mechanical parameters are calculated in the laboratory or from field tests in boreholes. In fact, preliminary estimations of settlements due to dewatering provided values well above the limit of 5 mm imposed by the Administration, because elastic parameters from field pressurometer tests under unloading-reloading paths were used for the analyses. Thus reducing all type of settlements became a priority. The experience gained from the dewatering confirms the high nonlinear behaviour of the elastic regime of the Barcelona Quaternary deposits. There are two factors that may explain this discrepancy: first, the strain level applied in the test, higher than the one applied in the pumping activities and, second, the breaking of cementation present in the quaternary clay, during the boring and installation of the pressurometer, thus giving a softer response for the soil.

The results from the Bruc shaft were similar. Pumping effects were computed and compared for three different scenarios. The depth of the enclosure was reduced in accordance with the position of the more permeable layers, which were identified with the pumping test and the geological description. In the first scenario, the diaphragm walls reached a depth of 60m depth (equal to the enclosure used to perform the shaft). In the second scenario, the diaphragm walls reached a depth of 54.1m, which entails a reduction of 730$m^2$ of diaphragm walls. In the third scenario, the diaphragm walls reached a depth of 51.5m, which involves a cumulative reduction of 1050$m^2$ of diaphragm walls. The results show that drawdown and settlements rise as the enclosure depth is reduced. But the magnitude of the increase is not high. On one hand, numerical results show that surface settlements were negligible in the first scenario, whereas they were 1.5mm in the second and 2.3mm in the third scenario. On the other hand, analytical settlements were also insignificant in the first scenario, while they were 1mm in the second and 2.4mm in the third scenario. Note that the maximum settlement was

attained at the bottom of the diaphragm walls. The settlements outside would not pose any risk to nearby buildings in any of the three scenarios, both because they would be very small and because they would not be differential, which is consistent with the observations at Padilla. The pumping rate necessary to achieve safe conditions is also increased. But its magnitude indicates that water could be pumped by using only one pumping well located in the middle of the excavation. The pumping rate increased from 6 (in the first scenario) to 520$m^3$/d (in the third scenario).

Therefore, the extra-cost of lengthening enclosures is not borne out by the results. If the soil is preconsolidated, excavations can be cheaper by combining short enclosures with pumping methods. If the soil is normally consolidated, the movements caused by pumping will be larger. In such a case, a non-linear coupled hydro-mechanical analysis should be performed to predict the movements prior to the construction of the enclosure. However, the estimation of the mechanical parameters is the crucial issue.

## 4.6. Conclusions

A number of conclusions may be drawn from the field measurements and from the analytical and the numerical results presented in this study.

The jet-grouting technique was invented to improve the shear strength of the soil. This capacity is not discussed since these properties have already been tested on several occasions. Jet-grouting is also used to waterproof soil and reduce the pumping effects outside excavations that need dewatering. This study demonstrates that the reduction in the hydraulic conductivity of a soil treated with jet-grouting may not be sufficient to eliminate drawdown and settlements outside enclosures. The hydraulic conductivity of jet-grouting is relatively high when used in coarse permeable soils. This fact is consequence of the lack of uniformity of the diameter of jet-grouting columns (Modoni *et al.,* 2006, Flora *et al.,* 2013 and Shen *et al.,* 2013c) and of the difficulties arising when this is performed in a coarse soil (the cement cannot be mixed effectively with sand soil) (Shen *et al*., 2009 and Shen *et al.,* 2013a). However, the technology is being improved, during the last years, to increase the uniformity of jet-grouted columns (Shen *at al.,* 2013a and Shen *et al.,* 2013b). As a result, pumping may still be necessary

to guarantee safe conditions during excavation. The effects of pumping were observed at Padilla although the enclosure was lengthened with jet-grouting piles. Drawdown measured outside the enclosure was high. However, settlements were relatively small. This is due to the preconsolidated state of the Barcelona soil, which therefore displays a relatively low compressibility and an elastic behaviour for the stress level involved in the dewatering activities described.

Two methodologies to calculate the pumping effects in preconsolidated soils are presented in this study. The analytical method, which considers that all the deformation takes place in the vertical direction, allows us to calculate settlements with a moderate error. The numerical method, whose results were also comparable with the measured values, considers that displacements can be in any direction. Both methodologies give suitable results considering that these were obtained in steady state and that the methods did not take into account the heave of the soil because of the excavation process. However, both methodologies are useful to approximate pumping settlements because the errors are relatively small and the predicted values are higher than the measured ones with the result that safety is not compromised.

Mechanical parameters necessary to predict soil movements caused by pumping were obtained from the storage coefficient of the soil, which was determined by a pumping test. This modus operandi is advantageous because it does not modify the soil properties as is the case of laboratory tests or mechanical field tests performed in boreholes.

Enclosures are often lengthened to reduce pumping effects, which considerably increases the cost of the excavation. However, these safeguards are not necessary in preconsolidated soils, provided that the stress level applied during dewatering does not exceed that preconsolidation stress (Sneed, 2001). In this study, a number of scenarios are analysed at both sites by varying the depth of the enclosure. None of the scenarios yield significant absolute settlements and the differential values are negligible. The extra-cost generated by lengthening the enclosure is not offset by the reduction in the pumping rate and in the pumping effects outside. The aforementioned safety precautions adopted at Bruc and Padilla were taken because the construction of the tunnel adjacent to the Sagrada Familia Basilica was a matter of concern in the city. In fact, a committee

appointed by UNESCO acted as external observers. That concern explains the low limits of allowable settlements imposed by the Administration in this particular case.

# 5. Hydraulic characterization of diaphragm walls for cut and cover tunnelling

## 5.1.Introduction

Tunnel construction through an aquifer under the water table can be complex. A number of methods can be adopted (Forth, 2004). A frequent choice for shallow tunnels is the "Cut and Cover Method" combined with drainage wells. The "Cut and Cover Method" consists in excavating under the protection of diaphragm walls (Gulhati and Datta, 2005). Diaphragm walls ensure that the excavation walls are stable and prevent lateral groundwater from entering the excavation. The main steps of this method are as follows (Figure 5.1):

1. Construction of diaphragm walls.
2. Drainage of the space between diaphragm walls using pumping wells.
3. Excavation of the space between diaphragm walls until the desired level.
4. Construction of tunnel vault and floor.
5. Filling of the gap between the vault and the ground surface

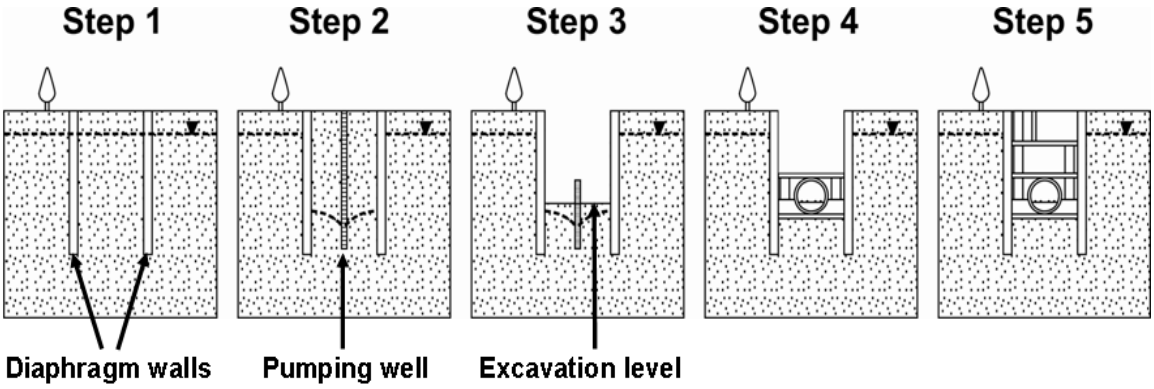


**Figure 5.1.** Cut and cover method steps.

Drainage must be continuous from step 2 through 4 in order to ensure dry conditions and the stability of the soil. Excavation with the "Cut and Cover Method" is not complicated, but unforeseen events during excavation can lead to serious problems (Rienzo *et al.,* 2008). Openings are relatively frequent in the construction of diaphragm

**This chapter is based on the paper: Pujades, E., Vázquez-Suñé, E., Carrera, J., Jurado, A., 2013. Dewatering of a deep excavation performed in a low permeability soil. Submitted.**

walls (Bruce *et al.,* 1989). If the openings are located above the excavation level, inflows may drag sediments, leading to the formation of sink holes outside the enclosure, which results in damage to nearby buildings (Pujades *et al.,* 2009). If the openings are located below the excavation level, inflow through them may cause a reduction in shear strength of the soil between diaphragm walls, leading to structure instability, bottom raising, bottom liquefaction and settlements (Xu *et al.,* 2009). These situations not only endanger the lifes of workers but also pose a threat to the works and, in urban areas, to adjacent buildings. Defects in the diaphragm walls detected before the excavation stage are relatively easy to repair by injecting sealing substances. However, defects spotted after excavation (step 3) are much more difficult and costly to repair because pumping cannot be interrupted to ensure the stability of the bottom of the excavation. Thus, groundwater flowing through the openings tends to drag the injected sealing substances. The question is whether it is possible to detect defects in the diaphragm walls before excavating.

Geophysical and hydrogeological methods can be used to spot openings. A typical geophysical method is crosshole sonic logging, which essentially consists in measuring the transit time of a sonic signal across the concrete (Paikowsky and Chernauskas, 2003; Rausche, 2004). High velocity indicates continuous concrete whereas slow velocity suggests a defect. The transmitter and receptor are introduced into two tubes separated by a given distance and set inside the diaphragm wall during its construction (Hollema and Olson, 2003). However, only the concrete between the access tubes can be assessed and the results may be influenced by a number of factors (White *et al*., 2008). Given that the access tubes must be cast during the construction of the diaphragm walls, they may break, fill up with concrete or become displaced, which makes them unusable. As an example, only five tests, out of the sixteen planned, could be performed in an excavation during the construction of high speed tunnel in Barcelona.

Hydrogeological methods consist in observing the response of groundwater to pumping (Ross *et al*., 1998; Knight *et al*., 1996; Vilarrasa *et al.*, 2011). If water levels drop as expected, it may be concluded that the enclosing system is satisfactory. Otherwise, repairs may be needed. This approach is advantageous because pumping and observation wells are essential to the construction (step 2) with the result that the only extra cost is that of data interpretation. Despite the potential interest in hydrogeological

methods, there are few studies in the literature. Most research concentrates on methods to calculate water inflows to tunnels constructed below the water table (Meiri, 1985; El Tani, 1999, 2003; Lei, 1999; Hwang and Lu, 2005; Park *et al.,* 2006; Kolymbas and Wagner, 2007; Li, *et al.,* 2009; Font-Capo, *et al.*, 2011). But little research focuses on the detection of hydraulic defects.

The only specific publications are those of Ross *et al*., (1998), Knight *et al*. (1996) and Vilarrasa *et al.* (2011). Ross *et al*., (1998) proposed a solution for evaluating the efficiency of the system. This solution consists in observing the spatial distribution and temporal evolution of water levels inside and outside the enclosed area. These authors did not seek specifically to calculate the effective transmissivity of the diaphragm walls or the location of the openings. Knight *et al.* (1996) analyzed a case of drainage on a large square closed perimeter in the United Kingdom. They used the ERNA (Electrical Resistance Network Analogue Model) to calculate steady state drawdown versus hydraulic conductivity of the diaphragm walls. The resulting graph allowed the evaluation of the hydraulic conductivity of the diaphragm walls using drawdown recorded in the area after a long pumping period. These authors observed that small defects in diaphragm walls can significantly alter their effective hydraulic conductivity. They sought to measure the drawdown outside the enclosure, but this is not practical for linear enclosures (e.g. highway or railway tunnel) given the need for a large number of observation points. Moreover, steady state may take a very long time to reach in some situations. Although the ultimate objective of the aforementioned works is essentially similar to what is proposed in the present chapter, these works cannot be implemented in other scenarios. Vilarrasa *et al*. (2011) developed a methodology to characterize the walls of a circular enclosure. The methodology, which is based on type curves to fit the observed time evolution of drawdowns, may be applied in different scenarios. However, in order to apply this methodology, drawdown must be measured outside the enclosure, which as stated above is not practical in linear excavations. Moreover, the methodology by Vilarrasa *et al*. (2011) is useful in circular enclosures but not for characterizing the diaphragm walls of linear excavations. Therefore, the question remains as to whether it is possible to characterize the diaphragm walls of linear enclosures using a methodology that is straightforward and generally applicable. The present chapter seeks to analyze the groundwater behaviour under different diaphragm wall conditions in an attempt to obtain a suitable methodology.

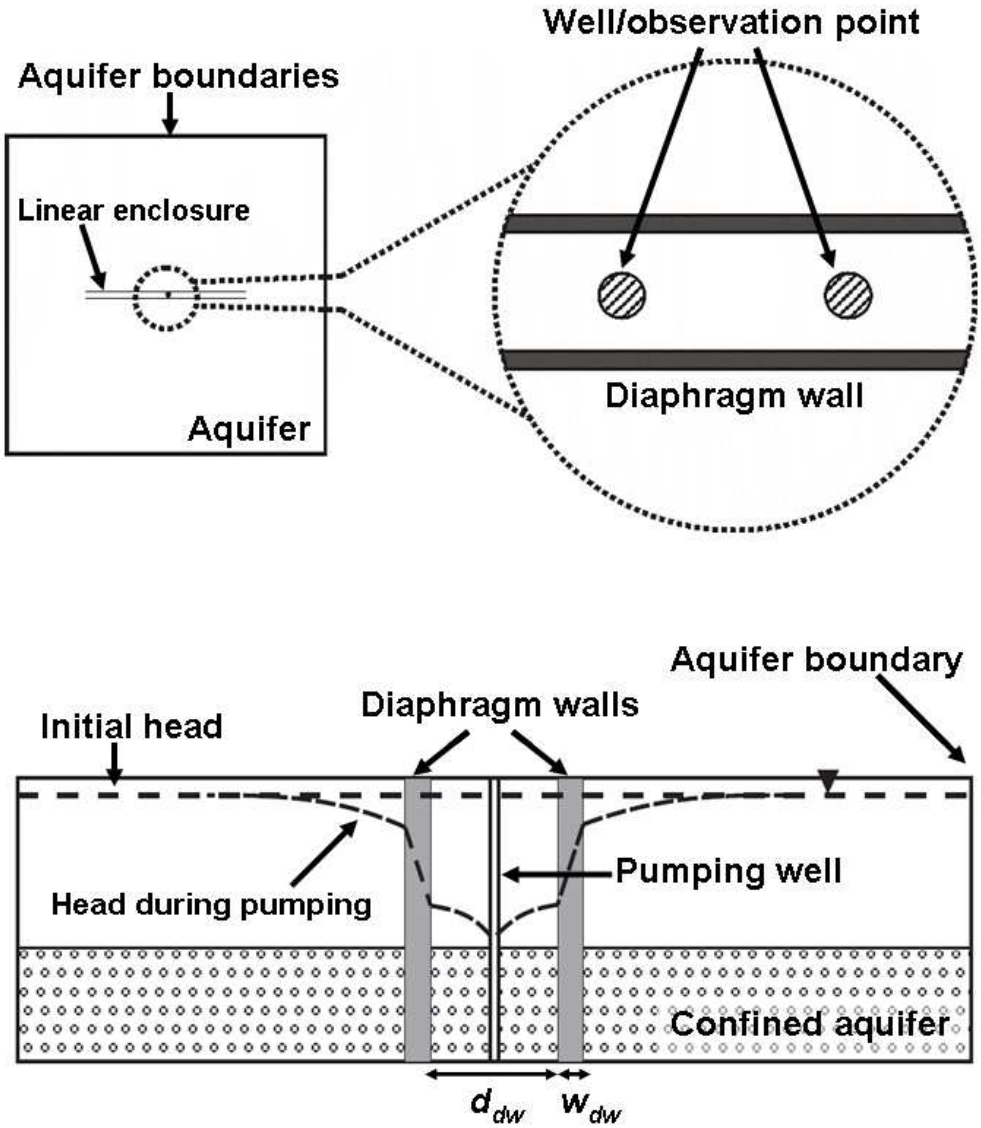


**Figure 5.2.** Problem statement. Above, plan view of the enclosure (general and detail of the middle). Below, schematic cross section where is shown the diaphragm walls and the pumping well.

## 5.2. Methods

### 5.2.1. Problem statement

The problem is formulated as shown in Figure 5.2. A tunnel is excavated below the water table using the "Cut and Cover Method" in a uniform confined aquifer. The diaphragm walls or similar supporting methods penetrate down to the base of the aquifer. It is assumed that the diaphragm walls are open at both ends of the underground construction. A pumping well is located in the centre of the excavation. The aquifer has

sufficient extension to ensure that the pumping cone does not reach the boundaries. Two types of problems are considered:

1. Homogeneous diaphragm walls are modeled with several values of effective conductance. Actually, diaphragm walls are heterogeneous bodies with very high conductivity contrasts between sections of concrete, where conductivity can be very low (Neville, 1995; Gens *et al.,* 1999), and the openings, where the aquifer conductivity may remain unchanged. Well constructed diaphragm walls do not present openings and their hydraulic conductivity is low. Diaphragm walls whose defects are uniformly distributed along the enclosure are regarded as homogeneous.

2. Heterogeneous diaphragm walls are modeled by simulating discontinuities with different characteristics (size and location with respect to the pumping well). We consider heterogeneous diaphragm walls with low hydraulic conductivity (e.g. $10^{-6}$ m/d) that have at least one opening.

The observation points are located at different distances from the pumping well, but in contrast to that proposed by Knight *et al*., (1996), they are situated between the diaphragm walls for the following reasons: 1) An opening in the enclosure produces a drawdown outside. This drawdown is concentrated around the opening (Figure 5.3), so that a large number of observation points would be needed to detect openings; and 2) wells drilled for pumping can be used as piezometers during the early stages.

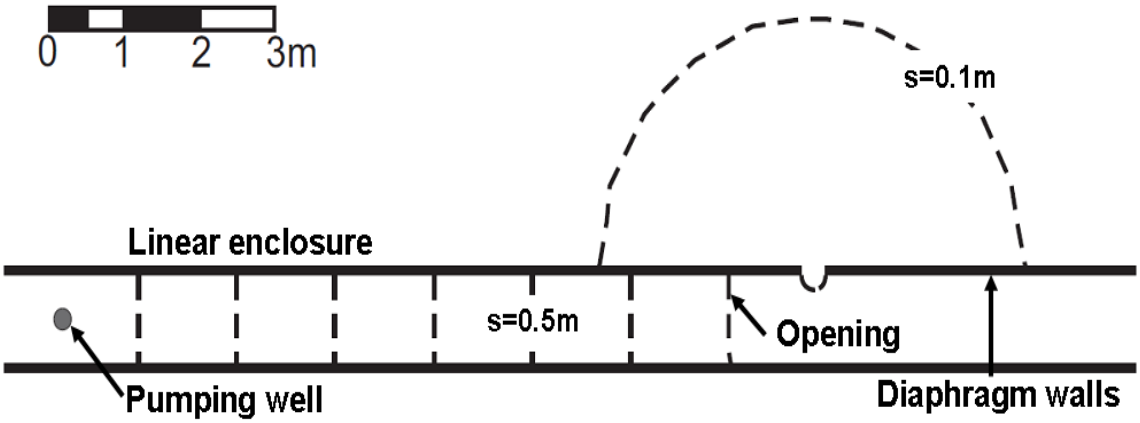


**Figure 5.3.** Steady state drawdown (s) caused by pumping between diaphragm walls. The diaphragm walls have an opening. It is shown the drawdown distribution near the well and the opening. The drawdown in the well is 1 meter. The distance between the diaphragm walls is 1 m. The drawdown distribution is obtained using a numerical model.

### 5.2.2. Mathematical formulation

Transient flow through a confined aquifer is governed by (Bear, 1972):

$$S\frac{\partial h}{\partial t} = \nabla \cdot (T\nabla h), \qquad (1)$$

where $h$ is head, $S$ is storage coefficient (which is assumed constant), $t$ is time and $T$ is transmissivity (also assumed constant throughout the aquifer ($T_{aq}$), except at the diaphragm walls ($T_{dw}$)).

We adopt a zero initial head in order to work with drawdowns. Two types of boundary conditions are considered at the pumping well: fixed flow or head. The former reads

$$Q_p = 2\pi T r_p \left.\frac{\partial h}{\partial r}\right|_{r=r_p} \qquad (2)$$

where $Q_p$ is the pumping rate, $r$ is the radial distance from the pumping well and $r_p$ is the radius of the pumping well. Alternatively, a prescribed head can be imposed at the well. In this case, head is fixed, but equation (2) is still used for computing the flow rate.

Solutions are presented in dimensionless form so that they can be applied to cases with similar geometry but different aquifer parameters. The equations that define the problem in dimensionless form are

$$\frac{\partial h_d}{\partial t_d} = \nabla_d \cdot (T_d \nabla_d h_d), \quad (3)$$

$$Q_d = 2\pi r_d \frac{\partial h_d}{\partial r_d}, \quad (4)$$

where $h_d$ is dimensionless head, $t_d$ is dimensionless time, $T_d$ is dimensionless transmissivity, $Q_d$ is dimensionless pumping rate and $r_d$ is dimensionless radial distance. Dimensionless variables are written as

$$\text{Dimensionless variable} = \frac{\text{Real variable}}{\text{Characteristic variable}} \quad (5)$$

where the characteristic variables for the problem are shown in Table 5.1.

| Type of variable | Characteristic variable | Equation |
|---|---|---|
| Transmissivity | Aquifer transmissivity | $T_c = T_{aq}$ |
| Storage coefficient | Aquifer storage coefficient | $S_c = S_{aq}$ |
| Length | Distance between diaphragm walls | $d_c = d_{dw}$ |
| Flow rate | Pumping rate | $Q_c = Q_p$ |
| Drawdown | Well drawdown | $s_c = s_p = Q_p / T_{aq}$ |
| Time | Pumping time | $t_c = S_{aq} d_{dw}^2 / T_{aq}$ |
| Leakage factor | Diaphragm walls leakage factor | $\alpha_c = T_{aq} / d_{dw}$ |

**Table 5.1**. Characteristic variables. Dimensionless variables are obtained by dividing real units variables by these characteristic variables. $T_c$ is the characteristic transmissivity, $S_c$ is the characteristic storage coefficient, $S_{aq}$ is the aquifer storage coefficient, $d_c$ is the characteristic distance, $d_{dw}$ is the distance between the diaphragm walls, $Q_c$ is the characteristic pumping rate, $s_c$ is the characteristic drawdown, $s_p$ is the well drawdown, $t_c$ is the characteristic time and $\alpha_c$ is the characteristic leakage coefficient.

### 5.2.3. Analytical solution for steady-state conditions

A steady state solution can be obtained by assuming that permeability of the diaphragm walls is sufficiently small to ensure that heads outside the wall remain unchanged. Therefore, a solution is only needed within the domain, i.e. inside the diaphragm walls. Integrating Equation (1) along the *y*-direction, dividing by $d_{dw}$, and applying the Gauss theorem leads to

$$S_{aq}\frac{\partial \bar{h}}{\partial t} = T_{aq}\frac{\partial^2 \bar{h}}{\partial x^2} + 2\frac{\alpha_{dw}}{d_{dw}}\left(H_{ext} - \bar{h}\right) + \sum_{i=0}^{N}\frac{Q_i \delta(x_i)}{d_{dw}} \qquad (6)$$

where $\bar{h}$ is the average head across the excavation, $H_{ext}$ is the head outside the diaphragm walls, $\alpha_{dw} = T_{dw} / w_{dw}$ is the leakage coefficient (conductance) of the wall, $w_{dw}$ is the thickness of the diaphragm wall and $x_i$ are the points with either pumping wells or openings in the diaphragm wall, where a flow rate, $Q_i$ , is extracted or added. The steady-state solution is obtained by intervals (see Annex 1)

$$\bar{h}_i = \bar{h}_{i-1}\frac{\sinh\left[\lambda(x_i - x_{i+1})\right]}{\sinh\left[\lambda(x_{i-1} - x_{i+1})\right]} + \bar{h}_{i+1}\frac{\sinh\left[\lambda(x_{i-1} - x_i)\right]}{\sinh\left[\lambda(x_{i-1} - x_{i+1})\right]}, \qquad (7)$$

where $\overline{h}_i$ is the average head in point *I* and $\lambda$ is the inverse of a characteristic distance (see Annex 1) given by

$$\lambda = \sqrt{2\alpha_{dw} / \left(T_{aq} d_{dw}\right)} \quad (8)$$

Note that $\lambda^2$ is a dimensionless leakage of the diaphragm walls and that the inverse of $\lambda$ is the length of the diaphragm walls affected by pumping when the pumped flow is equal to the flow that crosses the diaphragm walls. Therefore, if this length is greater than the distance between critical points $x_i$, the flow across the walls can be neglected. Conversely, if the distance between pumping wells is much smaller than $1/\lambda$, pumping will be balanced by the flow across the walls so that the head between the pumping wells will tend to the aquifer head outside the enclosure. The flow rate is calculated by applying Darcy's law, which yields

$$Q_i = -T_{aq} d_{dw} \lambda \left[ \overline{h}_i \left\{ \operatorname{cotgh}(\lambda(x_i - x_{i+1})) + \operatorname{cotgh}(\lambda(x_{i-1} - x_i)) \right\} + \frac{\overline{h}_{i+1}}{\sinh(\lambda(x_i - x_{i+1}))} + \frac{\overline{h}_{i-1}}{\sinh(\lambda(x_{i-1} - x_i))} \right] \quad (9)$$

Applying equation (9) to all singular points such as pumping wells or openings yields a linear system of equations, in terms of heads. Once heads at all singular points, $\overline{h}_i$, have been computed, head at each point in an interval can then be computed using Eq. (A.8) in Annex 1.Building this system requires either knowing, $Q_i$ or expressing it as a function of $\overline{h}_i$. For example, if the flow rate is extracted by a pumping well, an approximate equation is given by the Thiem solution (Thiem, 1906), applying the image method (Ferris *et al*., 1962)

$$Q_i = \frac{2\pi T_{aq} \left(\overline{h}_i - h_p\right)}{\ln\left(\frac{d_{dw}}{2r_p}\right)} \quad (10)$$

where $h_p$ is the head at the pumping well. In the case of an opening, the flow rate is given by Thiem (1906), applying the image method (Ferris *et al*., 1962)

$$Q_i = \frac{2\pi T_{aq}(\bar{h}_i - H_{ext})}{\left(2\ln\left(\frac{R_{ext}}{a/2}\right)\right) + \left(2\ln\left(\frac{d_{dw}}{a}\right)\right)} \qquad (11)$$

where $R_{ext}$ is the distance outside the diaphragm walls where the drawdown generated by the opening is negligible and $a$ is the size of the opening.

We display the case of diaphragm walls opened at the ends. If these ends were closed by diaphragm walls, the flow rate that enters the ends would be given by

$$Q_i = \alpha_{dw}\bar{h}_i d_{dw} \quad (12)$$

Note that the solution only depends on $\lambda$ and on the location and nature of the openings and pumping wells. The solution is compared with the numerical results in an idealized situation: two pumping wells within a 100 m long enclosure. An opening is located in the middle of the enclosure and the pumping wells are situated 10 m from each end. The head is fixed to the ends and two values of leakage coefficient of the diaphragm walls are simulated ($10^{-6}$ and $10^{-3}$ m/d). Results from the analytical solution are almost identical to those obtained with the numerical model (Figure 5.4). Note that by fitting field observations to the above solution (Eq. (9), (10) and (11)) it is possible to determine the state of the diaphragm walls. Furthermore, this equation is useful for designing a drainage system.

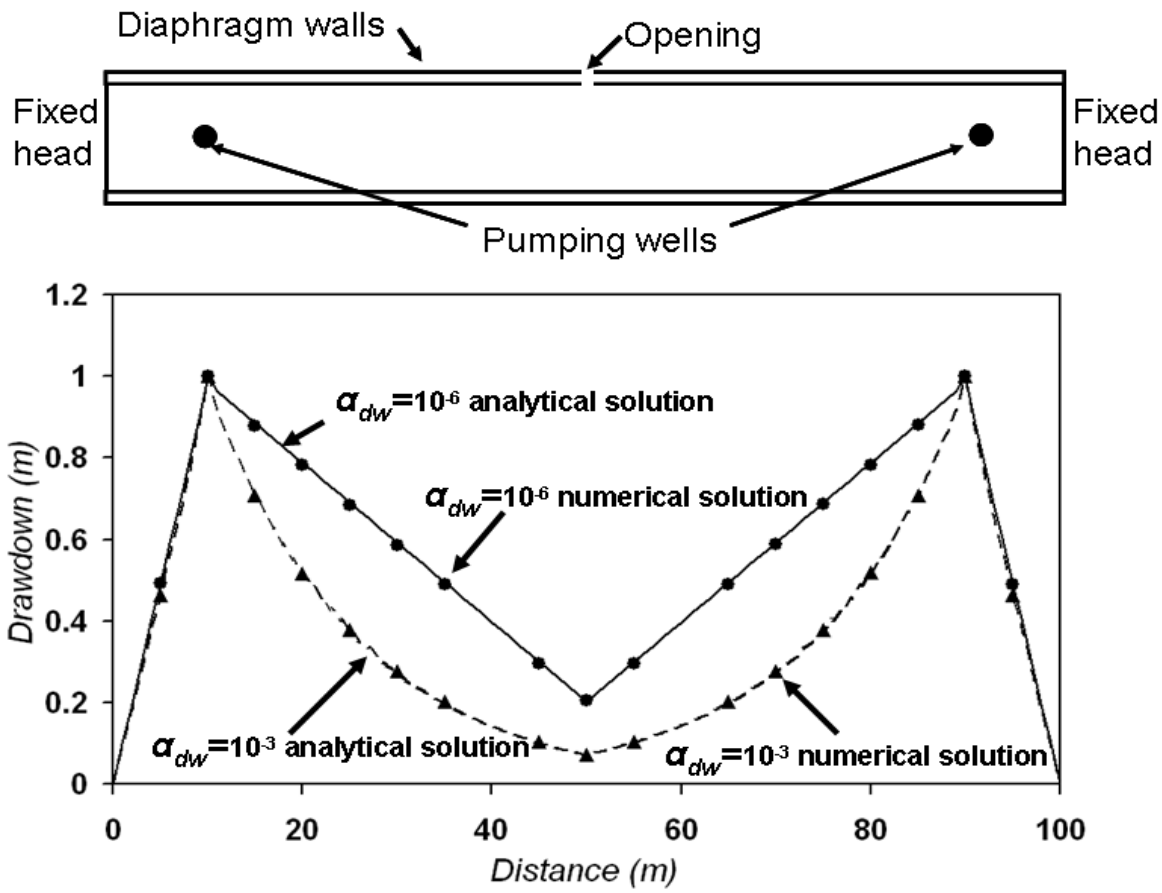


**Figure 5.4.** Drawdown between the diaphragm walls calculated by the model and with the analytical solution using two diaphragm walls leakage coefficient. This comparison enables us to validate the analytical solution.

### 5.2.4 Analytical results for transient conditions

A full transient solution is a possibility, but it would be unduly complex because of the openings. We will therefore rely on numerical solutions. Still, some relevant approximations can be made by analytical means. Two observations should be borne in mind. First, as mentioned in the introduction, the flow behaviour is controlled by the state of the diaphragm walls. Second, the nature of flow may evolve over time (Figure 5.5). During the early and later stages of pumping, the flow is radial and the evolution of heads can be approximated using the Theis equation (Theis, 1935)

$$h_p = \frac{Q_p}{4\pi T_{aq}} W(u). \qquad (13)$$

where $W(u)$ is the well function and $u = 1/(4t_d)$. This solution can be approximated using the Thiem solution(1906) with a transient boundary (Vilarrasa *et al.,* 2010) as

$$h(r) = \frac{Q_p}{2\pi T_{aq}} \ln \frac{r}{R} \qquad (14)$$

where $R = \sqrt{2.25 T_{aq} t / S_{aq}}$ is the radius of the pumping cone, which grows with the square root of time. If head at the well is fixed, this equation can also be used by setting $r = r_w$ and solving for $Q_p$, which would be time dependent (Perrochet et al., 2005).

Flow is linear for intermediate times (Figure 5.5) and the evolution of the flow rate can be calculated using the expression of Ferris *et al*. (1962)

$$q^* = 2 s_p \sqrt{\frac{S_{aq} \cdot T_{aq}}{\pi \cdot t}} \quad , \qquad (15)$$

where *q** is the flow rate drained per unit length.

Equations (14) and (15) summarize the behaviour of flow for 2D (radial) and 1D (linear) conditions, respectively. As shown in Figure 5.5, the behaviour of flow may evolve in time as the cone of depression encounters new impediments to flux.

Typically, the change in flow dimension can be noticed during the interval (0.1*tc, tc*), where *tc* is the characteristic time of a change in flow regime (Figure 5.5). The most important effects (and their respective characteristic times) are the following:

1) Effect of diaphragm walls (Figure 5.5 (1))

$$t_{cdw} = \frac{S_{aq} (d_{dw})^2}{T_{aq}} \qquad (16)$$

where the flow changes from radial to linear. This change is independent of the state of the diaphragm walls because the cone of depression has not reached them yet. Thus, this change is not observed when the distance between the piezometer and the pumping exceeds half the distance between the diaphragm walls.

2) Leakage through diaphragm walls (Figure 5.5 (2))

$$t_{cw} = \frac{S_{aq}\left(\frac{1}{\lambda}\right)^2}{T_{aq}} \qquad (17)$$

this change occurs when the diaphragm walls have a large leakage coefficient. Flow changes from linear to radial. Flow is not completely linear between $t_{cdw}$ and $0.1t_{cw}$ because a radial component of the flow increases with time in this period. However, the difference is usually negligible.

3) Large opening (Figure 5.5 (3))

$$t_{co} = \frac{S_{aq}\left(2d_o - d_p\right)^2}{T_{aq}} \qquad (18)$$

where $d_o$ is the distance between the pumping well and the opening and $d_p$ is the distance between the pumping well and the piezometer. This change is observed when the diaphragm walls are heterogeneous. The flow changes from linear to a mix between radial and linear. This occurs because the flow has a linear component until the pumping cone reaches the ends of the diaphragm walls. In the case where the diaphragm walls are heterogeneous the flow does not behave as radial until a characteristic time equal to $t_{cL}$.

4) Diaphragm wall end (Figure 5.5 (4))

$$t_{cL} = \frac{S_{aq}\left(2L - d_p\right)^2}{T_{aq}} \qquad (19),$$

where $L$ is the distance to the farthest end of the diaphragm walls. At this time, the flow changes from linear to radial. In Equations (18) and (19), the characteristic distance is greater than the distance between the pumping well and the opening or the ends of the diaphragm walls (boundaries). This is because the characteristic distance is equal to the addition of the distance from the piezometer to the boundary and the distance from the boundary to the image well. The image well is located at the same distance from the boundary as the pumping well but in the opposite direction (Figure 5.5). The dimensionless flow rate versus the logarithm of the dimensionless time (when the head is fixed at the pumping well) is plotted in Figure 5.5 to better understand the changes in flow behaviour during pumping. Two types of diaphragm walls are simulated,

homogeneous and heterogeneous. Linear and radial flow rates are also plotted. The changes in flow behaviour are explained above.

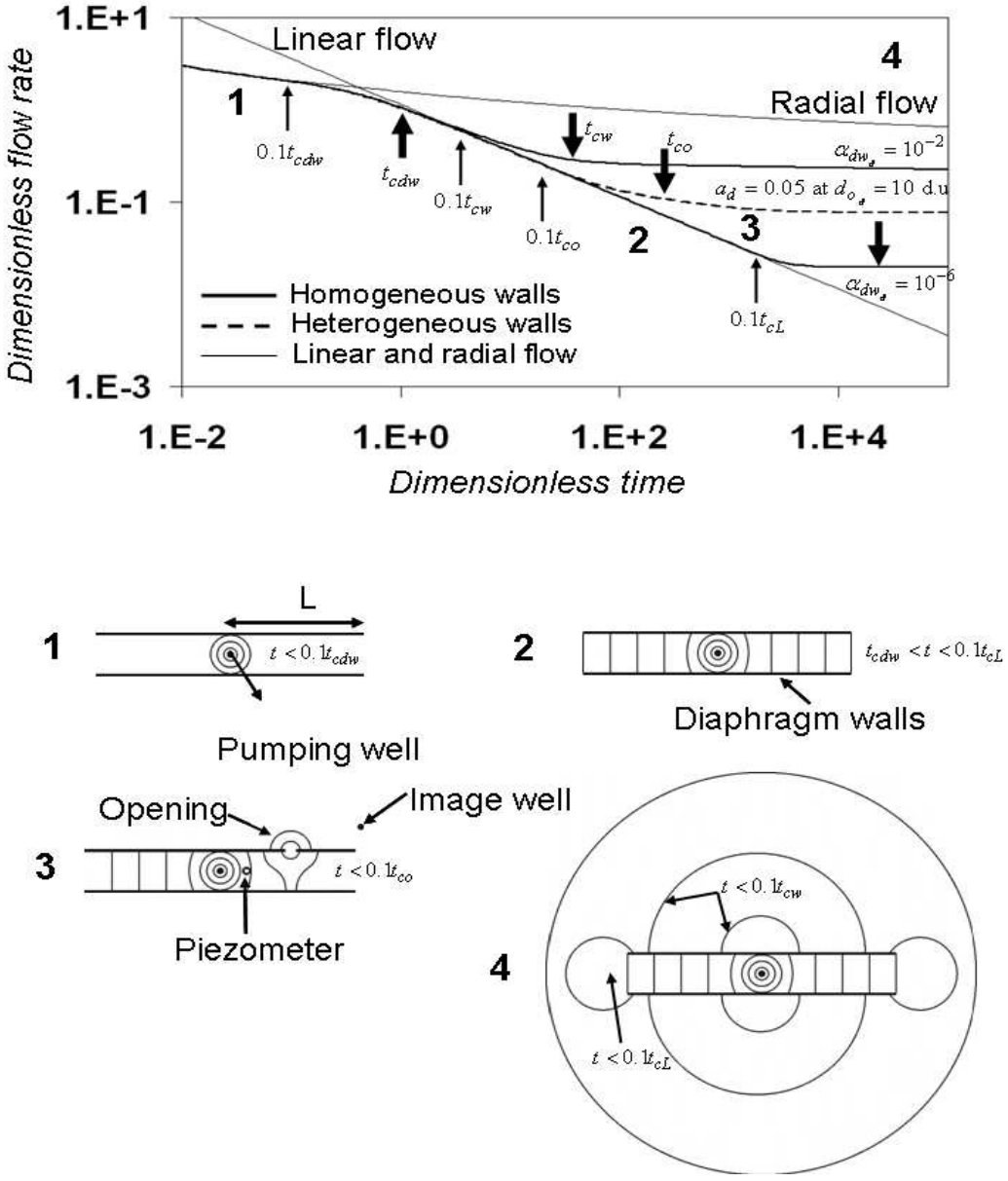


**Figure 5.5.** Flow rate versus time in transient state for different diaphragm walls conditions. Homogeneous diaphragm walls with leakage coefficient of 10-2 and 10-6 dimensionless units (d.u) are considered. The heterogeneous diaphragm walls simulated have an opening at 10 d.u to the pumping well. Flow rates at linear behaviour (Ferris equation) and at radial behaviour (Theis equation) are plotted.

### 5.2.5. Numerical solutions

Numerical solutions are obtained using the finite element code TRANSIN-IV (Medina and Carrera, 2004). The mesh (Figure 5.6) is generated using the mesh module of VISUAL TRANSIN (UPC, 2003), which is a visual interface for working with the TRANSIN-IV code. The numerical models were built in dimensionless units (d.u) and the results will therefore be obtained in a dimensionless form. The pumping well is located in the middle of the model (Figure 5.6). Drawdown is measured at several observation points located between the diaphragm walls. The aquifer boundaries are located too far to be affected by pumping.

Two conditions are studied at the pumping well: fixed head and fixed flow rate. The fixed head is more realistic for representing long term dewatering conditions, but more relevant information is obtained from fixing the flow in transient state, which is not easy to monitor with precision.

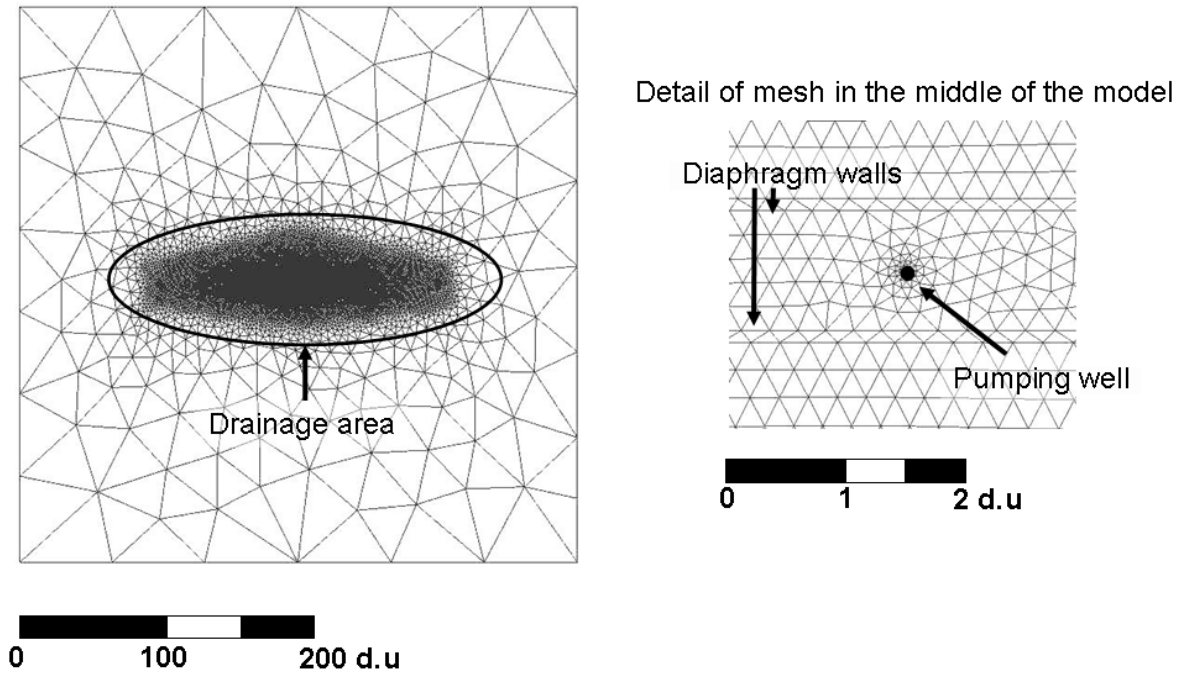


**Figure 5.6.** Model mesh used in the simulations. The element size at the middle of the model is 0.2 d.u and 100 d.u in the boundaries. Left, general view and right, detail of the middle of the model.

As stated in the problem statement section, two types of diaphragm walls are considered, homogeneous and heterogeneous. The leakage coefficient of homogeneous diaphragm walls and the characteristics of the discontinuities in the heterogeneous

diaphragm walls are changed in each simulation. Results are discussed in terms of drawdown and flow rate.

## 5.3. Results

### 5.3.1. Steady state numerical results

Figure 5.7a displays dimensionless drawdown versus dimensionless distance. Drawdown is displayed for half of the enclosure owing to symmetry from the pumping well to the end of the diaphragm walls. Results are shown for two types of diaphragm walls, homogeneous and heterogeneous. The flow rate is fixed at the pumping well, which is 1 dimensionless unit (d.u). It is possible to distinguish between homogeneous diaphragm walls or diaphragm walls with one opening. Diaphragm walls with one opening display heads with an inflexion point at the opening position. Large openings considerably modify head distribution and reduce drawdowns beyond the opening, hindering the identification of openings located further away. Therefore, an option is to analyse the diaphragm walls in short stretches. If an inflexion point is not observed at the head distribution, the diaphragm walls can be regarded as homogeneous and the leakage coefficient can be determined by comparison with the results of the analytical solution proposed in Section 5.2.3 or with the numerical results.

In short, diaphragm walls can be characterized hydraulically with a steady state analysis. However, a large number of observation points are necessary. Moreover, it may take a long time to reach steady state (around $SL^2/T_{aq}$). It is therefore worth studying the problem during its transient state.

A design conclusion can be derived from Figure 5.7. Notice that drawdown is about zero for dimensionless distances around $2/\sqrt{\alpha_{dw_d}}$ or actual distances of about $2/\lambda$. This illustrates again that the distance between pumping wells should be between $1/\lambda$ and $2/\lambda$. This also illustrates the importance of obtaining an estimate of $\lambda$ as soon as possible.

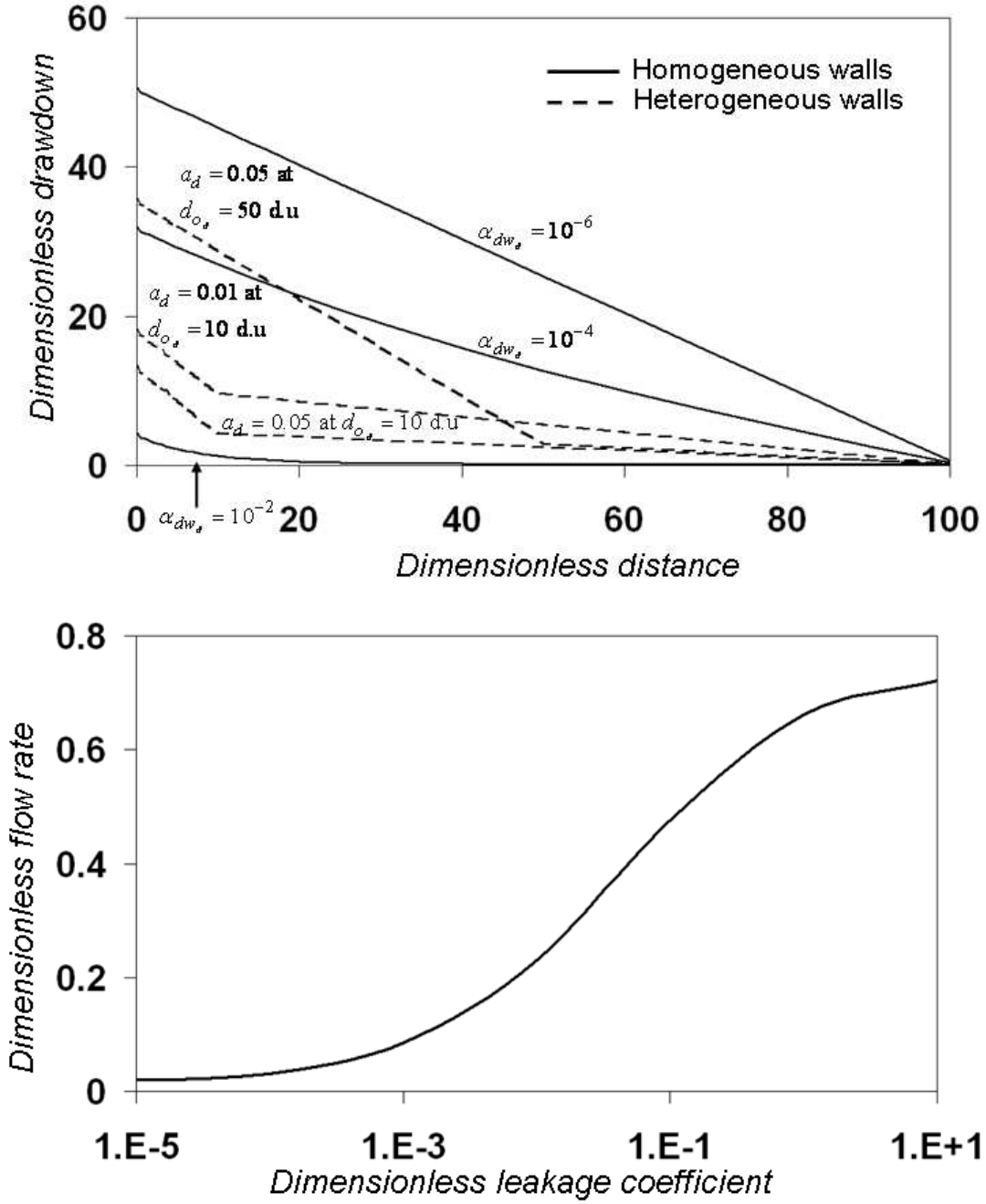


**Figure 5.7.** Above (a), steady state drawdown versus dimensionless distance along the enclosure for prescribed flow at the pumping well. Cases with homogeneous diaphragm walls (continuous lines) illustrate the role of the leakage coefficient, whereas the cases with openings (dashed lines), calculated for $\alpha_{dwd}$=10-6, illustrate the effect of size and distance to the pumping well. $a_d$ is the dimensionless opening size, $\alpha_{dwd}$ is the dimensionless leakage coefficient $\alpha_{dw} d_w / T_{aq} = (\lambda d_w)^2 = \alpha_{dw_d}$ and $d_{o_d}$ is the dimensionless distance between the pumping well and the opening. Below (b), flow rate versus diaphragm walls leakage coefficient.

Figure 5.7b displays the dimensionless flow rate versus the dimensionless leakage coefficient of diaphragm walls for the case where drawdown is fixed at 1 d.u in the pumping well. The pumping rate is independent of the leakage coefficient when its dimensionless value is lower than $10^{-5}$, but increases for higher leakage coefficients. Therefore, significant repairs to improve the hydraulic conditions of the diaphragm walls will be necessary only if the dimensionless leakage coefficient is higher than $10^{-3}$ d.u.

As stated in the problem statement section, two types of diaphragm walls are considered, homogeneous and heterogeneous. The leakage coefficient of homogeneous diaphragm walls and the characteristics of the discontinuities in the heterogeneous diaphragm walls are changed in each simulation. Results are discussed in terms of drawdown and flow rate.

### 5.3.2. Transient state results

Figure 5.8a displays dimensionless drawdown versus dimensionless time for homogeneous and heterogeneous diaphragm walls for prescribed flow rate at the pumping well. The observation point is located at the pumping well. The properties of the diaphragm walls are chosen so that the change in the flow behaviour takes place simultaneously for leakage ($t_{cw}$) and openings ($t_{co}$). This enables us to detect the main differences between the two walls. Thus, the leakage coefficient of the homogeneous diaphragm walls is calculated (equation (8)) for a characteristic distance equal to the distance from the well to the opening in the heterogeneous diaphragm walls. This distance is 10 d.u. The leakage coefficient of the homogeneous diaphragm walls is 0.00125 d.u, so that $t_{cw} = t_{co} = 400\ d.u$. Note that changes in the flow behaviour occur at the characteristic times explained in Section 5.2.3. The most striking feature in Figure 8a is that the departures from the linear behaviour indicate the location of the opening (heterogeneous diaphragm walls) or the leakage coefficient (homogeneous diaphragm walls). However, the head evolution is very similar in both situations (homogeneous and heterogeneous) and it is not easy to distinguish between them.

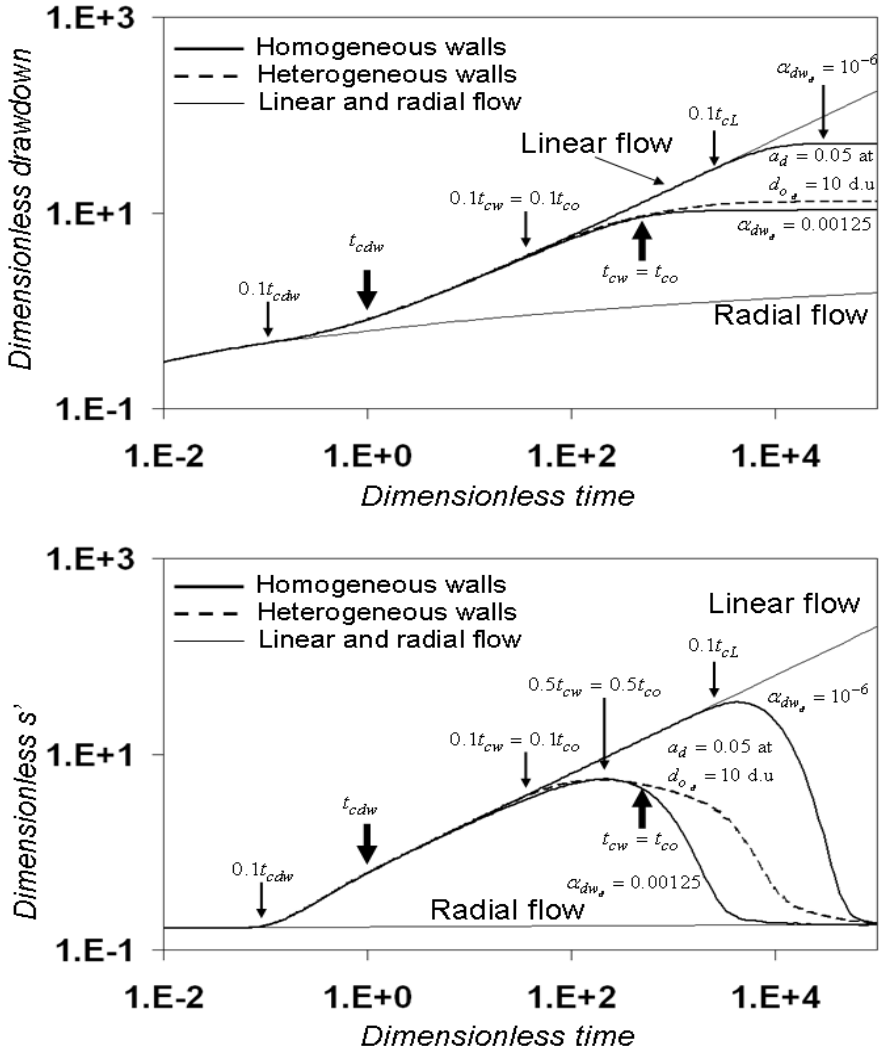


**Figure 5.8.** Above (a), drawdown at pumping well versus time for different states of diaphragm walls. The cases with homogeneous diaphragm walls (continuous lines) illustrate the role of the leakage factor, whereas the cases with openings (discontinuous lines), calculated for $\alpha_{dw_d} = 10^6$, illustrate the effect of size and distance to the pumping well. Drawdowns at linear behaviour and radial behaviour are included (thin continuous line). Below (b), diagnostic plot of drawdown measured at the pumping well with different diaphragm walls states.

Figure 5.8b displays the diagnostic plots calculated from the results shown in Figure 5.8a. The same diaphragm walls, pumping well and piezometer are used. Diagnostic plots consist in calculating the derivate of drawdown with respect to the logarithm of time (*s'*), and in plotting it versus time. The logarithmic derivate is highly sensitive to subtle variations in the drawdown evolution provided that measurements are accurate, the flow rate is constant and the heads are not affected by other perturbations.

Diagnostic plots allow us to detect behaviours that are difficult to observe in the drawdown evolution (Renard *et al.,* 2008). The flow behaviour changes faster to radial behaviour in homogeneous diaphragm walls than in heterogeneous diaphragm walls. The effect of radial flow starts at $0.1t_{cw}$ with homogeneous diaphragm walls and *s'* is maximum at $0.5t_{cw}$, when half of the pumped flow is radial. This proportion increases with time and at $t_{cw}$ the flow is completely radial and *s'* decreases. On the other hand, if the diaphragm walls are heterogeneous, the flow behaviour separates from the linear tendency at $0.1t_{co}$, but it does not become completely radial until $0.1t_{cL}$, when the pumping affects the ends of the diaphragm walls. Therefore, the evolution has a different shape, which allows us to differentiate between homogeneous and heterogeneous diaphragm walls. However, this becomes more difficult when $t_{cw} = t_{co} > 0.1t_{cL}$. Moreover, the evolution after $0.1\ t_{co}$ depends on the size of the opening.

Figure 5.9 displays dimensionless drawdown versus dimensionless time at two piezometers located at 20 d.u and 70 d.u from the pumping well. The flow rate is fixed at the well and again heterogeneous and homogeneous diaphragm walls are simulated. As before, the properties of the diaphragm walls were chosen so that the change in the flow behaviour takes place simultaneously at 20 d.u. from the pumping well. In the heterogeneous diaphragm walls the opening is located at 50 d.u from the pumping well. Therefore, the leakage coefficient of the homogeneous diaphragm walls is $7.8 \cdot 10^{-5}$ d.u. As a result, $t_{cw} = t_{co}$. The initial radial behaviour is not observed in these curves because the distance between the observation point and the pumping well is greater than that between the pumping well and the diaphragm walls. The drawdown measured at 20 d.u shows that both curves, homogeneous and heterogeneous, are similar. The two curves separate from the linear behaviour at the same dimensionless time. But the curves of the drawdown measured at 70 d.u. separate at different times from the linear tendency. While the curve of the homogeneous diaphragm walls separates at the same time as the curve measured at 20 d.u., the curve of the heterogeneous diaphragm walls separates before. Therefore, it is possible to differentiate between homogeneous and heterogeneous diaphragm walls by observing the drawdown behaviour at two piezometers.

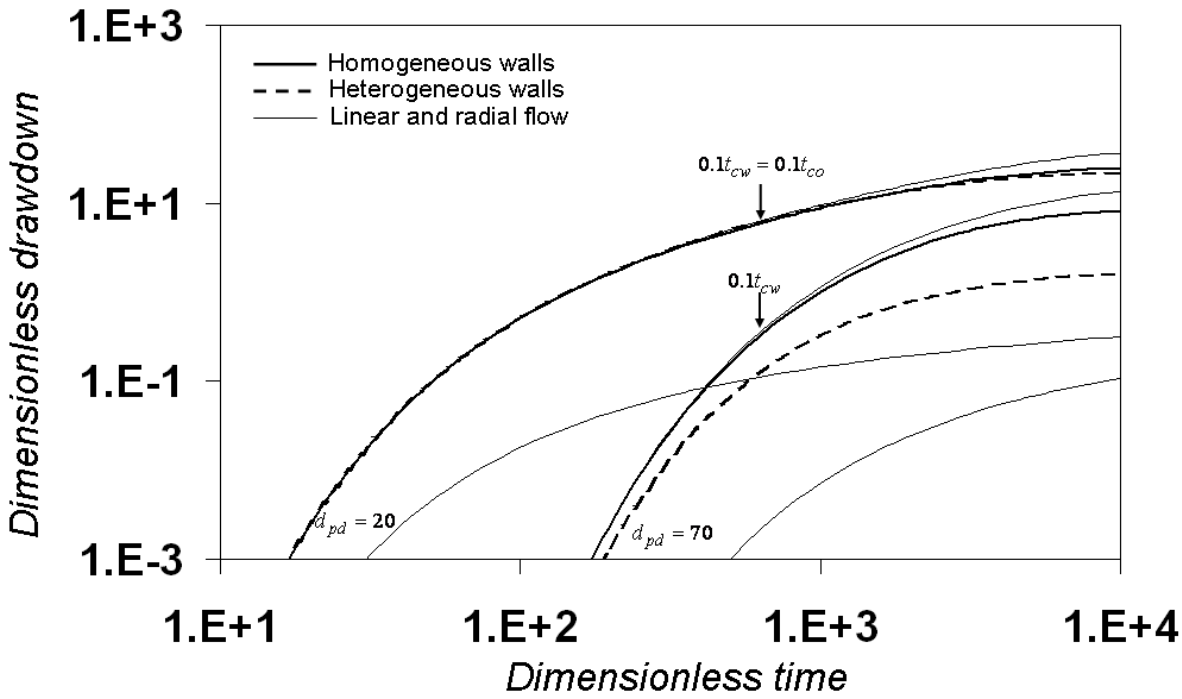


**Figure 5.9.** Drawdown at 20 and 70 d.u. to the pumping well versus time. The drawdown for linear and radial behaviour is plotted (thin continuous lines). Homogeneous diaphragm walls (continuous lines) have a leakage coefficient of 7.8·10-5 d.u. Heterogeneous diaphragm walls (discontinuous lines) have the opening at 10 d.u to the pumping well, their leakage factor is 10-6 d.u.

In short, there are two transient methods to characterize the diaphragm walls: measuring at two piezometers and using diagnostic plots. Both methods allow us to differentiate between homogeneous and heterogeneous diaphragm walls. The location of the opening or the leakage coefficient can be determined by knowing when the different changes occur. Both methods should be used together whenever possible, and the use of several piezometers increases the robustness of the results.

These methods obviate the need for making a numerical model of the problem because the drawdown measured at the observation points can be compared with the linear flow obtained by applying the Ferris equation. Moreover, the results can be verified by the flow rate evolution (Figure 5.5).

### 5.3.3. Application procedure

The proposed methodology to study the state of the diaphragm walls in a real situation consists in:

- Determination of the aquifer parameters from pumping tests.
- Pumping and measuring drawdown in all pumping and observation wells. A precise knowledge of the flow rate is essential (Pujades *et al.,* 2008).
- Writing the data in a dimensionless form applying equation (5) and the characteristic variables from Table 5.1.
- Plotting the dimensionless data when the steady state is reached. The type of diaphragm walls (homogeneous or heterogeneous) can be deduced from the shape of the head distribution along the enclosure. The opening can be located if an inflexion point exists. In the absence of an inflexion point, the leakage coefficient is obtained with the proposed analytical solution.
- Alternatively, when the steady state is not reached, the following transient methods are used:

    1. In the case of more than one piezometer, we plot the drawdown evolution at the different piezometers and determine the time when the curve separates from the linear behaviour. If the curves separate simultaneously, then the diaphragm walls are homogeneous. If the curves separate at different times, then the diaphragm walls are heterogeneous. The times when the flow behaviour changes from linear to radial indicate the leakage coefficient (eq. (8) and (18)) or the location of the opening (eq. (19)).

    2. In the case of one observation point, we study the diagnostic plot of the drawdown. The shape indicates the homogeneity or the heterogeneity of the diaphragm walls. Subsequently, the leakage coefficient is obtained by using $t_{cw}$ in equations (8) and (18). On the other hand, if there is an opening, its location is calculated by

detecting the departure of the linear behaviour and applying equation (19).

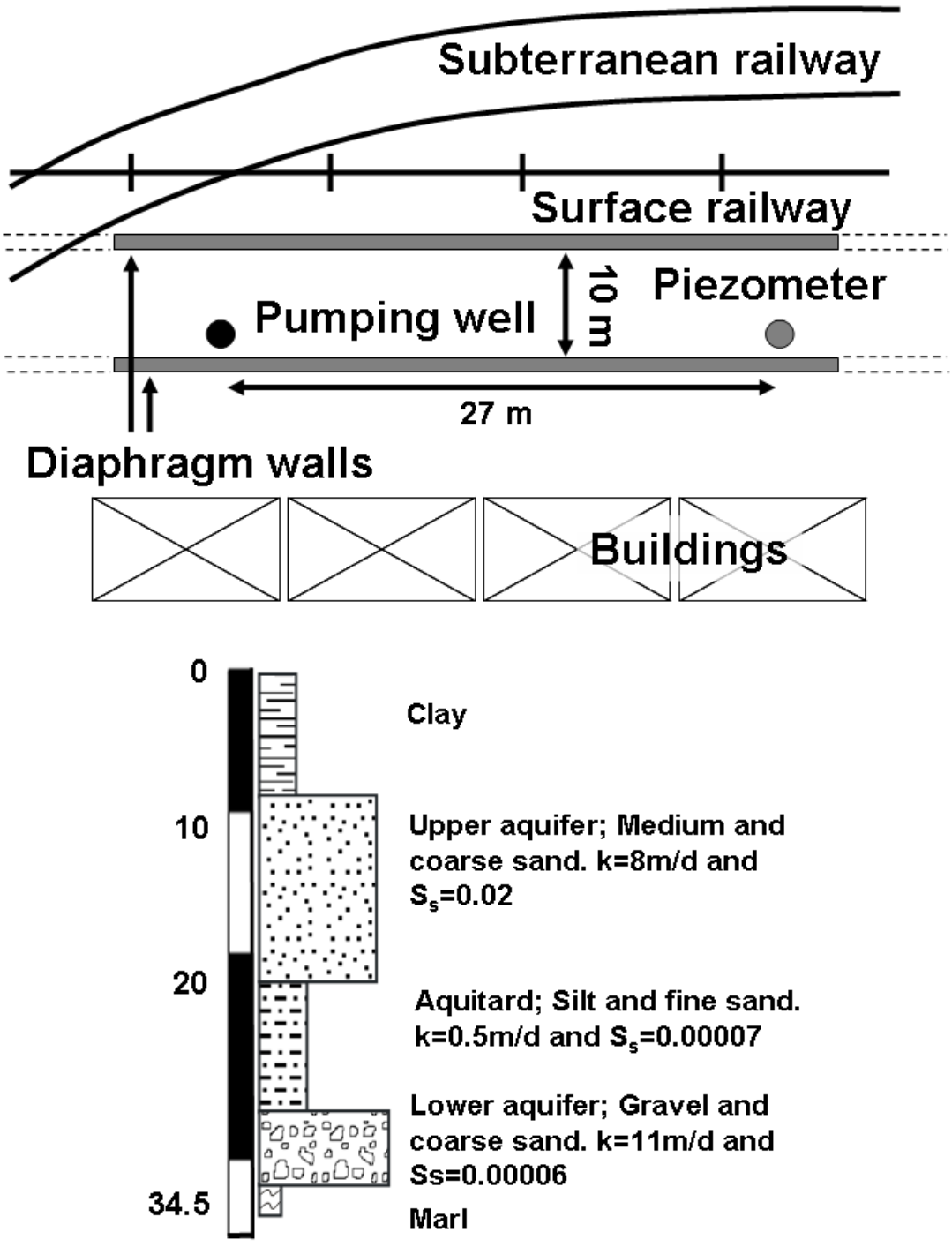


**Figure 5.10.** Above (a), plan view of the construction. Below (b) geological description. Aquifers parameters k and Ss are included.

3. In the case of one observation point, we study the diagnostic plot of the drawdown. The shape indicates the homogeneity or the heterogeneity of the diaphragm walls. Subsequently, the leakage coefficient is obtained by using $t_{cw}$ in equations (8) and (18). On the other hand, if there is an opening, its location is calculated by detecting the departure of the linear behaviour and applying equation (19).

## 5.4. Application

### 5.4.1 Case study

The diaphragm walls of the high speed train tunnel (Madrid-Barcelona) at Hospitalet de Llobregat (Barcelona) are characterized using the data collected during its construction. The tunnel was constructed in the delta of the river Llobregat, which is a heavily built-up area. Figure 5.10a displays the distribution of the wells, diaphragm walls, surface railways and buildings. The tunnel was excavated with the "Cut and Cover Method" and the diaphragm walls penetrated down to the base of the aquifer. Difficulties encountered in the construction of the diaphragm walls such as unexpected cemented layers gave rise to a large number of openings. As a result, groundwater and soil particles penetrated the openings inside the construction, ruling out the possibility of drainage. Moreover, holes appeared behind the diaphragm walls, putting at risk buildings. The holes were filled with concrete and the openings were sealed with pillars of reinforced concrete. The tunnel was eventually completed, but at an excessive cost in money and time. Construction problems not only endanger people but also pose a threat to buildings and infrastructure. The methodology presented in this chapter is used to determine the state of the diaphragm walls.

### 5.4.2 Hydrogeological description

The hydrogeology of the study area consists of two Quaternary aquifers separated by silty fine sands that overlie low permeability Tertiary sediments. A geological description of the site is shown in Figure 5.10b, which includes the hydraulic parameters, obtained by a pumping test interpretation. The Tertiary materials are

considered to be impermeable. The diaphragm walls cross all the Quaternary aquifers and end in the Tertiary materials.

### 5.4.3 Collected data

Pumping started sequentially at each well and head measurements were collected in the nearby wells. The flow rate was measured in the pumping well with a turbine flow meter. A number of problems were encountered during data collection: some piezometers were damaged by the construction machines and pumping was interrupted during drainage because of bad maintenance with the result that few data were obtained. To characterize the diaphragm walls, the data were measured in one piezometer located 27 m from the pumping well (Figure 5.10a).

### 5.4.4 Characterization of diaphragm walls

Drawdowns are written in a dimensionless form using equation (5) and plotted in a transient state graph (Figure 5.11a). Linear and radial behaviour are also plotted. The difficulty of differentiating between one opening (heterogeneous diaphragm walls) and uniformly distributed openings (homogeneous diaphragm walls) when the drawdown is measured in one piezometer was discussed in Section 5.3. The diagnostic plot method is used to characterize the diaphragm walls (Figure 5.11a) because only one piezometer is used. The end of the diaphragm walls is located at 1357 m from the pumping well (135.7 d.u.). If the diaphragm walls had only one opening, the flow behaviour would be completely radial at a dimensionless time equal to 7222 ($0.1t_{cL}$). In fact, *s'* decreases much earlier in our study, which suggests the presence of more than one opening. We interpret them as homogeneous walls. The dimensionless leakage coefficient can be obtained ($\alpha_{dw_a} = 1 \cdot 10^{-2}$ d.u) after identifying $0.1t_{cw}$, $0.5t_{cw}$ or $t_{cw}$ and applying equations (18) and (8). The results obtained when simulating the diaphragm walls with this leakage coefficient are consistent with the field measures (Figure 5.11a). The real leakage coefficient can be obtained using equation (5) and table (1), $\alpha_{dw} = 1 \cdot 10^{-3}$ m/d. In fact, a large number of openings were observed during the excavation stage (Figure 5.11b). If this methodology had been applied before the excavation, the

state of the diaphragm walls would have been determined. This would have enabled us to predict the defects of the diaphragm walls and repair them before excavation, which would have significantly reduced the cost and time of the works.

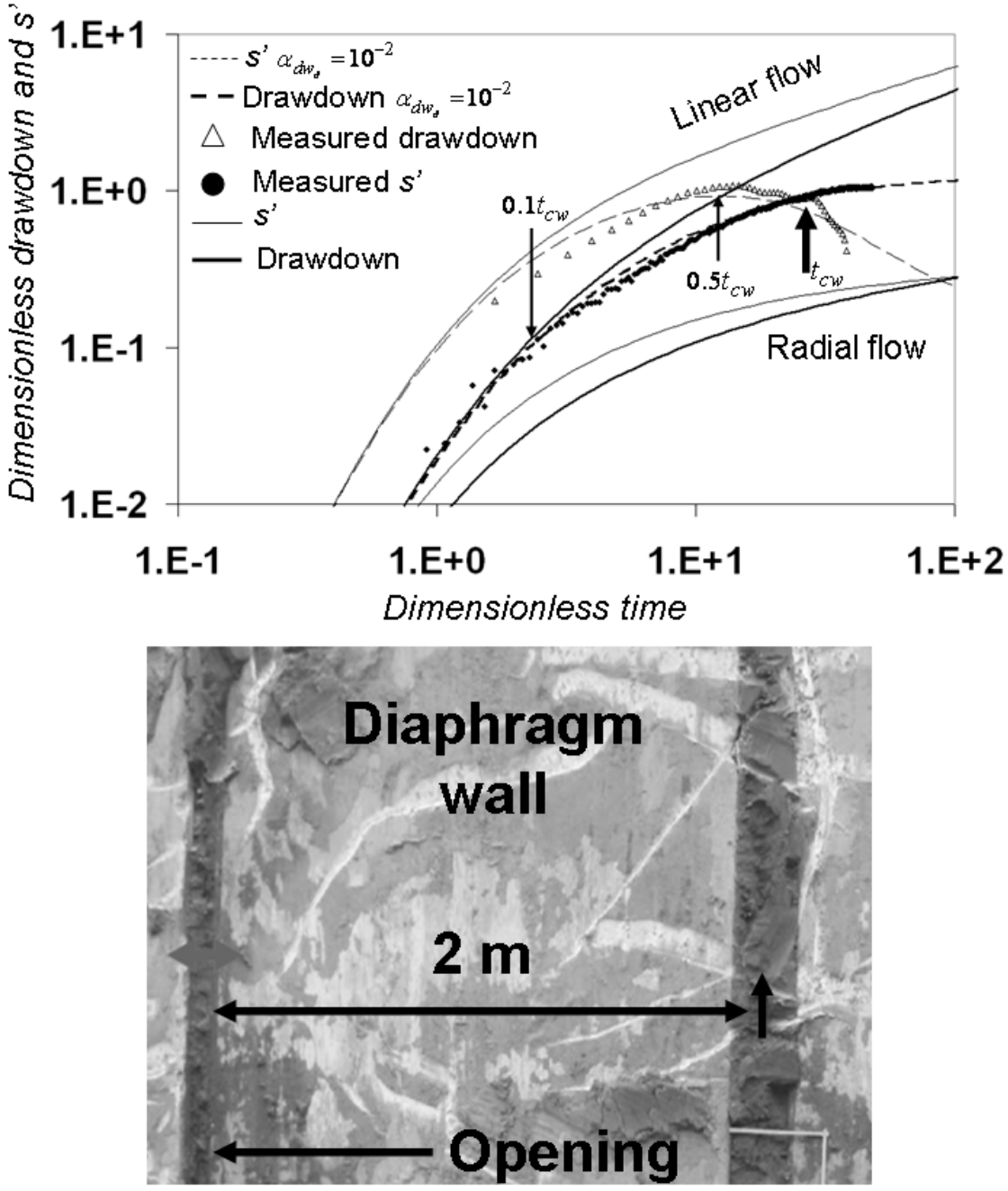


**Figure 5.11.** Above (a), in the same plot, drawdown versus time and diagnostic plot of the data measured. Linear and radial behaviour are included (continuous lines). Below (b), openings observed in the diaphragm walls during the excavation stage.

### 5.4.4 Characterization of diaphragm walls

Drawdowns are written in a dimensionless form using equation (5) and plotted in a transient state graph (Figure 5.11a). Linear and radial behaviour are also plotted. The difficulty of differentiating between one opening (heterogeneous diaphragm walls) and uniformly distributed openings (homogeneous diaphragm walls) when the drawdown is measured in one piezometer was discussed in Section 5.3. The diagnostic plot method is used to characterize the diaphragm walls (Figure 5.11a) because only one piezometer is used. The end of the diaphragm walls is located at 1357 m from the pumping well (135.7 d.u.). If the diaphragm walls had only one opening, the flow behaviour would be completely radial at a dimensionless time equal to 7222 ($0.1t_{cL}$). In fact, *s'* decreases much earlier in our study, which suggests the presence of more than one opening. We interpret them as homogeneous walls. The dimensionless leakage coefficient can be obtained ($\alpha_{dw_d} = 1 \cdot 10^{-2}$ d.u) after identifying $0.1t_{cw}$, $0.5t_{cw}$ or $t_{cw}$ and applying equations (18) and (8). The results obtained when simulating the diaphragm walls with this leakage coefficient are consistent with the field measures (Figure 5.11a). The real leakage coefficient can be obtained using equation (5) and table (1), $\alpha_{dw} = 1 \cdot 10^{-3}$ m/d. In fact, a large number of openings were observed during the excavation stage (Figure 5.11b). If this methodology had been applied before the excavation, the state of the diaphragm walls would have been determined. This would have enabled us to predict the defects of the diaphragm walls and repair them before excavation, which would have significantly reduced the cost and time of the works.

## 5.5. Discussion and conclusions

The state of the diaphragm walls can be determined by observing the head or the flow rate during the drainage stage. The flow behaviour depends on the characteristics of the diaphragm walls. A useful analytical solution to characterize the diaphragm walls is developed in steady state. The most important characteristics of this solution are as follows:

- The characteristic length for a homogeneous transmisive diaphragm walls is $1/\lambda$ where $\lambda = \sqrt{2\alpha_{dw}/\left(T_{aq} d_{dw}\right)}$. This characteristic distance is the distance affected by pumping when the diaphragm walls are penetrated by the total flow.
- This characteristic distance ($1/\lambda$) is the distance at which pumping wells should be located for excavation dewatering.
- It is possible to determine whether the diaphragm walls are tight, uniformly permeable or whether they contain individual openings by examining the spatial distribution of heads.

However, the steady state approach is not practical for the following reasons: (1) the time to reach steady state is too long, (2) an excessive number of piezometers are required and (3) the difference between a large opening and uniformly permeable diaphragm walls is small. A transient analysis is therefore more suitable.

Transient analysis consists in identifying the times at which changes in the flow behaviour occur. These times reflect the properties of the diaphragm walls such as the location of the opening when the diaphragm walls are heterogeneous or the leakage coefficient when they are homogeneous. However, it is not easy to distinguish between heterogeneous and homogeneous diaphragm walls using the observations obtained from one piezometer given that the drawdown curves are similar. Two methodologies are therefore proposed to characterize diaphragm walls.

One methodology consists in measuring drawdowns in at least two piezometers. The drawdown evolution separates from the linear tendency simultaneously in the two piezometers if the diaphragm walls are homogeneous. Should this simultaneous separation not occur, then the diaphragm walls are heterogeneous.

The second methodology proposed consists in studying the shape of the diagnostic plot of the drawdown obtained from one piezometer. The shape of the diagnostic curve indicates whether the diaphragm walls are homogeneous or heterogeneous.

Once the state of the diaphragm walls is determined, it is possible to locate the opening and to estimate the magnitude of the leakage coefficient. This is achieved by

observing the times when the flow changes from linear to radial and by applying the equations proposed in this chapter.

The best option is to use as many piezometers as possible, apply the two methodologies and compare the results. In elongated enclosures where there are a large number of pumping wells, pumping should start in chronological order and the other wells should be used as piezometers. If only one piezometer is built the diagnostic plot method is useful, but the piezometer must be close to the well because the drawdown evolution only yields valuable information when $t_{cw} = t_{co} > 0.1 t_{cL}$.

This approach was applied to a real case. We only had the transient data from one piezometer. The state of the diaphragm walls was determined using the methodology presented in this chapter and the leakage coefficient was calculated. Given the large number of openings, the diaphragm would have needed repairs. Characterization of the diaphragm walls before excavation is important because only then is it possible to interrupt pumping and repair the defects or design a new drainage system. If defects are observed subsequently (during excavation), they are difficult to remedy since pumping cannot be interrupted. The implementation of the methodologies proposed in this chapter will help us to gain a greater understanding of the nature of diaphragm walls.

# 6. Dewatering of a deep excavation performed in a low permeability soil

## 6.1. Introduction

New underground constructions at urban environments need to be deep to not affect existing structures (Li and Yuan, 2012). Therefore, they are usually built below the water table, which can result problematic (El-Nahhas, 1999). As a result, it is necessary to apply procedures which guarantee the safety of the excavation works in the presence of groundwater. Examples of these deep constructions are the vertical shafts performed to link tunnels with the surface (Ni and Cheng, 2011). These shafts are used as maintenance shafts during construction and as emergency or ventilation exits during operation. Generally, they consist of perform a deep circular excavation from the surface to the tunnel depth.

There are several techniques to perform deep excavations under the water table. The better procedure must to be chosen at each case to prevent the entrance of water inside the excavation and to avoid stability problems at the bottom of the excavation. Even it is possible to combine different techniques to improve their effectiveness (Forth, 2004). The method used depends on the characteristics of the soil, which require a deeply knowledge of the hydrogeology of the site (Stille and Palmström, 2008), which sometimes is not considered as much as it should, compromising the design and complicating the predictions (Jurado, *et al.,* 2012). An efficient method consists in combine the "cut and cover" method (Gulhati and Datta, 2005) with deep pumping wells (Powers, *et al,* 2007). On one hand, diaphragm walls avoid the lateral groundwater entrance and guarantee the verticality of the excavation walls (Xanthakos, *et al.,* 1994). On the other hand, deep pumping wells avoid the entrance of water from the excavation bottom and prevent unstable conditions. As a result, bottom uplift or liquefaction events are averted (Pujades, *et al.,* 2012). However, deep pumping wells are not recommended when the excavation is performed in a low hydraulic conductivity soil (Cashman and Prenne, 2001). At these cases, eductor wells, wick drains or perform the excavation under undrained conditions are alternatives. On one hand, eductor wells and wick drains are useful when poor rates of water must be extracted. On the other

**This chapter is based on the paper: Pujades, E., Vázquez-Suñé, E., Carrera, J., Jurado, A., 2013. Dewatering of a deep excavation performed in a low permeability soil. Submitted.**

hand, to perform the excavation under undrained conditions is possible when the drop of pressure consequence of the swelling of the soil caused during the excavation is enough to achieve stable conditions. Nevertheless, to apply these techniques is risky if the soil is not well known, because unexpected transmissive layers intercalated inside the low hydraulic conductivity materials lead to unstable conditions in the bottom of the excavation. Therefore, a detailed hydrogeological characterisation must be done. Borehole logging is the most used tool, however, layers of coarse sediments may be not noticed if the materials are not recovered with the core, which happens sometimes. Therefore, geophysical techniques should be used to improve the geology identified in the description of the boreholes. Similarly, grin size analysis and pumping tests should be performed to characterise the materials. Pumping tests are useful to notice intercalations of transmissive materials inside low hydraulic conductivity formations, since the transmissive layers rise considerably the effective transmissivity of the whole formation.

Soil characterisation also is important to determine the consolidation degree of the soil, which is relevant to predict the pumping settlements caused during a dewatering. These are small and elastic in preconsolidated soils as has been proved (Pujades *et al.,* 2013). In addition, a good characterisation allows constructing realistic numerical models to choose the best dewatering system. This is achieved by simulating several dewatering scenarios by varying the depth of the enclosure and/or the characteristics of the drainage.

However, to follow without hesitation all the required steps during the design process does not guarantee the success of the construction, since enclosures may has defects, which is not strange (Bruce *et al.,* 1989, Knight *et al.,* 1996, Vilarrasa *et al.,* 2012 and Pujades *et al.,* 2012). Defects in the enclosure (gaps or open joints) difficult the dewatering process and entail negative consequences (Pujades, *et al.,* 2012). On one hand, if these are located above of the excavation they cause inflows that may drag sediments, leading to the formation of sink holes outside the enclosure. On the other hand, if they are located below the excavation level, the water pressure is not dropped as much as necessary and unstable conditions may appear. These situations suppose serious risks that can be eliminated by testing the state of the enclosure. But the test must be performed before the excavation stage because if defects are detected before the excavation stage, they can be repaired by injecting sealing substances or the drainage

system can be redesigned to achieve the required drop of water pressure. However, if they are detected during the excavation stage, their reparation is difficult and costly because pumping cannot be interrupted, it continues being necessary to ensure the stability of the bottom of the excavation. Thus, groundwater flowing through the openings tends to drag the injected sealing substances. And if the system is redesigned, the works will be interrupted to construct the new drainage facilities. The existence of defects can be known easily by performing a Watertightness Assessment Test (WTAT) consisting on pumping inside and comparing the measured and the predicted drawdown. These can be located by applying hydrogeological tools (Knight, *et al.,* 1996, Ross and Beljin, 1998, Vilarrasa, *et al.,* 2012 and Pujades*, et al.,* 2012).

The High Speed Train (HST) tunnel in Barcelona (Spain) was constructed by using a tunnel boring machine (TBM). The tunnel crosses the city in the Southwest-Northeast direction. It goes below the Sagrada Familia Basilica, which was designed by Gaudi and it is a UNESCO World Heritage Site. The construction of the Basilica (designed by Antonio Gaudi) commenced in 1882 and is on going. The Basilica, which is an icon of Barcelona, attracts thousands of tourists every year. Given their importance, politicians and the public opinion feared for the safety of the Basilica during the tunnel excavation. As a result, additional safety measures were taken to minimize the effects of the construction (the monitoring points used were more than it is recommended, the Basilica was protected in front the tunnel excavation by a bored pile wall and the enclosures of the shafts were deepened to reduce pumping effects outside the excavations).

One ventilation and/or emergency shaft at each 700m of tunnel was required. Decisions and works developed to excavate one of these shafts are exposed in this chapter. The shaft, which has a circular shape, is located at the North of Barcelona, in the crossroads between the Mallorca and Trinxant streets. The shaft was built before the tunnel pass and the TBM entered through the enclosure to be repaired inside. Once the reparation finished, the machine continued excavating the tunnel. Two main problems arisen during the excavation of this shaft. The first related with the drainage technique since the initial geological characterisation of the site, which was too coarse, suggested that the materials located in the bottom of the excavation had a low hydraulic conductivity. The second, related with the state of the enclosure, where a defect was located after the excavation stage by performing a WTAT. Apart from these, other

questions emerged during the design and excavation stages, like the generally feared (at urban environments) pumping settlements, which were predicted and monitored, The shaft was finished successfully because a suitable methodology, which allowed to design the best dewatering system and to avoid unexpected events, was followed. This consisted on a hydrogeological characterisation, an efficient dewatering system designed numerically, a WTAT before the excavation stage and finally, a conscientious monitoring of groundwater and soil behaviour.

Thus, the objectives of this chapter are 1) to show the importance of the soil characterisation to choose the more efficient drainage method to perform a deep excavation under the water table and 2) to prove that although defects in deep enclosures are relatively common, these can be located easily by a WTAT. Moreover, the procedure arisen from the works developed to perform a deep excavation in Barcelona is shown.

## 6.2. Materials and methods

### 6.2.1. Problem statement

#### *6.2.1.1. General geographical, geological and hydrogeological description*

The excavation was performed to construct one of the emergency and ventilation shafts of the HST tunnel in Barcelona. The shaft is located at the North of Barcelona, at the crossroad between Mallorca and Trinxant streets and it is named “Trinxant shaft”. The soil of Barcelona is formed by Quaternary materials at the top and Tertiary materials at the bottom. The tunnel crosses mainly the tertiary materials, which belongs to the Pliocene Age. Trinxant shaft crosses both, Quaternary, Q, (0 to 14 m depth) and Pliocene, P, (14 to 33 m depth) (Figure 6.1b).

Tertiary materials belong to the Pliocene age. These are formed by clays and grey marls, from sea deposits, and sequences of conglomerate with a sandy-clay matrix. Pliocene is characterized by an alternation of these lithologies. Fine sediments are predominant at the bottom and the number and thickness of layers with coarse sediments increase at shallower depths.

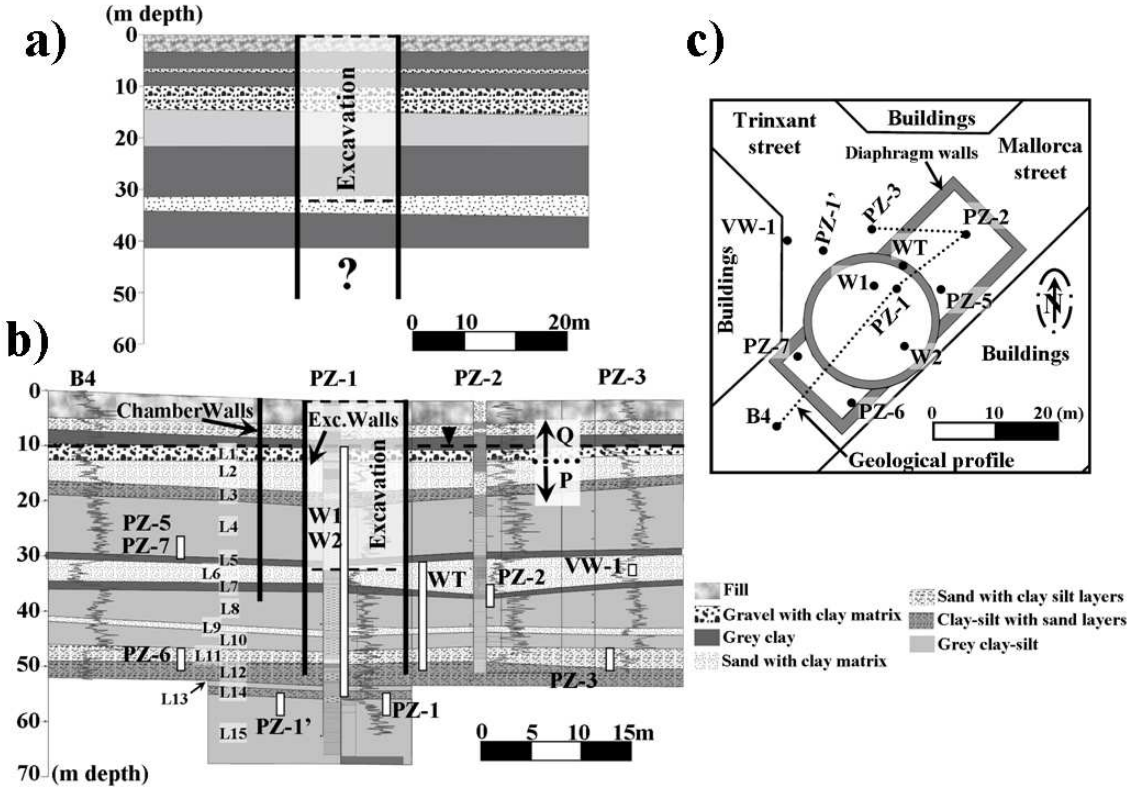


**Figure 6.1.** a) Initial coarse scale geology of the site. The detail of the study was not enough to identify the transmissive layers located below the excavation. b) Detailed geological profile of the site. Natural Gamma Ray register and borehole logging allowed us to identify 15 layers below the water table. The screens of the piezometers and the pumping wells are also displayed. c) Plan view of the site, including the enclosure and the location of piezometers and pumping wells.

Quaternary materials lie above the Pliocene. They can be divided into two: Pleistocene and Holocene. Pleistocene deposits are formed by gravels with a clay matrix at the bottom. These are alluvial fan deposits that are transformed into sands with a clay matrix in the seawards. Above these alluvial deposits are eolian deposits that consist of brown-yellow silts containing calcareous nodules. At the top of this sequence is a calcrete stratum. This series may be found three times. Finally, there are the Holocene deposits the main deposits of which are composed of:

- Torrential, alluvial and foothills deposits made up of fine detritic sediments (red clays or silts).

- Alluvial gravel and sands.

- Coastal plain sands.

Quaternary and Tertiary sediments can be considered as a layered aquifer with high vertical heterogeneity. The hydraulic conductivity ($k$) of clay layers ranges from 0.001 to 0.01 m/d and that of sand and gravel layers varies from 0.1 to 10 m/d. These values were derived from the numerous hydraulic tests performed during the HVT tunnel project and others projects.

#### *6.2.1.2. Soil state description*

Knowledge of the hydrogeological history of the soil is essential to predict its response to dewatering. The structure and deformational characteristics of the soil depend on its geological history. Like in many European cities, the early stages of urbanization in Barcelona were associated with an increase in industrial activity. Groundwater extraction by industry caused a significant lowering of groundwater levels. The subsequent decline of urban industries leads to the recovery of groundwater levels (Vazquez-Suñe, *et al.,* 2005). A side effect of groundwater fluctuations is the preconsolidation of the soil. Therefore, the soil in Barcelona is preconsolidated and it behaves elastically whenever the groundwater oscillations do not exceed the maximum drawdown reached during the period of industrial activity. Since this maximum drawdown was approximately 10-15 m at the study site, present day groundwater fluctuations usually remain in the swelling (elastic) branch of the oedometric curve. Moreover, if the drawdown necessary to excavate had exceed the maximum historical drawdown at some point, deformations would not have been elastic, but they would have been small, because the bigger deformations occur at the first stages of the oedometric curve. And these stages were beaten during the industrial period.

#### *6.2.1.3. Construction characteristics*

The shaft of Trinxant consisted in a deep circular excavation (Figure 6.1c). The excavation was 33 m of depth and 20 m of diameter. The water table was located at 10 m depth. The excavation was performed by combining the cut and cover method with deep pumping wells. Diaphragm walls, which were 50 m depth, were constructed using

a hydro-mill trench cutter and pumping wells were performed using the OD method (Ferrer, et al., 2008). The shaft had two outside chambers, one to facilitate the entrance of the TBM and the other the exit. They consist in two enclosures delimited by diaphragm walls of 38 m depth.

### 6.2.2. Basic concepts

#### *6.2.2.1. Hydrological numerical models*

A number of hydrological numerical models were used. We used the finite element code TRANSIN-IV (Medina and Carrera, 2003, and Medina *et al.,* 2000), with visual interface of VISUAL TRANSIN (UPC, 2003) to construct the models. Axisymmetrical and multilayer numerical models were used depending on the geometry of each case (Figure 6.2a and 6.2b). Lateral boundaries were at a sufficient distance from the site to ensure that they were not affected by pumping. Top and bottom boundaries were modelled as no flow boundaries because only the effect of pumping was analysed. Flow rate or head was prescribed at the pumping well depending on the objective of each simulation or the available data.

Numerical models were used to estimate the hydraulic parameters of the soil and the state of the enclosure by automatic parameter estimation (Carrera and Neuman, 1986a, b and c) and Medina and Carrera, 2003) employing the data measured during the pumping tests. They were also used to simulate a number of dewatering scenarios in order to find the best alternative. The safety factor of each dewatering design was computed analytically by using the numerical results.

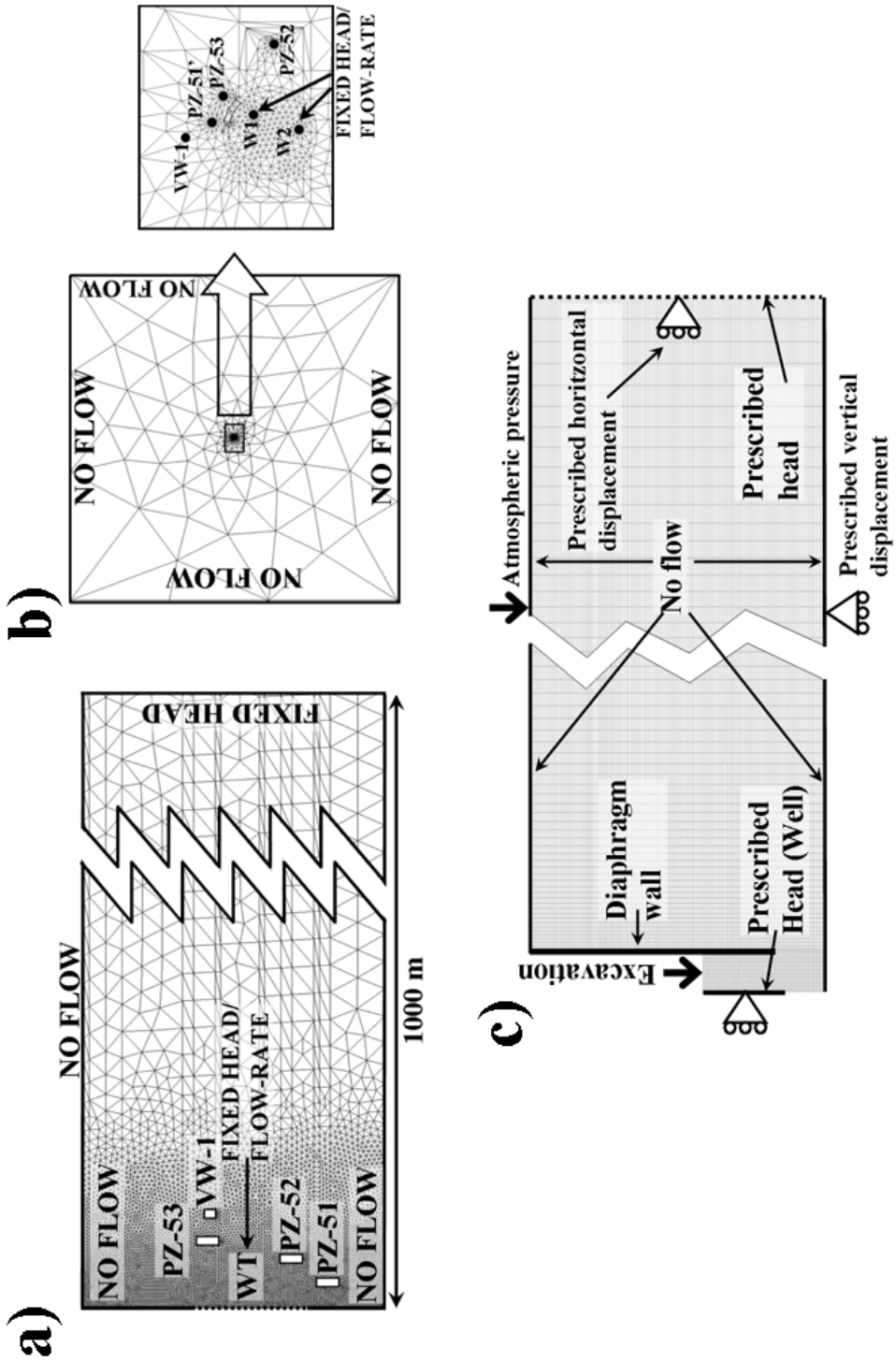


**Figure 6.2.** Schematic description of the numerical models. a) Boundary conditions and mesh of the hydraulic axisymmetrical numerical model. b) General and detailed plan views of the multilayered hydraulic model. Some piezometers are also displayed. c) Boundary conditions and mesh of the hydro-mechanical numerical model.

*6.2.2.2. Hydro-mechanical numerical models*

Coupled hydro-mechanical simulations were performed in order to predict the settlements caused outside the enclosure at the proposed dewatering design. We used the finite element numerical code CODE_BRIGHT (Olivella, *et al.,* 1994, Olivella, *et al.,* 1996) that solves coupled hydro-mechanical problems in porous media.

The models were axisymmetrical around the vertical well axis. Lateral boundaries were at a sufficient distance from the site to ensure that they were not affected by pumping and a prescribed head condition was imposed at the opposite boundary to the pumping well. Top and bottom boundaries were modelled as no flow boundaries. Finally, the head was prescribed in the pumping well (Figure 6.2c). Mechanical boundary conditions consisted on restrict the horizontal movements in the pumping well (symmetry axis) and in the lateral boundary (opposed to the pumping well) and on restrict the vertical movements in the bottom of the model.

The variables used at the models were the intrinsic permeability ($k_0$), the Young's modulus ($E_i$) and the Poisson ratio of each layer ($\upsilon_i$). Poisson's ratio used was 0.35 for every layer. Intrinsic permeability was obtained from the pumping test results and $E_i$ was calculated from the compressibility of the soil at each layer ($\alpha_i$), applying

$$E_i = \frac{3(1-2\upsilon_i)}{\alpha_i} \qquad (1)$$

where $\alpha_i$ was derived from the storage coefficient of each layer ($S_i$), which was obtained from the pumping test, applying the equation proposed by Jacob (1950) and cited by Ferris (1962) for elastic aquifers,

$$\alpha_i = \frac{S_i}{\gamma_w D_i} - \theta_i \beta \qquad (2)$$

where $\theta_i$ is porosity, $\gamma_W$ is the specific weight of the water and $\beta$ is water compressibility, which is much smaller than typical soil compressibilities and is often neglected. In fact, if $\beta$ is neglected $S_{Si} = \alpha_i \gamma_W$, where $S_{Si}$ is the specific storage coefficient of the $i$ th layer.

*6.2.2.3. Bottom stability (Safety Factor)*

The numerical results of several dewatering scenarios were compared. The main difference between them was the depth of the enclosure. All dewatering scenarios had to ensure the stability of the bottom of the excavation. Groundwater may give rise two stability problems at the bottom of the excavation: fluidization and base heave. Fluidization may occur when the excavation is carried out in unconfined aquifers and base heave when the excavation is made above a confined aquifer (Cashman and Preene, 2001). In practice, positive (i.e, compressive) effective stresses are essential at all stages when addressing these two problems. The vertical effective stress can be calculated by applying Terzaghi's equation in the vertical direction (Terzaghi and Peck, 1948)

$$\sigma'_V = \sigma_V - u \quad (3)$$

where $\sigma'_V$ is the effective vertical stress, $\sigma_V$ is the total vertical stress and $u$ is the water pressure. The total vertical stress is given by

$$\sigma_V = z\gamma_S \quad (4)$$

and the water pressure as

$$u = h\gamma_W \quad (5)$$

where $z$ is the depth of the point , $\gamma_S$ the specific weight of the soil, which was taken as 2 t/m$^3$, and $h$ is the piezometric head above the point. Unstable conditions are reached when $\sigma'_V \leq 0$. This occurs at excavations where the drainage system (wells and diaphragm walls) is not designed correctly. The drainage system must ensure that $\sigma_V > u$ or $\sigma_V / u > 1$ at each point below the excavation bottom. But in practice, owing to soil uncertainty, it is common to apply a safety factor ($SF$) to guarantee stability. There, we adopted a SF of 1.2,

$$SF = \frac{\sigma_V}{u} \geq 1.2 \qquad (6)$$

Since the soil is heterogeneous and that the drop of pressure is different in each geological layer, $SF$ was computed for each meter below the bottom of the excavation. The $SF$ value may appear small compared with the recommendations given by the EUROCODE 7 (Frank *et al.,* 2004), which suggest verify the hydraulic heave by comparing the total stress and the pore water pressure multiplied by the corresponding partial safety factors:

$$\gamma_{G,stb}\sigma_V = \gamma_{G,dst}u \qquad (7)$$

where $\gamma_{G,stb}$ and $\gamma_{G,dst}$ are the safety coefficients for stabilizing and destabilizing actions respectively. The Eurocode standards recommend $\gamma_{G,stb} = 0.9$ and $\gamma_{G,dst} = 1.35$ for this case. But we used a lower global safety factor of 1.2 due to the following reasons:

c) The Eurocode recommendation refers to straight walls, where the passive strength could be reduced dramatically if the soil effective stresses are reduced. In our case, the circular geometry of the shafts does not require any significant passive strength.

d) The Eurocode recommendation is based on a shallow pumping of the excavation bottom and not on a deep well pumping from the whole soil profile below the shaft, which is the case considered here. Therefore, the value of the pore water pressure could be measured (and controlled) directly from the pumping well, thus reducing the uncertainty of its value.

Moreover, shear resistance such as cohesion and friction forces were not considered as usual in this type of analyses (Frank *et al.* 2004). However, since these forces are opposed to the water pressure effects, our calculations were conservative.

Water pressure used to compute *SF* was obtained numerically from observation points located inside the enclosure but near from the diaphragm walls. These points measured the water pressure at different depths.

## 6.3. Application

### 6.3.1. Geological characterization

The site had been characterised geologically initially, but the study scale was too coarse (Figure 6.1a). Only one transmissive layer was characterised below the excavation bottom. This was not enough to decrease the water pressure and ensure the stability some meters below the excavation. Therefore, since the great majority of the soil seemed to have low values of hydraulic conductivity, the use of deep conventional pumping wells instead other pumping techniques was questioned. Wick drains, eductor wells or perform the excavation under undrained conditions were alternatives, which could be applied to drop the water pressure during the excavation. However, given the high risk of these techniques (if the soil is not well characterised) and given that conventional wells results a cost-effective technique, a detailed geological study was performed to assess the best alternative. Three tools were used. Firstly, four boreholes were performed (PZ1, PZ2, PZ4 and B4 in Figure 6.1b and 6.1c) and their core, which was obtained unaltered, was described. A number of layers of different lithology were identified (Table 6.1). After that, soil samples were taken of some depths (Table 6.1) to perform grain size analyses. With the results and taken as reference the Wentworth grade scale (Wentworth, 1992) the lithologies observed in the borehole logging were verified (Table 6.1). Finally, a register of Natural Gamma Ray was obtained from each borehole. This technique allows observing the continuity of the layers and identifying changes in lithology (Cripps and McCann, 2000). Results from the three techniques agreed.

Figure 6.1b shows the geological interpretation of the site. Quaternary and Tertiary are divided into several strata of different textural and lithological properties.

Fifteen layers were differentiated below the water table (Table 6.1) and most of the materials located below the water table belong to the Pliocene Age (Layers 2 to 15). Although the fine sediments were predominant, some fine layers of coarse materials located above the maximum excavation depth (Layer 9, 11 and 14) could facilitate the dewatering process by using deep conventional pumping wells. However, this was not enough and before to choose the drainage method the hydraulic conductivity of the layers had to be known.

| Layer | Grain size sample depth (m) | Grain size *K* (m/d) | Top depth (m) | Bottom depth (m) | Numerical *K* (m/d) | Numerical *Ss* | Grain size description |
|---|---|---|---|---|---|---|---|
| L1 | 10 | 0.37 | 10.0 | 11.0 | 0.5 | 1.00E-05 | Gravel with sandy-silty matrix |
| L2 | 11.5 | 3.45 | 11.0 | 14.0 | 0.009 | 9.99E-06 | Fine sands with clayey-silty matrix |
| | 11.75 | 0.17 | | | | | |
| | 12.9 | 0.04 | | | | | |
| L3 | | | 14.0 | 17.0 | 0.047 | 9.98E-06 | |
| L4 | 19.3 | 0.06 | 17.0 | 28.0 | 0.66 | 9.89E-06 | Fine sands with clayey-silty matrix |
| | 25.3 | 0.78 | | | | | |
| L5 | | | 28.0 | 30.0 | 0.0008 | 1.07E-05 | |
| L6 | 30.5 | 173.44 | 30.0 | 34.0 | 28.01 | 1.54E-05 | Coarse sands with some fine and medium sands |
| | 31.9 | 12.73 | | | | | |
| | 33.1 | 0.93 | | | | | |
| | 33.7 | 3.45 | | | | | |
| L7 | | | 34.0 | 35.0 | 0.017 | 1.06E-05 | |
| L8 | 37.1 | 1.64 | 35.0 | 42.0 | 0.77 | 3.64E-05 | Fine sands and silts with clayey matrix |
| L9 | 42.5 | 12.73 | 42.0 | 43.0 | 19.54 | 1.05E-05 | Coarse sands with some medium and fine sands |
| L10 | 45.1 | 4.16 | 43.0 | 46.0 | 6.07 | 1.20E-05 | Silts and fine sands with clayey matrix |
| L11 | 46.7 | 46.99 | 46.0 | 48.0 | 4.6 | 1.12E-05 | Coarse and fine sands |
| | 47.5 | 26.85 | | | | | |
| L12 | 48.3 | 365.78 | 48.0 | 52.0 | 0.045 | 1.36E-05 | Coarse and fine sands with silty-clayey matrix |
| | 49.1 | 46.99 | | | | | |
| | 49.3 | 68.24 | | | | | |
| | 49.5 | 12.73 | | | | | |
| | 49.9 | 22.28 | | | | | |
| | 50.5 | 1.36 | | | | | |
| L13 | 52.45 | 18.49 | 52.0 | 53.0 | 0.085 | 1.01E-05 | Clays and silts |
| L14 | 55.3 | 0.78 | 53.0 | 55.0 | 0.84 | 1.02E-05 | Silt and clays with fine sands |
| L15 | 61.6 | 1.97 | 55.0 | 65.0 | 0.11 | 1.05E-05 | Clays and silts |

**Table 6.1.** Characteristics of the layers located below the water table. The table displays the depth where the grain size analysis samples were taken, the hydraulic conductivity obtained from each analysis and the lithological description of the samples. This also shown all the identified layers located below the water table with the numerical results obtained from the pumping test characterisation.

### 6.3.2. Hydrogeological characterization

A pumping test was performed to know the hydraulic properties of the different geological layers. Pumping tests consist into pump water and to observe the groundwater response at several observation points (piezometers) located at different distances and screened at different depths. The boreholes performed to obtain the unaltered cores were used as Casagrande piezometers (PZ-1, PZ-2 and PZ-3) (Figure 6.1b and 6.1c). Additionally, head data from a vibrant wireless piezometer was used (VW-1). The screen of the piezometers was located at different depths to observe the

response at different layers. PZ-1 was screened from 54 to 57m depth, PZ-2 from 32 to 35m depth, PZ-3 from 46 to 50m depth and VW-1 from 33 to 34m depth. The testing well (WT) was screened from 20 to 50 m depth (Figure 6.1b and 6.1c). The pumping test lasted five days. It consisted in two days of pumping and three days of recovery. The pumping rate average during the test, which was measured using an electromagnetic flow-meter, was 5.6 l/s. Head evolution was measured at the piezometers and in the pumping well. Head measures were taken manually and automatically. The automatic data was measured at each minute using pressure sensors and the manual was taken with a groundwater level probe at times distributed logarithmically.

The hydraulic parameters, *K* and *Ss* of each layer, were obtained (Table 6.1) by an automatic parameter estimation performed with a hydrogeological numerical model, which was axisymmetrical (Figure 6.2a). The hydraulic conductivity used to start the estimation process was accordingly to the *k* obtained from the grain size results (Table 6.1). The empirical methods applied to compute *k* with the grain size analyses results were Hazen method (Custodio and Llamas, 1984), Kozeny method (Schoeller, 1962), Kozeny-Carman method (Batu, 1998), Harleman method (Schwarz and Zhang, 2003) and Bakhmeteff-Feodoroff method (Schoeller, 1962).

Good fits were obtained from the numerical estimation in all of the observation points, PZ-1, PZ-2, PZ-3 and VW-1 (Figure 6.3) and the estimated values were in order with the values from the grain size analyses and the lithology observed. Moreover, the effective transmissivity of the aquifer, which was calculated using the Jacob´s method (Cooper and Jacob, 1946), was about 170-200 $m^2$/d, which compared well with that obtained integrating the values of Table 6.1. The hydraulic conductivity values of the layers located below the excavation bottom (>0.1 m/d except the Layer 13) revealed that the best technique to perform the drainage was deep pumping wells, because the flow-rates required would be too high to the other methods. The hydrogeological characterisation shown that, although during the geological interpretation only the 11% of the saturated zone was described as transmissive (Layer 1, 6 and 9), the great majority of the layers (74.5%) had values of hydraulic conductivity higher than 0.1 m/d. This fact suggested the presence of unidentified thin transmissive layers intercalated inside the low transmissive materials.

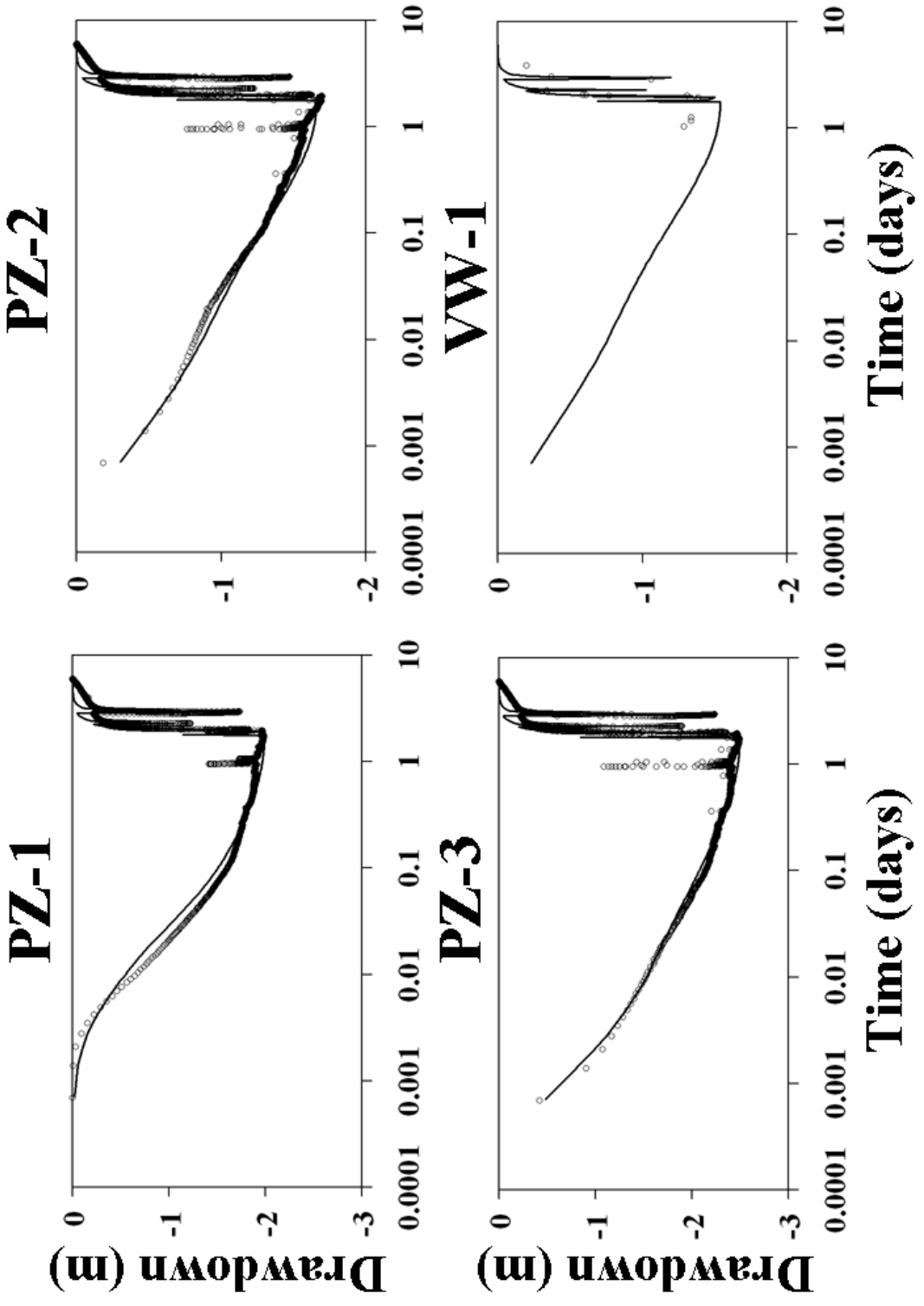


**Figure 6.3.** Evolution of measured (dots) and computed (lines) drawdowns during the pumping test.

### 6.3.3. Enclosure and dewatering design

Once the numerical model was calibrated, a number of dewatering scenarios were proposed and simulated. The simulations were performed using an axisymmetrical numerical model by prescribing the drawdown in the pumping well. The depth of the diaphragm walls, the screen of the pumping well and the drawdown in the well were varied at each simulation. Note that two premises had to be respected. The first was the minimum diaphragm walls depth, which guarantees the stability and the verticality of the walls. The second was not deepened the pumping well much more than the enclosure due to the fear in front of the pumping settlements. This second fact was consequence of the initial numerical analyses, which predicted large pumping settlements overtaking the warming limits defined by the Administrator. However, the initial analyses oversized the pumping settlements since the stiffness values used, which were obtained mainly from pressurometers analysing the unloading-reloading phase, were below the actual stiffness of the soil. But these values were recalculated using the storage coefficient values of the soil (Pujades *et al.,* 2013).

The well was located in the middle of the enclosure (symmetry axis) in the numerical simulations and the diaphragm wall at a distance equal to the radius of the enclosure. The results of each simulation were obtained in steady state. The safety factor was calculated at different depths below the excavation bottom applying the Equation 6. As an example, Table 6.2 displays the results obtained considering a pumping well screened as far as 55m, a 50m deep diaphragm walls and varying the drawdown inside the pumping well. Shade cells represent depths where *SF* is less than 1.2. A suitable dewatering design was obtained combining diaphragm walls of 50m depth, a pumping well screened from the water table to 55m depth and prescribing 40m of drawdown inside the pumping well. Numerical results indicated that conventional deep pumping wells could drain the Pliocene materials given their hydraulic conductivity. The expected steady state pumping rate was 2 l/s, which can be pumped with one pumping well. However, two pumping wells were recommended to avoid dangerous situations if one pump had resulted damaged.

| Depth | 25 m drawdown | 30 m drawdown | 35 m drawdown | 40 m drawdown |
|---|---|---|---|---|
| 33 | Non saturated | | | |
| 35 | 8.64 | | | |
| 37 | 3.22 | | | |
| 39 | 2.65 | | | |
| 41 | 2.43 | 9.49 | | |
| 43 | 2.32 | 5.37 | | |
| 45 | 2.26 | 4.16 | 26.73 | |
| 47 | 2.20 | 3.57 | 9.37 | |
| 49 | 1.59 | 1.96 | 2.54 | 3.63 |
| 51 | 1.13 | 1.19 | 1.27 | 1.36 |
| 53 | 1.10 | 1.14 | 1.18 | 1.23 |
| 55 | 1.14 | 1.18 | 1.22 | 1.27 |
| 57 | 1.17 | 1.21 | 1.24 | 1.28 |
| 59 | 1.20 | 1.23 | 1.26 | 1.30 |
| 61 | 1.23 | 1.26 | 1.29 | 1.32 |
| 63 | 1.26 | 1.28 | 1.31 | 1.34 |
| 65 | 1.28 | 1.31 | 1.34 | 1.37 |
| Q (l/s) | 1.25 | 1.5 | 1.75 | 2 |

**Table 6.2.** Safety factor at different depths in four different scenarios. All the scenarios have 50 m depth diaphragm walls and a 55 m depth pumping well. Drawdown in the pumping well varies at each scenario. Stable conditions are achieved with 40 m of drawdown in the pumping well. Flow-rate at each simulation is also shown.

The next step before of validate the dewatering system was to know the outside effects that the dewatering would cause (drawdown and settlements). Settlements were computed using a hydro-mechanical numerical model. Note that only the settlements caused by the dewatering were calculated. Figure 6.4a displays settlements in depth at 5, 10 and 20 meters from the enclosure. The predicted settlement at the surface is shown at Figure 6.4b. Greater settlements were concentrated around the enclosure, which agreed with the drawdown distribution. Given the great deep reached by the designed diaphragm walls, the predicted outside drawdown was small. As a result, outside settlements would not endanger the stability of the near buildings, since the biggest settlements would be 0.5 mm.

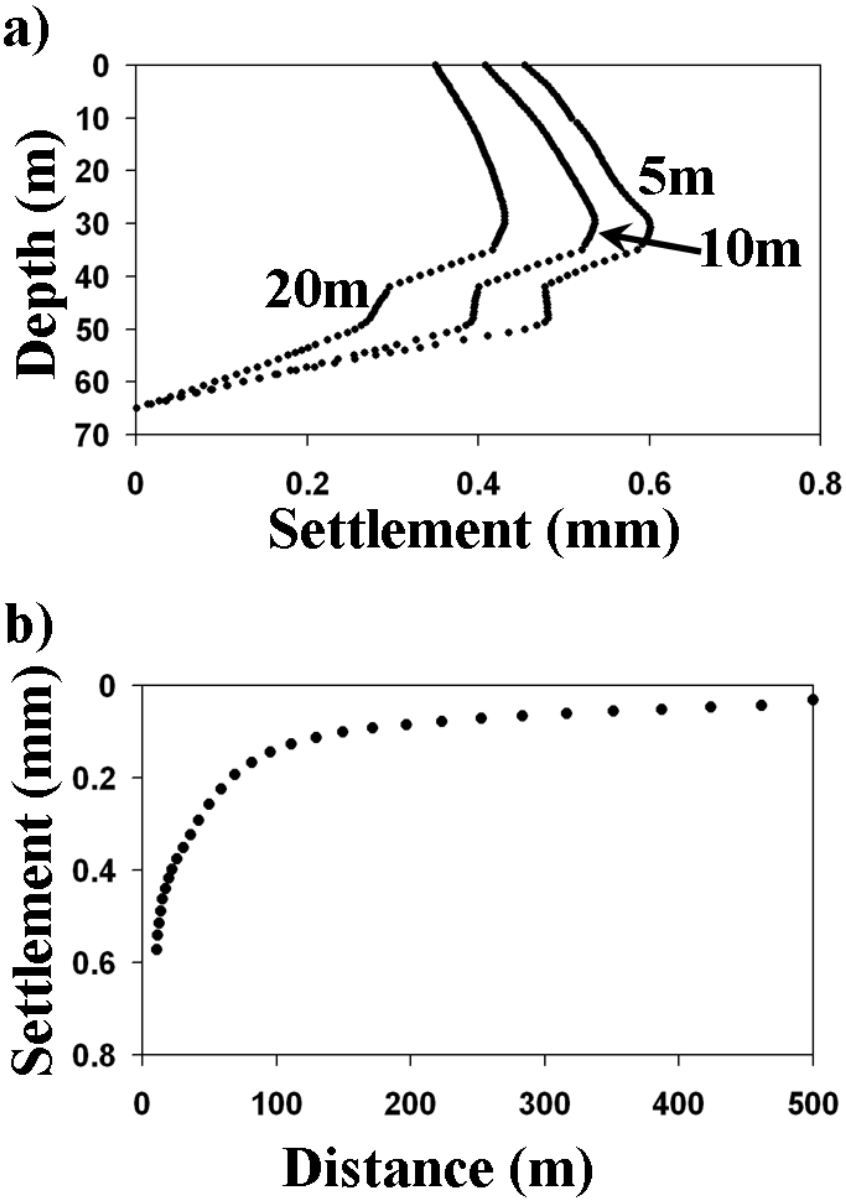


**Figure 6.4.** a) Computed settlements versus depth, at 5, 10 and 20 meters from the enclosure, caused by the proposed dewatering system. b) Computed surface settlements.

### 6.3.4. Watertightness Assessment Test (WTAT)

Enclosures may have open joints or gaps caused during their construction which can affect negatively their functions. If they are located above the excavation bottom, they may cause sink holes and if they are situated below, they may difficult the dewatering putting at risk the stability of the base. Therefore, it is essential to know the state of the enclosure before to start the excavation stage. The conditions of the enclosure can be known by using hydrogeological tools as pumping tests (Pujades, et.

al., 2012, Vilarrasa, et. al., 2012). For this reason, a pumping test, which consisted in pump inside the enclosure and measure outside, was performed when the enclosure was finished. The pumping test lasted 7 days, four of pumping and three of recovery. Two pumping wells were used (W1 and W2) which were screened from 10 to 55 m depth. Head was measured at the piezometers PZ-1', PZ-2 and PZ-3 (Figure 6.1b and 6.1c). VW-1 was not used because it had resulted damaged and PZ-1 was replaced by PZ-1' because the former also had been broken. Note that PZ-1' was located outside the enclosure. As in the first test, head measures were taken manually following a logarithmic frequency and automatically at each minute. Flow-rate was measured by using an electromagnetic flow-meter in W1 and a Woltman horizontal turbine flow-meter in W2. The averages of flow rate were 4 and 3 l/s at W1 and W2 respectively.

Simultaneously, the drawdown of the test was predicted with a multilayer numerical model (Figure 6.2b). It could not be axisymmetrical because there were two pumping wells. Therefore, the problem did not have an axisymmetrical geometry. The number of represented layers in the model had to be reduced to decrease the computation times. The multilayered model was made up by the more conductive layers linked by one-dimensional elements that represented the layers with low values of $k$.

When measured and predicted drawdowns were compared they did not fit (Figure 6.5). This fact indicated that the enclosure had a defect. Three more piezometers (PZ-5, PZ-6 and PZ-7) screened at different depths were drilled (inside the entrance and exit chambers) to locate the position of the gap. There were one piezometer screened below the diaphragm walls (PZ1'), two piezometers screened just at the end of the diaphragm walls (PZ3·and PZ6), two piezometers screened at intermediate layers between the end of the diaphragm walls and the water table (PZ5 and PZ7) and finally, one piezometer screened at the top of the saturated zone (PZ2) (Figure 6.1b and 6.1c). On one hand, the plan distribution allowed to locate the gap. On the other hand, the position of the screens made possible to approximate the deep of the defect. Bigger drawdowns were observed at the North side of the enclosure. Thus, it was deduced that the enclosure was open near from PZ1' and PZ3 (Figure 6.6a). The gap was situated at deep layers since the drawdown was higher in the deeper piezometers, moreover, defects in diaphragm walls usually appear at great depths because construction problems are more common than in shallow depths. New numerical results were obtained considering the gap to validate this deduction and they fitted correctly with the

data measured (Figure 6.5). The response time to the pumping, which depends on the hydraulic characteristics ($k$ and $S_S$) of the aquifer and the distance from the well to the piezometers, observed in the WTAT was increased in regard of the first pumping test. This occurred because groundwater had to dodge the enclosure to arrive until the well and therefore, groundwater ran more distance. The response time risen two orders of magnitude at the piezometers located far from the gap (PZ-2), but it risen less at the piezometers located in front of the gap (PZ-3), which verified the location of the gap.

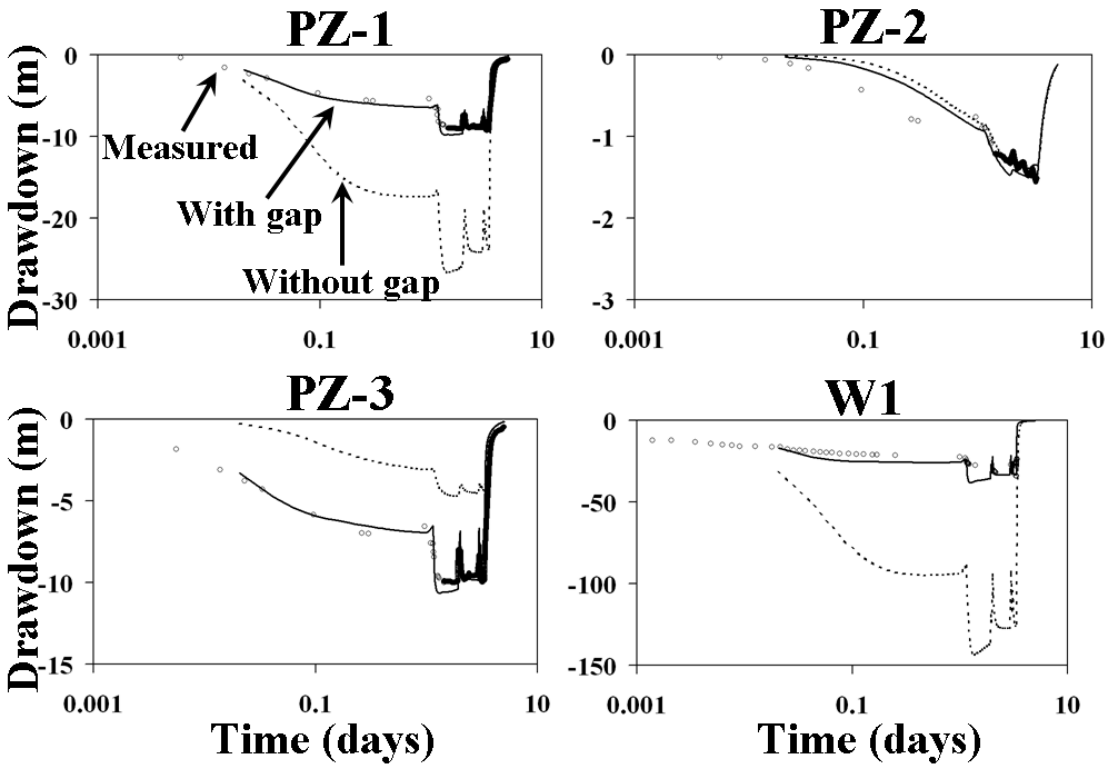


**Figure 6.5.** Evolution of measured (dots) and computed drawdowns during the Watertightness Assessment Test (WTAT). Numerical results are shown both with a gap in the enclosure (continuous line) and without a gap (dashed line).

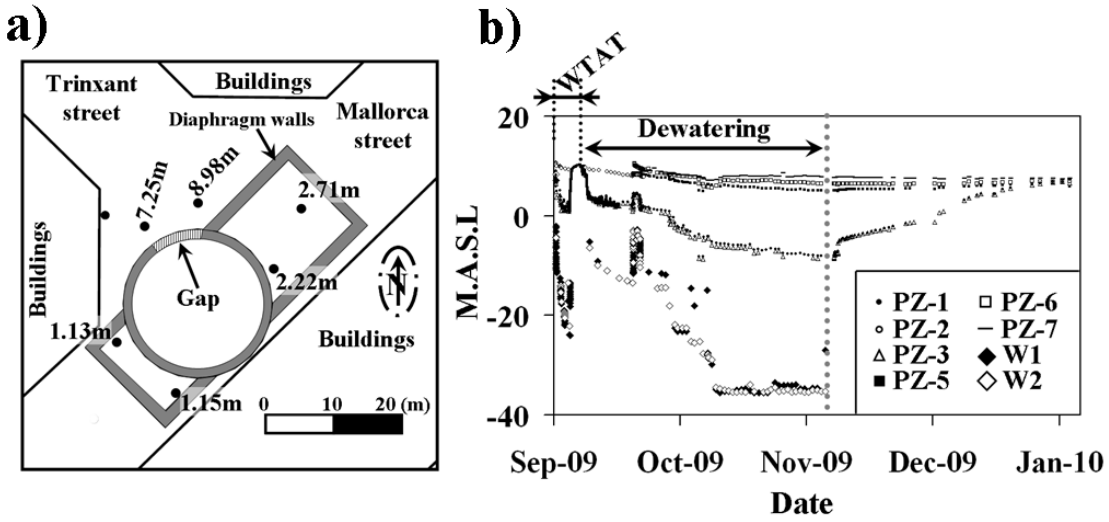


**Figure 6.6.** a) Measured drawdown during the WTAT at the piezometers located around the enclosure. Drawdown distribution indicated that the enclosure had a gap in the North side. b) Evolution of measured drawdown in the piezometers and in the pumping wells during the dewatering stage and after this.

It was necessary to check the stability and the pumping effects considering the gap because the previous dewatering predictions considered a perfect enclosure. Two pumping wells (W1 and W2) were needed to drop the water pressure as much as necessary. One of them was located close to the gap, which facilitated to achieve stable conditions at this area. The effect of the gap in the effectiveness of the enclosure was observed in the rise of the pumping rate required to stability. This rose from 2 to 6.6 l/s (+330 %), which indicates theat the effective transmissivity of the enclosure also rose. Bottom stability results, which were achieved by prescribing 40 m of drawdown inside the two wells, are shown at Table 6.3. Note that the safety factor only could be calculated in the middle of the modeled layers located in the saturated zone because the water pressure only could be known at these places with the multilayered numerical model.

Numerical settlements were recalculated with the presence of the gap. Given the difficulty of construct a 3D hydromechanical model, they were obtained using the axisymmetrical. To simulate the gap, the hydraulic conductivity of the diaphragm walls at deep layers was increased. An effective *k* was used considering that the area affected by the defect had 2 m width. Predicted settlements in the area close to the gap were 1.3

mm at 10 m from the enclosure, which is the distance where there are buildings. Settlements at other sides of the enclosure were not calculated, because outside drawdown caused by a gap is located around it (Vilarrasa, et al., 2012, Pujades, et al., 2012). Pumping rate and settlement caused by dewatering continued being acceptable. Therefore, the excavation continued as was expected.

Given the location of the gap (below the excavation bottom) and these results, the gap was not repaired by injection. On one hand, the rise of pumping rate and outside affectations were not disproportionate. On the other hand, the injections works would have interfered with the construction tasks. However, if the defect would have been above the bottom, it would have been injected to avoid soil dragging towards the excavation that would have caused an outside hole.

| Depth | 25 m drawdown |
|---|---|
| 33 | Non saturated |
| 38.5 | |
| 42.5 | |
| 44.5 | 2.39 |
| 47 | 1.58 |
| 54 | 1.37 |
| Q (l/s) | 6.6 |

**Table 6.3.** Safety factor computed numerically considering the gap in the enclosure. Predicted flow-rate is also shown.

### 6.3.5. Actual dewatering evolution

Head, flow-rate and soil movements were measured during the dewatering stage. Head was measured at the piezometers (PZ-1', PZ-2, PZ-3, PZ-5, PZ-6 and PZ-7) and in the pumping wells (W1 and W2) manually. Measures were taken daily to verify the correct dewatering of the excavation. Flow-rate was measured at pumping wells. It was not possible to use an electromagnetic flow-meter, because they are very fragile. Therefore, flow-rate was measured using a Woltman horizontal turbine flow-meter. Figure 6.6b displays the head evolution during the dewatering stage measured in the piezometers and in the pumping wells. Head inside the pumping wells achieve the necessary depth to guarantee the bottom stability. A drop and a recovering that belongs

to the watertight assessing test are observed the first days of September 2009. Subsequently, it was pumped until mid September to locate the gap, when the additional piezometers were constructed, where a recovery indicating the end of the pumping is observed. After, when the excavation arrived as far as the water table the dewatering started and this was continuous until November 2009.

Soil movements were measured during all the construction process at several monitoring points located around the enclosure. Figures 6.7a and 6.7b display the partial soil movements caused during the construction of the diaphragm walls and during the excavation and dewatering stages. On one hand, settlement caused by the construction of the walls was approximately 1 mm around the enclosure except in the North side, where the soil dropped 2 mm. This fact suggests that some problems appeared at this side during the walls construction, which matches with the presence of a gap. On the other hand, soil had an unusual behaviour during the excavation and dewatering stages. As a result, observed pumping settlements did not fit with the predicted. The magnitude of the settlements was different from the predictions. They were higher than the predictions at the South and South-east sides and smaller at the North. In the West side, no settlements were observed, contrary to the expected, the soil suffered a heave. Moreover, the awaited shape was circular with a protuberance around the gap, but although the protuberance could be intuited, the settlement distribution was not circular. The maximum settlements were delimited by an elongate area that followed the street direction.

Soil movement evolution from 8 monitoring points (Figure 6.8a) is shown at Figures 6.8b and 6.8c. Figure 6.8b displays the soil movements measured by monitoring points located at the North and West sides while Figure 6.8c shows the measures from monitoring points located at the South and South-east sides. Until the start of the excavation the movements were similar at all of the monitoring points. Only HN-8 measured more settlement and HN-1 did not vary its position during the construction of the walls. Similar observations were made at the settlement distribution plots. Once the dewatering started (second shady area at both plots) three behaviours can be observed. Points located at the South and South-east sides dropped until the end of the dewatering, points located at the West side rise and points located at the North side registered a moderated drop. When the pumping finished all of the monitoring points measured a small and quickly rise, but after that, the soil had different behaviours depending on the

side. While the South and South-east sides risen during the recovering period, the other sides dropped symmetrically.

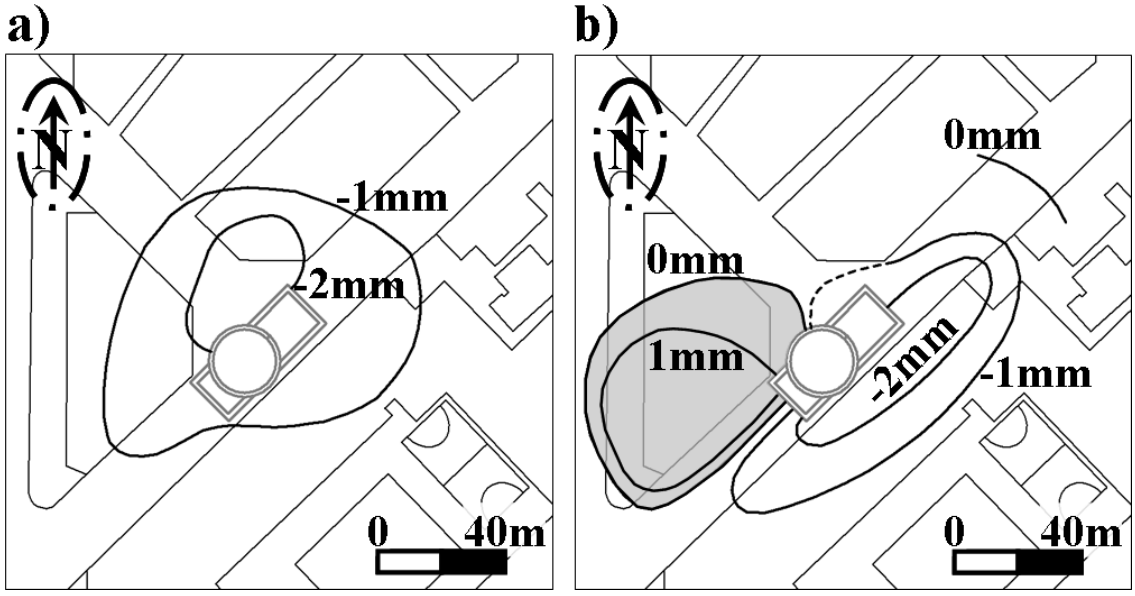


The difference between the expected and observed soil movements could be caused because it was assumed that all the soil was preconsolidated given the groundwater historical evolution and the observations at other sites of the HST tunnel construction in Barcelona. However, the soil could have lost this condition at the surroundings of the construction before the excavation. During the testing well construction two siphoning events occurred when two transmissive layers were being drilled (Layers 9 and 14 in Table 6.1). The bottom of the perforation siphoned and a big quantity of sand was dragged and was extracted to the surface. The well was finished satisfactory by raising the head inside the drilling machinery. During the filling of the gravel pack around the well, more quantity of gravel was required to fill the cavities generated during the siphoning events. 1 $m^3$ of gravel was necessary to fill the gravel pack between 30 and 32 m depth and 4 $m^3$ were needed to fill between 42 and 47 m depth. However, the alteration of the soil structure was too local and only affected the area located around the testing well. Of course that the siphoning events contributed to the pumping settlements, but it would be excessive to attribute all the differences between the predictions and the observations to the testing well construction. Moreover, the shape of the settlements distribution could not be caused by this fact.

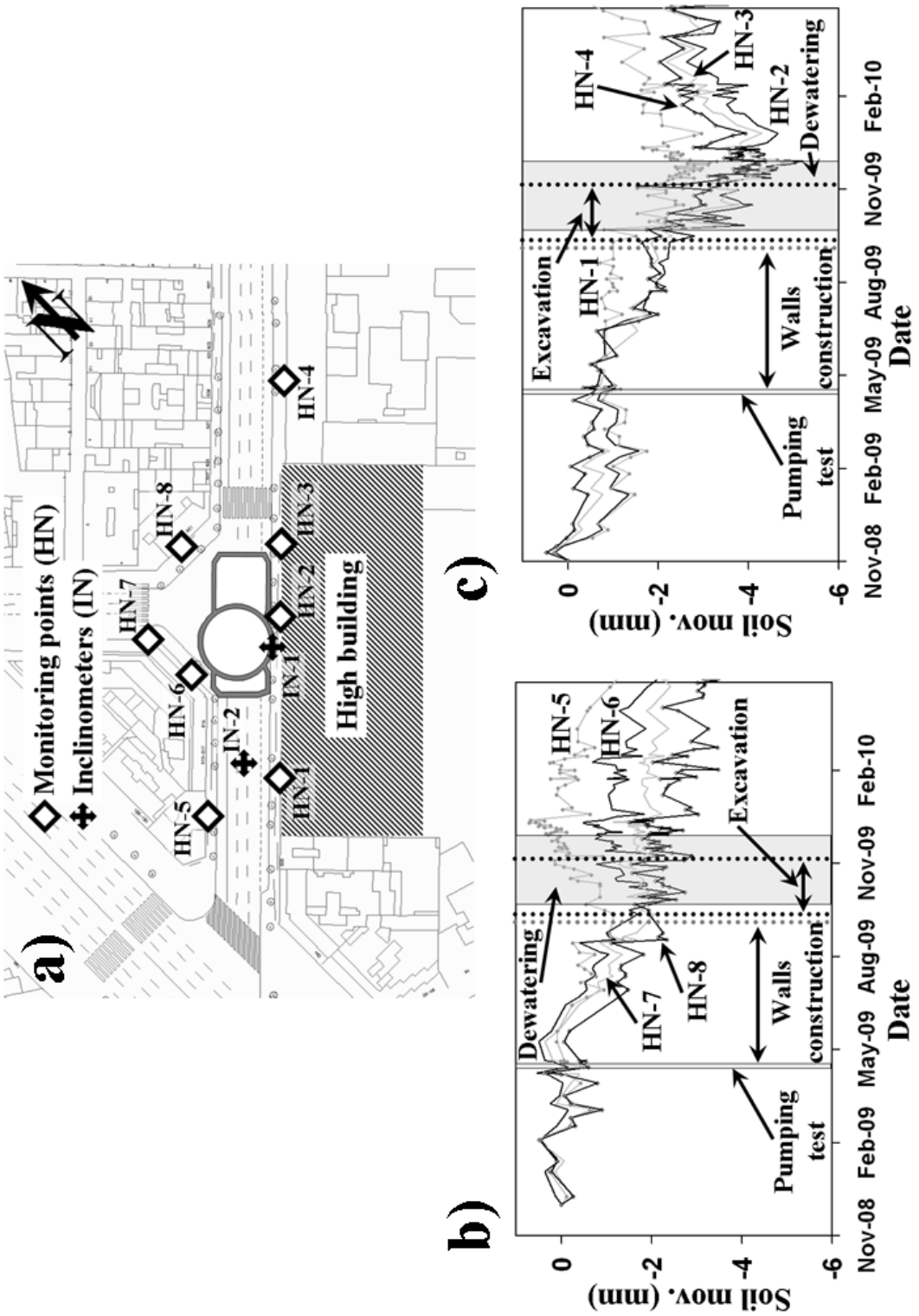


**Figure 6.8.** a) Plan view of the soil movement monitoring point and the inclinometers. b) Evolution of the soil movements measured in the monitoring points located at the West and North sides. c) Evolution of the soil movements in the monitoring points located at the South and South-east sides.

Nevertheless, the settlement distribution could be related with the building located at the South-East side on the shaft (Figure 6.8a). This building has 4 parkings floors, which arrive until the water table (located at 10 m depth), and it is deeper than the other buildings in the area. Probably, the excavation required to construct the 4 floors of parking modified partially the structure of the soil around the building, which could be consequence of the relaxation in the strain of the soil during the excavation. As a result, the affected area settled more during the dewatering than a preconsolidated soil. In fact, pumping settlements were similar in all of the area occupied by the building and they decrease sharply further away from the building. These settlements bended the soil and caused the heave of the North and East sides. But in the North side, no heave was observed because th dewatering settlements were higher due to the gap. Therefore, observed settlements were less than the predicted. Finally, as only the surroundings of the building would have lost the preconsolidation degree, the rest of the soil continued having an elastic behaviour. As a result, when pumping ceased, the West side settled to return as far as its initial position while the South-east side heaved. However, it is only a speculation since we do not have enough data to affirm this doubtless.

## 6.4. Discussion and Conclusions

Results show the importance of characterise the soil by combining different techniques and the utility of perform a pumping test to realize the presence of transmissive layers intercalated between low hydraulic conductivity materials. The initial geological studies of the site suggested to use drainage techniques focused on dewater low hydraulic conductivity materials, since this type of materials were observed at the bottom of the excavation. However, a posterior hydrogeological characterisation revealed thin intercalations of transmissive materials. Borehole logging, grain size analysis and Gamma Natural Ray logging were used to know the characteristics of the soil, and a pumping test revealed that the hydraulic conductivity was higher than 0.1 m/d in the 75% of aquifer thickness. This fact is not isolated, since the most of the materials characterised geologically as poor permeable have thin intercalations of transmissive sediments, which gives to the whole formation a significant transmissivity. The nature of the materials tips the balance and conventional deep pumping wells were used to perform the drainage of the excavation. If other drainage technique (focused on

dewater low hydraulic conductivity materials) would have been used, unstable conditions would have been achieved during the excavation, since water pressure would not have been dropped as much as necessary.

Defects in enclosures are relatively frequents (Bruce *et al.,* 1989, Knight *et al.,* 1996 and Vilarrasa *et al.,* 2012). However, they are not usually considered and only limited geophysics methods are used to know the state of some joints located between the diaphragm walls that form an enclosure (Pujades *et al.,* 2012). The results show the suitability of performs a WTAT consisting in pumping inside of an enclosure and compare the observed measures with the predicted. All the enclosure can be tested easily by performing a WTAT and the defects can be located. Moreover, this test does not interfere with construction works, and the results are, generally, obtained in a short period of time. The WTAT, which was performed with piezometers screened at different depths, also allowed knowing the depth of the gap. This fact was relevant because, if the gap would have been above the excavation bottom, it have been injected. Nevertheless, this was below the bottom and the excavation was stable only modifying the dewatering design. A fact of concern is the loss of efficiency of an enclosure that contains a defect. This raises enormously the effective transmissivity of the enclosure. Results show that the pumping rate required to stable conditions risen from 2 to 6.6 l/s (+330 %).

The importance of characterise the soil to design a suitable dewatering system and the necessity of evaluate the state of an enclosure before the excavation stage suggest the relevance of following a procedure to perform a deep excavation under the water table in safe conditions and guaranteeing the integrity of adjacent buildings and/or structures. This must include soil characterisation, dewatering numerical design, WTAT and monitoring of the drainage.

Apart from these, the development of the excavation of Trinxant proved that pumping settlements at preconsolidated soils are fairly small and elastic. In addition, they can be estimated with a moderate error by using stiffness parameters obtained from the storage coefficient values of the aquifer.

# 7. General conclusions

The following general results may be drawn from this thesis:

- Underground structures that intersect aquifers may cause head variations (barrier effect). The variations can entail negative consequences, from flooding or propagation of contaminants in the upgradient side to settlements seawater intrusion or drying of springs at the downgradient side. Generally, the head rise upgradient and drop downgradient. However, the nature of the boundaries plays a special role in the barrier effect distribution. The head rise is, in general, larger near of the barrier (local barrier effect) than at long distances (regional barrier effect). Similarly, the variations are larger near the middle of the structure than in the edges. Only two variables condition the magnitude of the barrier effect: the geometry of the barrier and the natural gradient prior to construction. Only these two variables are necessary to compute the barrier effect by using the solutions proposed. The solutions can be used to assess the barrier effect caused by an underground construction with a moderate error or to know the efficacy of a bypass system. The availability of the semi-empirical equations was proven using real data from the HST tunnel construction in Barcelona.

- Settlements caused by pumping at preconsolidated soils are relative small and elastic. Therefore, short diaphragm walls (as far as the minimum depth required structurally) and deep pumping wells are an efficient option to perform deep excavations in a safe manner. Outside impacts are similar to those of deep enclosures, but the cost is reduced. Deep enclosures have sometimes been used because preliminary estimations suggest large settlements. However, these predictions can be conditioned by the stiffness parameters of the soil used, which sometimes are lower than the real ones. The storage coefficient of the soil, which can be known easily by pumping test interpretation, also can be used to obtain the compressibility of the soil and to compute the soil movements caused

during dewatering. In fact, the displacements calculated using the storage coefficient match with the actual measurements. Apart from this, diaphragm walls are a good option to deepen an enclosure. Jet-grouting (often used to this purpose) does not reduce enough the hydraulic conductivity of the soil when it is applied at permeable materials. Therefore, given the width of the enclosure, the groundwater that flow towards the excavation is minimally reduced.

- Defects in enclosures used to perform deep excavations are a relative common problem. Small defects can entail negative consequences, if they are present in the enclosure, sinkholes can arise outside the excavation, the stability and development of the excavation are compromised and the pumping rate must be increased a lot to achieve stable conditions. Small defects increase considerably the effective parameters of all of the enclosure. However, the outside affectations are concentrated only around the defect. Their reparation is much easier if they are noticed before than during the excavation stage. Therefore, it is important to know the state of an enclosure before excavation. Hydrogeological tools can be used to assess the state of enclosures. In this thesis, I propose performing Watertightness Assessment Tests (WTAT) to the enclosures. In addition, one methodology to apply in steady state and two in transient state are proposed. On one hand, the steady state spatial distribution of drawdown along a linear enclosure indicates the position of the defects or, if there are many, the effective parameters of the enclosure. On the other hand, the drawdown and pumping rate evolutions depends directly of the state of the enclosure. Therefore, unexpected changes in the flow regime (between radial or linear) indicate us the existence or not of defects and its position.

- This thesis proposes methods and solutions, from a hydrogeological point of view, to improve the construction processes of underground structures below the water table. The methods allow us to assess the impacts caused by underground structures in aquifers, to design efficient dewatering systems of deep excavations and to evaluate the state of enclosures.

However, they are not useful if the soil is not accurately characterised from a hydrogeological point of view or if the historical processes suffered by the soil are not known. To this end, it is essential to define a clear methodology.

# 8. References

Allan, M., Kukacka, L., 1995. Analysis of core samples from jet grouted soil. Brookhave national laboratory – BNL-62357, Informal report, New York, United States of America.

Arai, Y., Kusakabe, O., Murata, O., Konishi, S., 2008. A numerical study on ground displacement and stress during and after the installation of deep circular diaphragm walls and soil excavation. Computers and Geotechnics, 35, 791-807.

Batu, V., 1998. Aquifer hydraulic, a comprehensive guide to hydrogeologic data analysis. John Wiley & Sons, ed. New York.

Bear, J., 1972. Dynamics of Fluids in Porous Media. Elsevier, New York.

Berry, G., Shiriaw, J., Hayata, K., Tan, S., 1988. A review of grouting techniques utilised for bored tunnelling with emphasis on the jet grouting method. Construction and Building Materials, 2 (1), 34-41.

Bruce, D., De Paoli, B., Mascardi, C., Mongilardi. E., 1989. Monitoring and quality control of a 100 metre deep diaphragm wall, in: Burland, J., Mitchell, J. (Eds.), Pilling and deep foundations, A.A. Balkema, Rotterdam. 23-32.

Bonomi, T., Bellini, R., 2003. The tunnel impact on the groundwater level in an urban area: a modelling approach to forecast it. Materials and Geoenvironment. 50, 45-48.

Butscher, C, 2012. Steady-state groundwater inflow into a circular tunnel. Tunelling and Underground Space Tecnology. 32, 158-167.

Cashman, P.M., Preene, M., 2001. Groundwater lowering in construction – A practical guide. Spon press, London.

Carrera, J., Neuman, S., 1986a. Estimation of aquifer parameters under transient and steady state conditions: 1. Maximum likelihood method incorporating prior information. Water Resources Research, 22 (2), 199-210.

Carrera, J., Neuman, S., 1986b. Estimation of aquifer parameters under transient and steady state conditions: 2. Uniqueness, stability and solution algorithms. Water Resources Research, 22 (2), 211-227.

Carrera, J., Neuman, S., 1986c. Estimation of aquifer parameters under transient and steady state conditions: 3. Application to synthetic and field data. Water Resources Research, 22 (2), 228-242.

Cooper, H. H., Jacob, C. E., 1946. A generalized graphical method for evaluating formation constants and summarizing well-field history, Eoc trans. AGU, 27(4), 526-534.

Chae, G.T., Yun, S.T., Choi, B.Y., Yu, S.Y., Jo, B.M., Kim, Y.J., Lee, J.Y., 2008. Hydrochemistry of urban groundwater, Seoul, Korea: The impacto f Subway tunnels on groundwater quality. Journal of Contaminant Hydrology. 101, 42-52.

Chiocchini, U., Castaldi, F., 2011. The impact of groundwater on the excavation of tunnels in two different hydrogeological settings in central Italy. Hydrogeology Journal. 19, 651-669.

Cripps, A., C., McCann, D., M., 2000. The use of the natural gamma log in engineering geological investigations. Engineering Geology, 55, 313-324.

Culí, L, 2011. Estudio de la relación entre el funcionamiento de una tuneladora (EPB) con la geología del terreno y las variaciones del nivel piezométrico. Minor thesis. Universitat Politècnica de Catalunya.

Custodio, E., Llamas, R., 1983. Hidrología Subterránea, Ed. Omega, España.

Custodio, E., Carrera, J., 1989. Aspectos generales sobre la contaminación de las aguas subterráneas. OP. 13, 96-112.

Davis, G. M., Horswill, P., 2002. Groundwater control and stability in an excavation in Magnesian Limestone near Sunderland, NE England. Engineering Geology, 66, 1-18.

Deveughèle, M., Zokimila, P., 2010. Impact of an impervious shallow gallery on groundwater flow. Bulletin of Engineering Geology and the Environment. 69, 143-152.

El- Nahhas, F. M., 1999. Soft ground tunnelling in Egypt: Geotechnical challenges ans expectations. Tunelling and Underground Space Technology, 14 (3), 245-256.

El Tani, M., 1999. Water inflow into tunnels, in: Alten, et al. (Eds.), Challenges for the 21st century. Balkema, Rotterdam. 61-70.

El Tani, M., 2003. Circular tunnel in a semi-infinite aquifer. Tunnelling and Underground Space Technology. 18, 49–55.

Ercelebi, S.G., Copur, H., Ocak, I., 2011. Surface settlement predictions for Istanbul Metro tunnels excavated by EPB-TBM. Environmental Earth Science. 62, 357-365.

Fang, Y. S., Liao, J.J., Sze, S. C., 1994. An empirical strength criterion for jet grouted soilcrete. Engineering Geology, 37, 285-293.

Ferrer, A., Davila, V., Sahuquillo, A., 2008. Descenso del nivel freático en centros urbanos. Diseño e instalación de una red de control eficiente y sostenible. In: Carmen, M., Vallejos, A., Valverde, M., Lambán, L. (Eds.), El agua y las infraestructuras en el medio subterráneo. Instituto geológico y minero de España, Madrid, pp. 335-353.

Ferris, J., Knowles, D., Brown, R., Stallman, R., 1962. Theory of aquifer tests. U.S. Geological Survey Water Supply Paper 1536-E.

Flora, A., Modoni, G., Lirer, S., and Croce, P., 2013. The diameter of single, double and triple fluid jet grouting columns: prediction method and field trial results. Geotechnique, 63 (11), 934-945. doi: 10.1680/geot.12.P.062.

Font-Capo, J., Vázquez-Suñé, E., Carrera, J., Martí, D., Carbonell R., Pérez-Estaún, A., 2011, Groundwater inflow prediction in urban tunneling with a tunnel boring machine (TBM), Engineering Geology 121 (2011), 46-54, Doi: 10.1016/j.enggeo.2011.04.012.

Forth, R.A., 2004. Groundwater and geotechnical aspects of deep excavations in Hong Kong. Engineering Geology. 72, 253–260.

Frank, R., Baduin, C., Driscoll, R., Kavvadas, M., Krebs Ovesen, N., Orr, T., Schuppener, B. 2004. Designer's Guide to EN1997-1, EUROCODE 7. Geotechnical Design-General Rules. Thomas Telford, London.

Furnival, G., Wilson, R., 1974. Regressions by leaps and bounds. Technometrics. 16, vol.4, 499-511.

Gatti, M.C., Cassani, G., 2007. Ground loss control in EPB TBM tunnel excavation, in: Barták, Hrdina, Romancov and Zlámal (Eds.), Underground Space – the 4th Dimension of Metropolises. Taylor and Francis Group, London.

Gavaskar, A., 1999. Design and construction techniques for permeable reactive barriers. Journal of Hazardous Materials, 68, 41-71.

Gens, A., Olivella, S.,Vallejan, B., 1999. Modelling of the THM behaviour of a concrete based engineered barrier (B waste canister), CRC OUPC 99-001/A, ANDRA, Châtenay-Malabry Cedex.

Goodman, R.F., Moye, D.G., Van Schaikwyk, A., Javandel, I., 1965. Groundwater inflows during tunnel driving. Bull. Assoc.Eng. Geologists 2 (1), 39–56.

Gómez, A. A., Rodríguez, L. B., and Vives, L. S., 2010. The Guarani Aquifer System: estimation of recharge along the Uruguay–Brazil border. Hydrogeology Journal, 18(7), 1667-1684.

Gue, S. S., Tan, Y. C., 2004. Two case histories of basement excavation with influence on groundwater. Keynote lecture, international conference on structural and foundation failures (ICSFF), Singapore, 2nd-4th August, 2004.

Guimera, J., 1992. Análisis experimental del flujo y comportamiento del ion nitrate en la zona no saturada y su influencia en el agua subterranean. PhD, diss., Dept. Geotechnical Engineering and Geosciences, Universitat Politècnica de Catalunya, UPC-BarcelonaTech, Barcelona, Spain.

Gulhati, S., Datta, M., 2005. Geotechnical Engineering. Tata McGraw Hill, Delhi.

Hollema, D.A., Olson, L.D., 2003. Crosshole sonic logging and velocity tomography imaging of drilled shaft foundations. Proc. NTTCE-03. DGZfP, Berlin.

Hsi, J., Small, J., 1992. Ground settlements and drawdown of the water table around an excavation. Canadian Geotechnical Journal, 24, 740-756.

Hsieh, P.A., Freckleton, R., 1993. Documentation of a computer program to simulate horizontal-flow barriers using The U.S. Geological Survey's Modular Three-Dimensional Finite-Difference Ground-Water Flow Model. Sacramento. Ca.

Hwang, R. N., Moh, Z. C., Kao, C. C., 2006. Design and construction of deep excavations in Taiwan. Proceedings of State-of-the-practice of Geotechnical Engineering in Taiwan and Hong Kong, 10-27.

Hwang, J.H., Lu, C.C., 2007. A semi-analytical method for analyzing the tunnel water inflow. Tunnelling and Underground Space Technology. 22, 39–46.

Iribar, V., J. Carrera, E. Custodio y A. Medina, 1997. Inverse modelling of sewater intrusion in the Llobregat delta deep aquifer. Journal of Hydrology, 198, 226-247.

Jacob,C . E., 1950. Flow of groundw ater, in Rousep, H. (Eds.), EngineeringH ydraulics. John Wiley, New York, pp. 321-386.

Jurado, A., De Gaspari, F., Vilarrasa, V., Bolster, D., Sánchez-Vila, X., Frenàndez-Garcia, D., Tartakovsky, D. M., 2011. Probabilistic analysis of groundwater-related risks at subsurface excavation sites. Engineering Geology. doi:10.1016/j.enggeo.2011.10.015.

Knight, D.J., Smith G.L., Sutton, J.S., 1996. Sizewell B foundation dewatering-system design, construction and performance monitoring. Géotechnique. 46(3), 473-490.

Kolymbas, D., Wagner, P., 2007. Groundwater ingress to tunnels – The exact analytical solution. Tunnelling and Underground Space Technology. 22, 23–27.

Kung, G. T. C., Hsiao, E. C. L., Schuster, M., Juang, C. H., 2007. A neural network approach to estimating deflection of diaphragm walls caused by excavation in clays. Computers and Geotechnics, 34, 385-396. doi: 10.1016/j.compgeo.2007.05.007

Kusumoto, S., Omae, H., Sato, T., Watanabe, M., Kobayashi, N., Nishida, K., 2004. Construction of preservation facilities on natural groundwater flows, in: Kono, Nishigaki and Komatsu (Eds.), Groundwater Engineering. Swets and Zeitlinger, Lisse, pp. 237-242.

Lancellotta, R., 1995. Geotechnical engineering, second ed. Taylor and Francis, Abingdon.

Lei, S., 1999. An analytical solution for steady flow into a tunnel. Groundwater. 37(1), 23-26.

Li, H., Kagami, H., 1997. Groundwater level and chemistry changes from túnel construction near Matsumoto City, Japam. Environmental Geology. 31, 76-84.

Li, D., Li, X., Li, C.C., Huang, B., Gong, F., Zhang, W., 2009. Case studies of groundwater flow into tunnels and an innovative water-gathering system for water drainage. Tunnelling and Underground Space Technology. 24, 260–268.

Li, X. G., Yuan, D. J., 2012. Response of a double-decked metro tunnel to shield driving of twin closely under-crossing tunnels. Tunnelling and Underground Space Technology, 28, 18–30.

López, A., 2009. Estudio analítico del efecto barrera: Definición, tipología, soluciones y aplicación a caso real. Msc thesis. Universitat Politecnica de Catalunya (UPC).

Marinos, P., Kavvadas, M., 1997. Rise of the groundwater table when flow is obstructed by shallow tunnels, in: Chilton, J. (Eds.), Groundwater in the urban environment: Problems, processes and management. Balkema, Rotterdam, pp. 49-54.

Medina A, Carrera J, 1996. Coupled estimation of flow and solute transports parameters. Water Resources Research, 32 (10), 3063-3076.

Medina, A., Alcolea, A., Carrera, J., Castro, L.F., 2000. Modelos de flujo y transporte en la geosfera: Código TRANSIN IV. [Flow and transport modelling in the geosphere: The code TRANSIN IV]. IV Jornadas de Investigación y Desarrollo Tecnológico de Gestión de Residuos Redioactivos de ENRESA. Technical publication 9/2000: 195-200.

Medina A, Carrera J, 2003. Geostatistical inversion of coupled problems: dealing with computational burden and different types of data. Journal of Hydrology, 281 (4), 251-264.

Meiri, D., 1985. Unconfined groundwater flow calculation into a tunnel. Journal of Hydrology. 82, 69-75.

Merrick, N., Jewell, M., 2003. Modelling of the groundwater impact of a sunken urban motorway in Sydney, Australia. Materials and Geoenvironment. 50, 229-232.

Modoni, G., Croce, P. & Mongiovì, L., 2006. Theoretical modeling of jet grouting. Geotechnique, 56(5), 335-347. doi: 10.1680/geot.2006.56.5.335.

Neville, A.M., 1995. Properties of Concrete. Longman, Harlow.

Ni, J., C., Cheng, W., 2011. Shield machine disassembly in grouted soils outside the ventilation shaft: A case history in Taipei Rapid Transit System (TRTS). Tunnelling and Underground Space Technology, 26, 435–443.

Nikbakhtan, B., Ahangari, K., Rahmani, N., 2010. Estimation of jet grouting parameters in Shahriar dam, Iran. International Science and Technology, 20, 472-477.

Olivella S., Carrera J., Gens A. & Alonso E.E. (1994). Non-isothermal multiphase flow of brine and gas through saline media. Transport In Porous Media, 15, 271–93.

Olivella, S., 1994. CODE_BRIGHT User's guide. Dept. Geotechnical Engineering and Geosciences, Universitat Politècnica de Catalunya, UPC-BarcelonaTech, Barcelona, Spain.

Olivella S., Gens A., Carrera J. & Alonso E.E. (1996). Numerical formulation for a simulator (CODE_BRIGHT) for the coupled analysis of saline media. Eng. Computations, 13, 87–112.

Paikowsky, S., Chernauskas, L., 2003. Review of deep foundations integrity testing methods and case histories, Bsces-geo-institute deep foundations seminar.

Paris, A., Teatini, P., Venturini, S., Gambolati, G., Bernstein, A.G., 2010. Hydrological effects of bounding the Venice (Italy) industrial harbour by a protection cut-off wall: a modeling study. Journal of Hydrologic Engineering. 15 (11), 882–891.

Park, K.H., Owatsiriwong, A., Lee, J.G., 2007. Analytical solution for steady-state groundwater inflow into a drained circular tunnel in a semi-infinite aquifer: A revisit. Tunnelling and Underground Space Technology. 23, 206–209.

Perrochet, P., 2005. A simple solution to tunnel or well discharge under constant drawdown. Hydrogeology Journal. 13 (5–6), 886–888.

Powers, J. P., Corwin, A. B., Schmall, P. C., Kaeck, W. E., 2007. Construction dewatering and groundwater control - New methods and applications, third ed. John Wiley and Sons, United States of America.

Pujades, P., Vázquez-Suñe, E., Carrera, J., 2008. Optimización de las lecturas de caudal durante el drenaje de obras y ensayos de bombeo, in: Carmen, M., Vallejos, A., Valverde,. M and Lambán, L. (Eds.), El agua y las infraestructuras en el medio subterráneo, Instituto geológico y minero de España, Madrid. 417-422.

Pujades, P., Mascuñano, E., Jurado, A., Vázquez-Suñe, E., Carrera, J., 2009. Detection faulty joints during the construction of tunnels excavated by the cut and cover method. Proceedings of the 9th international conference on tunnel construction and underground structures, 138-147.

Pujades, E., Carrera, J., Vázquez-Suñé, E., Jurado, A., Vilarrasa, V., Mascuñano-Salvador, E., 2012a. Hydraulic characterization of diaphragm walls for cut and cover tunnelling. Engineering Geology. 125, 1-10.

Pujades, E, López, A., Carrera, J., Vázquez-Suñé, E., Jurado, A., 2012b. Barrier effect of underground structures on aquifers. Engineering Geology, 145-146, 41-49.

Pujades, E., Vázquez-Suñé, E., Carrera, J., Vilarrasa, V., Jurado, A., De Simone, S., Ledesma, A., Ramos, G. Lloret, A. 2013a. Efficiency of deep enclosures versus pumping to reduce settlements during shaft excavations. Engineering Geology, Accepted.

Pujades, E., Vázquez-Suñé, E., Carrera, J., Jurado, A., 2013b. Dewatering of a deep urban excavation performed in a low permeability soil. Submitted.

Rausche, F., 2004, Non destructive evaluation of deep foundations. Proceedings of the fifth international conference on case histories in geotechnical engineering, New York.

Renard, P., Glenz, D., Mejias, M., 2008. Understanding diagnostic plots for well-test interpretation. Hydrogeology Journal. 17, 589-600.

Ricci, G., Enrione, R., Eusebio, A., 2007. Numerical modelling of the interference between underground structures and aquifers in urban environment. The Turin subway – Line 1, in: Barták, Hrdine, Romancov and Zlámal (Eds.), Underground Space. Taylor and Francis Group, London, pp. 1323-1329.

Rienzo, F., Oreste, P., Pelizza, S., 2008. Subsurface geological-geotechnical modelling to sustain underground civil planning. Engineering Geology. 96, 187–204.

Ross, R.R., Beljin, M.S., 1998. Evaluation of containment systems using hydraulic head data. Journal of environmental engineering. 124(6), 575-578.

Roy, D., Robinson, K. E., 2009. Surface settlements at a soft soil site due to bedrock dewatering. Engineering Geology, 107, 109-117.

Samper, J., Carrera, J., Medina, A., Garcia, Vera, M.A., Vallecillo, M.A., Manzano, M., 1991. Revisión del modelo de flujo y de transporte de contaminantes en las aguas subterráneas. ENRESA (public company in charge of the safe management, storage and disposal of the radioactive wastes produced in Spain), Madrid. Technical report.

Saurer, E., Lesnik, M., 2011. Grid space optimization of jet grouting columns, in: Anagnostopoulos, Pachakis and Tsatsanifos (Eds.), Proceedings of the 15th European conference on soil mechanics and geotechnical engineering, IOS Press, pp. 1055-1060. doi: 10.3233/978-1-60750-801-4-1055

Schneebeli, G., 1966. Hydraulique souterraine, Ed. Eyrolles, Paris.

Schoeller, H.,1962. Les eaux souterraines. Masson and cie. ed. Paris.

Schwarz, F. W., Zhang, H., 2003. Fundamentals of Groundwater. John Wiley & Sons, ed. New York.

Shen, S.L., Luo, C.Y., Xiao, X.C., and Wang, J.L., 2009. Improvement Efficacy of RJP method in Shanghai Soft Deposit, in: Han, J., Zheng, G., Schaefer, V. R. and Huang, M. (Eds.), Advances in Ground Improvement (GSP 188), ASCE Press, Reston, Virginia, pp. 170-177.

Shen, S.L., Wang, Z.F., Horpibulsuk, S, and Kim, Y.H., 2013a. Jet-Grouting with a newly developed technology: the Twin-Jet Method, Engineering Geology, 152(1), 87-95. doi: 10.1016/j.enggeo.2012. 10.018.

Shen, S.L., Wang, Z.F., Sun, W.J., Wang, L.B., and Horpibulsuk, S., 2013b. A field trial of horizontal jet grouting using the composite-pipe method in the soft deposit of Shanghai. Tunneling and Underground Space Technology, 35(2013), 142-151. doi: 10.1016/j.tust.2013.01.003.

Shen, S.L., Wang, Z.F., Yang, J., and Ho, E.C., 2013c. Generalized approach for prediction of jet grout column diameter, Journal of Geotechnical and Geoenvironmental Engineering, doi: 10.1061/(ASCE)GT.1943-5606.0000932.

Sneed, M., 2001. Hydraulic and mechanical properties affecting ground-water flow and aquifer-system compactation, San Joaquin Valley, California. U.S. Geological survey open-file report 01-35.

Stille, H., Palmström, A., 2008. Ground behaviour and rock mass composition in underground excavations. Tunnelling and Underground Space Technology, 23, 46–64.

Tambara, M., Nishigaki, M., Hashimoto, T., Shinshi, Y., Daito, K., 2003. Basic concept on preservation natural groundwater flows from intercepting by underground structure, in: Kono, Nishigaki and Komatsu (Eds.), Groundwater Engineering. Swets and Zeitlinger, Lisse, pp. 217-222.

Terzaghi, K., Peck, R.B., 1948. Soil mechanics in engineering practice, second ed. John Wiley and Sons, United States of America.

Theis, C.V., 1935. The relation between the lowering of the piezometric surface and the rate and duration of discharge of a well using groundwater storage. Am. Geophys. Union Trans. 16, 519-524.

Thiem, G., 1906. Hydrologische Methoden. Leipzig, Gebhardt.

Tinoco, J., Gomes, A., Cortez, P., 2011. Application of data mining techniques in the estimation of the uniaxial compressive strength of jet grouting columns over time. Construction and Building Materials, 25, 1257-1262.

Tubau, I., 2004. Estudio Hidrogeológico y propuesta de proceso constructivo para la excavación de un túnel entre pantallas en el delta del Llobregat. Minor thesis. Universitat Politecnica de Catalunya (UPC).

UPC (2003). Codigo Visual Transin 1.1 R65. Developed in the Department of Geotechnical Engineering and Geosciences (ETCG), UPC.

Usunoff, E., J. Carrera, S.F. Mousavi, 1992. An approach to the design of experiments for discriminating among alternative conceptual models. Advances in Water Resources, 15 (3), pp. 199-214.

Van Baars, S., 2011. Causes of major geotechnical disasters. In: Vogt, Schuppener, Straub and Braü (Eds.), ISGSR 2011. Bundesanstalt für Wasserbau, Germany.

Van der Boom, J., 2011. Tunelling in urbana reas: the use of lateral walls to Project abcient buildings. Minor thesis. Universitat Politecnica de Catalunya (UPC).

Vázquez-Suñe, E., Sánchez-Vila, X., Carrera, J., 2005. Introductory review of specific factors influencing urban groundwater, an emerging branch of hydrogeology, with referente to Barcelona, Spain. Hydrogeology Journal. 13, 522-533.

Velasco, V., Cabello, P., Vázquez-Suñé, E., López-Blanco, M., Ramos, E., Tubau, I., 2011. A sequence stratigraphic based geological model for constrining

hydrogeological modelling in the urabnized area of the quaternary Besòs delta (NW Mediterranean coast, Spain). Geological Acta. 10 (4), 373-393.

Vicenzi, V., Gargini, A., Goldscheider, N., 2009. Using tracer tests and hydrological observations to evaluate effects of túnel drainage on groundwater and surface Waters in the Northern Apennines (Italy). Hydrogeology Journal. 17, 135-150.

Vilarrasa, V., Bolster, D., Dentz, M., Olivella, S., Carrera, J., 2010. Effects of CO2 Compressibility on CO2 Storage in Deep Saline Aquifers. Transport In Porous Media. 85, 619-639.

Vilarrasa, V., Carrera, J., Jurado, A., Pujades, E., Vazquez-Sune, E., 2012. A Methodology for characterizing the hydraulic effectiveness of an annular low-permeability barrier. Engineering Geology 120 (2011), 68-80, Doi: 10.1016/j.enggeo.2011.04.005.

Wen, D., 2005. Chapter 13 Use of jet grouting in deep excavations, in: Buddhima, Indraratna and Jian Chu (Eds.), Ground improvement – Case histories. Elsevier Geo-Engineering Book Series, Elsevier, Oxford, Volume 3, pp. 357-370.

Wentworth, C.K., 1922, A scale of grade and class terms for clastic sediments. Journal of Geology, 30, 377-392.

White, B., Nagy, M., Allin, R., 2008. Comparing cross-hole sonic logging and low-strain integrity testing results, in: Santos, J.A. (Eds.), The 8th international application of stress wave theory to piles. IOS Press BV, Amsterdam.

Wong, L. W., Patron, B. C., 1993. Settlements induced by deep excavations in Taipei. Proceedings of 11th Southeast Asian Geotechnical Conference, Singapore, 787-791.

Wong, I. H., Poh, T. Y., 2005. Chapter 14 A case history of jet grouting in marine clays, in: Buddhima, Indraratna and Jian Chu (Eds.), Ground improvement – Case histories. Elsevier Geo-Engineering Book Series, Elsevier, Oxford, pp. 371-408.

Xanthakos, P., Abramson, L., Bruce, D., 1994. Ground control and improvement. John Wiley and Sons, United States of America.

Xu, Y.S., Shen, S.L., Du, Y.J., 2009. Geological and hydrogeological environment in Shangai with geohazards to construction and maintenance of infrastructures. Engineering Geology. 109, 241-254.

Zandarín, M., Oldecop, L., Rodríguez, R., Zabala, F., 2009. The rola of capillary water in the stability of tailing dams. Engineering Geology, 105, 108-118.

Zhang, J. F., Chen, J. J., Wang, J. H., Zhu, Y. F., 2013. Prediction of tunnel displacement induced by adjacent excavation in soft soil. Tunnelling and Underground Space Technology 36, 24-33.

Zhou, N.,Vermeer, P., Lou, R., Tang, Y., Jiang, S., 2010. Numerical simulation of deep foundation pit dewatering and optimization of controlling land subsidence. Engineering Geology 114 (3–4), 251-260.

# ANNEXES

## Annex I. Supplementary material of the Chapter 5

The two dimensional problem can be approximated by a one dimensional solution by integrating the flow equation in 1-D, which leads to

$$S_{aq}\frac{\partial \overline{h}}{\partial t}=T_{aq}\frac{\partial^2 \overline{h}}{\partial x^2}+2\frac{\alpha_{dw}}{d_{dw}}\left(H_{ext}-\overline{h}\right)+\sum_{i=0}^{N}\frac{Q_i\delta(x_i)}{d_{dw}} \qquad \text{(A.1)}$$

where $\overline{h}=\frac{1}{d_{dw}}\int_{-d_{dw}/2}^{d_{dw}} h(x,y)dy$, $\alpha_{dw}=T_{dw}/w_{dw}$ is the leakage coefficient of the wall, and $Q_i$ are the pumping rates of pumping wells located at $x_i$.

The solution in a generic interval $i(x_{i-1}, x_i)$ is obtained in a steady-state by solving first the homogenous equation and then imposing boundary conditions. The general solution

$$T_{ac}\frac{\partial^2 \overline{h}}{\partial x^2}-\frac{2\alpha_w \overline{h}}{d_{dw}}=0 \qquad \text{(A.2)}$$

is

$$\overline{h}=Ae^{\lambda x}+Be^{-\lambda x} \qquad \text{(A.3)}$$

where $\lambda=\sqrt{2\alpha_{dw}/\left(T_{aq}d_{dw}\right)}$ is a characteristic distance. In fact $1/\lambda$ is the distance so that a head drop, $\Delta h$, at a point in between the diaphragm walls will yield the same flow rate through the aquifer ($T_{aq}d_{dw}\lambda\Delta h$) and across the diaphragm walls ($2T_{dw}\Delta h/w_{dw}$).

$$Ae^{\lambda x_{i-1}}+Be^{-\lambda x_{i-1}}=h_1 \qquad \text{(A.4)}$$

$$Ae^{\lambda x_i}+Be^{-\lambda x_i}=h_2 \qquad \text{(A.5)}$$

Multiplying Eq.A.4 times $e^{-\lambda x_i}$, Eq.A.5 times $e^{-\lambda x_{i-1}}$, and subtracting yields

$$A = \frac{h_{i-1}e^{-\lambda x_i} - h_i e^{-\lambda x_{i-1}}}{2 \cdot sh\lambda(x_{i-1} - x_i)} \qquad \text{(A.6)}$$

Similarly, multiplying Eq.A.4 times $e^{\lambda x_i}$, Eq.A.5 times $e^{\lambda x_{i-1}}$, and subtracting yields

$$B = -\frac{h_{i-1}e^{\lambda x_i} - h_i e^{\lambda x_{i-1}}}{2 \cdot sh\lambda(x_{i-1} - x_i)} \qquad \text{(A.7)}$$

Substituting Eq.A.6 and A.7 in Eq.A.3 leads to

$$h(x) = h_{i-1}\frac{sh\lambda(x - x_i)}{sh\lambda(x_{i-1} - x_i)} + h_i \frac{sh\lambda(x_{i-1} - x)}{sh\lambda(x_{i-1} - x_i)} \qquad \text{(A.8)}$$

Finally, the flow rate pumped out (or flowing into) a point $x_i$ with head $h_i$, located between two points situated at $x_{i-1}$ and $x_{i+1}$ is:

$$Q_i = -T \cdot d \cdot \lambda \cdot \left[ h_i \cdot \{\text{cotgh}(\lambda(x_i - x_{i+1})) + \text{cotgh}(\lambda(x_{i-1} - x_i))\} + \frac{h_{i+1}}{\sinh(\lambda(x_i - x_{i+1}))} + \frac{h_{i-1}}{\sinh(\lambda(x_{i-1} - x_i))} \right]$$

(A.9)

# Annex II. Scientific papers and proceedings related with the elaboration of the thesis

## Annex II.1. Scientific articles

The following articles have been elaborated during this thesis. There is a copy of the published in the Annexes.

Pujades, E., Carrera, J., Vàzquez-Suñé, E., Jurado, A., Vilarrasa, V., Mascuñano-Salvador, E., 2012. Hydraulic characterization of diaphragm walls for cut and cover tunnelling. Engineering Geology, 125, 1-10. Doi: 10.1016/j.enggeo.2011.10.012.

Pujades, E., López, A., Carrera, J., Vàzquez-Suñé, E., Jurado, A, 2012. Barrier effect of underground structures on aquifers. Engineering Geology, 145-146, 41-49. Doi: 10.1016/j.enggeo.2012.07.004.

Pujades, E., Vàzquez-Suñé, E., Carrera, J., Vilarrasa, V., De Simone, S., Jurado, A., Ledesma, A., Ramos, G., Lloret, A., 2013. Deep enclosures versus pumping to reduce settlements during shaft excavations. Engineering Geology. Accepted.

Pujades, E., Vàzquez-Suñé, E., Carrera, J., Jurado, A., 2013. Dewatering of a deep excavation performed in a low permeability soil. Submitted.

Pujades, E., Vàzquez-Suñé, E., Carrera, J., Culí, L., Jurado, A., 2013. Hydrogeological impact assessment by tunnelling in high sensitive sites. Submitted.

Vilarrasa, V., Carrera, J., Jurado, A., Pujades, E., Vázquez-Suñé, E., 2011. A Methodology for Characterizing the Hydraulic Effectiveness of an Annular Low-Permeability Barrier. Engineering Geology, 120, 68-80. Doi: 0.1016/j.enggeo.2011.04.005.

J. Font-Capó; E. Vázquez-Suñé; J. Carrera; E. Pujades; V. Velasco; D. Monfort; 2013. Groundwater impact of lined tunnels constructed with Tunnel Boring Machine (TBM). Engineering Geology. Submitted.

## Annex II.2. Proceedings

The proceedings related to the thesis are listed below.

Pujades, E., Mascuñano, E., Jurado, A., Vilarrasa, V., Vázquez-Suñé, E., Carrera, J., 2009. Detección de juntas de pantalla defectuosas en excavaciones lineales drenadas, in: Cabrera, M.C., Vallejos, A., Valverde, M., Lambán, J.L., (Eds.), El agua y las infraestructuras en el medio subterráneo: testos de las ponencias y comunicaciones libres. Barcelona, 24-26 noviembre 2008. Publicaciones del instituto geológico y minero de España, Madrid, pp. 71-77.

Pujades, E., Vázquez-Suñé, E., Carrera, J., 2009. Optimización de las lecturas de caudal durante el drenaje de obras y ensayos de bombeo, in: Cabrera, M.C., Vallejos, A., Valverde, M., Lambán, J.L., (Eds.), El agua y las infraestructuras en el medio subterráneo: testos de las ponencias y comunicaciones libres. Barcelona, 24-26 noviembre 2008. Publicaciones del instituto geológico y minero de España, Madrid, pp. 417-422.

Pujades, E., Mascuñano, E., Jurado, A., Vilarrasa, V., Vázquez-Suñé, E., Carrera, J., 2009. Detection faulty joints during the construction of tunnels excavated by the cut and cover method, in: Likar, J., (Ed.), Proceedings of the 9th International Conference on Tunnel Construction and Underground Structures. Ljubljana, Slovenia, 16-18 September 2009. University of Ljubljana, Faculty of Natural Sciences and Engineering, Ljubljana, pp. 138-147.

Jurado, A., Pujades, E., Vilarrasa, V., Vázquez-Suñé, E., Carrera, J., 2009. Desarrollo de un método para resolver el drenaje de excavaciones entre pantallas, in: Cabrera, M.C., Vallejos, A., Valverde, M., Lambán, J.L., (Eds.), El agua y las infraestructuras en el medio subterráneo: testos de las ponencias y comunicaciones libres. Barcelona, 24-26 noviembre 2008. Publicaciones del instituto geológico y minero de España, Madrid, pp. 55-61.

Jurado, A., Pujades, E., Vázquez-Suñé, E., Carrera, J., 2009. Diseño y evaluación de la implementación de sistemas de drenaje en las obras de la L9 del metro en el delta del Llobregat, in: Cabrera, M.C., Vallejos, A., Valverde, M., Lambán, J.L., (Eds.), El agua y las infraestructuras en el medio subterráneo: testos de las ponencias y comunicaciones libres. Barcelona, 24-26 noviembre 2008. Publicaciones del instituto geológico y minero de España, Madrid, pp. 207-212.

Jurado, A., Bolster, D., Pujades, E., Vázquez-Suñé, E., Carrera, J., 2009. A methodology for analysing the drainage system in excavations between sheet pile walls, in: Likar, J., (Ed.), Proceedings of the 9th International Conference on Tunnel Construction and Underground Structures. Ljubljana, Slovenia, 16-18 September 2009. University of Ljubljana, Faculty of Natural Sciences and Engineering, Ljubljana, pp. 138-147.

Vilarrasa, V., Vázquez-Suñé, E., Carrera, J., Jurado, A., Pujades, E., 2009. Método para caracterizar la estanqueidad de recintos circulares poco permeables, in: Cabrera, M.C.,

Vallejos, A., Valverde, M., Lambán, J.L., (Eds.), El agua y las infraestructuras en el medio subterráneo: testos de las ponencias y comunicaciones libres. Barcelona, 24-26 noviembre 2008. Publicaciones del instituto geológico y minero de España, Madrid, pp. 103-109.

Vilarrasa, V., Jurado, A., Vázquez-Suñé, E., Carrera, Pujades, E., 2009. La modelación, un elemento clave en el seguimiento hidrogeológico de las obras de la LAV tramo La Torrassa-Sants, in: Cabrera, M.C., Vallejos, A., Valverde, M., Lambán, J.L., (Eds.), El agua y las infraestructuras en el medio subterráneo: testos de las ponencias y comunicaciones libres. Barcelona, 24-26 noviembre 2008. Publicaciones del instituto geológico y minero de España, Madrid, pp. 235-241.

# Annex III. Participation in congresses

**Event: Jornadas sobre "el agua y las infraestructuras en el medio subterráneo". Asociación Internacional de Hidrogeólogos – Grupo Español. Barcelona, España. November 2008.**

*Title:* Detección de juntas de pantallas defectuosas en excavaciones lineales drenadas.
*Authors:* Pujades, E., Mascuñano-Salvador, E., Jurado, A., Vilarrasa, V., Vàzquez-Suñé, E., Carrera, J.

*Title:* Optimización de las lecturas de caudal durante el drenaje de obras y ensayos de bombeo.
*Authors:* Pujades, E., Vàzquez-Suñé, E., Carrera, J.

*Title:* Desarrollo de un método para resolver el drenaje de excavaciones entre pantallas.
*Authors:* Jurado, A., Pujades, E., Vàzquez-Suñé, E., Carrera, J.

*Title:* Diseño y evaluación de la implementación de sistemas de drenaje en las obras de la L9 del metro en el delta del Llobregat.
*Authors:* Jurado, A., Pujades, E., Vàzquez-Suñé, E., Carrera, J.

*Title:* Método para caracterizar la estanqueidad de recintos circulares poco permeables.
*Authors:* Vilarrasa, V., Vàzquez-Suñé, E., Carrera, J., Jurado, A., Pujades, E.

*Title:* La modelación, un elemento clave en el seguimiento hidrogeológico de las obras de la LAV tramo La Torrassa-Sants.
*Authors:* Vilarrasa, V., Jurado, A., Vàzquez-Suñé, E., Carrera, J., Pujades, E.

---

**Event: 9th International conference on Tunnel Construction and Underground Structures. Slovenian Society for Underground Structures. Ljubljana, Eslovenia. September 2009.**

*Title:* Detection faulty joints during the construction of tunnels excavated by the cut and cover method.

*Authors:* Pujades, E., Mascuñano-Salvador, E., Jurado. A., Vilarrasa, V., Vàzquez-Suñé, E., Carrera, J.

*Title:* A methodology for analysing the drainage system in excavations between sheet pile walls.
*Authors:* Jurado. A., Bolster, D., Pujades, E., Vàzquez-Suñé, E., Carrera, J.

---

**Event: Las aguas subterráneas: Desafíos de la gestión para el siglo XXI. Asociación Internacional de Hidrogeólogos – Grupo Español. Zaragoza, España. September 2011.**

*Title:* Estudio del efecto barrera generado en acuíferos por construcciones subterráneas.
*Authors:* Pujades, E., López, A., Carrera, J., Vàzquez-Suñé, E., Jurado, A.

---

**Event: European Geosciences Union, General Assembly 2012. European Geosciences Union. Vienna, Austria. April 2012.**
*Title:* Barrier effect of underground structures on aquifers.
*Authors:* Pujades, E., López, A., Carrera, J., Vàzquez-Suñé, E., Jurado, A.

# Annex IV. Projects developed and related with the thesis

**Name of the Project:** Proyecto de construcción de plataforma L.A.V Madrid-Zaragoza-Barcelona-Frontera Francesa. Tramo: Hospitalet-La Torrassa. April 2007 to April 2008.

*Authors:* Pujades, E., Vàzquez-Suñé, E. and Carrera, J.

*List of reports:*

- Revisión del protocolo a seguir en el proceso de drenaje de las obras del AVE para el tramo L'Hospitalet-Torrassa.
- Seguimiento y evolución del proceso de drenaje durante la excavación del túnel del AVE, tramo L'Hospitalet-Torrassa, comprendido entre el pk 300+000 y el pk 302+460.
- Nota técnica sobre la colocación de las boyas de encendido y apagado, en el tramo comprendido entre los pk 300+780 y 301+090. Tramo L'Hospitalet-Torrassa, comprendido entre el pk 300+000 y el pk 302+460.
- Seguimiento y evolución del proceso de drenaje durante la excavación del túnel del AVE, tramo L'Hospitalet-Torrassa, comprendido entre el pk 300+000 y el pk 302+460.
- Seguimiento y evolución del proceso de drenaje durante la excavación del túnel del AVE, tramo L'Hospitalet-Torrassa, comprendido entre el pk 300+000 y el pk 302+460.
- Esquema constructivo para la realización de dos piezómetros en el interior del foso de FGC. Excavación del túnel del AVE tramo L'Hospitalet-Torrassa., comprendido entre el pk 300+000 y el pk 302+460.
- Seguimiento y evolución del proceso de drenaje durante la excavación del túnel del AVE, tramo L'Hospitalet-Torrassa, comprendido entre el pk 300+000 y el pk 302+460.
- Nota técnica sobre el drenaje bajo el paso del túnel de FGC, AVE L'Hospitalet-Torrassa.
- Seguimiento y evolución del proceso de drenaje durante la excavación del túnel del AVE, tramo L'Hospitalet-Torrassa, comprendido entre el pk 300+000 y el pk 302+460.
- Drenaje del túnel del AVE a su cruce con el túnel de FGC, tramo L'Hospitalet-Torrassa, comprendido entre el pk 300+000 y el pk 302+460.

- Descripción y nuevas propuestas sobre el sistema de drenaje de la excavación del túnel del AVE. Tramo L'Hospitalet-Torrassa, comprendido entre el pk 300+000 y el pk 302+460.
- Propuesta de dispositivo para minimizar el 'efecto barrera' en la obra para la construcción del tramo soterrado Hospitalet-Torrassa de la línea de tren de alta velocidad.

---

**Name of the Project:** Proyecto de construcción de plataforma L.A.V Madrid-Zaragoza-Barcelona-Frontera Francesa. Tramo: Montcada-Mollet del Valles. August 2009 to February 2010.

*Authors:* Escorcia, J., Serrano, A., Pujades, E., Vàzquez-Suñé, E. and Carrera, J.

*List of reports:*

- Propuestas de bombeo en el tramo del AVE Montcada – Mollet
- Cálculo de los caudales de drenaje para la excavación de los módulos 9 y 10 del túnel del tramo Montcada – Mollet. AVE Madrid-Barcelona.
- Drenaje para la excavación del túnel del tramo Montcada – Mollet. AVE Madrid-Barcelona.
- Nuevo dimensionado de los caudales de extracción en los pozos ubicados en las zonas de Tablestacas T! y T" para el drenaje de la excavación del Túnel del tramo Montcada – Mollet. AVE Madrid-Barcelona.
- Control del Factor de Seguridad ante el riesgo de levantamiento del suelo entre PK 200+000 y PK 200+286. Montcada – Mollet. (AVE Barcelona-Frontera Francesa).

---

**Name of the Project:** Proyecto de construcción de plataforma L.A.V Madrid-Zaragoza-Barcelona-Frontera Francesa. Tramo: Sants-Sagrera (Barcelona). December 2008 to February 2011.

*Authors:* Pujades, E., Vàzquez-Suñé, E. and Carrera, J.

*List of reports:*

- Bombeo en torno de "La torre del Fang".
- Aspectos hidrogeológicos en el entorno de las obras del AVE, sector c/Trinxant con c/Mallorca, Barcelona.
- Caracterización hidrogeológica en el entrono de las obras del AVE, sector c/Trinxant con c/Mallorca, Barcelona.

- Estudio del efecto barrera provocado por la construcción del AVE. Tramo Sant-Sagrera.
- Estudio previo a la ejecución de pantallas para la construcción del pozo de las obras del AVE, en el cruce entre las calles Mallorca y Trinxant. Calibración del ensayo de bombeo y cálculo del factor de seguridad.
- Protocolo de trabajos a realizar para la construcción de los pozos de ventilación en el tramo Sants-Sagrera del AVE.
- Diseño de los sondeos, piezómetros y pozo para la ejecución del pozo de ventilación situado en C/Padilla con C/Mallorca, Barcelona.
- Esquema constructivo de los piezómetros a ejecutar en el cruce entre las calles Padilla y Mallorca. AVE Sants-Sagrera.
- Bombeo previo a la excavación realizado entre las calles Trinxant y Mallorca.
- Esquema constructivo del pozo de bombeo a ejecutar en el cruce entre las calles Padilla y Mallorca.
- Reducción del bombeo en el pozo de mantenimiento situado en el cruce de las calles Trinxant y Mallorca.
- Seguimiento del drenaje durante la excavación del pozo de emergencia entre las calles Trinxant y Mallorca.
- Estudio previo a la ejecución de pantallas para la construcción del pozo de las obras del AVE en el cruce entre la calle Mallorca y Padilla. Calibración del ensayo de bombeo y cálculo del factor de seguridad.
- Bombeo previo a la excavación en el pozo de mantenimiento situado en el cruce de las calles Padilla y Mallorca.
- Piezómetros de control en la zona del túnel excavado entre pantallas.
- Ejecución de un piezómetro en la sección de control entre las calles Vizcaya y Navas.
- Cálculo del drenaje del pozo de mantenimiento situado en el cruce entre las calles Padilla y Mallorca utilizando columnas de jet-grouting.
- Eficiencia de los recintos de jet-grouting en el drenaje del pozo situado en la calle Padilla. Ajuste de los parámetros hidráulicos mediante la interpretación de un Segundo ensayo de bombeo.
- Seguimiento de la evolución del nivel piezométrico al paso de la tuneladora entre las calles Vizcaya y Trinxant.

- Diseño de los piezómetros para realizar el ensayo de bombeo en el cruce entre las calles Provença y Bruc – Tramo del AVE Sants-Sagrera.
- Características del ensayo de bombeo a realizar en el cruce entre la calle Provença y la calle Bruc.
- Características de los pozos de bombeo a construir para drenar el corralito de entrada al pozo de mantenimiento de Trinxant.
- Características del pozo de bombeo para drenar el corralito de salida del pozo de mantenimiento situado en la calle Trinxant.
- Ensayo de bombeo posterior a la ejecución de las columnas de jet-grouting en el pozo de mantenimiento de la calle Padilla.
- Bombeo en el corralito de entrada del pozo de mantenimiento situado en la calle Padilla.
- Sistema de drenaje para efectuar la excavación del pozo de mantenimiento en el cruce entre las calles Provença y Bruc.
- Bombeo en el corralito de entrada del pozo de mantenimiento situado en la calle Padilla.
- Piezómetros para realizar el ensayo de bombeo posterior a la ejecución de las pantallas en el cruce entre las calles Provença y Bruc- Tramo del AVE Sants-Sagrera.
- Ensayo de bombeo correspondiente al pozo de mantenimiento situado en la calle Enric Granados.
- Ensayo de bombeo posterior a la ejecución de las pantallas del pozo de mantenimiento sitiado en la calle Bruc.
- Conexión entre el pozo de ventilación y el túnel en la calle Nápoles. AVE Sants-Sagrera.
- Evolución del nivel piezométrico en el entrono de la Sagrada Familia –Histórica y actual.
- Piezómetros situados en el cruce entre las calles Provença y Enric Granados (AVE Sants-Sagrera).
- Características del pozo de bombeo a realizar en el cruce entre las calles Provença y Enric Granados (AVE Sants-Sagrera).
- Ensayo de bombeo en Rambla Cataluña para caracterizar los materiales a perforar por la tuneladora (AVE Sants-Sagrera).

- Evaluación de la profundidad de los pilotes durante el drenaje de la excavación a realizar en el cruce entre las calles Provença y Entença. (Ave Sants-Sagrera).
- Interpretación del ensayo de bombeo y sistema de drenaje para realizar las tareas de mantenimiento de la tuneladora en el cruce entre las calles Provença y Enric Granados. AVE Sants-Sagrera. (Ave Sants-Sagrera).
- Drenaje para la construcción de la primera fase de la galería de Conexión entre el pozo vertical y la tuneladora en el cruce entre las calles Enric Granados y Provença.. (Ave Sants-Sagrera).
- Propuesta de ensayo de bombeo en el cruce entre las calles Entença y Provença. Tramo Sants-Sagrera del AVE.
- Nota técnica: Drenaje para la excavación de la galería de conexión situada en el cruce entre las calles Provença y enric Granados. (AVE Madrid – Zaragoza – Barcelona – Frontera Francesa; tramo Sants – La Sagrera).
- Propuesta de ensayo de bombeo en la calle comte d'urgell para la caracterización hidráulica del terreno y posterior diseño del sistema de drenaje de la galería de conexión entre el pozo de emergencia y el túnel del AVE.
- Propuesta de ensayo de bombeo en la calle Nápoles para la caracterización hidráulica del terreno y posterior diseño del sistema de drenaje de la galería de conexión entre el pozo de emergencia y el túnel del AVE.

---

**Name of the Project:** Proyecto de construcción de la estructura de la estación de Sagrera. L.A.V Madrid-Zaragoza-Barcelona-Frontera Francesa. Tramo: La Sagrera-Nudo de la Trinidad. 2011.

*Authors:* Vàzquez-Suñé, E, Pujades, E., Escorcia, J., Serrano, A., and Jurado, A.

*List of reports:*

- Evaluación de caudales de drenaje durante la excavación del recinto de la estación de Sagrera (III).
- Evaluación de efecto barrera, efecto dren y caudales de drenaje durante la excavación del recinto de la estación de Sagrera.
- Protocolo a seguir en la fase inicial del bombeo para el agotamiento del nivel freático en la estructura de la estación de la Sagrera.

---

**Name of the Project:** Toronto – York Spadina Subway Extension. North Twin Tunnels (Canada). 2011.

*Authors:* Pujades, E., Vàzquez-Suñé, E. and Jurado, A.

*List of reports:*

- Technical report: Evaluation of the piles hydraulic conductivity at York University station.
- Toronto – York spadina subway extension York University station – Pumping test proposal.
- Toronto – York spadina subway extension York University station – Study of the drainage system that consist in pumping outside the enclosure.
- Toronto – York spadina subway extension York University station – Evolution of the drawdown measured outside the enclosure.
- Toronto – York spadina subway extension York University station – Some explanations about the "Report on a simplified estimation of settlements due to dewatering drainage of the York Spadina subway station.
- Toronto – York spadina subway extension York University station – Some considerations about the drainage of the York Spadina subway station (preliminary numericla model and recommendations).
- Toronto – York spadina subway extension York University station – Dewatering numericla simulation.
- Toronto – York spadina subway extension York University station – Dewatering plan for the TBM maintenance.
- Toronto – York spadina subway extension York University station – Test proposal.

**Name of the Project:** Estudio de climatología, hidrología, hidrogeología, drenaje y bombeo para el proyecto de metro Quito (Ecuador). February 2012 to April 2012.

*Authors:* Pujades, E., Vàzquez-Suñé, E., Alcaraz, M., Serrano, A.

*List of reports:*

- Modelo numérico hidrogeológico del valle de Quito. Calibración y predicción de posibles afecciones causadas por la construcción del metro. -Proyecto metro de Quito
- Modelo hidrogeológico del valle de Quito para el proyecto -Metro de Quito-


GHS


CSIC

UPC